Spherical wave reflection and transmission

Thesis

Spherical Wave Reflection and Transmission

Thesis submitted by

Yu Chen B.Sc., M.Phil.

for the degree of

Doctor of Philosophy

December 1991

Revised March 1992

Faculty of Technology

Open University

Milton Keynes

England

Abstract

This study is concerned with the reflection and transmission of spherical waves at a plane interface between two different media. The phenomenon of the reflection and transmission of spherical waves has been studied by means of analytical methods, numerical computation, and experimental tests.

A new integral representation for a spherical wave is obtained by transforming Lamb/Sommerfeld's integral representation. The new integral has no singularity so it allows more accurate numerical integration. A new proof of Lamb/Sommerfeld's integral representation for a spherical wave is presented based on the new integral.

By using the new form of solutions for reflected waves and existing solutions for transmitted waves, numerical studies have been carried out to examine the phenomenon of reflection and transmission of spherical waves at plane surfaces of discontinuity in material properties. It is shown that the effective critical angle for the total reflection of a spherical wave is greater than that of a plane wave at a hard boundary, and that when the source height increases the effective critical angle for the total reflection of a spherical wave tends to that of a plane wave. It is shown that recent predictions of spherical wave reflection and transmission coefficients greater than 1 at normal incidence under certain condition are probably due to numerical integration error. It also has been found that for spherical wave reflection and transmission, the time average energy flux, normal to a plane parallel to the plane of discontinuity, may locally be in the direction opposite to that of the direction of energy transmission over the plane as a whole. This so-called "backward wave" occurs in an interference between the direct and reflected waves, as well as in a transmitted wave.

An indirect test on the theory has been performed to check the pressure field, above a rigid boundary, predicted by the spherical wave theory. Theoretical and experimental results were in good agreement.

Acknowledgements

I am grateful for this opportunity of expressing my gratitude to my supervisor, Dr. Keith Attenborough, for his help and advice throughout my course of study. My thanks also go to Dr. N.Heap and Dr. A.Watson at the Faculty of Technology for their discussions on experimentation, to Dr. D.Broadhurst and M.L.Chen at the Department of Physics for their discussions on the principles of wave propagation, to the members of the Acoustics Group for maintaining a lively working atmosphere, and to P.Seabrook and B.Aengenheister for making up the equipment. I would like also to thank the staff of the Engineering Mechanics Discipline for their help. Useful suggestions by Professor P.E.Doak for improving this thesis are gratefully acknowledged.

This research was supported by a studentship grant from the Open University.

Contents

Chapter 1

Introduction

1.1 The aim of the research

The propagation of spherical waves is a fundamental form of motion. In general, when the extension of wave sources (except specially designed directional sources) is smaller than the wave length, at a distance which is not close to the source the waves can be treated as spherical: i.e., as waves generated by a point source.

Spherical wave propagation has been studied for many decades; however, we know less about spherical wave reflection or transmission than about the behaviour of plane waves at boundaries. We know that when a plane wave is incident at a plane interface between two different media, beyond a critical angle, the wave may be totally reflected; i.e., the time-space average energy transmission across the interface is zero in the direction perpendicular to the interface. In the case of spherical waves at such a plane interface of infinite extent, the whole range of incidence angles is involved from normal incidence to grazing incidence. An effective angle of incidence for a spherical wave may be defined as the angle of incidence of a ray which follows the specularly reflected path from source to receiver. Following this an effective critical angle for spherical wave reflection may be defined as the effective angle of incidence at which the time-space average energy transmission is zero in the direction perpendicular to the reflecting plane. It is not clear, from the literature, whether the effective critical angle for the total reflection of

a spherical wave is same as that for a plane wave. Theoretical treatments of spherical wave reflection and transmission have depended widely on classical integral representations due to Lamb and Sommerfeld. However some numerical results using these formulations have suggested the possibility of spherical wave reflection coefficients greater than one [46].

The research reported in this thesis has provided answers to some particular problems concerning spherical wave reflection at a plane interface between two different media. It is found numerically that when a spherical wave is incident on a boundary between an acoustically soft medium and a harder one (i.e., with a greater sound speed), the effective critical angle for total reflection for the spherical wave is greater than that for the corresponding plane wave. Beyond the effective critical angle there is some net time average energy transmission into the harder medium at some angles but no net time average energy transmission at others. It is also found that when the distance between a point source and the boundary increases, the effective critical angle for a spherical wave tends to that for a plane wave as expected. Further studies are carried out to solve problems where spherical waves are transmitted through several different media which have plane interfaces.

This study only deals with acoustic waves but the spherical wave theory developed here can be easily extended to other kind of waves, e.g., electromagnetic waves.

First we describe the differential equations which govern the general behaviour of waves in a medium. These differential equations are used widely in the theory of linear elasticity so sometimes the waves are also called elastic waves. The governing differential equation may be called the elastic wave equation. The waves in which we are interested, are linear and non-attenuated, except through geometrical decay caused by spherical spreading. The transporting medium can be either fluid or solid (a rigid porous medium can be treated as special case of a fluid), and all media are considered to be isotropic and homogeneous and the fluid is assumed to be inviscid. Secondly, boundary conditions at an interface between two different media will be given. Generally the radiation condition that, at infinite distance from a

source there are only waves outgoing from the source region, is applied. The boundary conditions to be applied, at a surface of fluid-fluid contact, are the continuity of the pressure and the continuity of normal displacement in the direction perpendicular to the interface. At a fluid-solid interface, besides the continuity of the normal displacements, we have the conditions that the pressure in the fluid is equal to the normal stress in the solid, and that the shear stress parallel to the interface vanishes (as the fluid is considered to be inviscid). Thus we have a clear problem to solve. What we aim to do is to find solutions to the differential equations subject to the boundary condition for a given geometry, and to interpret the solutions in physical terms so that we can obtain some understanding of the physical phenomena we are studying. Although this problem has been studied for many decades and there are several integral solutions to it, these solutions are very complicated, and thus there are difficulties in obtaining clear physical interpretations of them.

In this thesis, we are particularly interested in the classical type of integral solution which was first obtained by Sommerfeld for electromagnetic waves. A new form of solution is obtained which is shown to be equivalent to the classical Lamb/Sommerfeld type of solution.

To validate and interpret the solution, we have taken advantage of modern computers to calculate results for some specific problems where the geometry, wave frequency and material constants are given. Some of the theoretical results will be tested by experiment.

It is not the intention of this thesis to explain all theoretical results we have obtained, because the results have been obtained from a simplified mathematical model. Although this model is more complete than the widely-used impedance boundary model, several simplifications have been made. For example, variation of density in a gas is assumed to be negligible, and in calculations the density of a gas is taken to be a constant in a wave motion, although we know that air (say) is compressible. Also at an interface of a fluid and another medium it is assumed that the relative movement between two media parallel to the interface is free (i.e., slip is permitted at the interface). In many cases, it is difficult to judge how much these sim-

plifications have affected the results we have obtained unless we have some experimental verification. Convincing explanations would require considerably more theoretical studies and experimental verification than described here. Nevertheless attempts have been made to explain some results.

Before carrying out our investigation, the history of the study of spherical wave reflection is briefly reviewed.

1.2 Review

The classical functional mathematical expression for a spherical wave in an infinite space is well known and has a very simple form; the amplitude of the wave decreases in inverse proportion to the distance from a source. In cylindrical coordinates, an outgoing spherical wave of simple harmonic time dependence can be expressed as the complex function

$$\frac{exp(i(\omega t - k\sqrt{r^2+z^2}))}{\sqrt{r^2+z^2}}.$$

Unfortunately, this expression by itself is not sufficient when we deal with spherical wave reflection, because the reflected and transmitted waves in general do not have such a simple form. Based on this classical expression several alternative forms of spherical wave representation have been developed, which are useful in problems involving reflection and transmission.

An integral expression for a spherical wave can be found in a paper by Lamb [1], published in 1904, in which he was mainly concerned with surface waves. Lamb's formula for harmonic waves is expressed as

$$\frac{exp(-ik\sqrt{r^2+z^2})}{\sqrt{r^2+z^2}} = \int_0^\infty \frac{exp(-\sqrt{\xi^2-k^2}z)J_0(\xi r)\xi}{\sqrt{\xi^2-k^2}}\,d\xi, \qquad (1.1)$$

where the time dependency $exp(i\omega t)$ is omitted. In his derivation of this formula he started with an integral of the form of that on the right side of (1.1), and then used several arguments to demonstrate that equation (1.1) is true. A brief description of Lamb's derivation will be given in Chapter 5.

An alternative derivation of the complex conjugate of this integral representation was given by Sommerfeld in 1909 [4] $(exp(-i\omega t+ik\sqrt{r^2+z^2})/\sqrt{r^2+z^2}$,

represents an outgoing spherical wave when $exp(-i\omega t)$ is used for the time factor rather than $exp(i\omega t)$). A detailed account of Sommerfeld's derivation was presented by Stratton in 1941 in his book "Electromagnetic theory" (see pp.573-577 in [5]), he assumed that the integration variable ξ (or λ in [5]) can be any complex value. However, Sommerfeld in his book "Partial differential equations in Physics" (see pp.240-242 in [3]) published in 1949 specified ξ (or λ in [3]) as a positive real variable. He first derived the basic form of the integral in a two dimensional polar coordinate system by using a Fourier-Bessel transform, which he extended to the basic integral in three dimensions simply replacing r^2 by $r^2 + z^2$, and then deduced the correct explicit form of the integrand. When Ewing, *et al.*, discussed Sommerfeld's derivation in their book "Elastic waves in layered media" [11] published in 1957, they did not specify the nature of the integration variable, and used Lamb's formula (1.1) instead of its complex conjugate. So there is a lack of clarity in the various derivations of Lamb/Sommerfeld's formula. In fact, many mathematical handbooks (e.g., [62], [63]) do not include the important integral formula (1.1). When numerical integration is to be used, a particular problem is that, the singularity in the integrand of equation (1.1) will present a problem for the convergence of the integral at this point. In this thesis it is shown that the integral is convergent at the singularity and a simple proof of equation (1.1) is offered. The proof also provides a clear understanding of the integral expression.

Sommerfeld also gave an alternative form of integral for the complex conjugate of equation (1.1). The integrand contains a Hankel function instead of a Bessel function:

$$\frac{exp(ik\sqrt{r^2+z^2})}{\sqrt{r^2+z^2}} = \frac{1}{2}\int_{-\infty}^{\infty} \frac{exp(-\sqrt{\xi^2-k^2}z)H_0^1(\xi r)\xi}{\sqrt{\xi^2-k^2}}\, d\xi. \qquad (1.2)$$

The integral representations make possible the solution to the differential equations subject to the boundary conditions. The reflected and transmitted waves are characterised by different coefficients in the integrands which are functions of the integration variable only and independent of the space coordinates. The integrand coefficients can be determined from boundary conditions.

By using such integral expressions, many studies have been made of the problem of the reflection of electromagnetic spherical waves at a plane boundary between two semi-infinite homogeneous media. Sommerfeld [3], Van der Pol [6] and Norton [7] were among the early researchers. In 1947, Rudnick [8] extended the theory of spherical waves to the acoustic case for an interface between two semi-infinite media. His results are valid for a fluid-fluid interface as well as for a fluid-porous medium interface. The continuities of pressures and of normal particle velocities were applied at the boundary. Rudnick obtained the solutions in forms similar to the solutions given by Van der Pol. This problem was also studied by Paul [9]. He used Sommerfeld's integral in the form of equation (1.2) with the integrand containing the Hankel function.

An experiment was carried out by Lawhead and Rudnick [10] to check the adequacy of Rudnick's theoretical solution. The measurements were conducted in a large anechoic chamber. A spherical wave was generated from the open end of a brass tube which was coupled to a driver unit. The sound pressure generated by this approximate point source on a surface of fiberglass was measured with respect both to its amplitude and phase characteristics. In order to compute theoretical curves, the acoustic constants of the porous medium were obtained in measurements by using an impedance tube. The comparison between the measurements and an appropriate approximation of Rudnick's solution showed good agreement at the boundary. The difference between measured and theoretical results increased with increasing height of the receiver.

A book on elastic waves in layered media by Ewing, Jardetzky and Press [11] was published in 1957. In this book, the problems of waves from a point source in layered elastic media were discussed and the complete solutions to the elastic wave equations subject to the boundary conditions were presented. Ewing, Jardetzky and Press used the Lamb/Sommerfeld expression (1.1) for the waves produced by the point source. A numerical integration of the integral representation for the wave field was considered to be exceedingly difficult by Ewing *et al.*. Thus one does not expect to find any detailed

numerical results for spherical wave reflection in the pre-1957 literature.

In 1951, Ingard [12] used a different integral expression for spherical waves in spherical polar coordinates to study the reflection of a spherical wave at a plane boundary. He assumed that the boundary has a constant impedance, and the reflected wave is assumed to originate from an image source, the plane wave reflection coefficient being in the integrand of an appropriate integral. The form of integral expression for a spherical wave used by Ingard, is due to Weyl [13] and is given by

$$\frac{exp(ik\sqrt{x^2+y^2+z^2})}{\sqrt{x^2+y^2+z^2}} = \frac{ik}{2\pi}\int exp(ik(ax+by+cz)sin(\theta)d\theta d\phi. \qquad (1.3)$$

A further approximation was applied to the solution, and pressure contours were calculated from the approximation. At the same time Lawhead and Rudnick [14] carried out a similar study. They also assumed a constant impedance boundary condition, but used Lamb's expression for spherical waves. They expressed the integrand coefficient that they obtained from the boundary condition as an infinite integral. After some simplification, Lawhead and Rudnick exchanged the order of integrations and obtained an approximation which is similar to Ingard's approximation.

A derivation of the Weyl type of integral can be found in the book [15] by Brekhovskikh. Brekhovskikh describes the reflected wave as a combination of the usual reflected wave and a lateral wave. The idea is borrowed from the phenomenon of a wave beam displacement [16]. When a wave beam is incident on a plane boundary at an angle of total reflection, the reflected wave is spatially displaced with respect to the ray geometrically reflected at the interface. In a book [17] by Brekhovskikh and Lysanov published later, the Weyl type of integral was transformed into Sommerfeld's integral with a Hankel function. The Weyl type of integral was used by Doak [18] in 1952 to investigate the reflexion of a spherical acoustic pulse by an absorbent infinite plane. He describes the reflection wave field including a locally reflected wave and a scattered wave (or diffracted wave).

Theories developed by Ingard and by Rudnick were experimentally tested for porous media by Delany and Bazley [19] in 1969. The porous material

used was mineral wool. The experimental work is similar to that of Lawhead and Rudnick, but only the relative sound pressure level was measured. The agreement between their measurements and approximated theoretical results was found to be good. Their study was only concerned with highly attenuating media as the reflecting medium; they made the comment that for a medium which has a very low attenuation constant and relatively high phase velocity it is necessary to employ the more exact solution for the case of two semi-infinite media. Delany and Bazley also realised that numerical solution is probably the simplest procedure.

Further investigations on spherical wave reflection at a plane boundary have been made ([20] to [39]) by using either Lamb's integral or Sommerfeld's or Weyl's integral. Some new solutions have been presented. Many efforts have been made to simplify the integral solution for the reflected wave to an analytic approximation by various methods of integral analysis. A comprehensive review of studies on spherical wave reflection has been made by Chandler-Wilde [40] as a part of his Ph.D. thesis. Comparisons have been made for various representations of spherical wave reflection.

One of the reasons why efforts have been made to represent an integral solution by an analytic approximation is the difficulty in numerical integration, but with the increasing power of computers available, this becomes less difficult. Also for a problem of a multilayered medium a rigorous integral analysis in general will not produce a simple solution, because the solution is inherently a complicated one. With the development of modern computers, more and more use is being made of numerical methods to study spherical wave propagation. To deal with more complicated problems of waves in a plane multilayered medium from a point source, DiNapoli and Davenport [41] in 1980 presented a numerical method which is based on the Fast Field Program conceived by Marsh and Elam [42] . The wave field is expressed as a Fourier-Bessel transform with an unknown depth-dependent Green's function. First they replaced the Bessel function in the integral with the Hankel function associated with outward propagation; then they used a far field approximation so that the wave field can be expressed in a form suitable for

numerical integration. The Green's function is constructed from fundamental solutions of the classical Sturm-Liouville differential equation with discontinuous coefficients by use of the matrixant method. Results for the pressure field, plotted in terms of propagation loss verses range, were provided for three examples. Since approximation was used at a very early stage of their analysis, the method used by DiNapoli and Davenport cannot provide an exact answer for the problem of spherical wave reflection. Later, modifications to the basic algorithm were made by Richards and Attenborough [43] to improve its accuracy. Numerical examples for waves above a plane porous boundary showed significant improvements in accuracy.

In 1985, Schmidt and Glattetre [44] presented a numerical model of wave propagation in layered media based on the solution given in the book by Ewing *et al.*. Schmidt and Glattetre started from the solution in a form similar to Lamb's expression with unknown integrand coefficients representing the effect of reflection or of transmission and then used a matrix method developed a year earlier by Schmidt and Jensen [45] to determine the unknown integrand coefficients in the case of multilayered media. The numerical integration described in the paper by Schmidt and Jensen was performed in the complex plane to avoid singularities in the integrands. The model's capabilities were illustrated by two test cases. The first was the case where there is a point source in free space. They admitted that it was a challenge because of a singularity in the integrand. However no comparisons with the exact functional solutions were given. The model was also used to analyse the field radiated by a long horizontal array. According to the numerical results, different modes will propagate in slightly different directions.

More recently an investigation of spherical wave reflection by Piquette [46] produced the surprising result that when a spherical wave in a fluid is incident on a solid plate of infinite lateral extent, the amplitude of the reflected pressure and/or the transmitted pressure could exceed the maximum value of the amplitude of the incident pressure on the plate surface. Firstly Piquette obtained the solution of the elastic wave equations subject to the boundary conditions. The solution was of the form of Lamb's inte-

gral. The so called "overpressure" was obtained by numerical calculations for some special cases. The integration interval was split into a finite subinterval in which the integrand varies most rapidly and an infinite subinterval. The numerical integration over the finite subinterval was evaluated by using a Gauss-Legendre procedure and a 15-point Gauss-Laguerre numerical integration procedure was used over the infinite subinterval. To check these unexpected overpressures, Piquette calculated the power integral of the reflected and transmitted waves over both the front and back surfaces of the plate and found that the sum of the reflected and the transmitted power never exceeds the total incident power but can be greater than the incident power over certain finite areas. In order to verify his numerical finding, Piquette carried out an experiment to acquire reflection and transmission data. A square-shaped plate, 76 cm on a side, was immersed in water for measurement in the frequency range 1-5 kHz. The plate was steel or PMM. However he did not find the overpressures. We shall see later that his overpressure predictions are probably due to a computing error.

From the above narrative we can see that basically there are two theoretical models for the study of spherical wave reflection at a plane boundary. One model is that of two semi-infinite media. Wave fields must satisfy the wave equations in both media respectively and also satisfy appropriate boundary conditions. We shall use this exact model.

The other one is a simplified model. The assumption is made that the conditions at the reflecting boundary may be expressed in terms of a normal impedance independent of the angle of incidence so that the wave field in the medium that does not contain a source can be neglected. Since in general the specific normal impedance at a boundary between elastic media may depend strongly on the angle of incidence, this model is restricted and can not provide complete information on the reflection of a spherical wave at a plane solid boundary. However, this model may be a good approximation for outdoor sound propagation over certain types of ground (which behave as rigid porous media), and for some other problems of practical interest.

1.3 Outline

In the next two chapters, we shall describe the fundamental theories, the equations of linear elasticity and the computation methods, on which this research is based. Since we shall not make further approximations of the theoretical results that we obtain, the validity of the predictions will, to a large extent, rely on these fundamental theories and methods. Therefore the theories and computation methods are presented in some detail.

We start with simple plane wave cases in Chapter 4. To compare the results of spherical wave propagation, reflection and transmission with those of plane waves we need some plane wave results so the problems of plane wave reflection and transmission will be discussed first. Although the theory of plane wave propagation is well established, the results required are briefly re-derived for the sake of convenience of reference and completeness. Three cases will be examined. These are (*i*) plane wave incidence at an interface between two semi-infinite fluids, (*ii*) plane wave incidence from the fluid at a fluid-solid interface and (*iii*) plane wave incidence at the surface of a solid plate which is bounded by two semi-infinite fluid media. Since we are only interested in isotropic and homogeneous media, the waves can always be represented in two dimensional space introducing only two space coordinates. The conservation of energy flux in the direction normal to the interface will be discussed.

From the review in the previous section, we have seen that essentially there are three forms of integral representation for spherical waves which have been relatively widely used in the past. We are particularly interested in Lamb's integral (equation (1.1)). In Chapter 5, Lamb's integral representation for a spherical wave will be examined closely. First, it is shown that the integral in (1.1) is convergent. From the convergence analysis, a new form of integral for a spherical wave is obtained, given by

$$\frac{exp(-ik\sqrt{r^2+z^2})}{\sqrt{r^2+z^2}} = \int_{ik}^{\infty} J_0(r\sqrt{k^2+x^2})e^{-|z|x}\,dx. \qquad (1.4)$$

The path of integration is taken from k to 0 on the imaginary axis and then from 0 to infinity on the real axis. Verification of the convergence of the

Lamb's integral enables us to examine the integral by using a power series expansion. Based on the new integral, a new proof of the validity of (1.1) is offered.

From a table of integrals [62], we have found another formula for the complex conjugate of the formula (1.1), which is given by

$$\frac{exp(ik\sqrt{r^2+z^2})}{\sqrt{r^2+z^2}} = i\int_0^\infty H_0^{(1)}(z\sqrt{k^2-x^2})cos(rx)\,dx, \qquad (1.5)$$

where $H_0^{(1)}(z\sqrt{k^2-x^2})$ is a Hankel function of the first kind. The integral (1.5) has a singularity at $x = k$. It is not a reduction of Sommerfeld's integral and has not been used by previous researchers. The integral representation (1.5) will be used as another form for comparison, although we have not found it possible to prove directly that some resulting solutions in the presence of an interface satisfy the equations of motion. Since however the left side of (1.5) satisfies the equations of motion and the right side of (1.5) is equal to the left side then we have an indirect proof that the right side of (1.5) satisfies the equations of motion.

It is well known that the time average energy carried by a spherical wave crossing a plane surface of infinite extent per unit time is equal to half of the time average total output power generated by the point source which is placed at some distance away from the plane. A mathematical derivation of this result will be given in Chapter 5. This property of spherical waves will be used frequently.

With the help of a modern computer, one can solve almost any problem which can be defined properly in mathematical terms by using a numerical method. Although numerical methods are powerful, it is dangerous to rely purely on them without analytical guidance, or without experimental verification. Since most of our final results will be obtained by the NAG numerical routines, they are introduced in Chapter 3. Numerical test cases are given for two examples. Comparison will be made between the numerical integrations of the integrals in equations (1.1), (1.4) and the complex conjugate of equation (1.5) with the classical functional expression on the left side of equation (1.1). The comparisons show that the integral (1.4) gives more accurate

numerical integration results than the others, since the singularity is eliminated. However the accuracy of the numerical integration of (1.4) reduces as coordinates r and z increase, because the integrand oscillates rapidly. The first test is performed at some particular coordinate points, however no numerical routine can be guaranteed to work in all cases [47]. A wider range coordinate test is included indirectly in the second test. The second test is the numerical integration of the energy flux of a spherical wave over a plane surface. We shall see that as the area of the integration increases, the time average power across the area converges to half of the total output power, as it should.

Spherical wave reflection and transmission is studied in Chapter 6. The first use of Lamb's integral is for the study of the reflection of a spherical wave at a rigid boundary since this result can be compared with the result calculated from the classical functional expression. A new form of integral solution for the reflected wave is given. Pressure contours obtained by two methods show good agreement.

However it is found that in some regions a component of the time average energy flux is in a direction opposite to that of this component when it is integrated over the whole surface concerned. This phenomenon is sometimes called a "backward wave".

For the cases of spherical wave reflection at a fluid-fluid interface and at a fluid-solid interface, solutions are obtained which satisfy the wave equations and the boundary conditions and the reflection term is transformed into a new form. Comparisons of these results with those for the corresponding problems but with plane wave incidence show some similarities and some differences. The solutions for the reflected and transmitted waves are checked for energy conservation.

"Backward waves" are also predicted for reflection and transmission at a hard boundary.

Predicted pressure contours for the reflection at a fluid-solid interface are similar to those obtained for reflection from a perfectly rigid boundary for several fluid-solid interfaces of practical interest.

As a further application of the new integral (1.4), the transmission of a spherical wave through a solid plate which is immersed in various fluids is studied. The analytical solution in the form of an exact integral is obtained first and then numerical integration is carried out. The numerical results show that the reflection and transmission process for a spherical wave is consistent with that for the case of a plane wave for normal incidence and that the "overpressure" predicted by Piquette [46] does not exist.

In Chapter 6, the theoretical pressure contours above a model plate of infinite extent are presented and shown to be same as those computed from the functional result for rigid reflection. An experiment has been carried out to measure the pressure distribution caused by an incident spherical wave and the reflected wave. The experiments obviously had to be done by using a finite plate, but it has been assumed that the experimental results should correspond to the theoretical ones in regions not too close to the edges of a sufficiently large but finite reflector. A circular plate was used in this work. In order to speed up the measurement of the two dimensional pressure contours, a computer controlled measurement system was devised and built. The points of measurement correspond to those for theoretical calculation, and the same method of interpolation was used for both theoretical and experimental data. The experimental results show good agreement with the theoretical results except at the edge of the disc.

Some useful results will be discussed in the last chapter. We shall point out some further possible studies. The validity of applying Lamb's integral to porous media needs to be examined, and further research on "backward wave" propagation is recommended.

Chapter 2

Fundamental theory

The fundamental theory, on which this investigation is based, is a linear theory of elastic wave propagation. The theory concerns the transmission of infinitesimal mechanical disturbances in a medium. When an external disturbance is applied to any part of a body, this disturbance is transmitted through the body in the form of propagating waves, which cause deformation of the body, and consequently changes in the internal elastic forces.

Since the validity of results which we obtain later depends, to a large extent, on the theory of elastic wave propagation, a brief introduction of the theory is given here.

2.1 Linear elasticity

We start from the basic concepts. In elastic wave theory, the concept of stress is used to describe the internal elastic forces, and the deformation is described by displacement and strain. In the case of elastic waves in an inviscid fluid, we often use the term, pressure, for the isotropic stress.

Stress. At an arbitrary point P within a body we consider a small element of area δA with associated unit normal $\hat{n}$. We define the material which contains the positive unit normal to be on the positive side of δA. The material on the positive side of δA is assumed to exert a resultant force on the material on the negative side. As the area element at P approaches zero, the limit of the ratio of the force to the area is called a stress vector and it

is in the direction of the force. A stress vector will be denoted by $\hat{T}$ with components T_i. At any point in a body, we can define a stress vector on each of three planes parallel to the coordinate planes of a rectangular Cartesian coordinate system. The nine stress components of the three stress vectors are the components of a tensor. This tensor is called the stress tensor and is expressed as

$$[t_{ij}] = \begin{bmatrix} t_{11} & t_{12} & t_{13} \\ t_{21} & t_{22} & t_{23} \\ t_{31} & t_{32} & t_{33} \end{bmatrix}, \tag{2.1}$$

where t_{ij} represents the stress component acting in the x_j-direction on the surface normal to the x_i-direction. A stress component normal to the surface on which the force acts is called a normal stress and a stress component parallel to the surface is called a shear stress. Knowing the nine stress components at a point, we can determine the stress vector acting on any surface at the point. It is given by

$$T_i = n_j t_{ij}. \tag{2.2}$$

Here, and throughout this chapter, the summation convention is used for a repeated subscript in a term and the subscripts take on the values $1, 2, 3$, unless otherwise indicated. For example, equation (2.2) is equivalent to

$$T_1 = n_1 t_{11} + n_2 t_{12} + n_3 t_{13}, \tag{2.3}$$

$$T_2 = n_1 t_{21} + n_2 t_{22} + n_3 t_{23}, \tag{2.4}$$

$$T_3 = n_1 t_{31} + n_2 t_{32} + n_3 t_{33}. \tag{2.5}$$

Displacement. When a body is deformed, a particle in the body may move from its original location with coordinates (a_1, a_2, a_3) to a new location with coordinates (x_1, x_2, x_3). The displacement vector of the particle can be defined by those two points. Its components are given by

$$u_i = x_i - a_i. \tag{2.6}$$

If displacements are associated with all particles in the deformed position and they change with time, a displacement field can be used to specify the

deformation of a body. The displacement field of a deformed body relative to that of the body in its undeformed state can be described in terms of strain.

Strain. For infinitesimal deformation, Cauchy's definition of the strain tensor can be obtained as follows. Consider an infinitesimal line element da in an undeformed body. The square of the element's length in terms of the components da_i is given by

$$da^2 = \delta_{ij} da_i da_j, \tag{2.7}$$

where δ_{ij} is the Kronecker delta, defined by

$$\delta_{ij} = \left\{ \begin{array}{ll} 1 & \text{if } i = j \\ 0 & \text{if } i \neq j \end{array} \right\}. \tag{2.8}$$

After deformation, the square of the length element becomes

$$dx^2 = \delta_{ij} dx_i dx_j, \tag{2.9}$$

and by using equation (2.6) we may express da^2 in terms of the deformed position:

$$da^2 = \delta_{ij}(\delta_{ik} - \frac{\partial u_i}{\partial x_k})(\delta_{jl} - \frac{\partial u_j}{\partial x_l}) dx_k dx_l. \tag{2.10}$$

From equations (2.9) and (2.10) the difference between the squares of the length elements may be written as

$$dx^2 - da^2 = (\frac{\partial u_i}{\partial x_j} + \frac{\partial u_j}{\partial x_i} - \frac{\partial u_k}{\partial x_i}\frac{\partial u_k}{\partial x_j}) dx_i dx_j. \tag{2.11}$$

If the first derivatives of the displacement components are each very small the product terms in the bracket are negligible and Cauchy's strain tensor is defined by the rest of terms in the brackets divided by 2:

$$\epsilon_{ij} = \frac{1}{2}(\frac{\partial u_i}{\partial x_j} + \frac{\partial u_j}{\partial x_i}). \tag{2.12}$$

Hooke's law. For a linear elastic solid, stress is related to strain by Hooke's law, which states that the stress tensor is linearly proportional to the strain tensor. For isotropic media there are only two independent elastic constants and Hooke's law is expressed by

$$t_{ij} = \lambda \epsilon_{kk} \delta_{ij} + 2\mu \epsilon_{ij}, \tag{2.13}$$

where λ and μ are known as Lamé's constants.

For an inviscid fluid, the shear stress vanishes and the normal stress in any direction is called the pressure:

$$p = -t_{11} = -t_{22} = -t_{33}. \tag{2.14}$$

When a deformation in an inviscid fluid is infinitesimal, the pressure and the strain are related by

$$p = -K \epsilon_{kk}, \tag{2.15}$$

where K is called the bulk modulus.

2.1.1 Dynamics

Newton's second law of motion states that in an inertial frame of reference the rate of change of the linear momentum of a body is equal to the resultant of the applied forces. When elastic waves propagate through a medium, the motion of any part of the body must obey Newton's second law of motion.

Let us consider a region V, which does not contain a source, in a body. The region has a closed surface S. In linear elastic wave theory, the rate of change of the linear momentum of all the particles in V, in the x_i-direction, is given by

$$P_i = \int_v \rho \frac{\partial^2 u_i}{\partial t^2} \, dv, \tag{2.16}$$

where ρ is the original density. We have assumed that the change in the density is negligible. If the region is subjected to surface traction T_i and body force is neglected, the i th component of the resultant force is

$$f_i = \int_s T_i \, ds. \tag{2.17}$$

Expressing the surface traction in terms of the stress tensor by equation (2.2), transforming the surface integral into a volume integral by Gauss's theorem, and equating equations (2.16) and (2.17) we obtain

$$\int_v \rho \frac{\partial^2 u_i}{\partial t^2}\, dv = \int_v \frac{\partial t_{ij}}{\partial x_j}\, dv. \tag{2.18}$$

Since this equation must hold for an arbitrary volume V, the integrands on the two sides must be equal. Thus we obtain the equations of motion of linear elastic wave theory in a form without body force

$$\rho \frac{\partial^2 u_i}{\partial t^2} = \frac{\partial t_{ij}}{\partial x_j}. \tag{2.19}$$

The displacement field of a linear elastic wave in any region which contains no sources must satisfy equation (2.19).

By use of Hooke's law for isotropic media, equation (2.13), and equation (2.12), the equations of motion (2.19) can be expressed in terms of the displacement as

$$\rho \frac{\partial^2 u_i}{\partial t^2} = (\lambda + \mu) \frac{\partial^2 u_j}{\partial x_j \partial x_i} + \mu \frac{\partial^2 u_i}{\partial x_j \partial x_j}. \tag{2.20}$$

For convenience, we can express the components of the displacement in terms of two potentials, a scalar potential ϕ and the components of a vector potential, as ψ_i,

$$u_i = \frac{\partial \phi}{\partial x_i} + e_{ijk} \frac{\partial \psi_k}{\partial x_j}, \tag{2.21}$$

where e_{ijk}, the permutation symbol, is defined by

$$e_{ijk} = \left\{ \begin{array}{ll} 1 & \text{if } ijk \text{ represents an even permutation of 123} \\ 0 & \text{if any two of the } ijk \text{ indices are equal} \\ -1 & \text{if } ijk \text{ represents an odd permutation of 123} \end{array} \right\}. \tag{2.22}$$

On substituting equation (2.21) into equation (2.20) and rearranging terms we obtain

$$\frac{\partial}{\partial x_i}[(\lambda + 2\mu)\nabla^2 \phi - \rho \frac{\partial^2 \phi}{\partial t^2}] + e_{ijk} \frac{\partial}{\partial x_j}(\mu \nabla^2 \psi_k - \rho \frac{\partial^2 \psi_k}{\partial t^2}) = 0, \tag{2.23}$$

where

$$\nabla^2 = \frac{\partial^2}{\partial x_j \partial x_j}. \tag{2.24}$$

It can be seen that if the scalar potential and the vector potential satisfy the equations

$$\nabla^2\phi = \frac{\rho}{\lambda + 2\mu}\frac{\partial^2\phi}{\partial t^2}, \tag{2.25}$$

and

$$\nabla^2\psi_k = \frac{\rho}{\mu}\frac{\partial^2\psi_k}{\partial t^2}, \tag{2.26}$$

respectively, the displacement composed of the two potentials satisfies the equations of motion (2.23).

The scalar potential corresponds to a longitudinal wave which has a wave speed determined by

$$c_l = \sqrt{\frac{\lambda + 2\mu}{\rho}}. \tag{2.27}$$

A simple example of the longitudinal wave is

$$\phi = Acos(k_1 x_1 - \omega t), \tag{2.28}$$

where A is the constant amplitude, k_1 is the one-component wavenumber vector, and ω is the angular frequency. The wave represented by equation (2.28) has only one displacement component, u_1, which is parallel to the wavenumber vector. The vector potential corresponds to a transverse wave. Its wave speed is given by

$$c_t = \sqrt{\frac{\mu}{\rho}}. \tag{2.29}$$

An example of a transverse wave is

$$\psi_1 = 0, \psi_2 = Acos(k_1 x_1 - \omega t), \psi_3 = 0. \tag{2.30}$$

The only displacement component u_3 is normal to the wavenumber vector and the other displacement components are zero.

In an inviscid fluid, the assumptions for the derivation of equation (2.20) is also valid except $\mu = 0$ and $\lambda = K$, so the potential function for the displacement satisfies

$$\nabla^2\phi = \frac{1}{c_f^2}\frac{\partial^2\phi}{\partial t^2}, \tag{2.31}$$

where $c_f^2 = K/\rho$. From equations (2.31) and (2.15) we can find that the pressure in terms of the potential is given by

$$p = -\rho \frac{\partial^2 \phi}{\partial t^2}. \tag{2.32}$$

2.1.2 Two-dimensional formulae

We are interested in the reflection and transmission of plane or spherical incident waves at plane interfaces of infinite extent and hence the problems we consider can always be treated in a two dimensional space. In the case of plane waves, we use a rectangular Cartesian coordinate system x, y and z. If we set the x-axis parallel to the component of the wavenumber vector of the incident wave on the interface and the z-axis perpendicular to the interface, there will be no movement in the y-direction and the motion is independent of the y coordinate so that we only need consider problems in the x-z coordinate plane. For a spherical wave, we can take the z-axis of a cylindrical coordinate system perpendicular to the interface and passing through the point source so the motion is independent of the angular coordinate.

Let us consider plane waves first. Since the y-component of the displacement is zero the displacement can be expressed by

$$u = \frac{\partial \phi}{\partial x} - \frac{\partial \psi}{\partial z}, \tag{2.33}$$

$$w = \frac{\partial \phi}{\partial z} + \frac{\partial \psi}{\partial x}, \tag{2.34}$$

where u and w are the displacement components in the x and z directions respectively, ϕ is the potential function for the longitudinal waves and ψ is the single non-zero component of the vector potential function for the transverse waves. ψ is in the y-direction.

The potential functions must satisfy the equations of motion which are

$$\nabla^2 \phi = \frac{1}{c_l^2} \frac{\partial^2 \phi}{\partial t^2}, \tag{2.35}$$

$$\nabla^2 \psi = \frac{1}{c_t^2} \frac{\partial^2 \psi}{\partial t^2}. \tag{2.36}$$

The stress components are

$$t_{xx} = \lambda(\frac{\partial u}{\partial x} + \frac{\partial w}{\partial z}) + 2\mu\frac{\partial u}{\partial x}, \tag{2.37}$$

$$t_{yy} = \lambda(\frac{\partial u}{\partial x} + \frac{\partial w}{\partial z}), \tag{2.38}$$

$$t_{zz} = \lambda(\frac{\partial u}{\partial x} + \frac{\partial w}{\partial z}) + 2\mu\frac{\partial w}{\partial z}, \tag{2.39}$$

$$t_{zx} = \mu(\frac{\partial w}{\partial x} + \frac{\partial u}{\partial z}). \tag{2.40}$$

(2.41)

In an inviscid fluid, we have

$$t_{xx} = t_{yy} = t_{zz} = -p. \tag{2.42}$$

For spherical wave propagation, again we have two potential functions for the displacement, but the governing equation for the vector potential transformed from the rectangular coordinate system does not have the form of a wave equation. Fortunately because of the axial symmetry, we can use another potential which does satisfy the wave equation.

The displacement is related to the potentials by

$$u = \frac{\partial \phi}{\partial r} + \frac{\partial^2 \psi_t}{\partial r \partial z}, \tag{2.43}$$

$$w = \frac{\partial \phi}{\partial z} - \frac{\partial}{r\partial r}(\frac{r\partial \psi_t}{\partial r}), \tag{2.44}$$

where u and w are the displacement components in the r and z directions respectively, ϕ is a potential function for the longitudinal waves and ψ_t is the potential function for the transverse waves. The function ψ_t is not the transformation of ψ by a direct coordinate transform from a rectangular Cartesian coordinate system, but it is not difficult to show that if ϕ and ψ_t satisfy the equations

$$\nabla^2\phi = \frac{1}{c_l^2}\frac{\partial^2 \phi}{\partial t^2}, \tag{2.45}$$

$$\nabla^2\psi_t = \frac{1}{c_t^2}\frac{\partial^2 \psi_t}{\partial t^2}, \tag{2.46}$$

then the equations of motion (2.20) are satisfied. The two-dimensional Laplace operator ∇^2 is defined by

$$\nabla^2 = \frac{\partial^2}{\partial r^2} + \frac{1}{r}\frac{\partial}{\partial r} + \frac{\partial^2}{\partial z^2}. \tag{2.47}$$

The stress is given by

$$t_{rr} = \lambda(\frac{\partial u}{\partial r} + \frac{1}{r} + \frac{\partial w}{\partial z}) + 2\mu\frac{\partial u}{\partial r}, \tag{2.48}$$

$$t_{\theta\theta} = \lambda(\frac{\partial u}{\partial r} + \frac{1}{r} + \frac{\partial w}{\partial z}) + 2\mu\frac{u}{r}, \tag{2.49}$$

$$t_{zz} = \lambda(\frac{\partial u}{\partial r} + \frac{1}{r} + \frac{\partial w}{\partial z}) + 2\mu\frac{\partial w}{\partial z}, \tag{2.50}$$

$$t_{zr} = \mu(\frac{\partial w}{\partial r} + \frac{\partial u}{\partial z}). \tag{2.51}$$

2.2 Energy of waves

Travelling waves transport energy from one place to another. The amount of energy and the direction of energy transportation by a wave can be specified as the wave energy flux, or intensity. Obviously, the wave energy flux is a vector. The energy flux component along the direction of a particular coordinate axis is defined as the amount of energy crossing a unit area perpendicular to that axis per unit time. For a sound wave in a fluid, since the pressure has a constant value in any direction at one point, and by the definition of power, the energy flux component in the x_i-direction is given by

$$I_i = pv_i \tag{2.52}$$

where p is the pressure, and v_i is the i-th component of the particle velocity. The instantaneous energy flux is a function of both time and position. For a harmonic motion, the time average of the energy flux is defined by

$$< I_i >= \frac{1}{T}\int_0^T pv_i\, dt \tag{2.53}$$

where T is the period of the motion. If a complex representation is employed and harmonic motion is assumed, the time average energy flux over any period can be expressed as

$$< I_i >= \frac{1}{2}Re(p^* v_i) = \frac{1}{2}Re(pv_i^*) \tag{2.54}$$

where p^* and v^* are the complex conjugates of p and v respectively. Sometimes the complex product also gives the space average in certain directions.

Similarly in a solid, we can obtain the energy flux expression from the definition of the power, but we shall use a different approach by examining the energy balance equation. The law of energy conservation requires that the rate of change of energy in a volume V is equal to the energy crossing the surface S of the volume per unit time, which can be expressed as

$$\frac{\partial}{\partial t}\int_v \mathcal{E}\, dv = -\int_s \vec{I}\, d\hat{s}, \tag{2.55}$$

where $\mathcal{E}$ is the energy density and $\vec{I}$ is the energy flux vector. The energy density of waves is the sum of the kinetic and potential energy densities. As in the definitions used in the study of the mechanics of rigid bodies, the kinetic energy density is given by

$$\mathcal{E}_k = \frac{1}{2}\rho\frac{\partial u_i}{\partial t}\frac{\partial u_i}{\partial t}, \tag{2.56}$$

and the potential energy density is defined by

$$\mathcal{E}_p = \frac{1}{2}t_{ij}\epsilon_{ij}. \tag{2.57}$$

We can replace the surface integral by the volume integral on the right side of equation (2.55), and exchange the order of the time derivative and the integration on the left side of (2.55). Subsequently, after substituting equations (2.56) and (2.57) into equation (2.55) we have

$$\int_v (\rho\frac{\partial^2 u_i}{\partial t^2}\frac{\partial u_i}{\partial t} + \frac{\partial}{\partial t}(\frac{1}{2}t_{ij}\epsilon_{ij}))\, dv = -\int_v \frac{\partial I_i}{\partial x_i}\, dv. \tag{2.58}$$

Using the equation of motion in the first term of the left side of equation (2.58), using equation (2.13) in the second term, rearranging the terms, and using equation (2.13) again, we obtain

$$\int_v \frac{\partial}{\partial x_i}(t_{ij}\frac{\partial u_j}{\partial t})\, dv = -\int_v \frac{\partial I_i}{\partial x_i}\, dv. \tag{2.59}$$

From equation (2.59) we find that the component of the energy flux along the x_i-direction is given by

$$I_i = -t_{ij}\frac{\partial u_j}{\partial t}. \tag{2.60}$$

Equation (2.60) gives the rate of work being done by the force acting on an element of area normal to the x_i-direction. For the complex representation and harmonic motion, the time average energy flux can be expressed as

$$< I_i >= -\frac{1}{2}Re(v_j t_{ij}^*) = -\frac{1}{2}Re(v_j^* t_{ij}), \tag{2.61}$$

where v_j is the particle velocity, and $*$ denotes the complex conjugate. It is not difficult to verify equation (2.61) since the integral of a sum is equal to the sum of the integrals.

Since energy flux is a second order quantity, in general, the superposition principle for the composition of waves is not valid for energy flux. For example, if two waves are propagating in the same space and in the same direction, and the corresponding pressures are p_1 and p_2, and particle velocities v_1 and v_2 respectively, the instantaneous energy flux is defined by equation (2.52) as

$$I = (p_1 + p_2)(v_1 + v_2).$$

For the individual waves, we have

$$I_1 = p_1 v_1, \qquad I_2 = p_2 v_2.$$

In terms of the energy flux for the individual waves the instantaneous energy flux is expressed by

$$I = I_1 + I_2 + p_1 v_2 + p_2 v_1. \tag{2.62}$$

In general the cross terms in (2.62) caused by the interference between the two waves do not vanish, unless some particular relationship between the two waves is satisfied. However when we deal with the total energy of a whole system, the law of energy conservation requires that space average over any surface enclosing the sources of the time average energy flux caused by the interference between different waves must be zero [66]. A simple case is that of the interference between two spherical waves. Let us consider a surface which surrounds two point sources. The integral of the time average energy flux of the wave from one of the sources over the whole surface must be equal to the time average output power from that source. The sum of the two integrals of the time average energy flux of the waves from both sources

excluding the interference terms is the time average output power from the two sources together. At any point on the surface the interference terms do not always vanish, but the spatial average over the surface of the interference terms must vanish if the law of energy conservation is satisfied.

2.3 Boundary Conditions

Since we are interested in the reflection and transmission of waves, there is always at least one boundary involved. A simple case is that of a rigid boundary. This is an idealized model for the interface between one medium and another medium which has a relatively large rigidity. We shall show later that it is a good model for the interface between air and a metal. When a medium has a rigid boundary we assume that there has never been a displacement between the medium and the boundary at any time and anywhere on the boundary. The rigid boundary condition requires no movement at the boundary. That is the displacement component normal to the boundary is zero or the particle velocity normal component is zero. For harmonic motion the displacement and velocity conditions are equivalent. Some people prefer to use the velocity condition , but we shall adopt the displacement condition since we use displacement potential functions and the number of differentiations required to obtain the displacement component is one less than that to obtain the velocity component.

At an interface of two media, we assume that the two media are in close contact and that no medium penetrates into the other medium so we have a clearly defined and smooth boundary. When we consider the boundary conditions, we should remember the important assumption that the deformation caused by the waves is infinitesimal so that the boundary conditions can be imposed on the undisturbed boundary. From the above considerations we immediately have two conditions: the continuity of the displacement components normal to the interface and the continuity of the stress components normal to the interface. An equivalent condition to the continuity of displacement is the continuity of the corresponding velocity.

Until now we have assumed that the fluid which we are interested in is inviscid. This assumption implies that we allow a relative movement parallel to the interface at the interface between two fluids or between a fluid and a solid so that the tangential velocities can be discontinuous over the boundary, and also the shear stress vanishes at a fluid-solid interface. However, we shall bear in mind that this is another approximation. In fact, we know that all real fluids have some viscosity no matter how small.

Thus we shall consider the following three types of boundary conditions:

1) at a rigid boundary, the normal component of the particle displacement vanishes;

2) at an interface between fluid and fluid, the normal component of the particle displacement is continuous and the pressure is continuous;

3) at an interface between fluid and solid, the normal component of the particle displacement is continuous and the pressure in the fluid is equal to the normal stress component in the solid, and the shear stress component vanishes.

In this thesis, we are interested only in continuous, steady state wave fields so that no initial conditions are required.

At infinity the geometrical spreading of a spherical wave implies that the wave field vanishes. A stronger condition was introduced by Sommerfeld. This condition is called the "radiation condition". It specified that no energy may be radiated from infinity into a region containing sources. This implies that there can be no waves propagating inwards from infinity into the region of finite extent under consideration in free field problems; all waves hence must propagate "outwards" from the sources concerned. (see "Methods of mathematical physics" by Courant and Hilbert [48], and "Acoustic and electromagnetic waves" by Jones [50]).

Ultimately, the radiation condition is a consequence of the law of causality which can be stated fully as follows: (i) if there is no cause there is no effect; (ii) the cause must always precede the effect. Thus if there are no sources of waves there are no waves. A wave emitted by any source can be perceived by an observer elsewhere only when the wave reaches the observer: i.e., only

after the lapse of the appropriate finite travel time. Thus in the absence of any reflecting surfaces, the wave must always travel outwards from the source. Waves from sources at infinity can never reach an observer, as it would take them an infinite time to do so. When there is a reflecting surface at any finite distance from the source, the reflected wave must arrive at the observer at a time later than that of the original wave direct from the source. The wave energy density, however, does not satisfy the wave equation, in general, and hence its flux does not necessarily satisfy the "outwards travelling" radiation condition, and in particular may not when the wave field has both directly radiated and reflected components [66].

Instead of using the radiation condition in its basic form, we shall use the following conditions: (1) the sum of the integrals of the time average energy flux of individual waves over a surface which surrounds the sources must be equal to the total output power generated by the sources; (2) the energy flux must decay to zero as the distance away from the sources tends infinity. These conditions are sufficient for the problems and solutions to be considered. For most of our solutions it is difficult to show analytically whether these conditions of energy radiation are satisfied, but the results of some numerical studies will be given.

The boundary conditions which discussed above are very much idealized but have been widely used by many researchers (for example, [11] by Ewing *et al.*, and [51] by Morse and Ingard). Some times the boundary conditions have been expressed in terms of impedance (see [52] by Kinsler *et al.*) but essentially these are the same as the pressure and displacement conditions for elastic wave propagation.

Chapter 3

Computational methods

3.1 Methods of numerical integration

Integral expressions have been used for studies of spherical wave propagation for many decades, but the complicated integral forms make analytical analysis very difficult. Many analytical studies have concentrated on the far field approximation for a single medium with an acoustic impedance boundary. If we consider a more complicated model, for example, two fluid half spaces, analytical analysis of the integral solution can become very difficult indeed. Even in cases where analytic integration is possible, the results may still be very complicated and require approximation before being evaluated numerically. In such cases, direct numerical evaluation of the integrals may provide a better way to solve the problem. Numerical integration is also known as quadrature. The method of numerical integration involves expressing an integral as a linear or nonlinear combination of the values of the integrand. In recent years, with the development of computers, it has become more and more popular. As the need for methods of numerical integration have grown, increasing numbers of commercial computer software packages have appeared on the market. Such standard computer software makes research work easier, because one can concentrate on the essential problem, rather than on developing a numerical technique. Furthermore the standard programs are written by experts who specialise in numerical methods, so these programs are usually more efficient than those which are 'homegrown'. Despite this,

we should understand the principle of the method.

The NAG library is a collection of such standard computer programs and is widely used in the United Kingdom. The NAG library offers a number of routines for numerical evaluation of definite integrals in one or more dimensions. We will consider only the one dimensional case. The routines are designed to suit different forms of integrations; for example, the integrand many have algebraic singularities at certain points, the interval of integration may extend to infinity, etc.. Basic assumptions are that integrands are composed of piecewise analytic functions and that Taylor series or other expansions provide good approximations, at least over small enough intervals.

In the numerical study, the NAG routines D01ajf, D01atf, D01amf, D01ahf, D01baf have been used.

D01ajf is a general purpose routine for numerical integration over a finite interval. It is an adaptive extrapolation routine, which uses the Gauss 10-point and Kronrod 21-point rules. D01ajf does not require particular information about the integrand and can be used when the integrand has singularities of some types.

D01atf is the same as D01ajf except that it requires a subroutine to evaluate the integrand at an array of abscissae.

D01amf calculates an approximation to the integral of a function over an infinite or semi-infinite interval. An adaptive procedure, based on the Gauss 7-point and Kronrod 15-point rules is employed on the transformed integral, in the form

$$\int_a^{\infty} f(x)\,dx = \int_0^1 f(a + \frac{1-t}{t})\frac{1}{t^2}\,dt.$$

D01baf computes an estimate of the definite integral of a function of known analytical form, using a Gauss quadrature formula with a specified number of abscissae. Depending on the type of interval, a subroutine is called. We have used two subroutines. D01baz is for Gauss-Legendre quadrature on a finite interval. D01bay is for Gauss-rational quadrature on a semi-infinite interval and it suits a rational type of decay integrand. The reason that we have chosen D01bay instead of an exponential decay quadrature is because the energy flux is a rational type of decay function as we shall show later.

D01ahf computes a definite integral over a finite range to a specified relative accuracy using the method described by Patterson. This routine is used as a double check or as an alternative when there is a difficulty in using D01ajf or D01atf.

Next we shall describe the theoretical background for the NAG routines which we have chosen. For the methods used in NAG routines, an integral is generally expressed as an approximation in the form of a weighted sum of integrand values,

$$\int_a^b w(x)f(x)\,dx \approx \sum_{i=1}^{N} W_i f(x_i). \qquad (3.1)$$

The points x_i within the interval [a, b] are called the abscissae and the W_i are the weights. The quadrature rule is a particular method used to determine the abscissae and the weights. The integration rules which we have been using are of Gauss type. The theory of integration rules of the Gauss type is related to the theory of orthogonal polynomials.

For a given weight function $w(x) > 0$ it is possible to define a sequence of orthogonal polynomials $p_0(x)$, $p_1(x)$, ..., of integer degree n, which satisfies

$$\int_a^b w(x)p_m(x)p_n(x)\,dx = 0, \qquad m \neq n. \qquad (3.2)$$

A relevant theorem is as follows: let $w(x) > 0$ be a weight function defined on [a, b], and corresponding to orthogonal polynomials $p_n(x)$. If we let the zeros of $p_n(x)$ be the abscissae x_1, x_2, ...,x_n , the weights W_1, W_2,...,W_n can be determined such that formula (3.1) is of degree of precision $2n - 1$. The degree of precision is maximal.

In general the weights and abscissae are obtained for the weight function defined on the interval [-1, 1], and are available in tabular form.

An n-point Gauss rule is one with the weight function $w(x) = 1$, and is also called a Gauss-Legendre rule. This type of rule will be often used in the later calculations.

For a non-polynomial function there is an error involved. Usually, we wish to know not only the value of an integration, but also the possible error involved in its calculation. One of the methods used to estimate the error is to compare the result obtained by using one rule with that obtained by using

another rule of different degree. In this case it is not very economical to use Gauss rules alone since the abscissae of Gauss rules of any order are distinct from those of any other order (except for the mid-point, when the number of points is odd). In order to use all the abscissae in the previous low order formula in the rule of higher order, a new type of formula can be used,

$$\int_a^b f(z)\,dz \approx \sum_{k=1}^{m} a_k f(y_k) + \sum_{k=1}^{n} b_k f(x_k), \tag{3.3}$$

where the y_k are the abscissae of a given m-point rule and where a_k, b_k and x_k can be determined so that the rule is exact for polynomials of the highest possible degree.

This type of rule is due to Kronrod and developed by Patterson. The Kronrod formula is obtained when y_k is determined by a m-point Gauss rule and $n = m + 1$ in formula (3.3). Again from the theory of orthogonal polynomials, it is possible to obtain such a rule which is exact for a degree of precision $3m + 1$. The a_k are different from those determined by the m-point Gauss rule.

Patterson offered a method which allows us to obtain a rule with a large number of abscissae. He starts with the 3-point Gauss rule, and 4 abscissae are added to produce a 7-point formula of degree 11. Then 8 abscissae are added to this formula to produce a 15-point formula of degree 23. The process can be continued for a large number of abscissae. In the program D01ahf, the largest number of abscissae is 255. The effective degree of these n-point formulae is $(3n - 1)/2$.

For a simple numerical integration, like D01baf, a definite integral can be expressed explicitly by its approximation, and a fixed number of abscissae is used. The algorithm proceeds in the same way for each problem and only the number of abscissae is chosen, depending on the complexity of the problem. No estimate is made of the accuracy of the result.

An automatic numerical integration generally involves a complicated logical process aimed at reducing the error and the computation time. The number of abscissae is gradually increased until the estimated error is reduced to a certain level as requested by the user. The basic input information required by an automatic program comprises: (1) the limits of integration, (2)

a routine for computing the integrand, (3) a relative tolerance t_r, and (4) an absolute tolerance t_a.

A simple automatic program may be based on the Kronrod formula or the Patterson formula. A series of rules which uses increasing number of abscissae are successively applied over the whole interval. Complicated automatic programs, like D01ajf, D01atf and D01amf are adaptive routines. This means that the distribution of abscissae is adapted to the shape of the integrand. The interval of an integral is repeatedly divided into a number of sub-intervals and quadrature rules are applied separately to each sub-interval. The position of the integration points of the nth iteration depends on information gathered from iterations, 1,...,n-1, so the sub-division process is carried out in such a way that many points are located in the neighbourhood of difficult spots of the integrand. An automatic integration program with use of some extrapolation technique even allows jump discontinuities and singularities of some types to be integrated.

There are three main elements involved in the process of an adaptive numerical integration. They are as follows:

1. quadrature rules for evaluating the integral over a sub-interval;

2. a method for estimating the local error of the numerical integration over a sub-interval; this local error will provide the information for deciding on the subdivision process;

3. criteria for deciding on the subdivision process and for deciding when to terminate.

The first of these three elements has already been discussed. The second is concerned with the error. There are two types of errors, truncation error (formula error) and computer round-off error. The former arises from the fact that the sum from a quadrature formula is only an approximation to an integral of an arbitrary function. The formula error is the difference between the sum and the exact value of the integral. The computer round-off error is due to the limitation on the accuracy in the computer. For a simple calculation, the round-off error is usually negligible; however, for a complicated numerical integration, the round-off could seriously affect the

result of an integration since a large number of arithmetic operations are involved.

Sometimes the analytical form of the formula error is available, but, practically, different methods are used to determine the formula error. For example, in the NAG routine, D01ahf, the local error over a sub-interval is determined by the difference of the two values obtained from two successive rules. In D01ajf, D01atf and D01amf, the local error on an interval J is determined by

$$E_J = D_{mea} min(1, (200 D_J / Q_{abs})^{3/2}), \tag{3.4}$$

where D_J is the modulus of the difference of a quadrature sum and some integral approximation of lower degree, and where

$$Q_{abs} = \sum W_i |f(x_i)|,$$

$$D_{mea} = \sum W_i |f(x_i) - M|,$$

with

$$M = \frac{1}{length\ of\ J} \sum W_i f(x_i).$$

The formula (3.4) is an empirical one.

The third element in an adaptive routine is the criteria for deciding the subdivision process and when to terminate.

For the programs which we have used, the sub-division process is decided by the local error. The algorithm used by D01ajf, D01atf,and D01amf is described as follows. The first calculation is performed over the whole interval. If the error E_0 calculated for this interval satisfies the equation

$$E_0 < max(t_a, t_r |Q_0|),$$

where Q_0 is the first numerical integration, the value of the numerical integration will be given by Q_0 with estimated error E_0; otherwise the interval is bisected, the integral and error contributions over both halves are calculated, and the total integral and error estimates are accordingly adjusted. If the equation

$$\sum_j E_j < max(t_a, t_r |\sum_j Q_j|) \tag{3.5}$$

is satisfied, computations are terminated with the value of integration $\sum_j Q_j$ and error $\sum_j E_j$. Otherwise, the sub-interval which has a large local error is selected for a further bisection and the sums of the local integration and of the local error are used in criterion (3.5). The procedure is repeated until criterion (3.5) is satisfied.

D01ahf uses an algorithm different from that used by D01ajf, D01atf, D01amf. A series of rules is successively applied over the whole interval. When the difference of two results obtained by two successive rules is less than t_r, the last result is taken as the value of the integral. If all rules have been applied without achieving the required accuracy, the interval is divided into two sub-intervals. The series of rules is then applied to the first sub-interval. If the required accuracy is not obtained, the interval is stored for future examination and the second sub-interval is examined. If the result on this second interval again fails to meet the required accuracy then the sub-interval is further subdivided and the whole process repeated. In contrast to the criterion used by D01ajf, D01atf and D01amf, routine D01ahf requires only the local error satisfying the specified accuracy.

Program D01ahf uses two criteria for abnormal termination: 1. an upper bound for the number of function evaluations has been reached; 2. too many unsuccessful levels of subdivision have been invoked; but programs D01ajf, D01atf and D01amf use different five criteria:

1. round-off error is detected;
2. a too small interval must be subdivided;
3. further calculations are not expected to yield any improvement;
4. an upper bound for subdivisions has been reached;
5. the integral is probably divergent or slowly convergent.

Most of the above criteria are empirical.

To speed up the process of calculation, some extrapolation technique may be used. The ε-algorithm for extrapolation is an often used convergence acceleration technique. It attempts to replace the original sequence by faster converging sequences.

Assume that a sequence s_n converges to the limit s,

$$s = s_n + \sum_{i=1}^{p} a_i q_i^n,$$

with a_i independent of n and

$$|q_p| < \ldots < |q_1| < 1.$$

For a given sequence of real numbers s_0, s_1,..., we can define a triangular table

$$\begin{array}{ccccc}
\varepsilon_{0,0} & & & & \\
\varepsilon_{1,0} & \varepsilon_{0,1} & & & \\
\varepsilon_{2,0} & \varepsilon_{1,1} & \varepsilon_{0,2} & & \\
\ldots & & & & \\
\ldots & & & & \\
\varepsilon_{l,0} & \varepsilon_{l-1,1} & & & \\
\varepsilon_{l+1,0} & & & &
\end{array}$$

by means of the relations

$$\varepsilon_{l,-1} = 0,$$

$$\varepsilon_{l,0} = s_l, \qquad l = 0, 1, \ldots.,$$

$$\varepsilon_{l,j+1} = \varepsilon_{l+1,j-1} + \frac{1}{\varepsilon_{l+1,j} - \varepsilon_{l,j}}.$$

This table has the property

$$\varepsilon_{l,2j} = s_n + o((q_{j+1}^l)).$$

When the value of a numerical integration is considered as a sequence as the number of sub-intervals is increased, a theorem guarantees that this sequence converges to the exact value of the integral as its limit when the number of equal sub-intervals tends to infinity. Therefore the ε-algorithm can be applied to evaluate a numerical integration. It can be shown that $\varepsilon_{i,i}$ converges to s more rapidly than the sequence s_i. A study [53] has shown that the ε-algorithm may also be used even when the sub-intervals are not equal and when integrands have singularities.

3.2 Automatic symbolic manipulation

With modern computers, not only have numerical methods been revived, but automatic symbolic manipulation has also become possible. REDUCE is an example of software that deal with automatic symbolic manipulation. The program utilises a specialised computer language, LISP; however it is not necessary for a user to have any knowledge of LISP.

The program follows the rules of algebraic manipulation and deals only with elementary functions. It does not make any mistakes, but it cannot solve a problem which mathematicians cannot solve.

A reason for using the REDUCE program is to save time and to obtain an accurate result when a large amount of simple manipulation is involved. For example when studying wave transmission through a plate, there are three boundary conditions on the surface of each side of the plate, so there is a total of six conditions determining six equations with six unknowns for given material, geometry and wave parameters. The coefficients of the equations are functions of these parameters. Solving such a system of six equations is not difficult work in principle, but is very lengthy and tedious. With the help of REDUCE, the solution can be obtained accurately and quickly although its expression will take up many pages if printed out.

Using REDUCE to do a manipulation is very similar to what we do by hand. This can be best illustrated by a simple REDUCE program. For a given potential function of a spherical wave, in order to obtain a component of the corresponding time average energy flux, we need to derive the appropriate velocity component of a particle and the pressure by differentiation, and take the complex conjugate of one of them. The component time average energy flux is given by one half of the real part of the product of the complex conjugate of the pressure (say) and the velocity component. The example program is as follows:

```
factor i;
on rat;
let d=sqrt(r* * 2+z * * 2);
let f1=exp(i* (w* ti-k* d))/d;
```

```
let f2=exp(-i* (w* ti-k* d))/d;
let p=-rho* df(f2,t,2);
let vz=df(f1,t,z);
let fluxz=p* vz/2;
end;.
```

This program will produce the z-component of the time average energy flux. Symbol ';' is necessary for completing each statement. In the program there are two potential functions 'f1' and 'f2'; one is the complex conjugate of the other. The space dependence 'd' is given as a function of the coordinates. When executing the program, the substitution will automatically take place. 'df' is a differentiation operator. It will give the derivatives of the first argument in the brackets with respect to the rest of the variables. If there is a number in the brackets, it represents the number of differentiations with respect to the variable which it follows. 'rho' denotes a constant density.

REDUCE can be used in an interactive mode or a batch mode. We use only an interactive mode since we do not have a very large job. We can write a file for a program, like the one given above. After getting into REDUCE, then upon using an 'in' command to load the file, typing 'fluxz;' and finally typing the "return" key, the result will be displayed:

$$\frac{i*w^3*z*rho}{2(r^4+2*r^2*r^2+r^4)}+\frac{SQRT(r^2+z^2)*k*w^3*z*rho}{2(r^4+2*r^2*r^2+r^4)},$$

The real part of this expression is the required result.

REDUCE provides several switches for a user to display results in different forms. In the example program, 'i' was declared as a factor and the 'rat' switch was on so that REDUCE separates the term involving 'i' from others.

The method of displaying a result is important when using REDUCE. It involves choosing variables, declared factors and switches, etc.. A good choice will enable us to express a result in a simple form or in an easily understood form from the physical point of view. For example the coefficients of reflection and transmission are related to wave speeds, wavenumber components, angle of incidence, material constants, etc.. If we are not careful in choosing appropriate variables, the expressions for the coefficients could

include all variables whereas a simple expression would include only some of them.

Most of the analytical results in this thesis have been obtained with use of REDUCE. It has been used in the derivation of integrand coefficients, the series expansion in the proof of (1.1), and so on. To obtain the integration coefficients from boundary conditions, three operators also used are 'sub', 'lcof' and 'det' . The 'sub' operator was used in the following way:

```
let con0(i)=sub(z=0, conz(i));.
```

It makes a substitution $z = 0$ into conz(i) and gives a boundary condition con0(i) at $z = 0$. Unlike 'let', the 'sub' operator is used for a local substitution.

The operator 'lcof' was expressed by

```
let a(i,j)=lcof(con0(i),c(j));.
```

It gives a(i,j) as the coefficient of an unknown c(j) in equation con0(i). This operator enables us to obtain the coefficients of the system equations determined by the boundary conditions.

The system of boundary condition equations can be solved directly by using a 'solve' operator, which is designed to solve simultaneous linear equations. However with a large order system of equations, it will take a very long time. An alternative method has been used as we know that a solution of a system of equations can be expressed by the ratio of two determinants which are determined by the coefficients of the system equations.

The 'det' operator was used together with the 'mat' operator which is in turn used to define a matrix:

```
det mat( matrix1 );
```

where 'matrix1' represents a matrix of coefficient elements. The operators return the determinant expansion of the matrix.

A useful switch is 'fort'. When 'fort' is on, a result will be printed in the

FORTRAN format. The 'out' command allows a result to be directly written into a file. As mentioned earlier, the result for wave transmission in layered media could take up several pages, but with use of the 'out' command and with 'fort' on we can obtain the result written in a file in FORTRAN format for use in the next step of the numerical study. Some results obtained by using REDUCE can be found in Appendixes (B) to (D).

Chapter 4

Plane wave reflection and transmission

A plane wave and a spherical wave are two extreme mathematical models for realistic waves. At a long distance away from a point source, a spherical wave can be treated as a plane wave. Light waves from the sun are a very good example of plane waves as seen by observers on the earth. A plane wave is relatively easy to deal with in mathematical terms and the theory of plane wave propagation is well established. The main object of this thesis is to study spherical wave propagation and one of the interesting features of spherical waves, which we would like to know more about, is how the reflection and transmission of a spherical wave differs from that of a plane wave. In order to make the comparison easy, we shall present the results for plane waves first. Some of the many well known solutions for problems of plane wave propagation can be found in the literature: e.g., the publications by Schoch [16], Ewing, *et al.* [11], Kinsler *et al.* [52], but their results are not always presented in forms which are appropriate for purposes of comparisons with spherical waves. In this chapter, we shall study systematically several cases of plane wave propagation and present the results in forms which can be directly used for comparison with those for spherical waves. Some results for plane waves in multilayered media are less well known. The problems of transmission to be considered are only those in fluids. The transmission of spherical waves in a solid is very complicated and the numerical study will require large computing CPU time. Since we are not particularly interested

in the waves in a solid in this thesis, the transmission of waves in solids will be discussed briefly.

The mathematical model used here is very much idealised and is applied to the continuous, steady state, wave field and the results in some respects may not apply for wave pulses or wave beams, since for the cases of wave pulses or beams, there are some regions in which the medium is not disturbed at some time. Discussions of the reflection and transmission of pulses can be found in [49] and [18]. We shall see that the model for plane waves used in this thesis is not valid at grazing incidence.

4.1 Rigid boundary

The first case that we consider is that of plane waves propagating in a semi-infinite fluid which has a rigid plane boundary. At the boundary, as we have discussed in Chapter 2, the condition is that the component of displacement normal to the boundary is zero. Assuming that the origin is at the boundary, we have the condition

$$w = 0 \qquad \text{at } z = 0. \tag{4.1}$$

We seek a solution in the form

$$\phi = A\ exp(i(\omega t - kx + qz)) + A\ R\ exp(i(\omega t - kx - qz)), \tag{4.2}$$

where ϕ represents the displacement potential and Snell's law that the angle of incidence is equal to the angle of reflection has been assumed. The first term represents an incident wave, in which A is an amplitude constant which is dependent on the strength of the source; the second term corresponds to the reflected wave and R is the reflection coefficient. The reflection coefficient for the pressure is the same as that for the potential function. ω is an angular frequency and k and q are the x and z-components of the wavenumber vector. The angle of incidence can be determined by the two components of the wavenumber as

$$\theta = tan^{-1}(\frac{k}{q}). \tag{4.3}$$

It is easy to verify that equation (4.2) is a solution of the equation of motion if the following relationship is satisfied

$$\kappa^2 = k^2 + q^2 \tag{4.4}$$

where $\kappa = \omega/c$ is the wavenumber, c being the wave speed. On substituting equation (4.2) into the boundary condition, we obtain

$$exp(i(\omega t - kx))(-iq)(R-1) = 0. \tag{4.5}$$

Equation (4.5) gives

$$R = 1. \tag{4.6}$$

For convenience, later we shall assume that the amplitude of the incident wave is unity.

For a plane wave, the time-space average energy flux along the z-axis is defined by

$$< I_z >= \frac{1}{2} Re(p(\frac{\partial w}{\partial t})^*) = \frac{1}{2} Re(p^* \frac{\partial w}{\partial t}), \tag{4.7}$$

where $(\frac{\partial w}{\partial t})^*$ and p^* are the complex conjugates of the z-component of the particle velocity and the pressure respectively.

We use the second of equations (4.7) for the calculation. From equation (4.2), we have

$$p^* = \rho\omega^2 A(exp(-i(\omega t - kx + qz)) + exp(-i(\omega t - kx - qz))) \tag{4.8}$$

and

$$\frac{\partial w}{\partial t} = -q\omega A(exp(i(\omega t - kx + qz)) - exp(i(\omega t - kx - qz))). \tag{4.9}$$

A little complex manipulation yields

$$< I_z >= 0. \tag{4.10}$$

This result means that no time-space average energy crosses any plane surface parallel to the boundary (the plane wave source, strictly, must be assumed to be infinitely distant from the boundary if the boundary is of infinite extent). The average energy flow reflected by the rigid boundary must cancel out that

moving towards the boundary because of the nature of the rigid boundary. As it was pointed out earlier, this mathematical model is invalid at grazing incidence. At grazing incidence, q in (4.2) becomes zero, so the boundary condition (4.1) is no longer applicable.

4.2 Fluid-fluid interface

Let us consider the situation where two fluid media are in a close contact so that the z-components of the displacements and the pressures are equal at the interface. Assuming that the incident wave is in medium 1 and the transmitted wave in medium 2, we have the boundary conditions

$$\left\{ \begin{array}{rcl} w_1 & = & w_2 \\ p_1 & = & p_2 \end{array} \right\} \text{at } z = 0, \tag{4.11}$$

where the subscripts indicate the media concerned.

A solution of the equation of motion can be expressed as

$$\phi_1 = exp(i(\omega t - k_1 x + q_1 z)) + R\ exp(i(\omega t - k_1 x - q_1 z)), \tag{4.12}$$

$$\phi_2 = T\ exp(i(\omega t - k_2 x + q_2 z)), \tag{4.13}$$

provided that

$$\kappa_1^2 = k_1^2 + q_1^2, \qquad \kappa_2^2 = k_2^2 + q_2^2, \tag{4.14}$$

where $\kappa_1 (= \omega/c_1)$ and $\kappa_2 (= \omega/c_2)$ are the wavenumbers for waves in medium 1 and medium 2 respectively. Again Snell's law of equality of the angles of incidence and reflection has been assumed. R is the reflection coefficient, T is the transmission coefficient and we assume that the amplitude of the incident wave is unity. As in the case of the rigid boundary, this solution is not valid at grazing incidence.

The reflection coefficient for the pressure is the same as that for the potential function and the transmission coefficient for the pressure is given by the product of T and the density ratio ρ_2/ρ_1. The reflection and transmission coefficients are determined by the boundary conditions (4.11). On substituting equations (4.12) and (4.13) into the conditions, we have $k_1 = k_2 = k$

(or $sin(\theta_1)/sin(\theta_2) = c_1/c_2$ relating the angle of incidence θ_1 to the angle of refraction θ_2) and

$$q_1 R + q_2 T = q_1, \tag{4.15}$$

$$-\rho_1 R + \rho_2 T = \rho_1. \tag{4.16}$$

For given material constants and angle of incidence, R and T are the unknowns of this system of two equations. Solving this system we obtain

$$R = \frac{\rho_2 q_1 - \rho_1 q_2}{\rho_2 q_1 + \rho_1 q_2}, \tag{4.17}$$

$$T = \frac{2\rho_1 q_1}{\rho_2 q_1 + \rho_1 q_2}. \tag{4.18}$$

The coefficients R and T are independent of the frequency of the wave and are functions of the angle of incidence. This can be seen easily by rewriting the z-component wavenumbers in the forms

$$q_1 = \frac{\omega}{c_1} cos\theta, \qquad q_2 = \frac{\omega}{c_1}\sqrt{\frac{c_1^2}{c_2^2} - sin^2\theta}, \tag{4.19}$$

where θ is the angle of incidence. On substituting equations (4.19) into equations (4.17) and (4.18) we obtain the reflection and transmission coefficients in terms of the angle of incidence and the material constants as

$$R = \frac{\rho_2 cos\theta - \rho_1\sqrt{(c_1^2/c_2^2) - sin^2\theta}}{\rho_2 cos\theta + \rho_1\sqrt{(c_1^2/c_2^2) - sin^2\theta}}, \tag{4.20}$$

$$T = \frac{2\rho_1 cos\theta}{\rho_2 cos\theta + \rho_1\sqrt{(c_1^2/c_2^2) - sin^2\theta}}. \tag{4.21}$$

When the wave speed in medium 1 is less than the speed in medium 2, $c_1 < c_2$, and the angle of incidence is greater than the critical angle which is defined by

$$\theta_c = sin^{-1}\frac{c_1}{c_2}. \tag{4.22}$$

the incident x-component wavenumber k is greater than κ_2. In this case, q_2 becomes imaginary and the reflection and transmission coefficients become complex quantities. This means that the reflected and transmitted waves are no longer in phase with the incident wave. The reflected wave (in (4.12))

would be still a travelling wave, but *no body wave* would be stimulated in medium 2. There would be only a surface wave propagating with a phase speed which is same as that of the incident wave or the reflected wave along the interface. The amplitude of this surface wave (4.13) decays exponentially in the z-direction. There may be also a corresponding surface wave in medium 1.

If the wave speed in medium 2 is less than the speed in medium 1, i.e. $c_1 > c_2$, then the reflection and transmission coefficients are always real quantities; in other words the reflected and transmitted wave are always in phase with the incident wave.

Let us examine the energy transmission in these two cases. From the definition, we know that the energy flux in the z-direction is the product of the pressure and the z-component particle velocity. Since the boundary conditions require the continuity of pressure and the continuity of particle displacement in the z-direction, which gives the velocity continuity, the conservation of energy flux in the z-direction is automatically satisfied. By using equations (4.12) and (4.13), it is easy to obtain the time-space average energy flux components, which are

$$< I_{z1} >= -\frac{1}{2} Re((R-1)(R^*+1)\rho_1 q_1 \omega^3) \tag{4.23}$$

in medium 1 and

$$< I_{z2} >= \frac{1}{2} Re(T^* T \rho_2 q_2 \omega^3) \quad \text{at } z = 0. \tag{4.24}$$

R^* and T^* are the conjugates of the reflection and transmission coefficients respectively.

When $c_1 > c_2$ or when $c_1 < c_2$ and $\theta < \theta_c$ there is always time-space average energy transmitted into the second medium. By using equations (4.17) and (4.18) we can obtain the transmitted energy flux which is

$$< I_{z1} >=< I_{z2} >= \frac{4(\rho_1 q_1)^2 \rho_2 q_2 \omega^3}{(\rho_1 q_2 + \rho_2 q_1)^2} \quad \text{at } z = 0. \tag{4.25}$$

Complete transmission occurs at the angle of incidence at which the reflection coefficient is zero. This angle for complete transmission can be determined

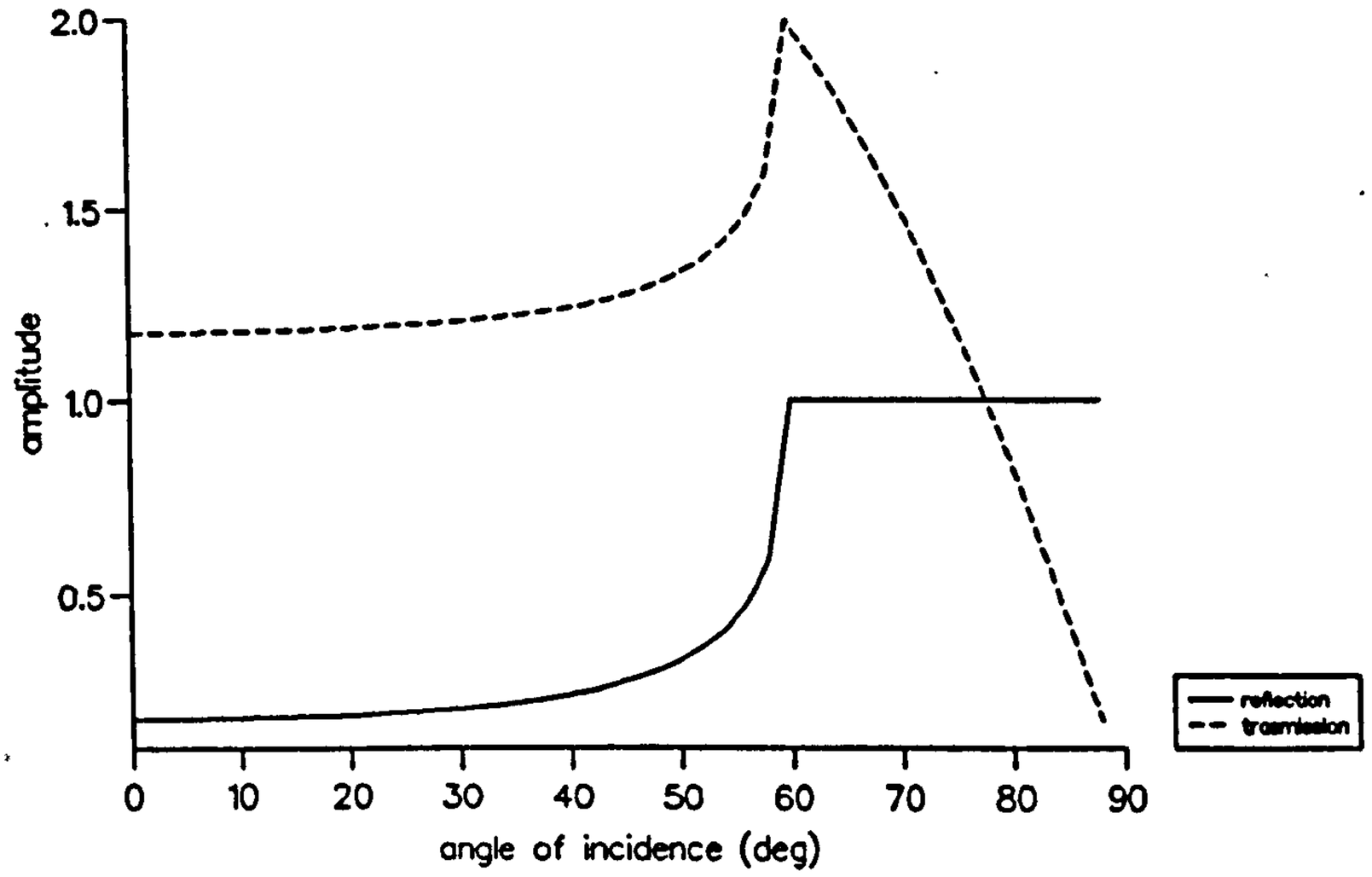

Figure 4.1 Amplitudes of the reflection and transmission coefficients for the pressure of a plane wave at a kerosene-water interface. The incident wave is in the kerosene.

from the formula

$$sin\theta_t = \sqrt{\frac{\rho_2^2 c_2^2 - \rho_1^2 c_1^2}{\rho_2^2 c_2^2 - \rho_1^2 c_2^2}}. \tag{4.26}$$

When $c_1 < c_2$ and and the angle of incidence is greater than the critical angle, i.e., $k > \kappa_2$, then, by examining equation (4.24), we find that the product of the conjugates is purely real and q_2 is purely imaginary so that $< I_{z2} >$ becomes zero. In this case, the phenomenon of total reflection takes place: i.e., no time-space average energy crosses the interface. In this case by using real variables, it is easy to find that the instantaneous energy flux associated with the interference between the incident wave and the reflected wave is not zero throughout a time period, and that the instantaneous transmitted energy flux is attenuated exponentially in the negative z-direction.

For a given angle of incidence and material constants, we can calculate the modulus and the phase of the reflection and transmission coefficients. Numerical examples are shown for the kerosene-water combination in Figures (4.1) and (4.2), and for the water-kerosene combination in Figure (4.3). The incident wave is in the first medium of these combinations.

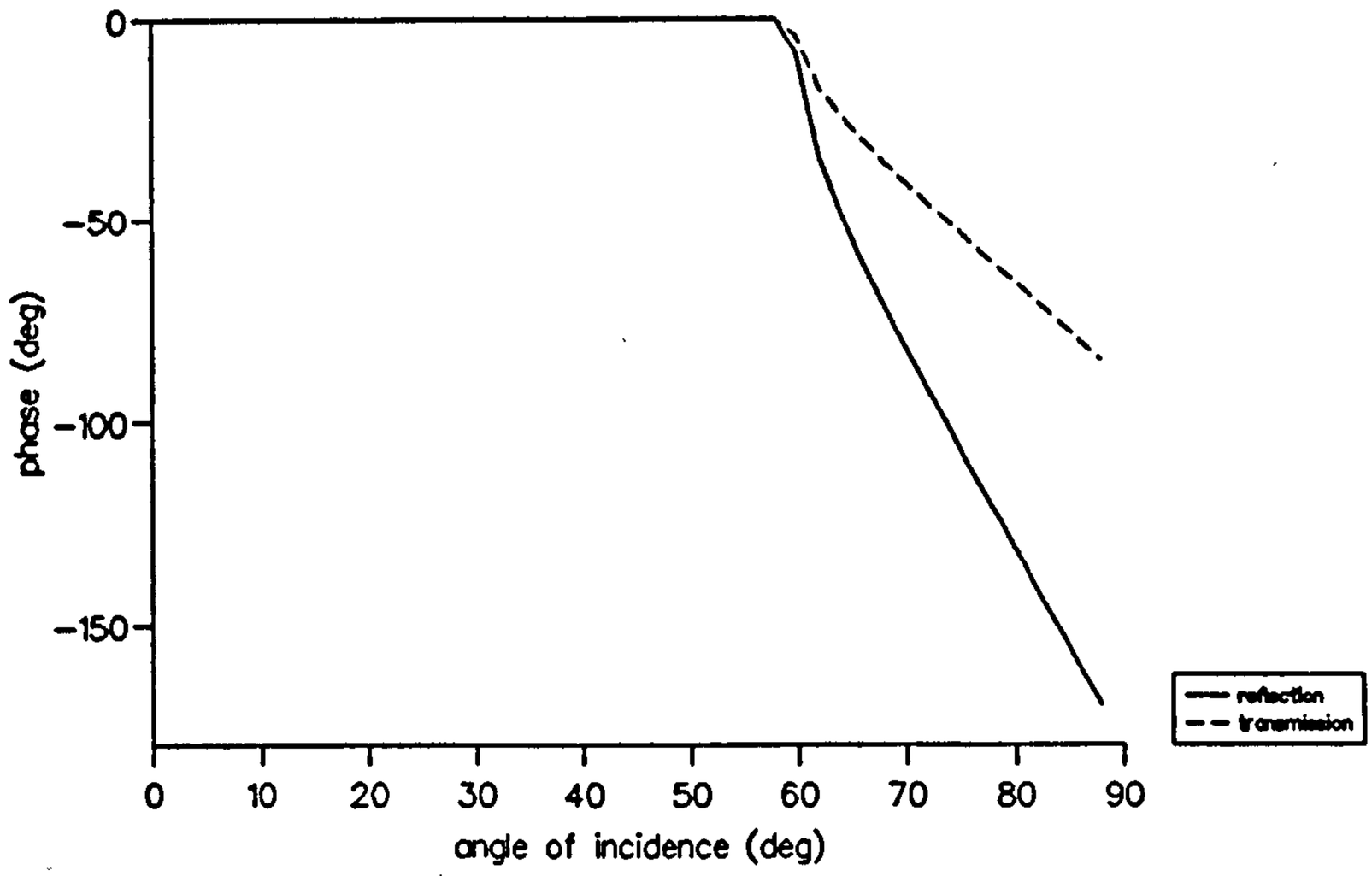

Figure 4.2 Phases of the reflection and transmission coefficients (relative to the phase of the incident wave) for the pressure of a plane wave at a kerosene-water interface. The incident wave is in the kerosene.

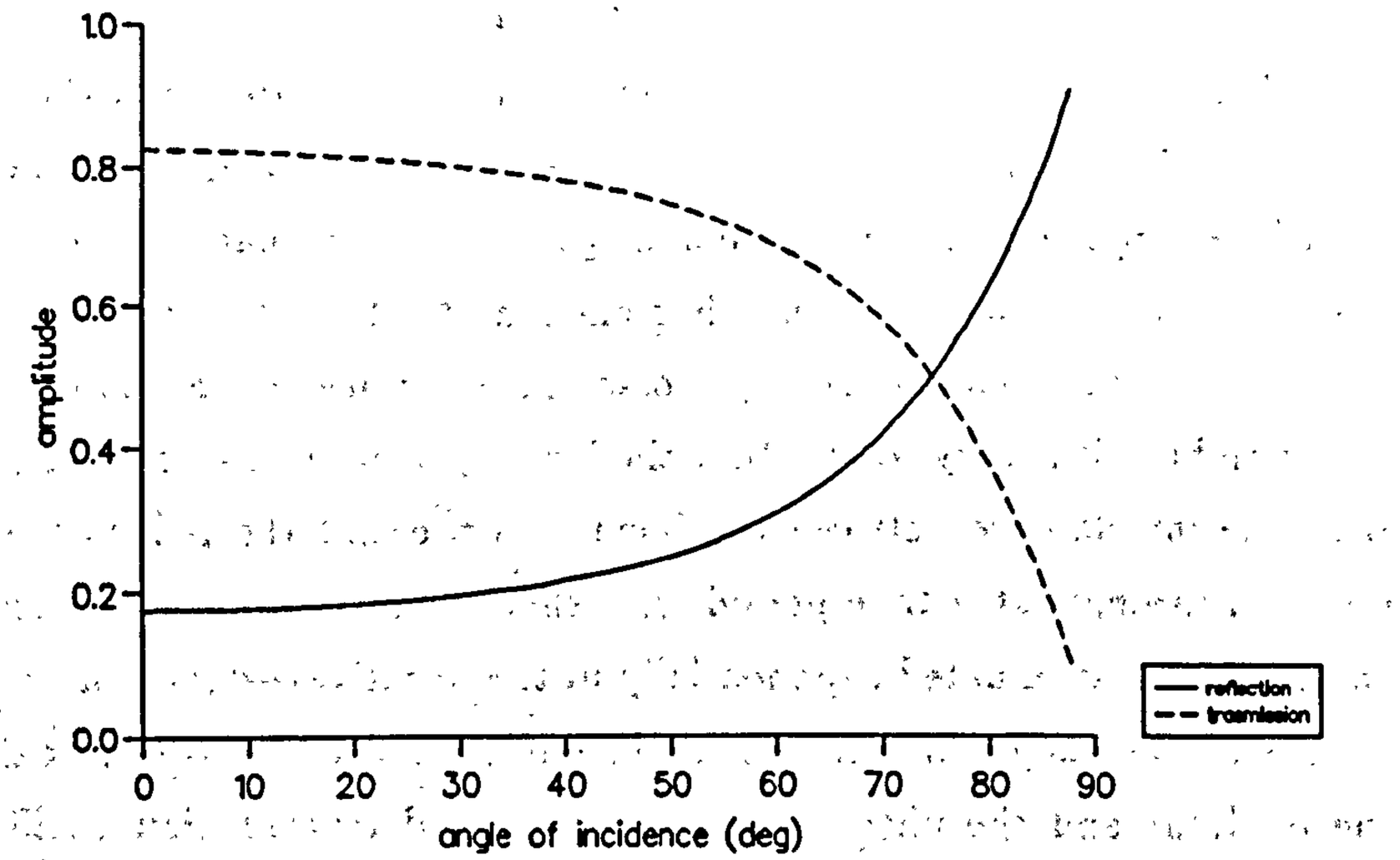

Figure 4.3 Amplitudes of the reflection and transmission coefficients for the pressure of a plane wave for pressure at a water-kerosene interface. The incident wave is in the water.

The material constants used for the calculation are given in Table (4.1) [61]. In Figures (4.1) and (4.2), the critical angle for this combination is given by

$$\theta_c = 59.8°. \tag{4.27}$$

We can see that for angles of incidence less than the critical angle, the amplitudes for both the reflected and transmitted waves are increasing with the angle of incidence and change rapidly when approaching θ_c; beyond θ_c the amplitude for the reflected wave becomes unity and the amplitude for the transmitted wave decreases to zero. Figure (4.2) shows that the phases of both the reflected and transmitted waves (relative to that of the incident wave) remain unchanged at zero degrees before the critical angle, and that the phases of the reflected and transmitted waves change after the critical angle. The phases of the reflected and transmitted waves decrease monotonically as the angle of incidence increases beyond the critical angle. The negative phases would imply that the phases of the reflected and transmitted waves are behind that of the incident waves.

Since for the water-kerosene combination $c_1 > c_2$ and the phases of the reflection and transmission coefficients are zero, we show only the amplitudes. In Figure (4.3) it can be seen that the reflection coefficient is monotonically increasing and the transmission coefficient is monotonically decreasing. Both of the coefficients are less than one.

medium	density	longitudinal wave speed	transverse wave speed
air	1	331	
kerosene	810	1324	
water	1000	1531	
aluminium	2700	6420	3040
brass	8600	4700	2110
steel	7800	5960	3235
lead	11400	2160	700

Table 4.1 Material constants (SI units)

4.3 Fluid-solid interface

When a wave impinges at an angle upon an interface between a fluid and a solid both longitudinal and transverse waves can be stimulated in the solid. At normal incidence only the longitudinal wave is stimulated. At an interface between an inviscid fluid and a solid, the boundary conditions require that the normal component of the displacement is continuous, the pressure in the fluid is equal to the normal stress in the solid and the shear stress in the solid vanishes since an inviscid fluid cannot sustain a shear stress. We call the fluid medium 1 and the solid medium 2. The boundary conditions for a plane interface are

$$\left\{\begin{array}{rcl} w_1 & = & w_2 \\ -p_1 & = & t_{zz} \\ t_{zr} & = & 0 \end{array}\right\} \text{at } z = 0. \tag{4.28}$$

We consider a solution in the following form, with Snell's laws being assumed:

$$\phi_1 = exp(i(\omega t - kx + q_1 z)) + R\ exp(i(\omega t - kx - q_1 z)), \tag{4.29}$$

$$\phi_2 = T_l\ exp(i(\omega t - kx + q_l z)), \tag{4.30}$$

$$\psi_2 = T_t\ exp(i(\omega t - kx + q_t z)). \tag{4.31}$$

Here

$$q_1 = \sqrt{\kappa_1^2 - k^2}, \quad q_l = \sqrt{\kappa_l^2 - k^2}, \quad q_t = \sqrt{\kappa_t^2 - k^2}. \tag{4.32}$$

R is the reflection coefficient and T_l and T_t are the transmission coefficients for the longitudinal and transverse waves respectively. They are determined by a system of three equations obtained from the boundary condition, and are given by

$$R = \frac{\rho_2 q_1((2k^2 - \kappa_t^2)^2 - 4q_l q_t k^2) - (\kappa_t^4 q_l \rho_1)}{\rho_2 q_1((2k^2 - \kappa_t^2)^2 - 4q_l q_t k^2) + (\kappa_t^4 q_l \rho_1)}, \tag{4.33}$$

$$T_l = \frac{2(2k^2 - \kappa_t^2) q_1 \kappa_t^2 \rho_1}{\rho_2 q_1((2k^2 - \kappa_t^2)^2 - 4q_l q_t k^2) - (\kappa_t^4 q_l)\rho_1}, \tag{4.34}$$

$$T_t = -\frac{4k q_1 q_l \kappa_t^2 \rho_1}{\rho_2 q_1((2k^2 - \kappa_t^2)^2 - 4q_l q_t k^2) - (\kappa_t^4 q_l \rho_1)}. \tag{4.35}$$

As in the case of two fluid half spaces, the reflection and transmission coefficients (4.33), (4.34) and (4.35) are independent of frequency. Solutions (4.29) to (4.31) are not valid at grazing incidence. At normal incidence, the x-component wavenumber k is zero, and from equation (4.35) we can see that the transverse wave cannot be stimulated.

The time-space average energy flux in the z-direction in the fluid is given by the second of equations (4.7) as,

$$< I_{z1} >= \frac{1}{2} Re(p^* \frac{\partial w}{\partial t}), \tag{4.36}$$

and the time-space average energy flux in the z-direction in the solid is defined by

$$< I_{z2} >= \frac{1}{2} Re(t^*_{zz} \frac{\partial w_2}{\partial t} + t^*_{zr} \frac{\partial u_2}{\partial t}). \tag{4.37}$$

From the boundary conditions (4.28), it is easy to see that conservation of the energy flux in the z-direction across the boundary is satisfied, since the displacement condition is equivalent to the velocity condition for a harmonic wave.

When the wavenumber κ_1 for a wave in the fluid is greater than κ_t and the angle of incidence is greater than the critical angle defined by

$$\theta_c = sin^{-1} \frac{c_1}{c_t} \tag{4.38}$$

the phenomenon of total reflection may be expected to occur. In this case, both q_l and q_t are imaginary and the z-component of the time-space average energy flux in medium 1 is given by

$$< I_{z1} >= \frac{1}{2} Re((R+1)(R^*-1) q_1 \rho_1 \omega^3). \tag{4.39}$$

The expression for R is not very simple, but we do not need to substitute the analytical expression for R into equation (4.39) to analyze the energy flux. Examining the reflection coefficient in equation (4.33), we find that when the angle of incidence is greater than the critical angle, the numerator is the conjugate of the denominator, and a little complex analysis shows that $(R+1)(R^*-1)$ is purely imaginary, so for $k > \kappa_t$, $< I_{z1} >$ is zero.

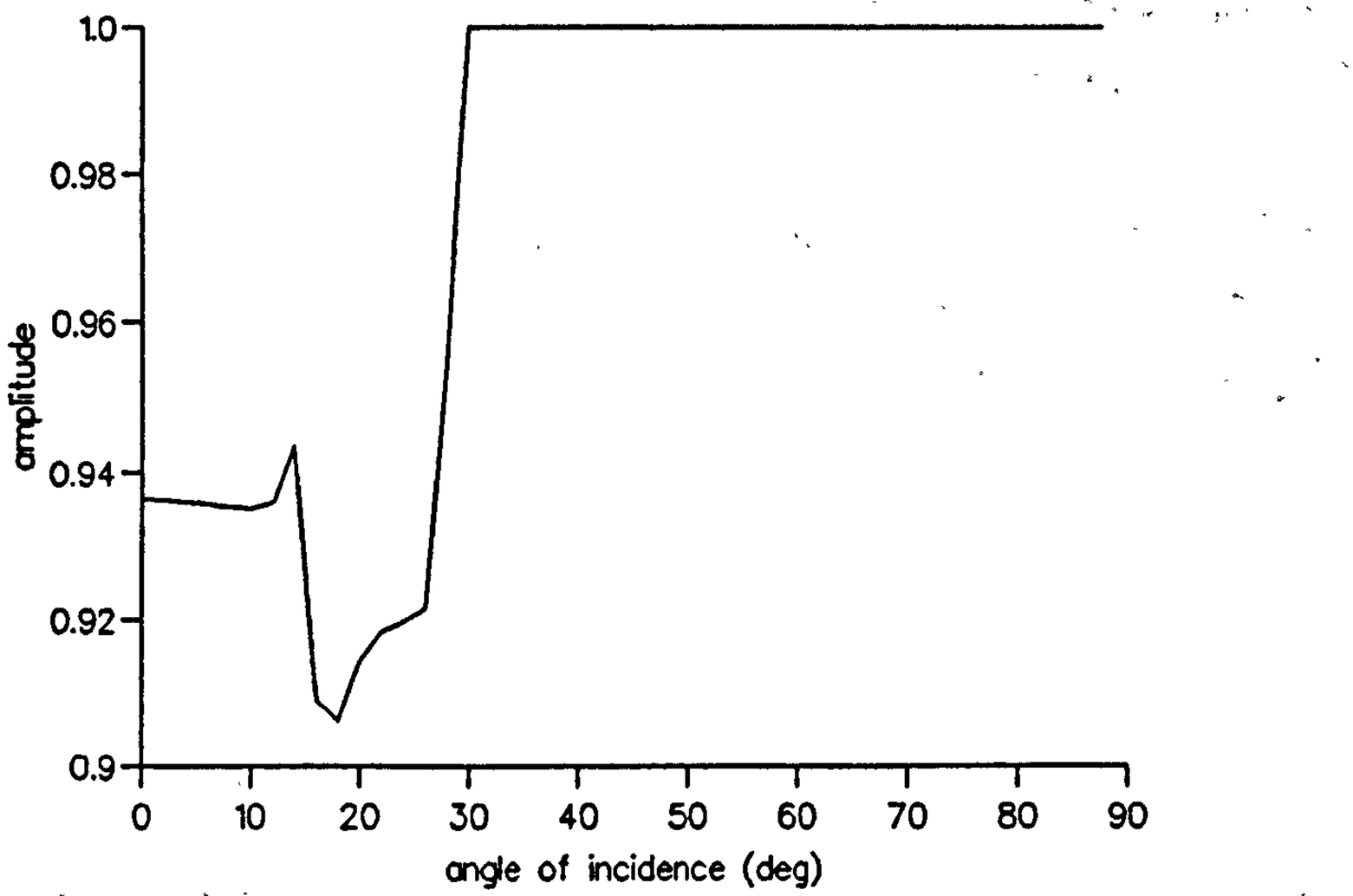

Figure 4.4 Amplitudes of the reflection coefficient for the pressure of a plane wave at a water-steel interface. The incident wave is in the water.

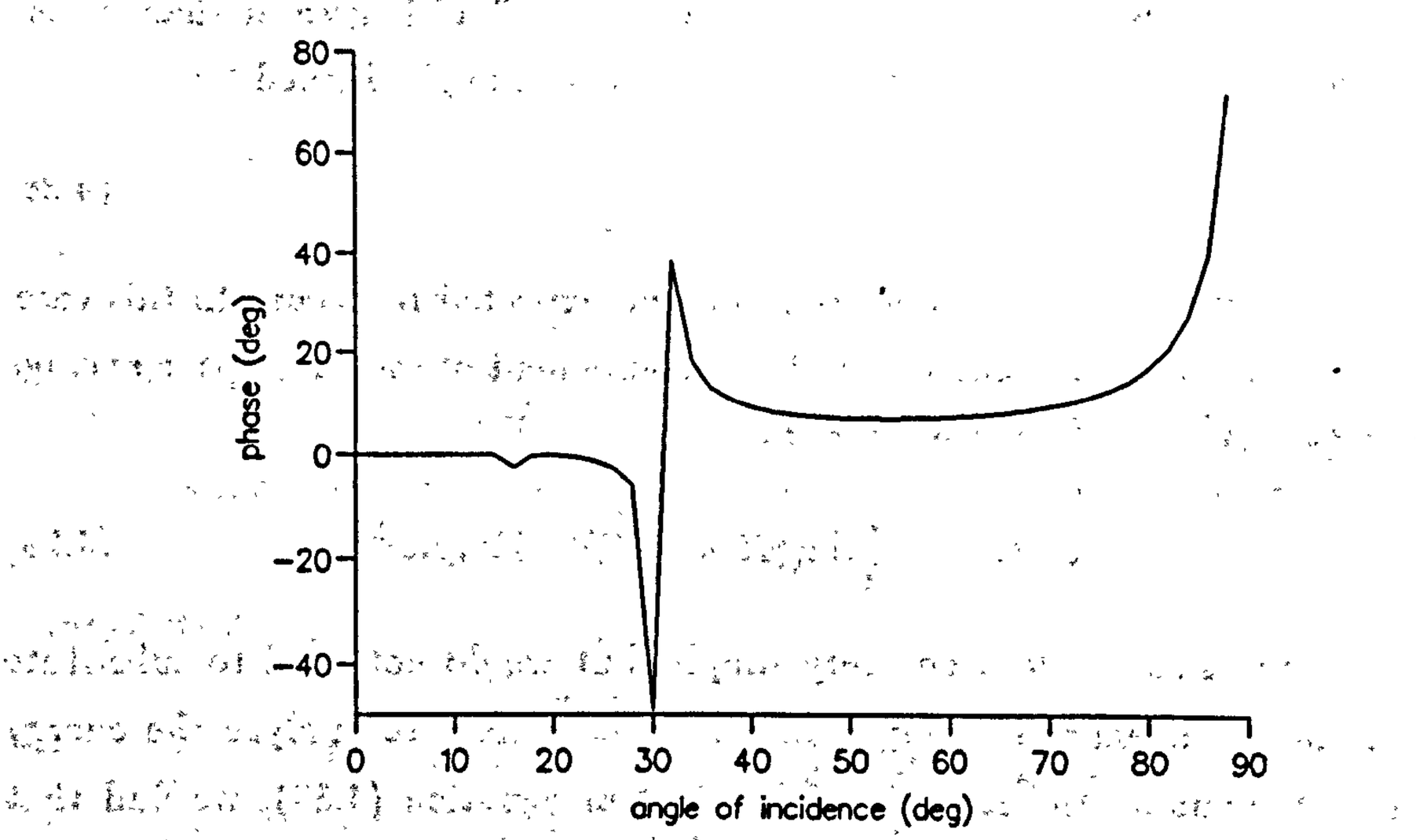

Figure 4.5 Phases of the reflection coefficient for the pressure, relative to that of the incident wave, for a plane incident wave at a water-steel interface. The incident wave is in the water.

The reflection coefficient has calculated for the water-steel combination. The modulus and the phase are given in Figures (4.4) and (4.5). The critical angle for this combination is

$$\theta_c = 28.2^\circ. \tag{4.40}$$

It can be seen that the amplitude is always less than one for the angles of incidence less than the critical angle, and that the amplitude becomes unity for angles of incidence grater than or equal to the critical angle. In contrast to the case of fluid-fluid combination, the phase remains at zero degrees until the angle of incidence is about 14°, but thereafter decreases until the critical angle is reached.

4.4 Fluid-solid-fluid

We consider a solid plate in a fluid. The solution to this problem can be extended to the situation where fluids on the two sides of the plate are different. The boundary conditions at an interface are the same as we described in the last section. We have two interfaces so there are six conditions. The boundary conditions are given by

$$\left\{ \begin{array}{rcl} w_1 & = & w_2 \\ -p_1 & = & t_{zz} \\ t_{zr} & = & 0 \end{array} \right\} \text{at } z = 0, \tag{4.41}$$

$$\left\{ \begin{array}{rcl} w_3 & = & w_2 \\ -p_3 & = & t_{zz} \\ t_{zr} & = & 0 \end{array} \right\} \text{at } z = -l \tag{4.42}$$

where l is the thickness of the plate. We consider a solution in the following form for the z-component wavenumber of the incident wave being greater than zero, again assuming Snell's laws:

$$\phi_1 = exp(i(\omega t - kx + q_1 z)) + R\ exp(i(\omega t - kx - q_1 z)), \tag{4.43}$$

$$\phi_2 = C_a\ exp(i(\omega t - kx + q_l z)) + C_b\ exp(i(\omega t - kx - q_l z)), \tag{4.44}$$

$$\psi_2 = C_c\ exp(i(\omega t - kx + q_t z)) + C_d\ exp(i(\omega t - kx - q_t z)), \tag{4.45}$$

$$\phi_3 = T\ exp(i(\omega t - kx + q_3 z)). \tag{4.46}$$

Here q_1, q_l and q_t are given by equations (4.32); R is the reflection coefficient at the first fluid-solid interface and T is the transmission coefficients at the second solid-fluid interface; C_a, C_b, C_c and C_d are complex amplitude coefficients for the waves in the solid. The coefficients are determined by the system of six equations from the boundary conditions. If written down explicitly, the expressions of those coefficients will take up several pages so we shall not give them here. The reflection and transmission coefficients are shown in Appendix (B). Since the solution satisfies the boundary conditions at the two interfaces this guarantees the continuity of the energy flux in the z-direction.

The reflection and transmission coefficients are frequency dependent. This is due to the finite thickness of the plate. The frequency dependence of the reflection and transmission coefficients may be easily seen by considering a simple case of normal incidence.

When medium 1 is the same as medium 3, and in the case of normal incidence where $k = 0$, the reflection and transmission coefficients reduce to

$$R = \frac{-(exp(2id\kappa_l) - 1)(\kappa_l^2\rho_1^2 - \kappa_1^2\rho_2^2)}{exp(2id\kappa_l)(\kappa_l\rho_1 + \kappa_1\rho_2)^2 - (\kappa_l\rho_1 - \kappa_1\rho_2)^2} \tag{4.47}$$

$$T = \frac{4exp(2id\kappa_l)exp(2id\kappa_1)\kappa_l\rho_1\kappa_1}{exp(2id\kappa_l)(\kappa_l\rho_1 + \kappa_1\rho_2)^2 - (\kappa_l\rho_1 - \kappa_1\rho_2)^2} \tag{4.48}$$

It is easy to verify that equation (4.47) is the same as the reflection coefficient given in the book by Kinsler *et.al.* [52]. When the thickness of the plate is very small compared with the wavelength of the longitudinal wave, we have the relation $d\kappa_l << 1$. In this case from equation (4.47) we can see that the reflection coefficient is very small, and the transmission coefficient is close to one. This result is independent of the material combination.

A simple transmission situation also occurs when the frequency and the thickness of the plate satisfy the relation

$$d\kappa_l = n\pi, n = 1, 2, 3...; \tag{4.49}$$

i.e., the thickness of the plate is an integer number of half-wavelengths for the longitudinal wave. The reflection and transmission coefficients for different

material combinations have been calculated by using equations (4.47) and (4.48), and are shown in Table (4.2) since we intend to check the result obtained by Piquette [46]. It can be seen that at low frequencies, i.e, for large wavelengths, the metal plates have very small reflection coefficients which increase as the frequency increases.

medium	aluminium	brass	steel	lead
reflection (modulus)				
1000 Hz	0.05840	0.1799	0.1653	0.2402
5000 Hz	0.2806	0.6752	0.6430	0.7771
transmission (modulus)				
1000 Hz	0.9981	0.9833	0.9864	0.9706
5000 Hz	0.9594	0.7384	0.7662	0.6292

Table 4.2 Reflection and transmission coefficients of a plane wave. In the case of a metal plate in water, the thickness of the plate l=0.01m.

We can calculate the reflection and transmission coefficients as a function of angle to obtain some idea how the waves behave with change in the angle of incidence. We are particularly interested in the reflection and transmission in the fluid so the calculated values for R and T have been obtained and are shown in Figures (4.6) to (4.9) for the cases of the water-steel-water combination and the water-aluminium-water combination at 5000 Hz. The incident wave is in the water in both cases.

We find that two sets of curves for the water-aluminium-water combination and for the water-steel-water combination have similar features, except for differences in values. It can be seen that the amplitude and the phase of the reflection coefficients (Figures (4.6) and (4.7)) change smoothly with increasing angle of incidence until certain angles near grazing incidence are reached, and then the gradients of the curves have sudden changes. The curves in Figures (4.6) and (4.7) have little bumps at 15-20 degrees which correspond to the critical angles for the longitudinal waves in the solids. (The data for the phase curve of the steel in (4.6) change very slightly so when plotting out, the curve does not appear to have the bump.)

It is interesting to see that in Figures (4.8) and (4.9) the amplitude and phase of the transmission coefficients oscillate around constant values with

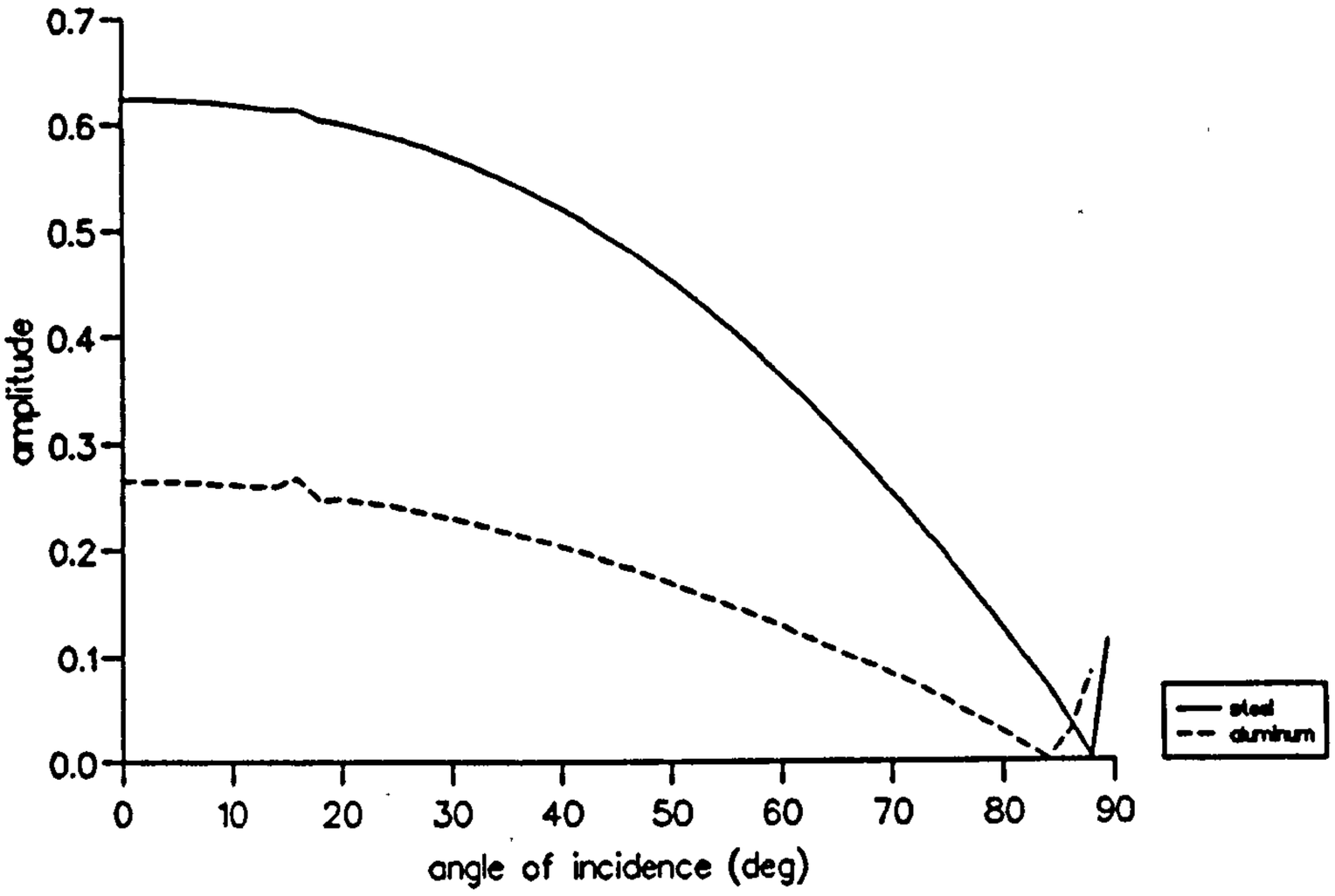

Figure 4.6 Amplitude of the reflection coefficient for the pressure of a plane wave in the case of water-solid-water combination.

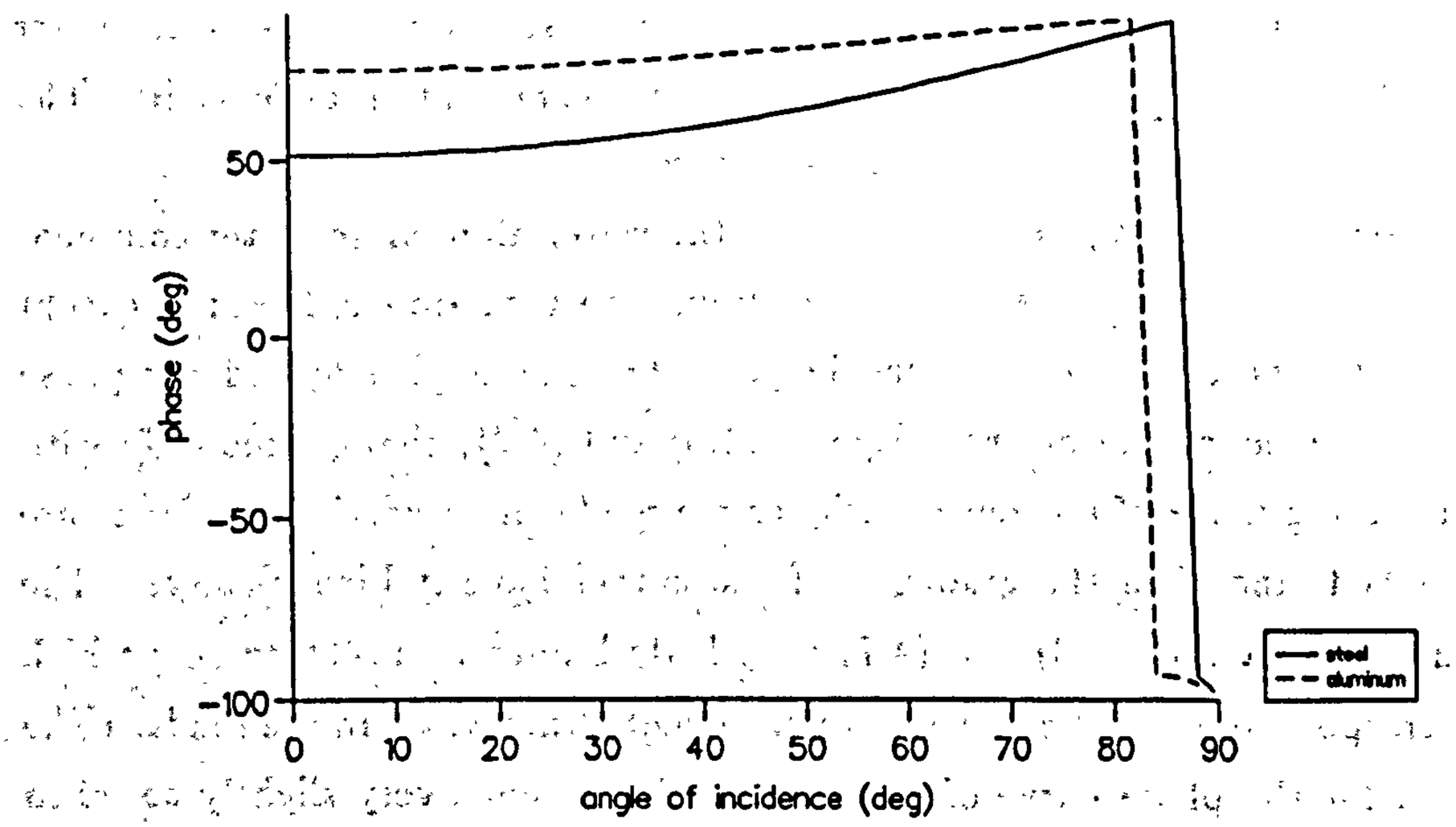

Figure 4.7 Phase of the reflection coefficient for the pressure of a plane wave in the case of water-solid-water combination.

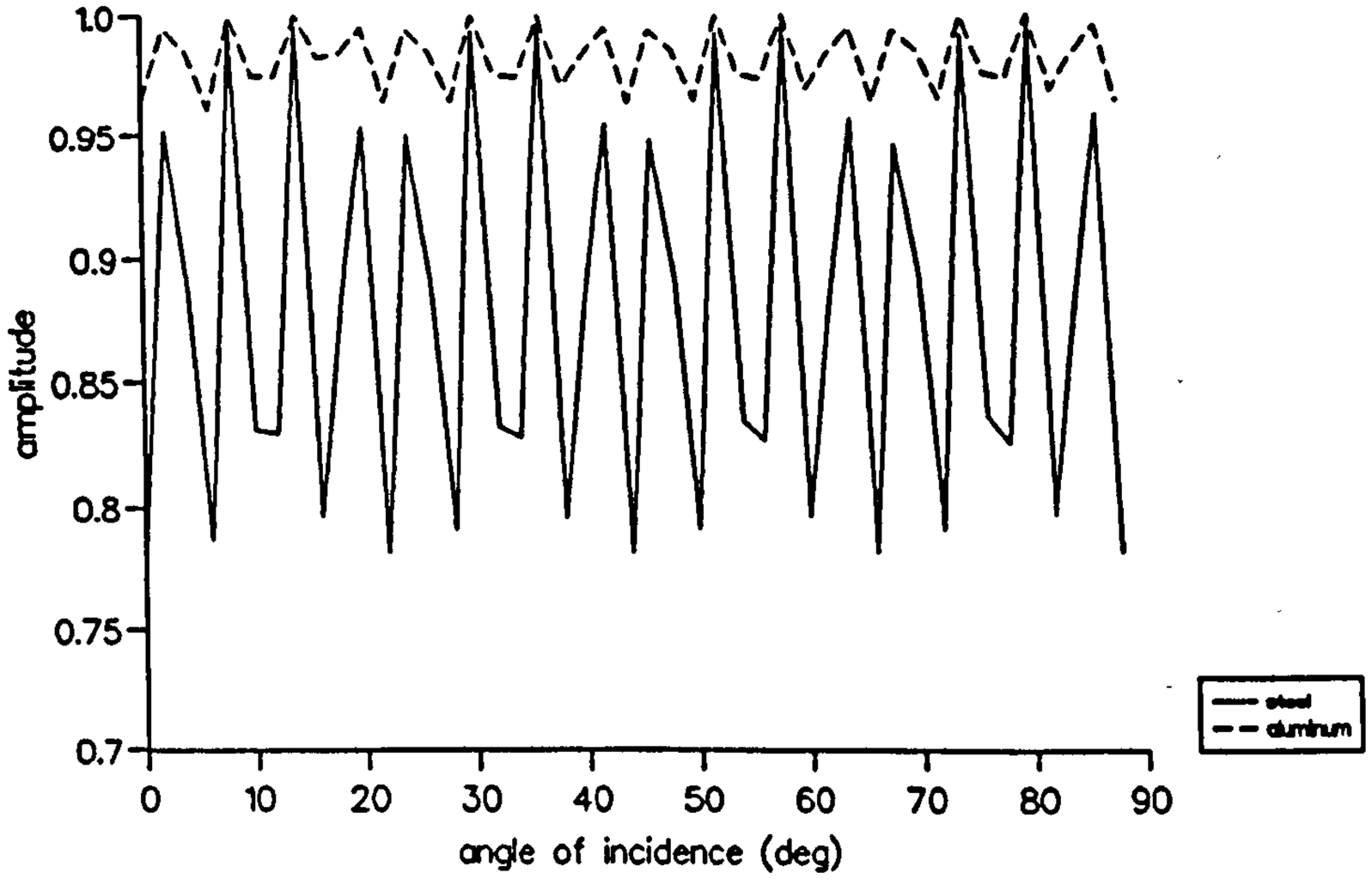

Figure 4.8 Amplitude of the transmission coefficient for the pressure of a plane wave in the case of water-solid-water combination.

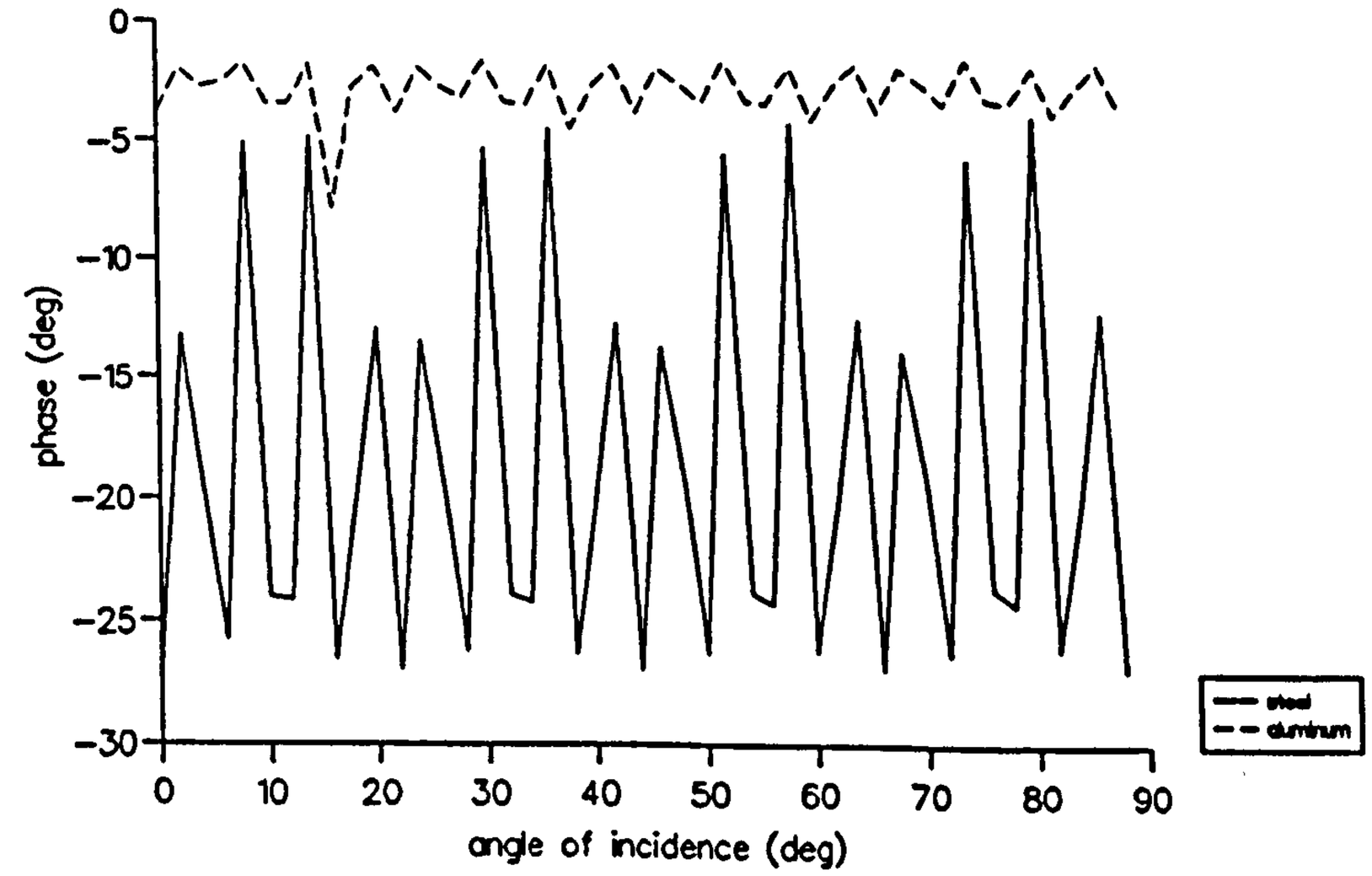

Figure 4.9 Phase of the transmission coefficient for the pressure of a plane wave in the case of water-solid-water combination.

variation of angle of incidence. At the interface between medium 2 and medium 3, there are two different types of incident waves (longitudinal and transverse waves) in the solid; the oscillation of the transmission coefficient is probably due to the interference between the longitudinal and transverse waves. The curves for the reflection coefficient in Figures (4.6) and (4.7) are not oscillatory, this may be because when the reflection of the longitudinal and transverse waves at the interface between medium 2 and medium 3 reaches the interface between medium 2 and medium 1, the interference effects, from the reflected longitudinal and transverse waves and the direct longitudinal and transverse waves generated by the wave incident in medium 1, would be cancelled out at that interface.

Chapter 5

Spherical waves in infinite space

5.1 Integral representations for spherical waves

The investigation of spherical wave propagation is based on the integral relationship

$$\frac{exp(-ik\sqrt{r^2+z^2})}{\sqrt{r^2+z^2}} = \int_0^\infty \frac{J_0(r\xi)exp(-|z|\sqrt{\xi^2-k^2})\xi}{\sqrt{\xi^2-k^2}}\, d\xi. \qquad (5.1)$$

It is easy to show that these expressions, on both the left and right sides, are solutions of the wave equation.

As we mentioned earlier, when the integral in formula (5.1) has been used recently for numerical studies of spherical wave propagation in elastic media (e.g., [44], [46]) some unexpected results have been reported. For example, Piquette [46] has predicted numerically the so-called 'overpressure phenomenon', whereby the reflected wave amplitude exceeds the incident wave amplitude under certain conditions, but his results have not been verified either by experiments or by other independent methods. In such a situation, it is natural for a researcher to check carefully the methods being used, not only the method used to produce the results but also the fundamental theoretical method. Although the integral in formula (5.1) has been used for study of spherical waves for decades, it seems possible that as was mentioned in the introduction there may be some ambiguities in its mathematical foundations. Therefore before we carry out any further study, we shall examine the integral in (5.1) closely.

5.1.1 A brief history of the classical integral

The earliest derivation of the formula (5.1) was given by Lamb [1]. He started from a solution of wave equation in the form of integral in (5.1), and used three arguments to assert that equation (5.1) is true. The first argument was involved in the derivation of the equation

$$\frac{exp(-ikz)}{z} = \int_0^\infty \frac{exp(-z\sqrt{\xi^2 - k^2})\xi}{\sqrt{\xi^2 - k^2}}\, d\xi. \tag{5.2}$$

The second argument due to Weber [54] is that the mean value of a solution of the scalar Helmholtz equation, taken over the surface of a sphere of radius $R = \sqrt{r^2 + z^2}$ not enclosing any singularities, is equal to

$$\frac{sin(kR)}{kR}\phi_0,$$

where ϕ_0 is the value at the centre. The third argument, due to Thomson and Tait [2], is that in any case of symmetry round an axis, if the potential is constant through a certain finite distance, however short, along the axis, it is constant throughout the whole space that can be reached from this portion of the axis, without crossing any of the masses.

Lamb's derivation is very simple, but it is not easy to understand the connections between these arguments and Lamb's derivation. An alternative derivation which is often found in textbooks (see [4], [5] and [11]) is due to Sommerfeld [3]. It should be noticed that Sommerfeld's derivation was for the complex conjugate of equation (5.1) in the book "Electromagnetic theory" [4] and this has been used also by Stratton [5], but later when Ewing, Jardetzky and Press quoted Sommerfeld's derivation in the book 'Elastic waves in layered media' [11] they used a different sign in their expressions without accounting for the change.

By using a cylindrical coordinate system, Sommerfeld derived the two-dimensional formula in the coordinate plane $z = 0$

$$\frac{exp(ikr)}{r} = \int_0^\infty \frac{J_0(r\xi)\xi}{\sqrt{\xi^2 - k^2}}\, d\xi \tag{5.3}$$

(with ξ (or λ in [4]) being defined as a real and positive variable), so that, when the z dependence is added, the three-dimensional wave equation is satisfied (i.e. the expression would become one for $exp(ik\sqrt{r^2 + z^2}/\sqrt{r^2 + z^2})$. He

pointed out that the fact that the integral in the three-dimensional formula (5.1) coincides with the integral in the two-dimensional formula (5.3) for z=0 ensures that it also gives the correct representation of $exp(ik\sqrt{r^2+z^2})/\sqrt{r^2+z^2}$ for $z \neq 0$. The argument behind this statement would be the uniqueness theorem for the solution, since the integral in the three-dimensional formula (5.1) satisfies the governing differential equation and the condition at $z = 0$.

Both of the studies by Lamb and Sommerfeld of formula (5.1) might have been inspired by the Sonine and Gegenbauer type integrals [57]. The Sonine and Gegenbauer type integrals involve infinite integrals of the products of two Bessel functions of forms similar to the integral in (5.1). A discussion of the Sonine and Gegenbauer type integrals can be found in the book 'Theory of Bessel functions' by Watson [57]. In this book, formula (5.1) and its complex conjugate are given as a particular case of the discontinuous integrals of Sonine and Gegenbauer; formula (5.1) is not given in the original works by Sonine [58] or Gegenbauer [59]. Watson did not explain how formula (5.1) was derived. Following Sonine's method, an attempt has been made to derive formula (5.1) and it was found that the derivation was possible only if some conditions on integrals of exponential functions could be ignored. In other words we failed to obtain formula (5.1) by using a method similar to Sonine's on a rigorous and understandable basis, and regarding the integration to be strictly along the real axis. A detailed discussion of this attempt is given in Appendix (A).

Another possible method for the proof of formula (5.1) is that of power series expansion, but we have not found any study using this method in the literature. The method of power series expansion can only be applied to a convergent integral. Since we are not able to find any discussion of the convergence of the integral in (5.1), before using the method of power series expansion to prove (5.1), we have to show that the integral is convergent.

Watson in his book considered the integral in formula (5.1) as a contour integration to avoid the singularity at $\xi = k$, however he did not define the integration path clearly. Although Stratton also assumed that integration variable ξ (or λ in [5]) can be any complex value, Sommerfeld [4], as remarked

earlier, did not do so explicitly. In fact he specified the range of his integration variable as $0 \leq \xi < \infty$. On the other hand Ewing, *et al.*, [11] did not specify the nature of the integration variable. This suggests that there is lack of clarity in published derivations of Lamb/sommerfeld's formula. It is possible that the complex conjugate of (5.1), presented by Sommerfeld, Watson and others may be regarded as a contour integral over complex variables, but the path of integration must be specified because of the singularity in the integrand. It appears from the literature that so far no one has clearly defined the path of integration when interpreting the complex conjugate of (5.1) as a contour integral. We shall show that, when the coordinates r and z are *real* variables, the wavenumber k and the integration variable ξ are *real* and positive, the integral is convergent at the singularity and formula (5.1) is valid only when the argument of the exponential on the right side of (5.1) is negative. The condition on the wavenumber k meets the requirement for the investigation of spherical wave propagation in a medium which is not energy absorbing.

5.1.2 Convergence of the integral and a new representation

First we rewrite the improper integral in (5.1) as

$$\frac{e^{-ikd}}{d} = lim_{a\to\infty} lim_{b\to 0}\left(\int_0^{k-b} \frac{J_0(r\xi)e^{-|z|q}\xi}{q}\, d\xi + \int_{k+b}^{a} \frac{J_0(r\xi)e^{-|z|q}\xi}{q}\, d\xi\right), \quad (5.4)$$

where $d = \sqrt{r^2+z^2}$ and $q = \sqrt{\xi^2-k^2}$. We can eliminate the singularity by substituting $\xi = \sqrt{k^2+x^2}$ into equation (5.4). Then we have

$$\frac{e^{-idk}}{d} = lim_{a\to\infty} lim_{b\to 0} \left(\int_{ik}^{\sqrt{b^2-2kb}} J_0(r\sqrt{k^2+x^2})e^{-|z|x}\, dx + \int_{\sqrt{b^2+2kb}}^{\sqrt{a^2-k^2}} J_0(r\sqrt{k^2+x^2})e^{-|z|x}\, dx\right). \quad (5.5)$$

It is easy to see that when b tends to zero, the limit $\sqrt{b^2-2kb}$ and the limit $\sqrt{b^2+2kb}$ both become zero so we have

$$\frac{e^{-ikd}}{d} = lim_{a\to\infty} \left(\int_{ik}^{0} J_0(r\sqrt{k^2+x^2})e^{-|z|x}\, dx -\right.$$

$$+ \int_0^{\sqrt{a^2-k^2}} J_0(r\sqrt{k^2+x^2})e^{-|z|x}\,dx) \qquad (5.6)$$

The first integral is independent of the parameter a, and it is convergent over the finite range. Let us look at the second one. When a tends to infinity, $\sqrt{a^2-k^2} \to \infty$. By the Dirichlet test theorem, the second integral of equation (5.6) is convergent when the parameter a tends to infinity, because $\int_0^b J_0(r\sqrt{k^2+x^2})\,dx$ is a bounded function for all $b \geq 0$, $exp(-|z|x)$ vanishes as x tends to infinity, and the integral of the derivative of $exp(-|z|x)$ with respect to x over an infinite range is absolutely convergent. Hence we have shown that the integral on the right side of equation (5.1) is convergent and we also obtain a new expression for a spherical wave which avoids the singularity in the classical representation. When written in a compact form, equation (5.6) becomes

$$\frac{exp(-ikd)}{d} = \int_{ik}^{\infty} J_0(r\sqrt{k^2+x^2})exp(-|z|x)\,dx. \qquad (5.7)$$

The integration path is taken from $x = ik$ to $x = i0$ along an imaginary axis and from $x = 0$ to $x = \infty$ along a real axis.

5.1.3 A proof of the new integral

The integral in (5.1) has been shown to be convergent, but it is difficult to prove formula (5.1) by direct expansion. Since we have also shown that the integral in (5.1) is equivalent to (5.7) we can use formula (5.7) instead. First we separate the real and imaginary parts which are written as

$$\frac{cos(k\sqrt{r^2+z^2})}{\sqrt{r^2+z^2}} = \int_0^k -J_0(r\sqrt{k^2-y^2})sin(|z|y)\,dy$$

$$+ \int_0^{\infty} J_0(r\sqrt{k^2+x^2})exp(-|z|x)\,dx, \qquad (5.8)$$

$$\frac{sin(k\sqrt{r^2+z^2})}{\sqrt{r^2+z^2}} = \int_0^k J_0(r\sqrt{k^2-y^2})cos(|z|y)\,dy, \qquad (5.9)$$

where we have converted the integrations on the imaginary axis to the real axis by the substitution $x = iy$.

Let us consider (5.9) first, expanding $sin(k\sqrt{r^2+z^2})$ in power series in its argument this gives

$$\frac{sin(k\sqrt{r^2+z^2})}{\sqrt{r^2+z^2})} = k - \frac{k^3(r^2+z^2)}{3!} + \frac{k^5(r^2+z^2)^2}{5!} - \frac{k^7(r^2+z^2)^3}{7!} + ..., \quad (5.10)$$

where $-\infty < k\sqrt{r^2+z^2} < \infty$.

By expanding $J_0(r\sqrt{k^2-y^2})$ and $cos(|z|y)$ in their arguments respectively, the integrand can be written as

$$J_0(r\sqrt{k^2-y^2})cos(|z|y) = 1 - \frac{r^2(k^2-y^2)}{2^2} - \frac{(yz)^2}{2!} + \frac{(rzy)^2(k^2-y^2)}{2^2\cdot 2!}$$
$$+\frac{r^4(k^2-y^2)^2}{2^2\cdot 4^2} + \frac{(yz)^4}{4!} - \frac{r^6(k^2-y^2)^3}{2^2\cdot 4^2\cdot 6^2} - \frac{(yz)^6}{6!}$$
$$- \frac{r^2z^4y^4(k^2-y^2)}{2^2\cdot 4!} - \frac{r^4z^2y^2(k^2-y^2)^2}{4^2\cdot 2^2\cdot 2!} + ... \quad (5.11)$$

for $-\infty < r\sqrt{k^2-y^2} < \infty$ and $-\infty < |z|y < \infty$, where we have assumed that the product of the two convergent series is also convergent [56]. Integrating the right side of equation (5.11) term by term, and rearranging the terms gives the required result

$$\int_0^k J_0(r\sqrt{k^2-y^2})cos(|z|y)\,dy$$
$$= k - \frac{k^3(r^2+z^2)}{3!} + \frac{k^5(r^2+z^2)^2}{5!} - \frac{k^7(r^2+z^2)^3}{7!} + ... \quad (5.12)$$

It is little more complicated to prove equation (5.8). First we rewrite the expression on the left side of (5.8) as

$$\frac{cos(k\sqrt{r^2+z^2})}{z\sqrt{(r^2/z^2)+1}}. \quad (5.13)$$

Expanding the numerator in its argument and expanding $1/(z\sqrt{(r^2/z^2)+1})$ in r^2/z^2 for $z > r$, we have the product

$$\frac{cos(k\sqrt{r^2+z^2})}{z\sqrt{(r^2/z^2)+1}} = \sum_{n=0}^{\infty}\sum_{m=1}^{\infty}(-1)^{n+m}\frac{r^{2n}z^{2m-1}k^{2n+2m}}{p_e(2)^2(2m-1)!)}\left(\frac{1}{2n+2m}\binom{n}{1}\right.$$
$$\left. - \frac{1}{2n+2m-2}\binom{n}{2} + \frac{1}{(2n+2m-4)}\binom{n}{3} - ...\right)$$

$$+\sum_{n=0}^{\infty}\sum_{m=0}^{\infty}(-1)^n\frac{r^{2n}z^{-2m-1}k^{2(n-m)}}{(2n-2m)!}(\frac{p_o(2n-1)}{p_e(2n)}\binom{n}{1}$$

$$-\frac{p_o(2n-3)}{p_e(2n-2)}\binom{n}{2}+\frac{p_o(2n-5)}{p_e(2n-4)}\binom{n}{3}-...), \tag{5.14}$$

where

$$p_e(2n)=2n\cdot(2n-2)\cdot(2n-4)...,$$

$$p_o(2n-1)=(2n-1)\cdot(2n-3)\cdot(2n-5)....$$

Next we consider the integrand in the first integral on the right side of (5.8). Upon expanding $J_0(r\sqrt{k^2-y^2})$ and $sin(|z|y)$ in their arguments, respectively, the product, the integrand, becomes

$$J_0(r\sqrt{k^2-y^2})sin(|z|y)=\sum_{n=0}^{\infty}\sum_{m=0}^{\infty}\frac{r^{2n}|z|^{2m+1}}{p_e(2n)^2(2m+1)!}y^{2m+1}(k^2-y^2)^n. \tag{5.15}$$

Performing integration term by term on the series in (5.15) gives

$$\int_0^k -J_0(r\sqrt{k^2-y^2})sin(|z|y)\,dy$$

$$=\sum_{n=0}^{\infty}\sum_{m=1}^{\infty}(-1)^{n+m}\frac{r^{2n}z^{2m-1}k^{2n+2m}}{p_e(2)^2(2m-1)!)}(\frac{1}{2n+2m}\binom{n}{1}$$

$$-\frac{1}{2n+2m-2}\binom{n}{2}+\frac{1}{(2n+2m-4)}\binom{n}{3}-...). \tag{5.16}$$

For the integrand of the second integral in (5.8), we expand only the Bessel function in a power series in its argument, so

$$J_0(r\sqrt{k^2+x^2})exp(-|z|x)$$

$$=exp(-|z|x)(1-\frac{r^2(k^2-x^2)}{p_o(2)^2}+\frac{r^4(k^2-x^2)^2}{p_o(4)^2}-...). \tag{5.17}$$

Integrating the series from 0 to b and then letting b tend to infinity, and rearranging terms, we obtain

$$\int_0^{\infty} J_0(r\sqrt{k^2+x^2})exp(-|z|x)\,dx$$

$$=\sum_{n=0}^{\infty}\sum_{m=0}^{\infty}(-1)^n\frac{r^{2n}z^{-2m-1}k^{2(n-m)}}{(2n-2m)!}(\frac{p_o(2n-1)}{p_e(2n)}\binom{n}{1}-\frac{p_o(2n-3)}{p_e(2n-2)}\binom{n}{2}+...). \tag{5.18}$$

Comparing the sum of the series in equations (5.16) and (5.18) with the series in (5.14) proves the formula (5.8) for $z > r$.

The formula (5.8) is valid for any r and z, since the integrals in equation (5.8) satisfy the reduced wave equation (omitting the time dependence) and certain boundary conditions, for example at the surface $z = 2r$. From the above proof we can see that for a real positive k the formula (5.1) is valid only when the argument of the exponential function on the left side has a minus sign.

We could avoid using the theory of differential equations if we could show that

$$\int_k^0 J_0(r\sqrt{k^2-y^2})sin(|z|y)\,dy + \int_0^\infty J_0(r\sqrt{k^2+x^2})exp(-|z|x)\,dx$$

$$= \int_k^0 J_0(z\sqrt{k^2-y^2})sin(|r|y)\,dy + \int_0^\infty J_0(z\sqrt{k^2+x^2})exp(-|r|x)\,dx. \quad (5.19)$$

We have attempted to prove equation (5.19), but have failed to do so.

5.1.4 Numerical test of the integrals

Numerical integration using the integral in (5.7) should give more accurate results than that using the integral in equation (5.1), since the singularity is eliminated.

However, from a table of integrals [62], we have found another formula for the conjugate of the functional expression. This is

$$\frac{exp(ik\sqrt{r^2+z^2})}{\sqrt{r^2+z^2}} = i\int_0^\infty H_0^{(1)}(z\sqrt{k^2-x^2})cos(rx)\,dx \quad (5.20)$$

where $H_0^{(1)}(z\sqrt{k^2-x^2})$ is a Hankel function of the first kind. The integral in (5.20) also has a singularity at $x = k$. The complex conjugate of the representation in (5.20) may be used also for comparison with the classical integral.

By use of the computer software, NAG library, we can evaluate these integrals for given constants. The NAG library offers several integration routines. We can test the routines by using Lamb's representation (5.1), the

new representation (5.7) and representation (5.20). The results of comparison with the functional expression will also show us how good each of the representations are for the purposes of numerical integration. For the test we have used two recommended and reliable programs which will often be used later. D01ajf was used for the finite interval, from 0 to k and D01amf for the infinite interval from k to infinity. Routine D01ahf will be used later for a particular case, so an example is also given. The calculation uses double precision. The relative accuracy is specified as 10^{-4} and the absolute accuracy is 0.0. The calculations were obtained for given dimensionless kr and kz. In a typical case of frequency 1000 Hz and wave speed $c = 331\text{m/s}$, $kr = 3000$ and $kz = 20$ correspond to $r \sim 150\text{m}$ and $z \sim 1\text{m}$ respectively.

Comparisons of the integrations with the functional expression for $r < z$ and $r > z$ are shown in Table (5.1). Note that the results are given for the modulus of the real and imaginary components; the sign of the calculations has been omitted, but, for example, the complex conjugate of the results from (5.20) has been calculated. The functional expression that has been used corresponds to the left side of equation (5.1). The calculations for the real component involve an infinite integration range so they are less accurate than the calculations for the imaginary component (see equation (5.6)). For the small values of kr and kz, comparison of results for the imaginary component (the second column) shows that the integrations for equations (5.7) and (5.20) have similar accuracy and give much better results than those for equation (5.1). For the small values of kr and kz, comparison of the real components shows that the result from the integral in equation (5.20) is better than that from the integral in (5.1), and the result from the integral in equation (5.7) is better than those of both equations (5.1) and (5.20). As the value of kr increases, the accuracy of the numerical integration using (5.7), particularly for the real component, reduces. Indeed the accuracy of computations by (5.7) and (5.20) for the real component is less than that from (5.1) at $kr = 1000$. This is because for large values of kr the Bessel function oscillates rapidly. Nevertheless, the imaginary components continue to be computed more accurately by (5.7) and (5.20).

$kr = 1, kz = 2$	modulus of real part	modulus of imaginary part
functional	5.240153942228524	6.678872052315230
integration (5.1)	5.240153325900175	6.678873336210182
integration (5.7)	5.240153942092239	6.678872052315229
integration (5.20)	5.240154235716217	6.678872052315230
(5.20) with D01ahf	5.240121699482819	6.678871631622314
$kr = 2, kz = 1$		
functional	5.240153942228524	6.678872052315230
integration (5.1)	5.240153725243341	6.678872384175797
integration (5.7)	5.240153948170988	6.678872052315230
integration (5.20)	5.240153067361828	6.678872052315230
(5.20) with D01ahf	5.240168762583650	6.678871631622314
$kr = 1000, kz = 20$		
functional	0.007343092434411	0.017500518592507
integration (5.1)	0.007343098284159	0.017500538149762
integration (5.7)	0.007343423361133	0.017500518592507
integration (5.20)	0.007343027431859	0.017500518592508
(5.20) with D01ahf	0.007343027373487	0.017500517889857
$kr = 2000, kz = 20$		
functional	0.004351225772965	0.008434512931526
integration (5.1)	0.004351233768200	0.008434512224196
integration (5.7)	0.004351229113076	0.008434512931526
integration (5.20)	0.004351217913059	0.008434512931526
(5.20) with D01ahf	0.004351217400386	0.008434512624567
$kr = 3000, kz = 20$		
functional	0.006252146147347	0.000972552714254
integration (5.1)	0.006252097091458	0.000972553516250 3
integration (5.7)	0.006252111504118	0.000972552714257
integration (5.20)	0.006252144476359	0.000972552714244
(5.20) with D01ahf	0.006252144467865	0.000976058479864 1

Table 5.1 Comparison of numerical integrations with the functional expression.

The results of (5.20) with D01ahf were obtained by using the integral in (5.20) and D01ahf was used on the sub-interval, $(0, k)$, and D01amf on (k, ∞). The results are less accurate than calculations using D01ajf for small values of kr and kz, but the accuracy of the results is stable for both large and small values of kr and kz, and meets the required accuracy. The integration with the Hankel function, (5.20), uses slightly more CPU time. The accuracy of the numerical integrations for any of the three expressions can be improved at the cost of more CPU time.

The test in Table (5.1) is given for several values of kr and kz to see what accuracy of numerical integrations can be achieved by using NAG routines and how different they are for various forms of integrals; however it cannot guarantee that the programs will work for all values of kr and kz, since the quadrature rules are only approximations. (An example of such failure by using the Gauss-Kronrod program is illustrated by Squire [47].) A test for wider range of r is included indirectly in the next test.

5.2 Energy of a spherical wave

Energy transport is an important feature of wave propagation. A good theory of wave propagation must satisfy the law of energy conservation. Spherical wave propagation in an infinite space is a simple case where we can study the energy aspect analytically. Later when checking solutions for energy conservation, we shall integrate the energy flux over an infinite range, with the energy flux being determined by a product of two integrals. To obtain an idea of the accuracy for such complicated numerical integrations we shall use the spherical wave in infinite space as a test case.

The law of energy conservation requires that the time average total energy per unit time crossing a surface which surrounds a point source must be equal to the output power generated by the source. By using this law, the total output power generated by a point source can be evaluated easily in a spherical coordinate system.

Let us consider a surface of a sphere with the centre at a point source.

The energy flux is in the radial direction and of the same magnitude at all points on the surface because of the spherical symmetry, so the time average power crossing the surface, $\dot{E}$, is given by the product of the time average energy flux and the area of the surface. This result is expressed by

$$\dot{E} = 2|A|^2 \pi \rho \omega^3 k, \tag{5.21}$$

where A is the possibly complex amplitude constant and $|A|^2 = AA^*$. The above result will be often used later when we test solutions for energy conservation.

For most practical problems we do not have such spherical symmetry, but axial symmetry is common. In a cylindrical coordinate system, for the problem of spherical wave propagation in an infinite space, a convenient way to examine the energy transport is to replace the spherical surface by two parallel infinite extended plane surfaces normal to the z-axis with a source located on this axis half way between the two surfaces. We are going to show that the time average of the energy carried by a spherical wave crossing a plane surface of infinite extent, per unit time, is equal to half of the total time average power generated from the point source. Let us consider a cylindrical coordinate system. The plane surface is $z = h(> 0)$ with the point source at the origin. The time average power crossing the surface is given by

$$\dot{E}_z = \int_0^\infty \frac{1}{2} Re(p^*(r,t) v_z(r,t))\, 2\pi r dr \tag{5.22}$$

where $p^*(r,t)$ is the complex conjugate of the pressure, and $v_z(r,t)$ is the particle velocity.

The spherical wave displacement potential is

$$\phi = \frac{A \exp(i(\omega t - k\sqrt{z^2 + r^2}))}{\sqrt{z^2 + r^2}}, \tag{5.23}$$

where A is an amplitude constant. The time average energy flux crossing the surface can then be expressed as

$$\begin{aligned} \dot{E}_z &= \int_0^\infty \rho \omega^2 Re(\phi^* \frac{\partial^2 \phi}{\partial z \partial t})|_{z=h}\, \pi r dr \\ &= \int_0^\infty \frac{\pi A^2 \rho \omega^3 k r h}{(h^2 + r^2)^{3/2}}\, dr. \end{aligned} \tag{5.24}$$

From the last expression in (5.24) it can be seen that when either h or r tends to infinity, the energy flux becomes zero. On using b for the upper limit, the integration with respect to r gives

$$\dot{E}_z = lim_{b\to\infty} - \frac{|A|^2\rho\pi\omega^3 k(h\sqrt{h^2+b^2} - h^2 - b^2)}{(h^2+b^2)}$$
$$= |A|^2\pi\rho\omega^3 k. \qquad (5.25)$$

$\pi|A|^2\rho\omega^3 k$ is half of the time average power generated by the point source. It is obvious that the time average power crossing a surface, at $z = -h$, say, on the other side of the point source will be another half of the total power.

Using the algebraic expression of the energy flux, and from the law of energy conservation, we have shown that the power output of a point source is given by $2|A|^2\pi\rho\omega^3 k$. From this result and formula (5.1), we can derive a rather surprisingly simple result. Using the integral expression (5.1) to express the potential (5.23) we have

$$\phi = A\int_0^\infty \frac{J_0(r\xi)exp(-|z|\sqrt{\xi^2-k^2})\xi}{\sqrt{\xi^2-k^2}}\, d\xi exp(i\omega t). \qquad (5.26)$$

The z-component of the particle velocity is given by

$$v_z = \frac{\partial^2\phi}{\partial z\partial t} = -Ai\omega\int_0^\infty J_0(r\xi)exp(-|z|q)\xi exp(i\omega t)\, d\xi \qquad (5.27)$$

By applying this result and the complex conjugate of (5.26) to equation (5.24), after transforming the complex conjugate of (5.26) into the form of (5.7), and using the result (5.25), we obtain, at $z = h(>0)$,

$$Re(\int_0^\infty(\int_{ik}^\infty J_0(r\eta)exp(-h\xi)\, d\xi)^* i\int_0^\infty J_0(r\xi)exp(-hq)\xi\, d\xi)rdr) = k \qquad (5.28)$$

where $q = \sqrt{\xi^2-k^2}$, $\eta = \sqrt{\xi^2+k^2}$ and the superscript $*$ indicates the complex conjugate. Equation (5.28) is equivalent to (5.25). It is remarkable to see that such a complicated integral results in a simple constant.

Equation (5.28) includes an integral with a new form of integrand, which corresponds to the particle velocity. This type of integral will be involved in the calculations of the energy flux later. The numerical integration for the particle velocity should not be very difficult since it does not have any

singularity; however as with the numerical integration of (5.7), the accuracy of the calculation may be reduced for large values of r and z because of the oscillatory feature of the integrand. We shall not test the accuracy of numerical integration of the particle velocity explicitly but it is checked indirectly by the next test. Since the exact analytical result of (5.28) is available it provides a good way of testing the program for numerical calculation of the time average power crossing a surface. We shall test the formula (5.28) numerically for given h (or z) and k. The integrations corresponding to the energy flux use NAG routines D01atf and D01amf, and we choose other two NAG routines for the integration with respect to r, D01ajf for a finite interval and D01bay for a semi-infinite interval, since it is not permissible to call a routine within a calculation by the same routine. This test serves three purposes. The first one is to test the program for numerical calculation of the time average power crossing a surface and to check the new routines D01atf and D01bay. The second purpose is to indirectly test the integral representation of the particle velocity and the third is to indirectly check the integrals for the pressure and particle velocity for wider range of r at a given z. If the program for calculating the time average power gives a satisfactory result, we would expect that the calculations for the pressure and particle velocity should also give reasonable accurate results.

The routines D01atf and D01ajf use the same algorithm, but D01atf requires the integrand to be calculated at an array of points, and it is more efficient. Obviously we wish to calculate the integrations corresponding to the energy flux more quickly since it is the integrand for another integration. From equation (5.24) we can see that the energy flux is a rational type decay function with increasing r, so we choose D01baf for the semi-infinite integration with respect to r. The finite interval for D01ajf is from 0 to 100, and is divided into 10 equal sub-intervals. D01bay is used from 100 to infinity. For the integrations corresponding to the energy flux, again the value k is the point separating the finite interval and the semi-infinite interval. For D01ajf, D01atf, and D01amf, the relative accuracy is specified as 10^{-3} and the absolute accuracy is 0.0.

A comparison is given in Table (5.2) between the result of the integration for k using the suitably normalized algebraic expression (see (5.25) for the energy flux (5.24) and that obtained by using the integral expression (5.28).

intervals (m)	normalized integration (5.24)	integration (5.28)
0-10	4.2734023638535 75	4.27341604232 7881
10-20	0.2352221291039 64	0.2352196574211121
20-30	0.0788852297647 94	0.0788851752877 23541
30-40	0.0394959826461 61	0.0402158685028 55301
40-50	0.0237099590963 22	0.0237102676182 98531
50-60	0.0158106995430 00	0.0158105194568 63403
60-70	0.0112950005119 76	0.0112944608554 24404
70-80	0.0084720171203 21	0.0084723671898 24581
80-90	0.0065897429700 87	0.0065895849830 85288
90-100	0.0052720158410 72	0.0052721798419 95239
100- ∞	0.0475370522141456	0.0477889776229 85840
sum	4.7456080076083 75	4.7466751011088 49

Table 5.2 Comparison of numerical integrations. Frequency f=1000 Hz, wave speed c=331 m/s, $k = (2\pi f/c) = 4.745608009960716$, source height h=1m.

The value of π is obtained from a NAG routine X01aaf. Examining the results for the sub-intervals, we can see that the two integrations agree to about 4 or 5 digits. This accuracy is little less than that obtained by the single integration for the pressure for large values of r in Table (5.1). The sum in Table (5.2) shows that integration (5.28) can reach the accuracy to 3 digits, and integration (5.24) can obtain accuracies to 9 digits, in comparison with the exact value of k given in the caption to Table (5.2).

The calculation of the integrand in (5.28) had a few failures for values of $r > 100$. The maximum number of subdivisions allowed with the given workspace in computer memory which was specified as 50000 has been reached without the accuracy requirements being achieved. This is because for large values of r the integrands in the integrals for the pressure

$$\int_{ik}^{\infty} J_0(r\eta)exp(-|z|\xi)\, d\xi$$

or for the particle velocity

$$\int_0^\infty J_0(r\xi)exp(-|z|q)\xi\, d\xi$$

become rapidly oscillatory. If the workspace is further increased , the computer's internal round-off error specified by the software will limit the accuracy; consequently there is no further improvement in accuracy. The failures of calculation at some particular points and some particular ranges do not seriously affect the whole integration process. In fact a calculation failure does not always imply a large error. The relative error is about 0.0002, which is smaller than the specified relative accuracy for D01ajf, D01atf and D01amf. It is difficult to increase the accuracy further.

Chapter 6

Spherical wave reflection and transmission

In this chapter we shall start with using the classical integral representation (1.1) to study problems concerned with the reflection of spherical waves at a plane boundary; then we transform the reflected wave expressions to new forms which are subsequently used in numerical studies. The solutions based on the formula with the Hankel function (equation (1.5)) are also used.

As in the case of plane waves, we consider only the continuous, steady state, wave field; hence the results obtained here may not be applicable wave pulses or wave beams. The problem of transmission is discussed only for waves in a fluid. There are solutions for the problems of reflection at a rigid boundary, and reflection and transmission at the interface between two media. They can be found, for example, in the book 'Elastic waves in layered media' by Ewing, *et al.* [11]. Since the existing solutions, which are based on Lamb's integral, have singularities, numerical integrations are extremely difficult. This has been pointed out by Ewing, *et al.*. Transformation of the classical solution into a new form of solution has enabled us to overcome some difficulties in the numerical integration and so we have obtained more accurate integration results, and carried out a detailed numerical study of spherical wave reflection and transmission. The results offered in this chapter are consistent with those obtained in the previous chapter for plane waves.

It is not our intention to explain all of the new results obtained in this chapter, since convincing explanation would require further theoretical stud-

ies and experimental verifications. Nevertheless some attempt has been made and is given in Appendix (E).

For spherical wave propagation, a cylindrical coordinate system is used. If we choose the z-axis to pass through the point source and normal to the reflection surface, the wave field is symmetrical about the z-axis and depends only on the coordinates z and r.

6.1 Rigid boundary

The exact algebraic solution is well known for spherical wave reflection at a plane rigid boundary, so it provides a benchmark for checking the integral solutions. Let us assume that the point source is at $z = h(> 0)$ above the boundary which is at $z = 0$. At a rigid boundary, the z-component of particle displacement is zero and this condition is expressed by

$$w = 0 \qquad \text{at } z = 0. \tag{6.1}$$

Since we are interested only in a continuous steady state wave field, initial conditions are ignored. We consider a solution of the equation of motion in the form

$$\varphi = \frac{exp(i\omega t - i\kappa\sqrt{r^2 + (h-z)^2})}{\sqrt{r^2+(h-z)^2}} + R\frac{exp(i\omega t - i\kappa\sqrt{r^2 + (h+z)^2})}{\sqrt{r^2+(h+z)^2}}, \tag{6.2}$$

with

$$\omega = \kappa c,$$

c being the wave speed and κ being the wavenumber. The first term in equation (6.2) represents the incident wave and the second term is for the reflected wave. The geometrical decay is proportional to the distance travelled along the incident and reflected wave paths, respectively, and R is the reflection coefficient. The consideration of spherical spreading is an important factor when we initially guess an integral form of solution. We have assumed unit amplitude for the incident wave. Since we only consider the case of time harmonic motion we shall omit the time dependent term $exp(i\omega t)$ (or

$exp(-i\omega t)$ depending on the sign of the space dependent term) whenever it is not relevant.

From the boundary condition, following the same procedure as we did in the case of plane wave, it is easy to obtain that the reflection coefficient is given by

$$R = 1. \tag{6.3}$$

Let us examine the solution for energy conservation. Solution (6.2) is a sum of the incident wave and the reflected wave. Consider now a plane surface, at $z = 2h$, say, in the incidence medium, above the point source, parallel to the reflecting surface. The sum of the time average powers from the direct and reflected waves crossing the plane surface must be equal to the total output power of the point source, which is $2\pi\rho\omega^3 k$. The reflected wave can be regarded as a spherical wave generated from an imaginary source on the z-axis at $z = -h$. We have shown, in Chapter 5, that the time average power crossing a plane surface due to a single spherical wave is $\pi\rho\omega^3 k$ and the result is independent of the distance between a source and the plane. It is obvious that the totally reflected spherical wave from the image source will also contribute this amount of power crossing the plane surface. Therefore the sum of the time average powers from the direct wave and reflected wave, respectively, meets the requirement of energy conservation. The energy flux may not be zero locally across an element of such a plane surface, due to the interference between the incident and reflected waves, although the spatial integration of the time average energy flux of the interference terms must be zero. An interesting result was obtained when calculating the time average local energy flux component

$$< I_z >= \frac{1}{2} Re(p^* \frac{\partial w}{\partial t}), \tag{6.4}$$

where p^* is the complex conjugate of the pressure. It was found that in some regions above the point source, although both the direct wave and the reflected wave are supposed to be travelling away from the boundary, the z-component of the time average total energy flux of the two waves is locally in the negative z-direction. An example of such a calculation is given in Table

coordinate r (m)	1.16	1.18	1.20	1.22	1.24
energy flux	0.042	0.012	-0.0028	-0.0091	0.018

Table 6.1 An example of a negative time average energy flux component in the z-direction for spherical waves in air reflected at a rigid boundary. Frequency 1000Hz; source height 1m; height of plane $z = 2$m.

(6.1). The results given in Table (6.1) were calculated from (6.4) and were normalized to $\pi\rho k\omega^3$. Since it is a simple algebraic calculation, the negative sign of the time average energy flux cannot be caused by numerical error. A discussion of this so called "backward wave" will be given in the last chapter.

An equivalent integral solution of the equation of motion can be written as

$$\varphi = \int_0^\infty \frac{J_0(r\xi)e^{-|h-z|\sqrt{\xi^2-\kappa^2}}\xi}{\sqrt{\xi^2-\kappa^2}}\,d\xi + \int_0^\infty R\frac{J_0(r\xi)e^{-|h+z|\sqrt{\xi^2-\kappa^2}}\xi}{\sqrt{\xi^2-\kappa^2}}\,d\xi, \tag{6.5}$$

provided that

$$\kappa c = \omega.$$

Use of the boundary condition gives

$$\int_0^\infty (J_0(r\xi)e^{-h\sqrt{\xi^2-\kappa^2}}(1-R))\,d\xi = 0 \quad \text{at } z = 0. \tag{6.6}$$

A sufficient condition for the integration to be zero is that the integrand vanishes for any ξ and for an arbitrary r, so we have

$$R = 1, \tag{6.7}$$

as required. Equation (6.5) is written in a form of two separate terms corresponding to the incident wave and the reflected wave respectively. If we change the integration variable by a substitution $\xi = \sqrt{x^2+\kappa^2}$, a new form of solution is obtained, which is, written in compact form,

$$\varphi = \int_{i\kappa}^\infty J_0(r\sqrt{x^2+\kappa^2})(exp(-|h-z|x^2) + exp(-|h+z|x^2))\,dx, \tag{6.8}$$

where the path of integration is defined as in equation (5.7).

Following a similar procedure, but using the formula with the Hankel function instead, we can obtain an alternative, complex conjugate, form of the integral solution

$$\varphi = i\int_0^\infty [H_0^{(1)}(|z-h|\sqrt{\kappa^2-x^2}) + H_0^{(1)}((h+z)\sqrt{\kappa^2-x^2})]cos(rx)\,dx, \quad (6.9)$$

with $\kappa c = \omega$. It is not difficult to show that the four solutions, (6.2), (6.5), (6.8) and (6.9), are equivalent except that solution (6.9) has a phase different from the other three, (6.2), (6.5) and (6.8), due to its being the complex conjugate. Using NAG routines, we can calculate the data for pressure contours using equations (6.5), (6.8) and (6.9). The routine D01ajf is used for the integration from 0 to κ, and D01amf for that from κ to infinity. The three solutions give very similar results to that obtained from (6.2). The accuracy is similar to that obtained for the test case of Table (4.1). The pressure is proportional to the potential function, and in dB the pressure can be expressed as

$$p = 20log_{10}(|\varphi|) + CONST, \quad (6.10)$$

where $|\varphi|$ is the modulus of φ, and CONST is a constant which depends on the amplitude of the incident wave, and on the reference pressure. The value of CONST is 74 dB for the calculations presented here.

Pressure values were calculated at the crossover points of a mesh lying on a plane formed by taking r and z as a two-dimensional Cartesian coordinate pair. Since one of the results of the calculation here will be used later for the experimental comparison, the pressure contours were obtained in the real space, instead of the dimensionless space. The results can be easily converted to the dimensionless space. A frequency of 1000 Hz was used for waves in air or in water. The wavelength of the wave in the air is about 331mm, and that in the water is about 1531mm. Neighbouring points in each of the r and z-directions are 50mm apart. In the case of air, we have also considered separations of 100mm or 25mm. It is found that using 100mm intervals gives less detailed pressure contours, and that the results obtained by using 25mm intervals are similar to those when using 50mm intervals. Since a sparser network density uses less CPU time we chose the length of the interval to be 50mm.

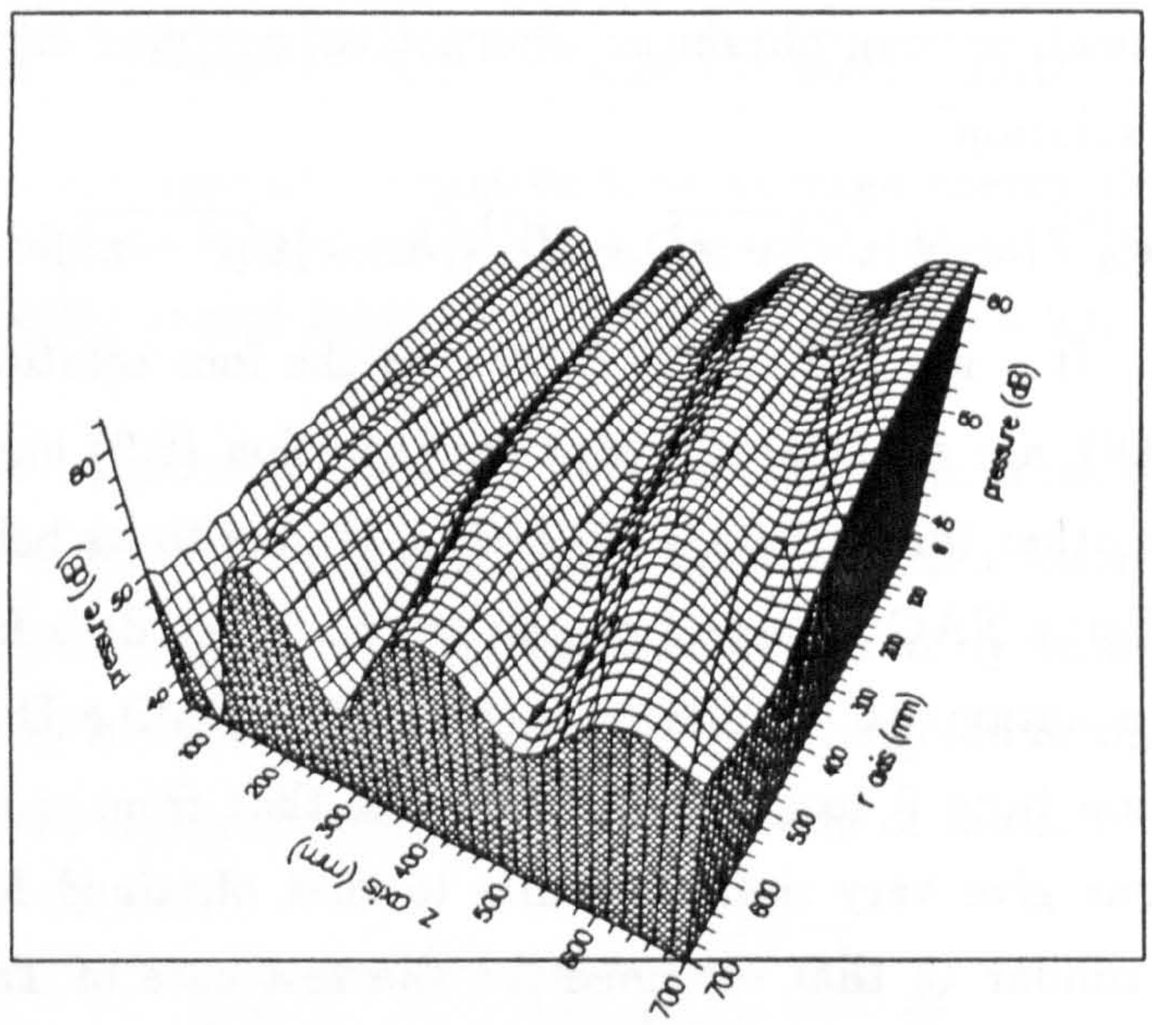

Figure 6.1 Three dimensional pressure contours for spherical waves in air reflected at a rigid boundary. The point source is located at 1m on the z-axis and the boundary is at $z = 0$m; frequency 1000 Hz.

The results are shown in Figures (6.1) and (6.2) for waves in air and in water respectively. The contours were produced by using the UNIMAP software package. The results are presented in the form of three dimensional contours. This allows us to easily identify the pressure level peaks or troughs. In Figure (6.1) there are four troughs but only one in Figure (6.2) which is for the longer wavelength. In the region between the source and the boundary, the number of peaks or troughs which may exist of course depends on the relation between the wavelength and the distance of the observation point to the boundary.

We shall see that the rigid boundary is a good approximation to a fluid/solid metal interface, and in some cases for a gas-liquid interface, but the rigid boundary is not suitable for describing the interface condition where two fluid media which have similar acoustic properties are in contact.

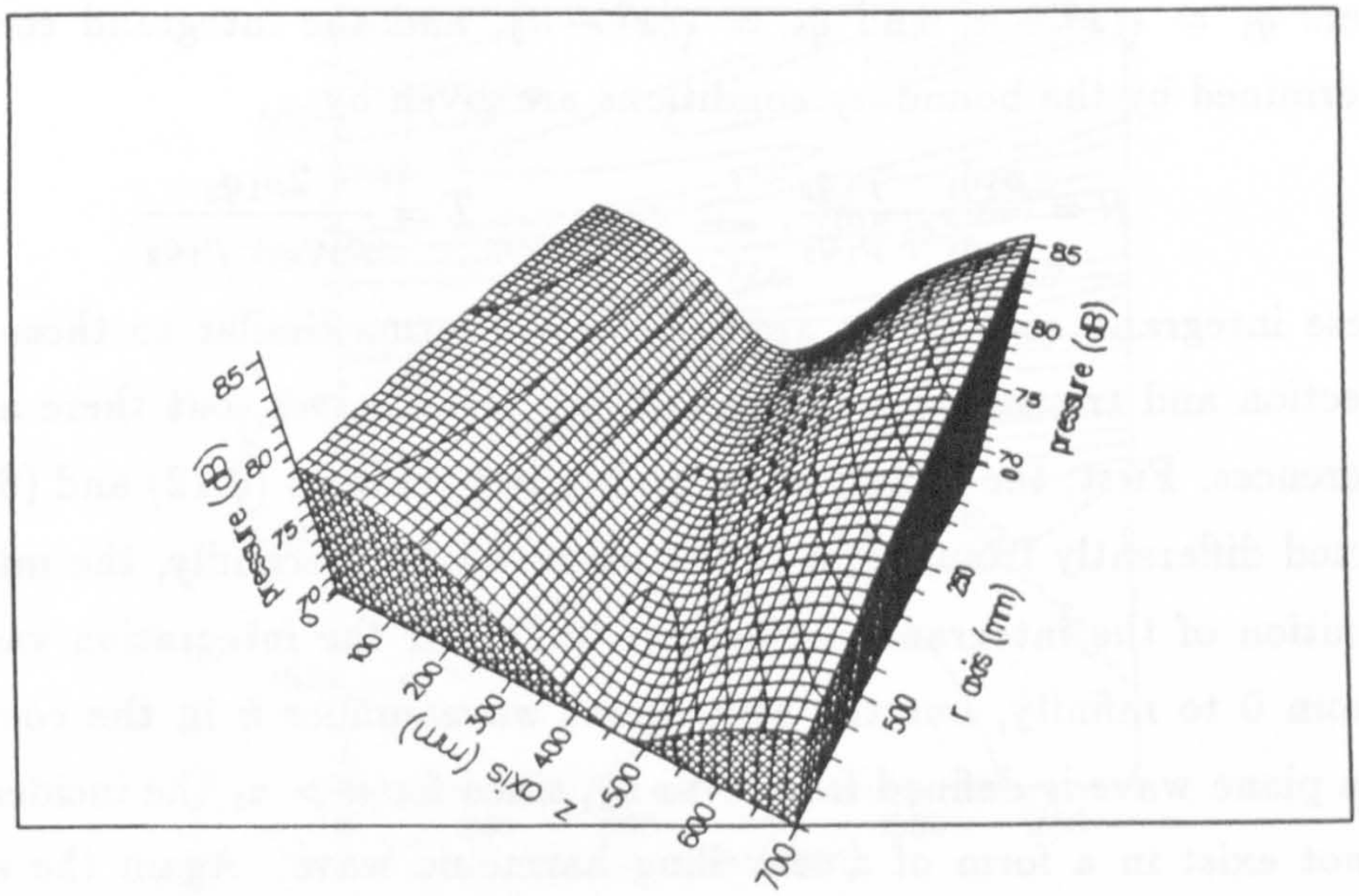

Figure 6.2 Three dimensional pressure contours for spherical waves in water reflected at a rigid boundary. The point source is located at 1m on the z-axis and the boundary is at $z = 0$m; frequency 1000 Hz.

6.2 Interface between two fluid media

Next let us consider the problems of spherical wave reflection and transmission at a plane interface of two semi-infinite fluid media. The boundary conditions at an interface of two fluids (at $z = 0$) are similar to the case of plane waves, and are given by

$$w_1 = w_2, \qquad p_1 = p_2, \qquad \text{at } z = 0. \tag{6.11}$$

Again the point source is at $z = h(> 0)$. The classical solutions in terms of Lamb's integral can be found in the book 'Elastic waves in layered media' by Ewing, *et al.* [11], and may be written as

$$\varphi_1 = \int_0^\infty \frac{J_0(rx)e^{-|z-h|q_1}x}{q_1}\,dx + \int_0^\infty R\frac{J_0(rx)e^{-(h+z)q_1}x}{q_1}\,dx, \tag{6.12}$$

$$\varphi_2 = \int_0^\infty T\frac{J_0(rx)e^{-hq_1+zq_2}x}{q_2}\,dx, \tag{6.13}$$

where $q_1 = \sqrt{x^2 - \kappa_1^2}$ and $q_2 = \sqrt{x^2 - \kappa_2^2}$, and the integrand coefficients determined by the boundary conditions are given by

$$R = \frac{\rho_2 q_1 - \rho_1 q_2}{\rho_2 q_1 + \rho_1 q_2}, \qquad T = \frac{2\rho_1 q_2}{\rho_2 q_1 + \rho_1 q_2}. \tag{6.14}$$

These integrand coefficients appear to have forms similar to those for the reflection and transmission coefficients for plane waves, but there are basic differences. First, the quantities q_1 and q_2 in equations (6.12) and (6.13) are defined differently from those of the plane waves. Secondly, the interval of definition of the integrand coefficients (6.14) for the integration variable x is from 0 to infinity, but the component wavenumber k in the coefficients for a plane wave is defined from 0 to κ_1, since for $k > \kappa_1$ the incident wave cannot exist in a form of a travelling harmonic wave. Again the solution for the reflected wave can be transformed into a new form. The solution for the transmitted wave will keep its present form since the singularity has been eliminated by the form of the transmission coefficient. The transformed solution for the reflected wave is

$$\varphi_r = \int_{i\kappa_1}^{\infty} \frac{\rho_2 x - \rho_1 \sqrt{x^2 + \kappa_1^2 - \kappa_2^2}}{\rho_2 x + \rho_1 \sqrt{x^2 + \kappa_1^2 - \kappa_2^2}} J_0(r\sqrt{x^2 + \kappa_1^2}) exp(-(h+z)x)\, dx, \tag{6.15}$$

where φ_r denotes the second term on the right side of (6.12).

By using the the integral representation with the Hankel function for a spherical wave, one can obtain the complex conjugate solution in the form

$$\varphi_1 = i \int_0^{\infty} [H_0^{(1)}(|z-h|\eta_1) cos(rx) + R' H_0^{(1)}((h+z)\eta_1) cos(rx)]\, dx, \tag{6.16}$$

$$\varphi_2 = i \int_0^{\infty} T' H_0^{(1)}((h-z)\eta_2) cos(rx)\, dx, \tag{6.17}$$

where $\eta_1 = \sqrt{\kappa_1^2 - x^2}$ and $\eta_2 = \sqrt{\kappa_2^2 - x^2}$. Although the first term of the integrand in equation (6.16) is a solution of the equation of motion, it is difficult to show whether the integral of the second term in equation (6.16) and the integral (6.17) satisfy the equation of motion. Using the boundary conditions we obtain

$$R' = \frac{H_0^{(2)}(h\eta_1) H_0^{(1)}(h\eta_2)\eta_1\rho_2 - H_0^{(1)}(h\eta_1) H_0^{(2)}(h\eta_2)\eta_2\rho_1}{H_0^{(2)}(h\eta_1) H_0^{(1)}(h\eta_2)\eta_1\rho_2 + H_0^{(1)}(h\eta_1) H_0^{(2)}(h\eta_2)\eta_2\rho_1}, \tag{6.18}$$

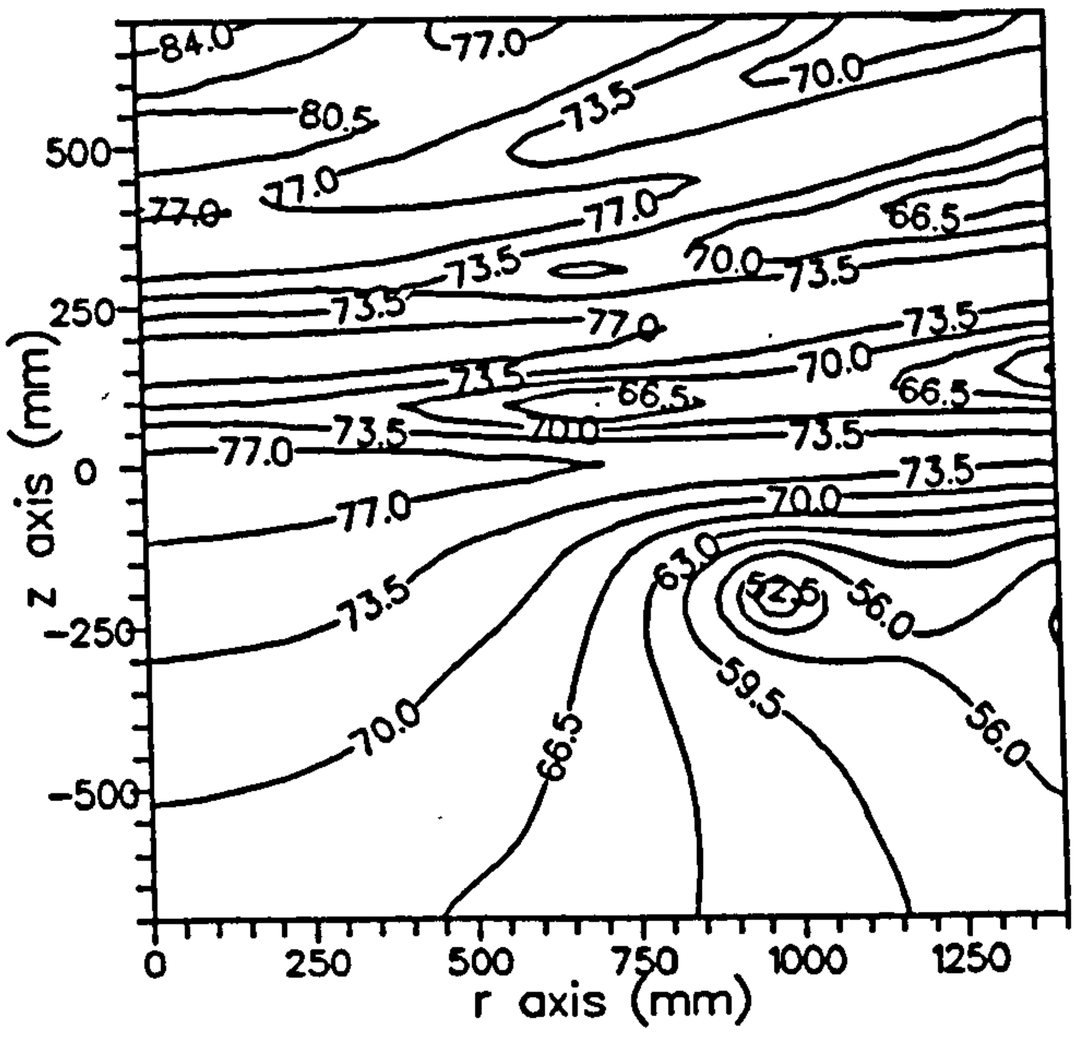

Figure 6.3 Pressure contours when a spherical wave is incident on an air-water interface. The point source is located at 1m on the z-axis, in the air, and the interface is at $z = 0$m. Frequency 1000 Hz.

$$T' = \frac{2H_0^{(2)}(h\eta_1)H_0^{(1)}(h\eta_1)\eta_1\rho_2}{H_0^{(2)}(h\eta_1)H_0^{(1)}(h\eta_2)\eta_1\rho_2 + H_0^{(1)}(h\eta_1)H_0^{(2)}(h\eta_2)\eta_2\rho_1}. \tag{6.19}$$

The coefficients (6.18) and (6.19) appear very different from those given in equation (6.14), and numerical calculations also show differences. However, numerical integrations of solutions (6.12) (with the transformed second term (6.15)) and (6.13) give very similar results to those obtained from integrations of (6.16) and (6.17). The values of the pressures in terms of dB agree within 1 dB. However numerical integration of (6.12) or (6.13) uses much less CPU time than that of (6.16) or (6.17). Pressure contours obtained by using equations (6.12) (with (6.15)) and (6.13) are shown in Figures (6.3) and (6.4).

The contours are presented in a two-dimensional form, so that we can clearly see the distortion of the spherical wave pattern caused by the reflected wave. Figure (6.3) is for an air-water interface and Figure (6.4) is for a kerosene-water interface. Air and water are less well acoustically matched than the kerosene and water. For the larger impedance change (Figure (6.3)), the spherical wave pattern is strongly distorted because the hard boundary

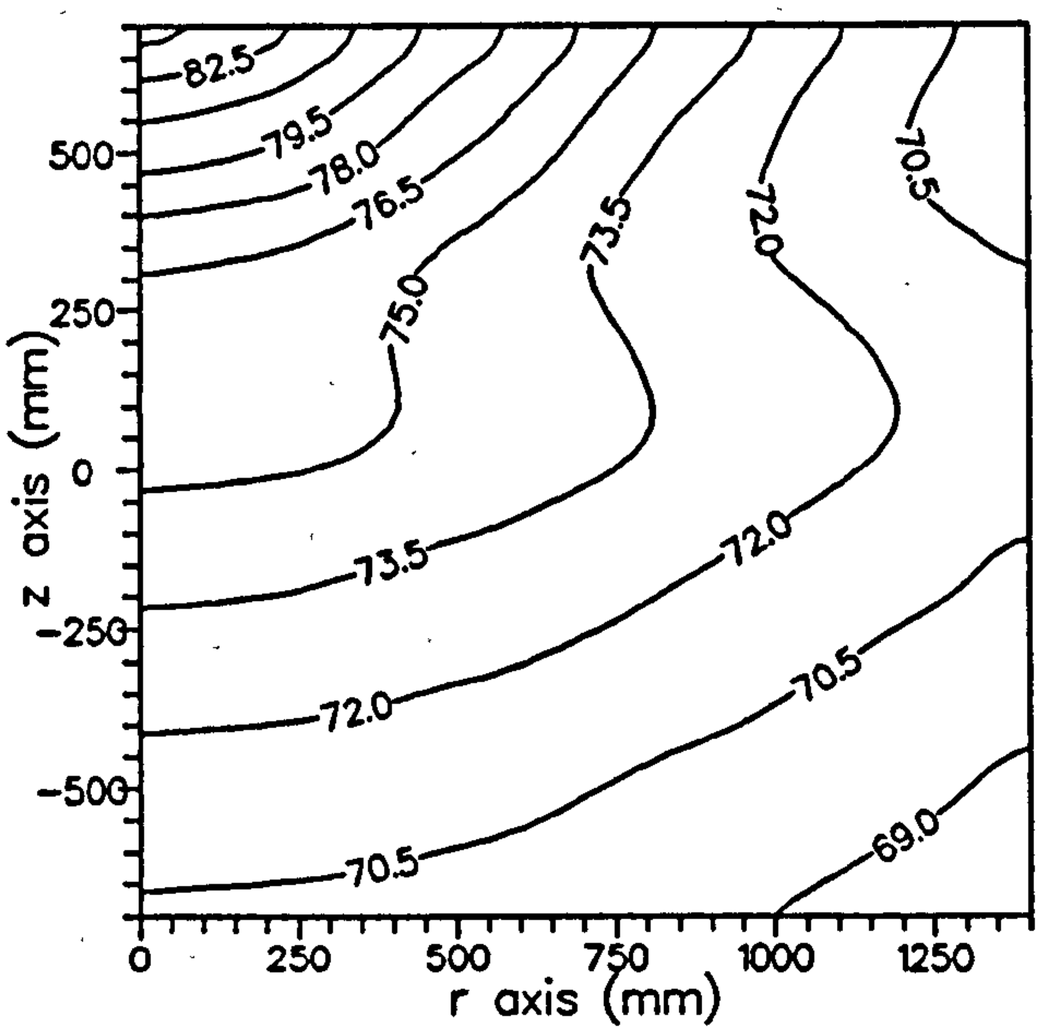

Figure 6.4 Pressure contours when a spherical wave is incident on a kerosene-water interface. The point source is located at 1m on the z-axis, in the kerosene, and the interface is at $z = 0$m. Frequency 1000 Hz.

produces a stronger reflected wave as expected. In Figure (6.3) it is interesting to see that there is a point of minimum pressure in the transmission area where $z < 0$, in the neighbourhood of $r \sim 1000$ mm and $z \sim$ -250 mm.

By analogy with the case for plane wave incidence, given an incident spherical wave at an interface between two fluid half spaces, one can define the specular reflection and transmission coefficients for the pressure by

$$R_p = \frac{\varphi_r}{\varphi_i}, \tag{6.20}$$

$$T_p = \frac{\varphi_2 \rho_2}{\varphi_i \rho_1}, \tag{6.21}$$

where φ_r is the reflected wave, φ_i is for the incident wave, and the subscript numbers indicate the media concerned as before.

The spherical wave integral solutions for the reflection and transmission coefficients should tend towards those for plane wave incidence when the observer is a very long distance away from the point source. We have calculated the reflection and transmission coefficients for spherical wave incidence for different source heights, for comparison with the coefficients for plane waves.

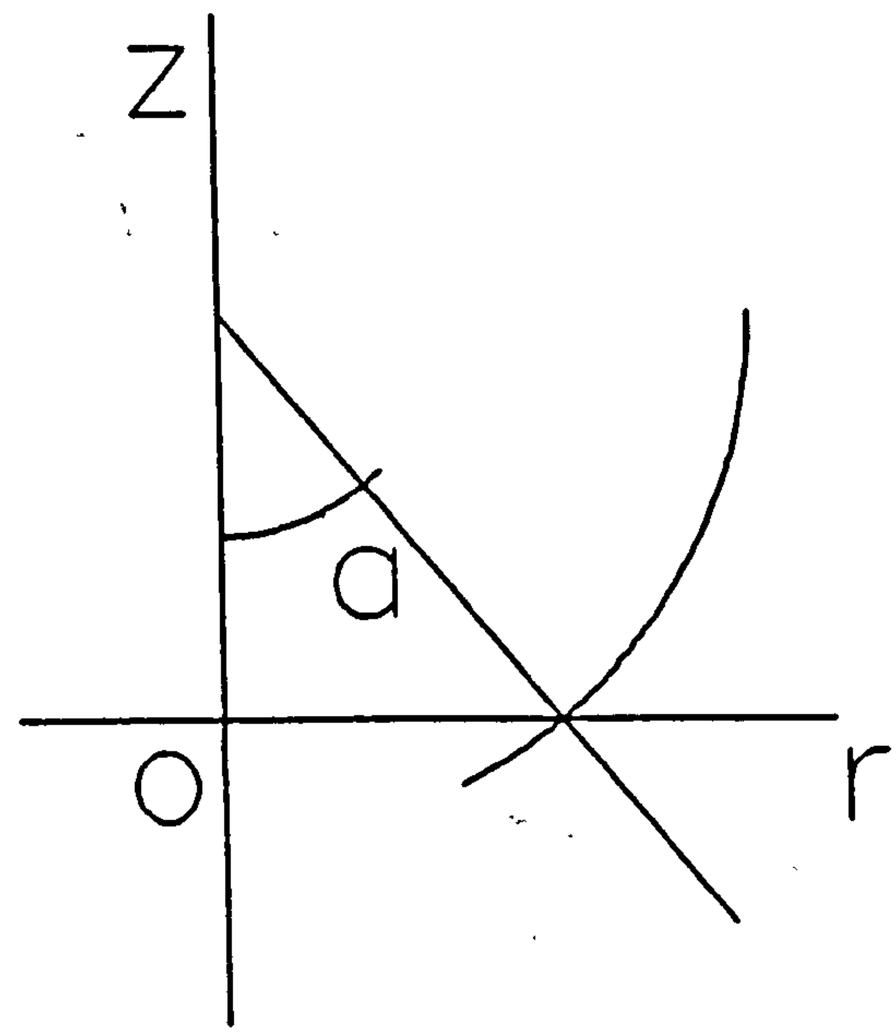

Figure 6.5 The angle of incidence for a spherical wave is defined by a.

The angle of incidence for a spherical wave is defined as the angle between the normal to the boundary and the normal to the wave front at the joint point of the front and the boundary as shown in Figure (6.5)

The results are shown in Figures (6.6) to (6.9). They show that in the case of a kerosene-water interface, the coefficients (6.20) and (6.21) depend on the height of the source, and that as the height of the source increases they tend towards those for a plane wave. Examining Figures (6.7) and (6.9), we find that the reflected wave or the transmitted wave has a phase different from that of the incident wave; in other words, the reflection and transmission coefficients for the spherical wave are always complex quantities. This situation is different from that for the plane wave. In Figures (6.7) and (6.9) the phase curves for a plane wave are plotted with a positive sign, which allows us to make an easy comparison. The positive phase for spherical waves would imply that the phases of the reflected and transmitted waves are ahead of that of the incident wave, or the phases of the reflected and transmitted waves are behind that of the incident wave at degrees of $360° - \alpha$, where α indicates the phase value at a given angle of incidence in Figures (6.7) and (6.9). The reason for this positive phase is not very clear; it may be related

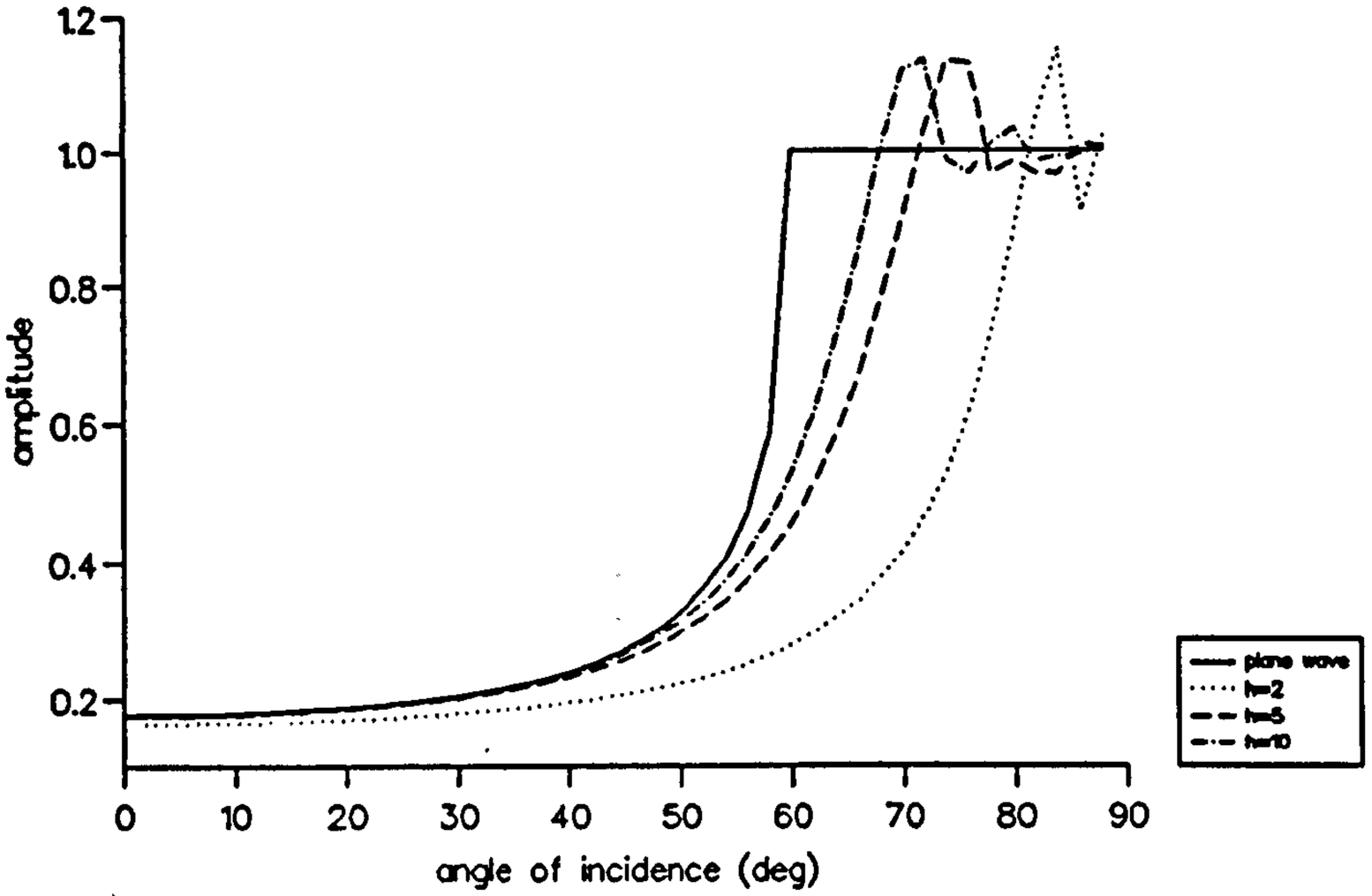

Figure 6.6 Amplitudes of the reflection coefficients of spherical waves for pressure incident in kerosene on a kerosene-water interface for different source heights, h, compared with those for plane wave incidence. Frequency 1000 Hz.

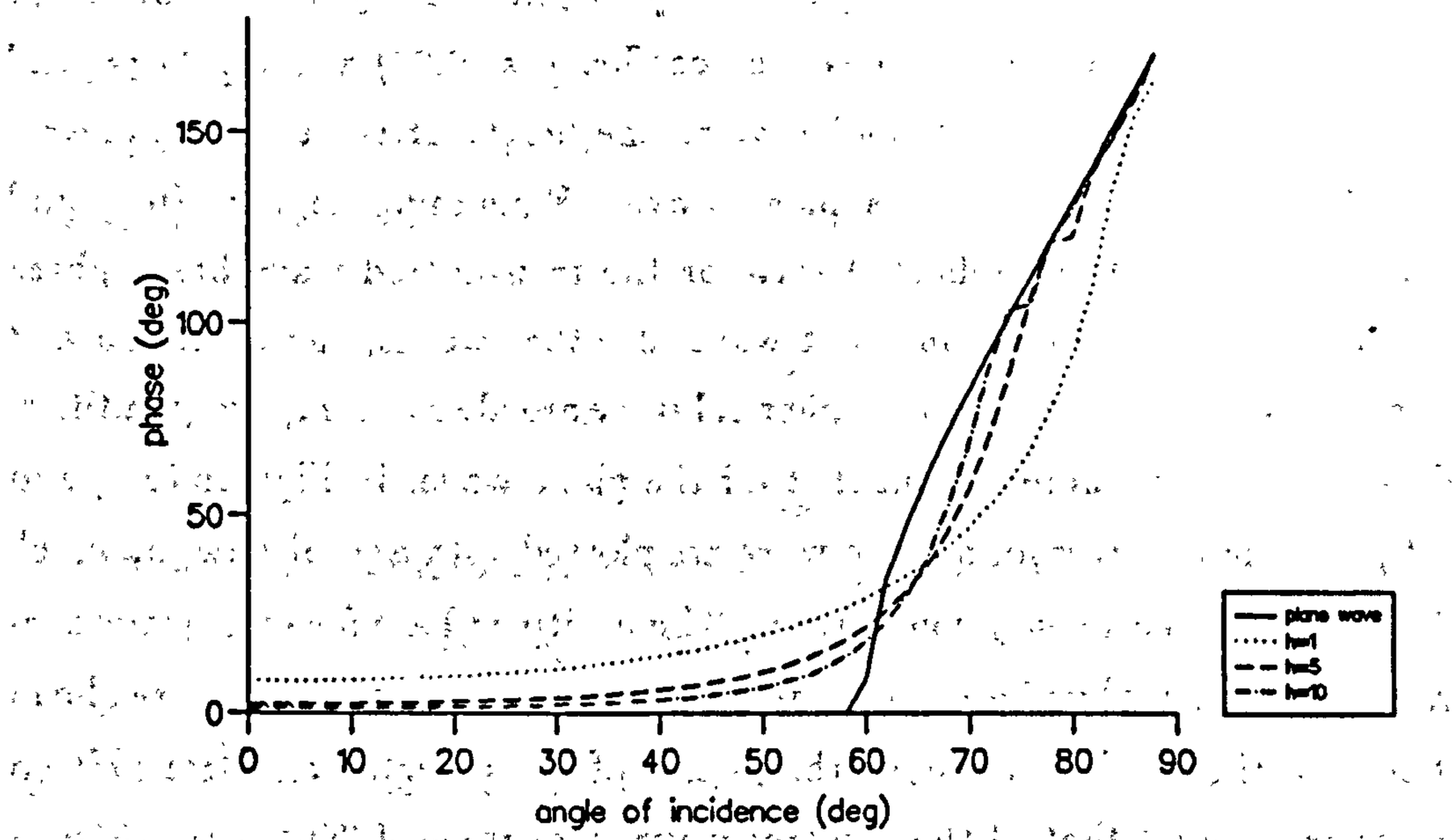

Figure 6.7 Phases of the reflection coefficients of spherical waves for pressure incident in kerosene on a kerosene-water interface for different source heights, h, compared with those for plane wave incidence. Frequency 1000 Hz.

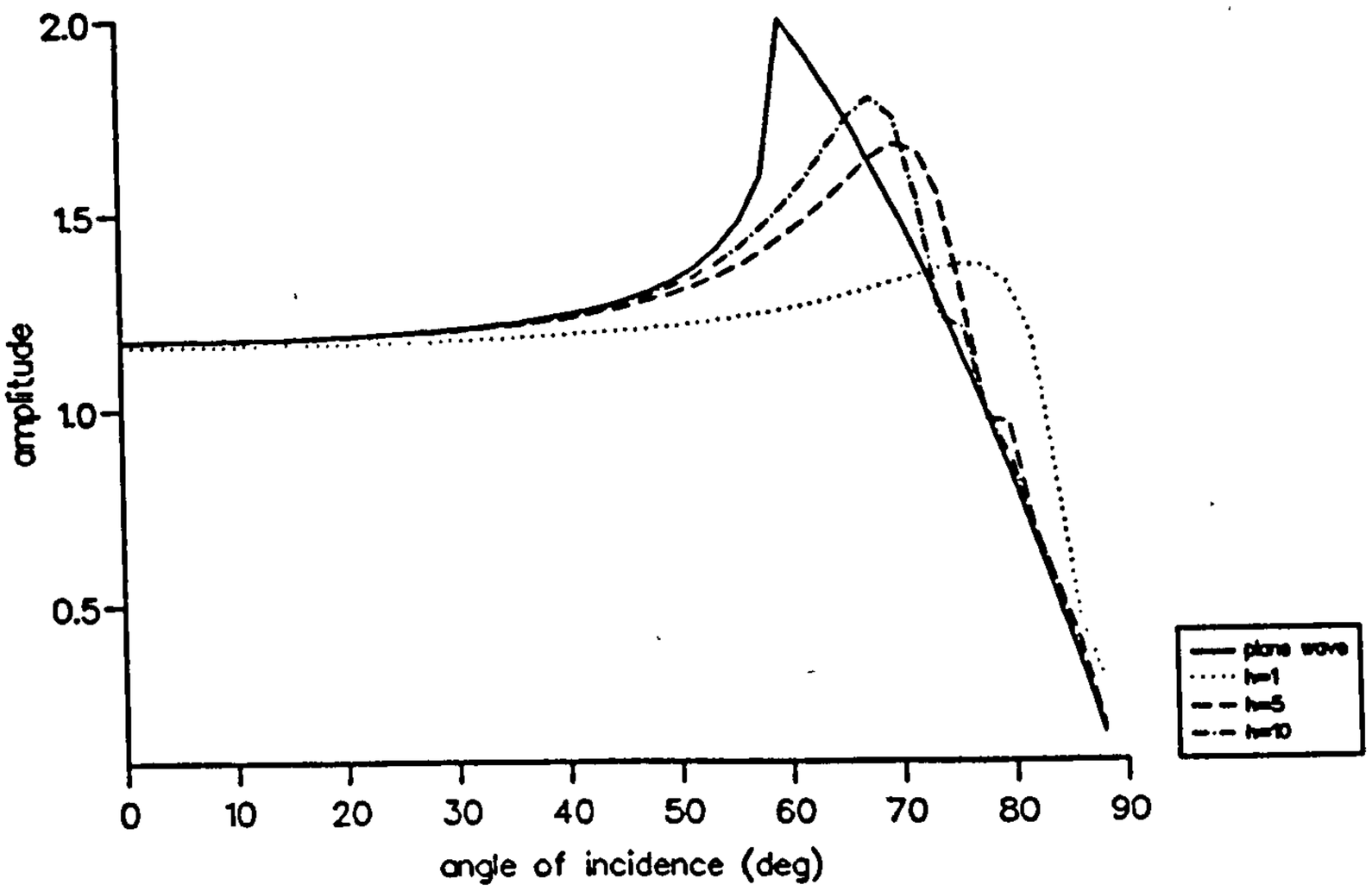

Figure 6.8 Amplitudes of the transmission coefficients of spherical waves for pressure incident in kerosene on a kerosene-water interface for different source heights, h compared with those for plane wave incidence. Frequency 1000 Hz.

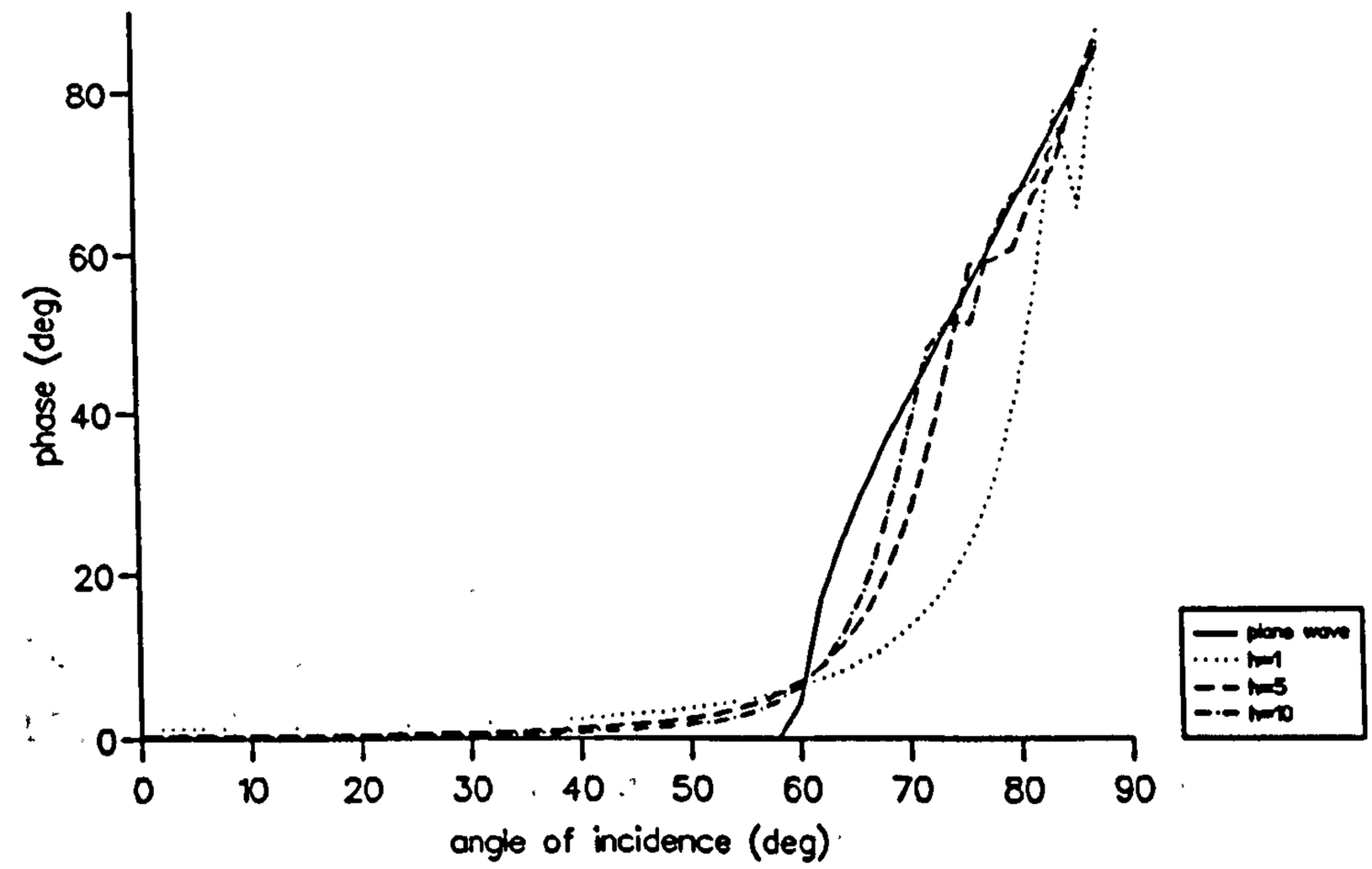

Figure 6.9 Phases of the transmission coefficients of spherical waves for pressure incident in kerosene on a kerosene-water interface for different source heights, h, compared with those for plane wave incidence. Frequency 1000 Hz.

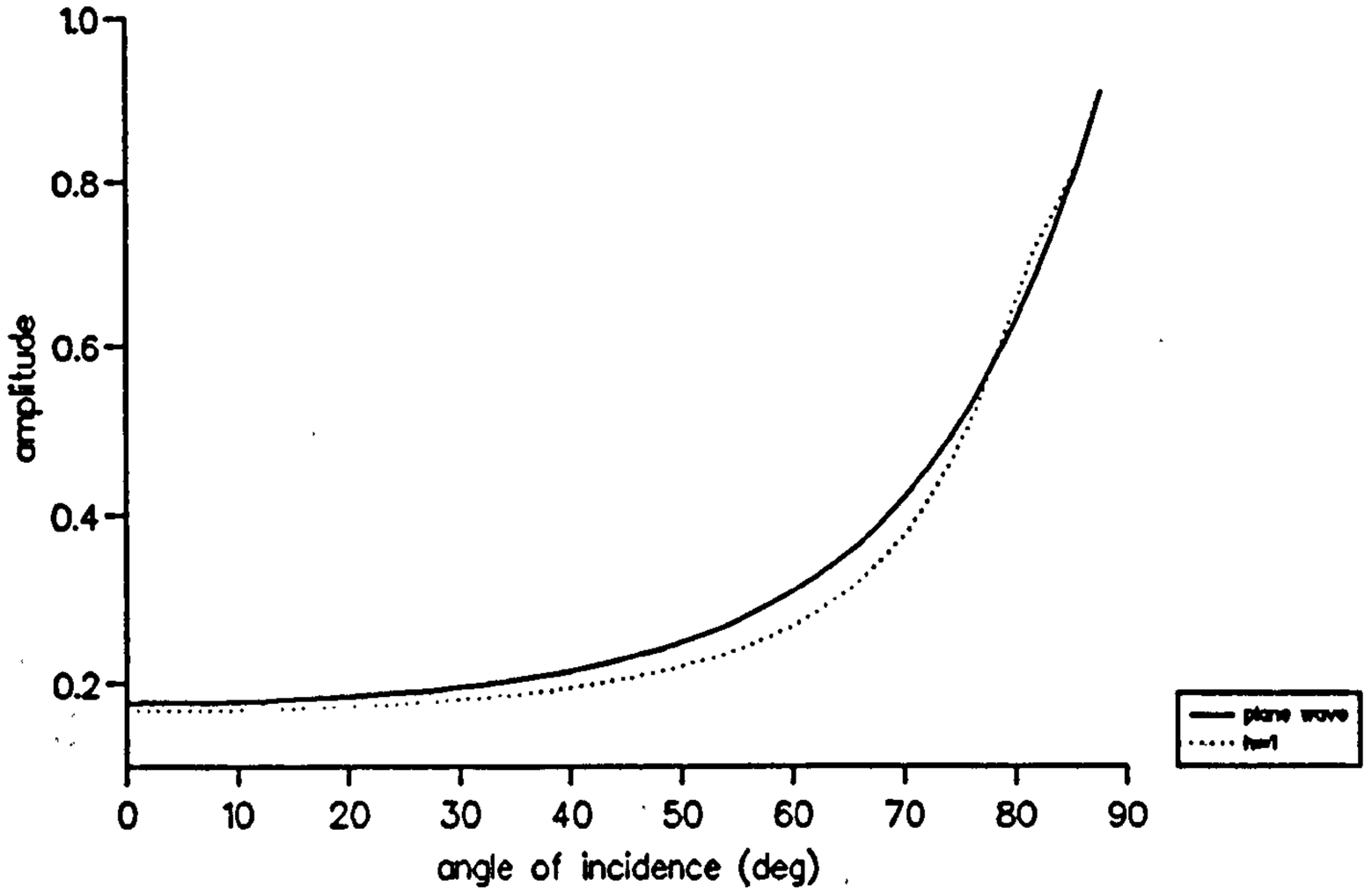

Figure 6.10 Amplitudes of the reflection coefficients of spherical waves for pressure incident in water on a water-kerosene interface for different source heights, h, compared with those for plane wave incidence. The curves for $h = 5$ and $h = 10$ coincide with that for plane wave. Frequency 1000 Hz.

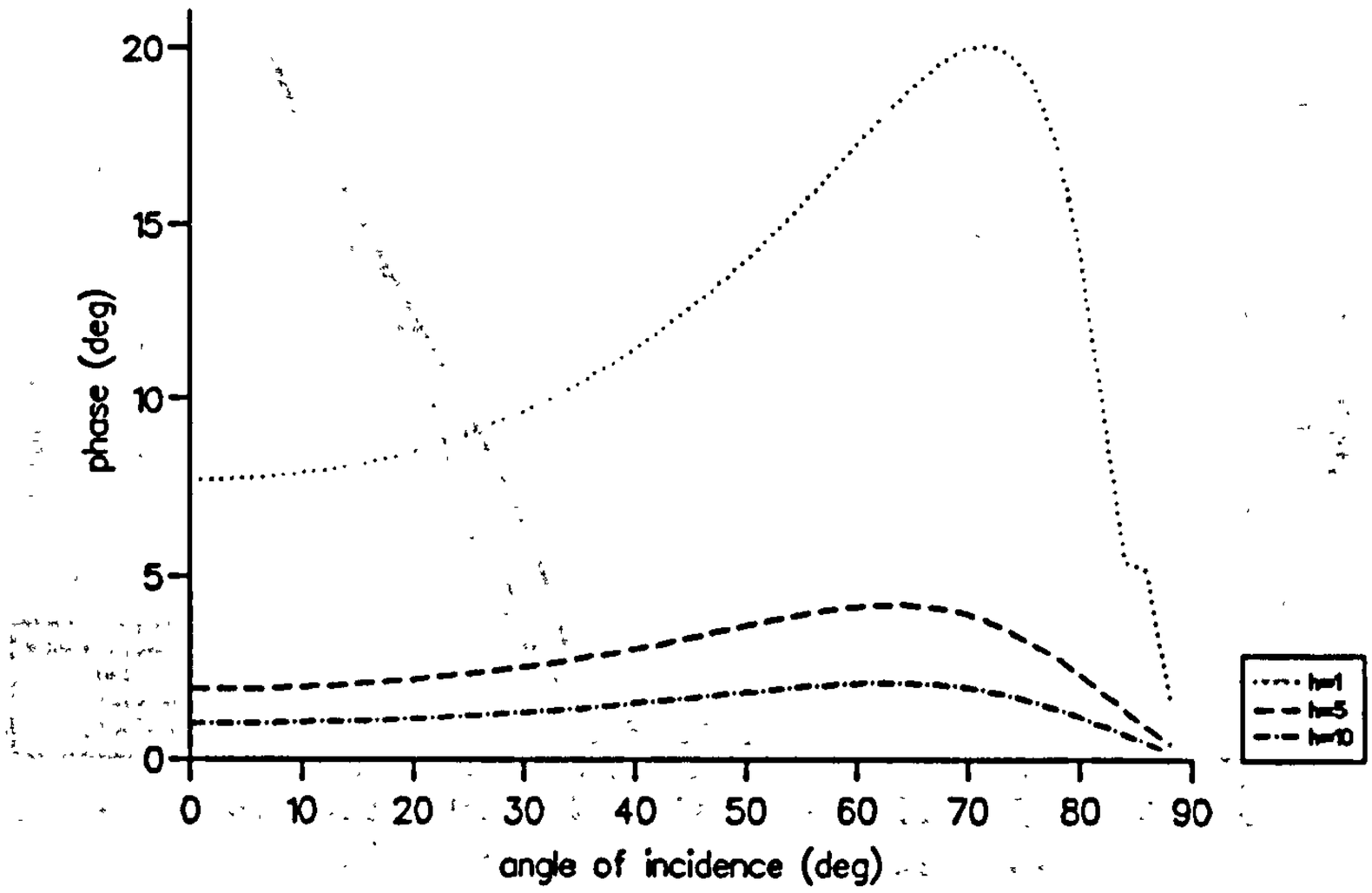

Figure 6.11 Phases of the reflection coefficients of spherical waves for pressure incident in water on a water-kerosene interface for different source heights, h compared with those for plane wave incidence. Frequency 1000 Hz.

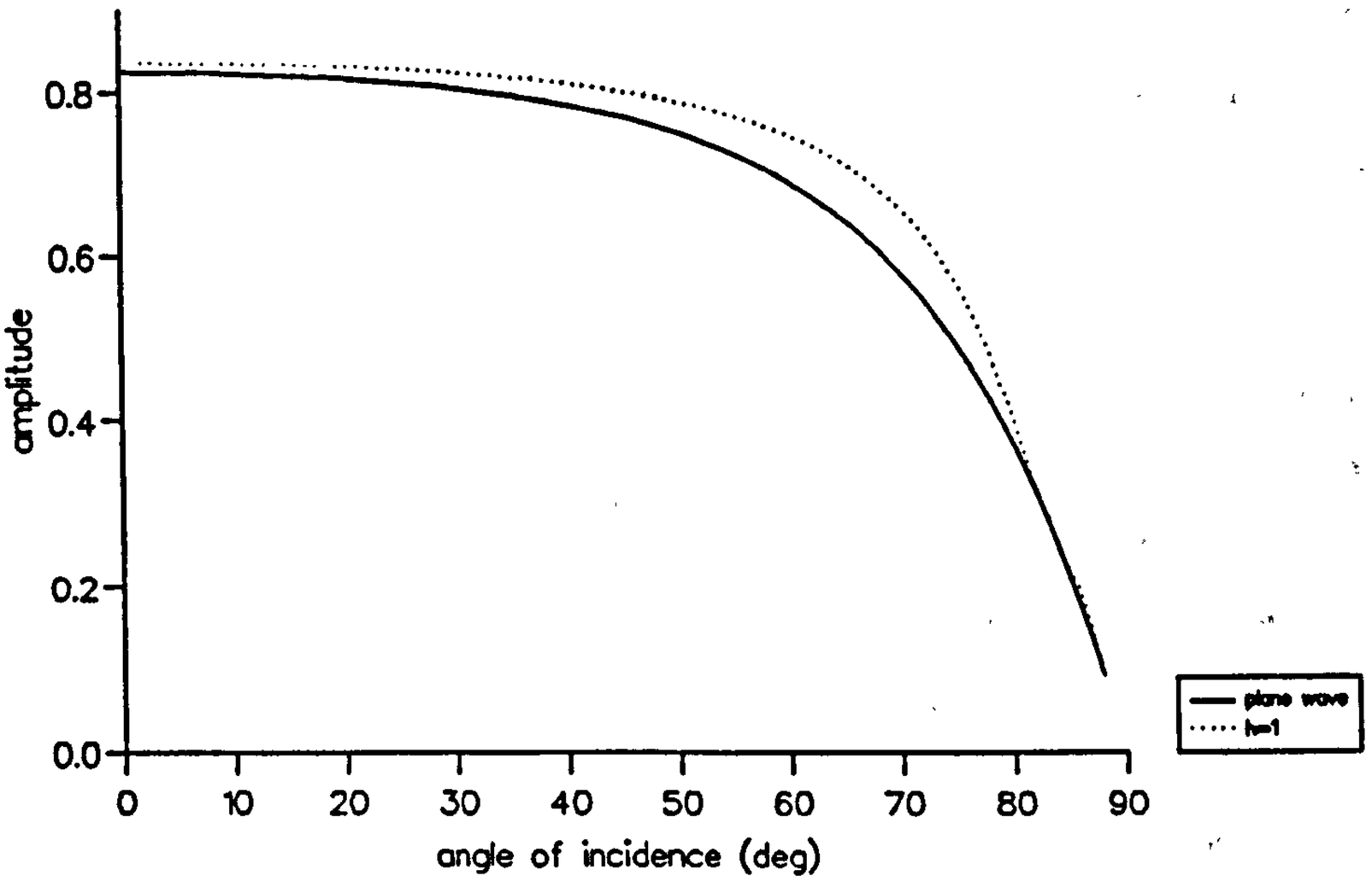

Figure 6.12 Amplitudes of the transmission coefficients of spherical waves for pressure incident in water on a water-kerosene interface for different source heights, h compared with those for plane wave incidence. The curves for $h = 5$ and $h = 10$ coincide with that for plane wave. Frequency 1000 Hz.

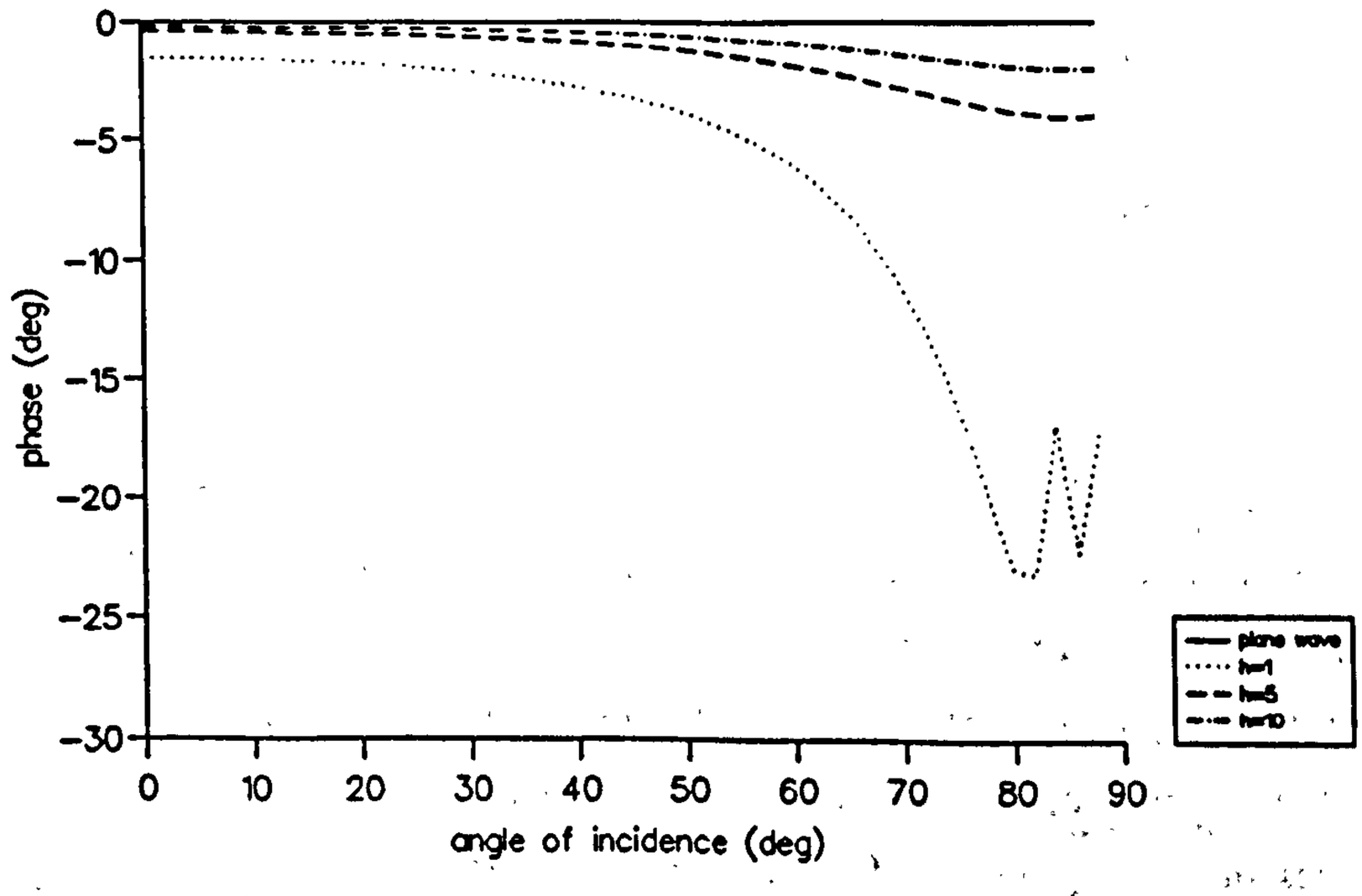

Figure 6.13 Phases of the transmission coefficients of spherical waves for pressure incident in water on a water-kerosene interface for different source heights, h compared with those for plane wave incidence. Frequency 1000 Hz.

to the following discussion.

An interesting feature is shown in Figures (6.6) and (6.7), i.e., for large angles of incidence the reflection coefficient becomes oscillatory. An explanation of the oscillation may be obtained from the description of spherical wave incidence at a plane interface suggested by Doak [66] (also see [49]). Doak points out that when a spherical wave is incident at a plane interface with a medium having a higher sound speed than the medium containing the source, there is a diffracted wavefront ahead of the totally reflected portion of the reflected wavefront; there is a diffracted wave everywhere behind this diffracted wavefront which is composed of contributions from the initially transmitted wave, and therefore the field in the source medium has three components: the incident wave, the reflected wave (including its totally reflected portion), and the diffracted wave (see Fig.4.8 in [49] for incidence of a spherical pulse). The oscillation of the reflection coefficient may be due to the interference between the reflected and diffracted waves. It should be mentioned that we have attempted to study the possibility of such interference by decomposing the reflected wave term (6.15) and some results are given in Appendix (E). The positive phases of the reflection and transmission coefficients may also be the effect of the diffracted wave.

In the case of a water-kerosene interface, (Figures (6.10) to (6.13)), the coefficients for spherical waves reduce to that for a plane wave rapidly and apparently very nearly monotonically with increasing source height.

As in the case of plane waves, it can be seen from the definition (6.4), that if the solution satisfies the boundary conditions the continuity of the energy flux in the z-direction is automatically guaranteed. We have seen earlier that the direct wave satisfies the law of energy conservation. With the reflecting/transmitting surface being $z = 0$ and the point source at some point $z = h(> 0)$, the reflected wave satisfies the wave equation with no sources in the region $z > 0$ and accordingly its time average energy flux is solenoidal in this region, so that its time average energy is conserved there. Similarly the transmitted wave satisfies the wave equation with no sources in the region $z < 0$ and accordingly its time average energy flux is solenoidal

in this region, so that its time average energy is conserved there [66].

To test the numerical integration procedures against those conclusions, consider the point source to be at $z = 1$m, and suppose that there are two planes parallel to $z = 0$: in the source medium at $z = 0.5$m (between the source and the reflecting/transmitting plane), and at $z = 1.2$m (above the source plane). In the transmission medium, consider a plane at $z = 0$, (just below the reflecting/transmitting plane) and one at $z = -1$m. The time average powers of the reflected wave crossing the plane at $z = 0.5$m and the plane $z = 1.2$m should be the same for a solenoidal energy flux, as should those of the transmitted wave crossing the planes $z = 0$ and $z = -1$m. The sum of the reflected and transmitted powers should be equal to half of the total time average output power generated by the point source.

The time average power crossing an area of radius r on each such plane is given by the integration of the time average energy flux over the area:

$$\dot{E} = \int_0^r < I_z > 2\pi x dx \tag{6.22}$$

The z-component of the energy flux, $< I_z >$, is defined by (6.4).

In integrations with respect to x, the NAG routine D01baz was used for the finite ranges $0 \leq x \leq r$. It is very difficult to evaluate the integral on a semi-infinite interval since for large values of r, the integral for the pressure, or that for the velocity, becomes very unreliable (due to the oscillatory natures of the integrands), the situation being worse than that we have found in Chapter 5 for a spherical wave in infinite space, perhaps, as a result of the integrand coefficients being involved. For the calculations of pressure and velocity we used the routines D01ajf, D01atf, D01amf. The results for the reflected and transmitted waves separately are shown in Table (6.2). The calculated powers in Table (6.2) are normalized to half of the total time average output power generated by the point source. By examining the reflected wave powers, it can be seen that with increasing radius, the difference between the two values for the areas of the same radius decreases. The values for the transmitted wave start from small values and increase as the integration area becomes larger. The transmitted power at the interface has one peak and the power crossing the surface at $z = -1$m has two peaks; after the peak values, the

reflection						
radius r(m)	20	100	200	300	500	1000
$z = 0.5$	0.4261	0.5311	0.5438	0.5480	0.5514	0.5539
$z = 1.2$	0.3926	0.5240	0.5403	0.5457	0.5500	0.5532
transmission						
radius r(m)	2	6	8	12	20	1000
$z = 0.0$	0.4946	0.5372	0.4834	0.4460	0.4451	0.4435
$z = -1$	0.2337	0.3986	0.4456	0.4429	0.4438	0.4435
sum of the reflected and transmitted powers for $r = 1000$						
$(z = 0.5) + (z = 0.0) = 0.9974$						
$(z = 0.5) + (z = -1) = 0.9974$						
$(z = 1.2) + (z = 0.0) = 0.9967$						
$(z = 1.2) + (z = -1) = 0.9967$						

Table 6.2 Calculation of time average powers crossing plane surfaces for the reflected wave and the transmitted wave. The kerosene-water interface is at $z = 0$, frequency 1000 Hz, source height 1m

power values for both surfaces approach the same constant. Comparing the reflected and transmitted wave powers, we can see that the reflected powers converge more slowly than the transmitted powers. For the reflected powers the values at $r = 500$m have two digits in agreement with the last values (at $r = 1000$m) but for the transmitted powers at $r = 12$m for $z = 0$ or at $r = 8$m for $z = -1$m, the values already converge to the two digit accuracy. The energy integration for the transmitted wave power on the surface at $z = -1$m is shown in Figure (6.14). The sum of the reflected wave power and the transmitted wave power at $r = 1000$m is about 0.997. Since the accuracy of the integrations is reduced at large values of r because of the oscillation of the integrands, and in view of the accuracy that we could achieve in Chapter 5 for a spherical wave in infinite space, we can see that our numerical solutions are in good agreement with the law of energy conservation.

The fact that the values for the transmitted wave decrease after the peak value implies the existence of "backward waves", i.e., there is energy propagating in the direction opposite to that of the transmission of the total integrated power, which is along the negative z-axis. For spherical wave re-

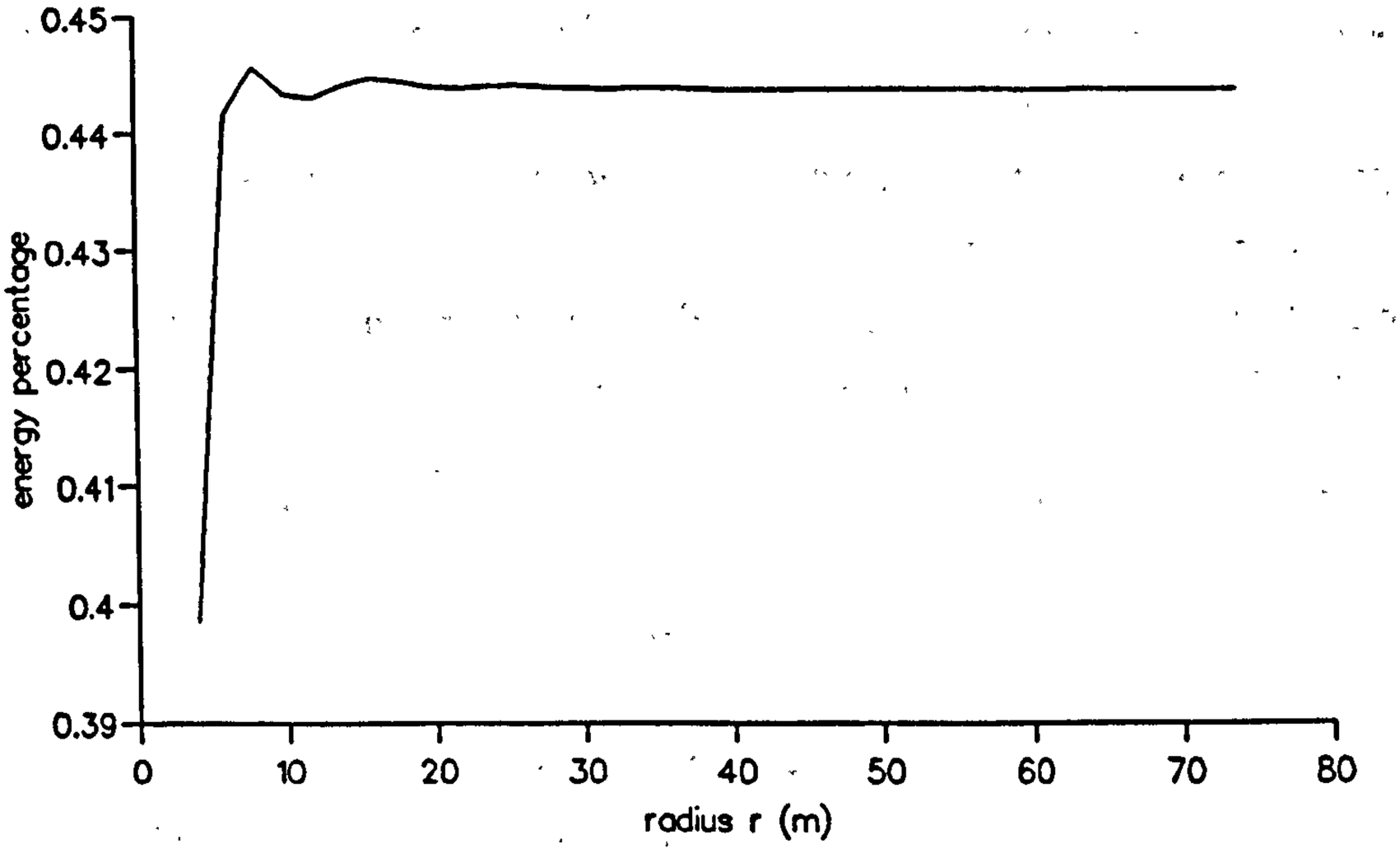

Figure 6.14 The time average power of the transmitted spherical wave crossing an area of radius r of the surface at $z = -1$ in the water, the kerosene-water interface is at $z = 0$, and the source is at a height of 1m in the kerosene.

flection at an acoustically hard boundary (air-water or kerosene-water), the calculation of the local time average energy flux component above the point source also shows such a "backward wave" feature in some regions. The "backward waves" occur near the source as well as at some distance away from the source. For example, in the case of air-water boundary, on the plane, $z = 2$m above the point source which is in the air, at $h = 1$m, the negative time average energy flux occurs at $r = 2.7$m and $r = 23.3$m.

The reflection and transmission of energy at the interface has been examined further numerically. Similar to the case of plane waves, the critical angle of the total reflection for a spherical wave is defined as the angle at which the energy total reflection just takes place when the angle of incidence is increased from zero degrees, and it can be determined by calculating the transmitted time average energy flux in the z-direction against the angle of incidence, and the angle at which the sign of the energy flux first changes gives the critical angle. It is found that the total energy reflection for a spherical wave does not take place at the critical angle for a corresponding plane

wave. In other words, the critical angle for a spherical wave is different from that of the corresponding plane wave. There is a displacement and it depends not only on the combination of the materials but also on the height of the source. The calculation of the critical angle for spherical waves incident on a kerosene-water interface from different source heights is shown in Table (6.3). From Table (6.3) we can see that as the height of source increases, the

Source height (m)	1	21	41	61	81	∞(plane wave)
Critical angle (deg)	69.8	64.6	63.2	62.6	62.2	59.8

Table 6.3 Critical angles

critical angle decreases. The critical angle for the total reflection of a plane wave is 59.8 degrees and the calculated critical angles for spherical waves decrease monotonically to this angle with increasing source height. It should be mentioned that, beyond the critical angle, at some angles of incidence there is some net time average transmitted energy but no net transmission at other angles. This may be caused by the interference between the incident and diffracted waves.

6.3 Interfaces between fluid and solid.

The boundary conditions at an interface between a fluid and a solid are

$$\left.\begin{array}{rcl} w_1 & = & w_2 \\ -p_1 & = & t_{zz} \\ t_{zr} & = & 0 \end{array}\right\} \text{at } z = 0. \tag{6.23}$$

We consider the case where the incident wave is in the fluid. The Sommerfeld type solution can be found again in the book by Ewing, *et al.* [11] and is

$$\varphi_1 = \int_0^\infty \frac{J_0(r\xi)e^{-|z-h|q_1}\xi}{q_1}\,d\xi + \int_0^\infty R\frac{J_0(r\xi)e^{-(h+z)q_1}\xi}{q_1}\,d\xi \tag{6.24}$$

in the fluid, and

$$\phi_l = \int_0^\infty T_l\frac{J_0(r\xi)e^{-hq_1-zq_2}\xi}{q_l}\,d\xi, \tag{6.25}$$

$$\psi_t = \int_0^\infty T_t \frac{J_0(r\xi)e^{-hq_1 - zq_2}\xi}{q_t}\, d\xi \tag{6.26}$$

in the solid, where h is the source height, $q_1 = \sqrt{\xi^2 - \kappa_1^2}$, $q_l = \sqrt{\xi^2 - \kappa_l^2}$, $q_t = \sqrt{\xi^2 - \kappa_t^2}$, and the integrand coefficients are given by

$$R = \frac{\rho_2 q_1((2\xi^2 - \kappa_t^2)^2 - 4q_l q_t \xi^2) - (\kappa_t^4 q_l \rho_1)}{\rho_2 q_1((2\xi^2 - \kappa_t^2)^2 - 4q_l q_t \xi^2) + (\kappa_t^4 q_l \rho_1)}, \tag{6.27}$$

$$T_l = \frac{2(2\xi^2 - \kappa_t^2) q_1 \kappa_t^2 \rho_1 \rho_2}{\rho_2 q_1((2\xi^2 - \kappa_t^2)^2 - 4q_l q_t \xi^2) - (\kappa_t^4 q_l \rho_1)}, \tag{6.28}$$

$$T_t = -\frac{4\xi q_1 \kappa_t^2 \rho_1 \rho_2}{\rho_2 q_1((2\xi^2 - \kappa_t^2)^2 - 4q_l q_t \xi^2) - (\kappa_t^4 q_l \rho_1)}. \tag{6.29}$$

An incident spherical wave at the surface of a solid always generates two types of waves in the solid. ϕ_l is a longitudinal wave and ψ_t a transverse wave. The integrand coefficients R, T_l and T_t are determined by the three boundary condition equations. The new form solution for the reflected wave is

$$\varphi_r = \int_{i\kappa_1}^\infty R J_0(r\sqrt{x^2 + \kappa_1^2}) exp(-(h+z)x)\, dx, \tag{6.30}$$

where the integrand coefficient R is defined by (6.27) with $\xi = \sqrt{x^2 + \kappa_1^2}$, $q_1 = x$, $q_l = \sqrt{x^2 + \kappa_1^2 - \kappa_l^2}$ and $q_t = \sqrt{x^2 + \kappa_1^2 - \kappa_t^2}$.

Again we hypothesize a form of complex conjugate solution based on the integral representation with the Hankel function (1.5), which is

$$\begin{aligned} \varphi_1 &= i\int_0^\infty H_0^{(1)}(|z-h|\sqrt{\kappa_1^2 - x^2}) cos(rx)\, dx \\ &+ i\int_0^\infty R H_0^{(1)}((h+z)\sqrt{\kappa_1^2 - x^2}) cos(rx)\, dx \end{aligned} \tag{6.31}$$

in a fluid, and

$$\phi_l = i\int_0^\infty T_l H_0^{(1)}((h-z)\sqrt{\kappa_l^2 - x^2}) cos(rx)\, dx, \tag{6.32}$$

$$\psi_t = i\int_0^\infty T_t H_0^{(1)}((h-z)\sqrt{\kappa_t^2 - x^2}) cos(rx)\, dx \tag{6.33}$$

in a solid, where $\eta_1 = \sqrt{\kappa_1^2 - x^2}$, $\eta_l = \sqrt{\kappa_l^2 - x^2}$, $\eta_t = \sqrt{\kappa_t^2 - x^2}$,

$$R = \frac{A_1 + A_2}{A_1 - A_2}, \tag{6.34}$$

$$T_l = \frac{2H_1^{(1)}(h\eta_1)H_0^{(1)}(h\eta_1)h\eta_1\kappa_t^2\rho_1(2H_1^{(1)}(h\eta_t)\eta_t + H_0^{(1)}(h\eta_t)h(2x^2-\kappa_t^2))}{(A_1-A_2)\rho_2}, \tag{6.35}$$

$$T_t = -\frac{4H_1^{(1)}(h\eta_1)H_0^{(1)}(h\eta_1)H_1^{(1)}(h\eta_l)h^2x\eta_1\eta_l\kappa_t^2\rho_1}{(A_1-A_2)\rho_2}. \tag{6.36}$$

Here

$$\begin{aligned} A_1 &= 4H_1^{(1)}(h\eta_1)H_1^{(1)}(h\eta_l)H_1^{(1)}(h\eta_t)\eta_1\eta_l\eta_t(h^2x^2+1) \\ &- 2H_1^{(1)}(h\eta_1)H_1^{(1)}(h\eta_l)H_0^{(1)}(h\eta_t)h\eta_1\eta_l\kappa_t^2 \\ &- 2H_1^{(1)}(h\eta_1)H_0^{(1)}(h\eta_l)H_1^{(1)}(h\eta_t)h\eta_1\eta_t(2x^2-\kappa_t^2) \\ &+ 4H_1^{(1)}(h\eta_1)H_0^{(1)}(h\eta_l)H_0^{(1)}(h\eta_t)h^2\eta_1(2x^2-\kappa_t^2)^2, \end{aligned} \tag{6.37}$$

$$A_2 = H_0^{(1)}(h\eta_1)H_1^{(1)}(h\eta_l)H_0^{(1)}(h\eta_t)h^2\eta_l\kappa_t^4\frac{\rho_1}{\rho_2}. \tag{6.38}$$

We have calculated pressure contours in the fluid. The graphical representation of the wave field in the solid is more complicated, since the stress is a tensor. The calculation of the stress field or displacement is still possible but it will require a large CPU time, and hence we shall not present any discussion of the wave field in the solid.

We found that numerical integrations using integrals (6.30) and (6.31) give very similar results if there is a large difference in the properties of the two media; otherwise there is a significant difference between the two numerical integrations. An example of calculations obtained from (6.30) and (6.31) is given in Table (6.4). It can be seen that for an air-steel interface, the difference between the two solutions is less than 0.01 dB, and the difference for a water-steel interface is about 0.5 dB. In a small range, pressure contours calculated from solutions (6.30) and (6.31) for an air-water interface give almost an identical picture.

Figure (6.15) shows calculated pressure contours above the air-steel interface, and Figure (6.16) shows those above the water-steel interface. The contours are presented in two-dimensional form. We have also calculated the pressure contours in air above a rigid boundary and in water above a rigid boundary. We find that the contours in air above steel and in air above a rigid boundary are almost identical. Similarly, the contours in water above steel and in water above a rigid boundary cases are indistinguishable. We have

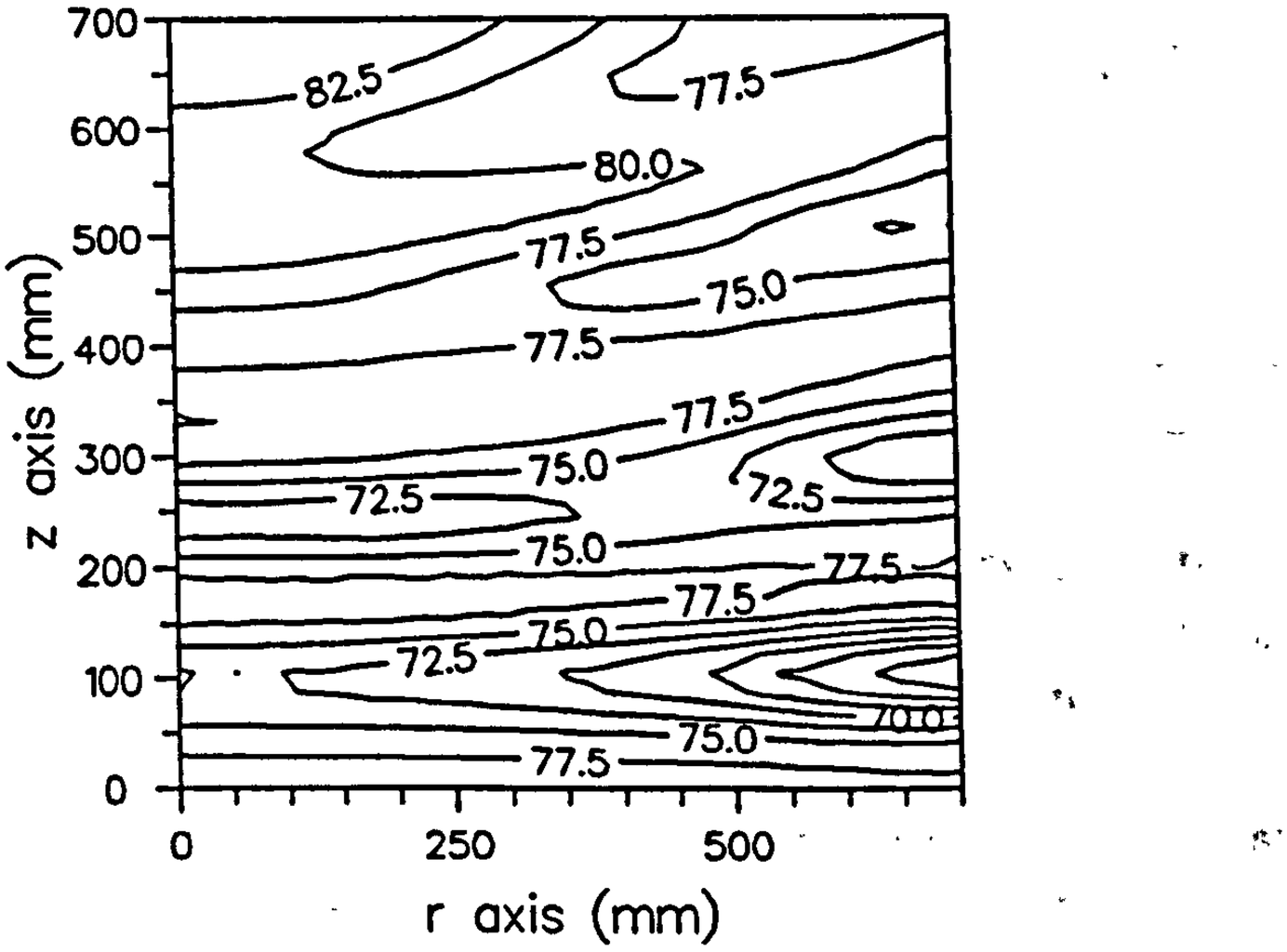

Figure 6.15 Two-dimensional pressure level contours (dB) for a spherical wave in air incident on a rigid boundary, or at an air-steel interface. A point source is located at 1m on the z-axis and the interface is at 0m. Frequency 1000 Hz.

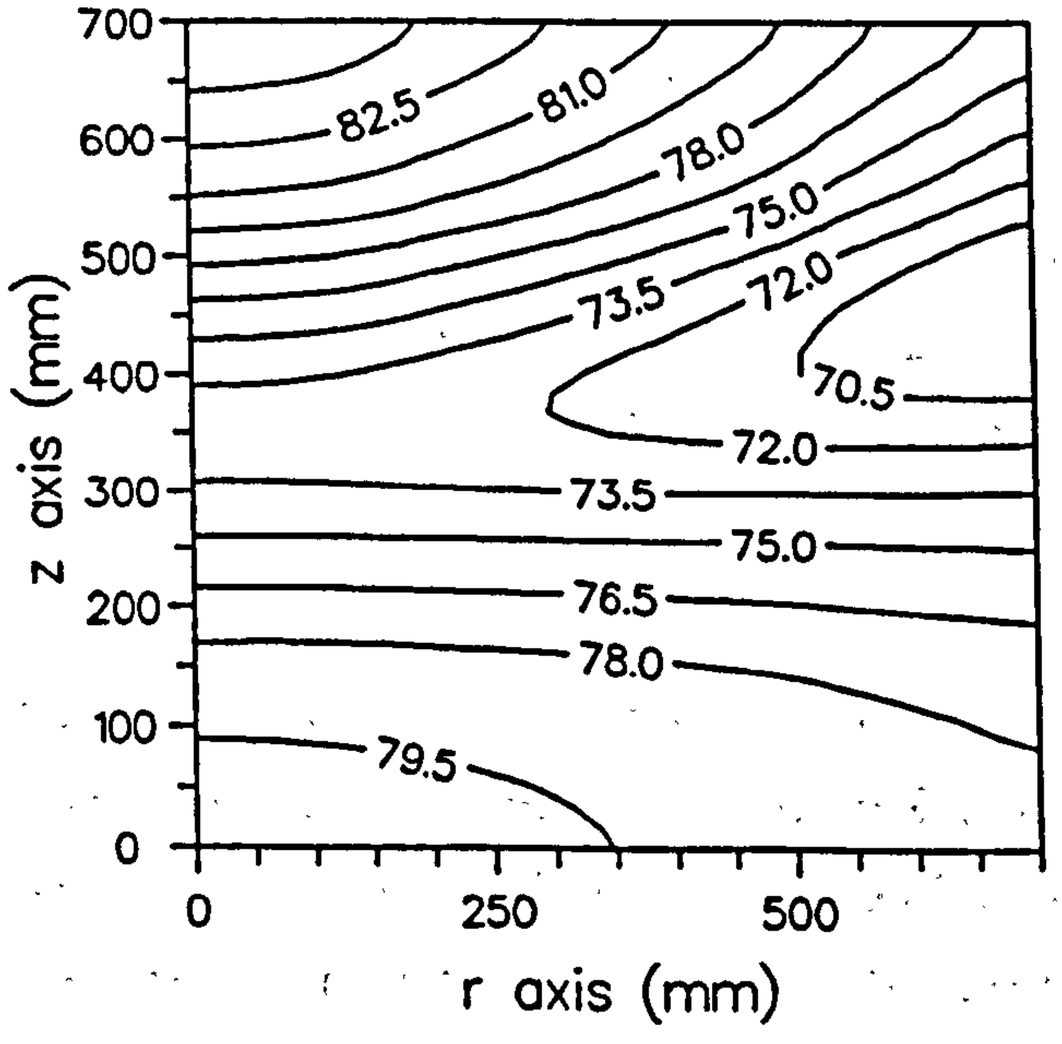

Figure 6.16 Two-dimensional pressure level contours (dB) for a spherical wave in water incident on a rigid boundary, or at a water-steel interface. A point source is located at 1m on the z-axis and the interface is at 0m. Frequency 1000 Hz.

Air-Steel, source height $h = 1$m						
coordinates (m)	(0,0)	(0,.05)	(0,.1)	(.05,0)	(.05,.05)	(.05,.1)
(6.30)	57.520	57.509	57.479	52.877	52.880	52.889
(6.31)	57.521	57.510	57.479	52.867	52.871	52.884
Water-Steel, source height $h = 2$m						
coordinates (m)	(0,0)	(0,.05)	(0,.1)	(.05,0)	(.05,.05)	(.05,.1)
(6.30)	45.903	45.901	45.893	46.487	46.484	46.476
(6.31)	46.411	46.407	46.396	47.049	47.045	47.034

Table 6.4 Comparison between calculations for the pressure using (6.30) and (6.31). The direct wave was calculated from the non-integral expression for the both cases, frequency 1000 Hz.

calculated the pressure contours above other fluid-solid (metal) interfaces, and have found similar results. Therefore the theoretical model of spherical wave propagation in a fluid above a rigid boundary can be used as a very good approximation for propagation above a fluid-metal interface in many circumstances.

If we concentrate on the top left quarter of Figure (6.3) (noting that only the upper half is above the boundary in Figure (6.3)), and compare it with Figure (6.15), we find that they are very similar. This means that even for an air-water interface, considering the water as a rigid boundary for waves in air can be a good approximation. It is obvious from Figure (6.4) that water cannot be treated as a rigid boundary for waves in kerosene.

The reflection coefficient defined by

$$R_p = \varphi_r/\varphi_i \tag{6.39}$$

has been calculated for a water-steel interface. Solution (6.30) was used for the calculation but we found difficulty in the integration at some large values of r. The difficulty is caused by a singularity in the integrand between $(0,\ \kappa_1)$. Although, the routine D01ajf is designed to handle singularities it is impossible to obtain an adequate result. The integrand changes too sharply around the singularity. This singularity is caused by a zero in the denominator of the integrand coefficient for the reflection (6.27). In order to overcome this difficulty the location of the zero was determined by using

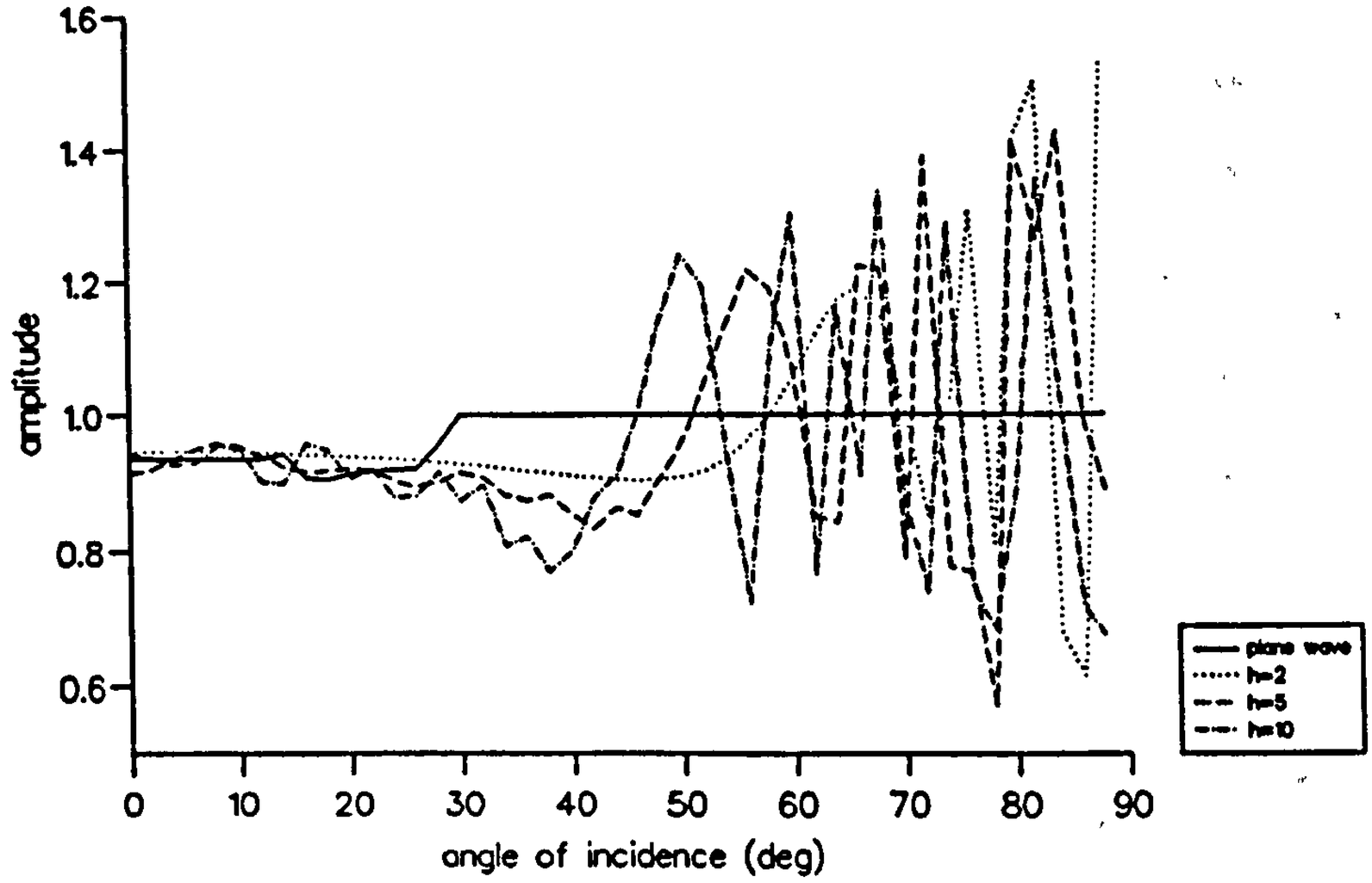

Figure 6.17 Comparison between amplitudes of the reflection coefficients of spherical pressure waves in water incident on a water-steel plane interface for different source heights, and, for a plane wave. Frequency 1000 Hz.

routine C05agf and then the interval was split up at this point. Another routine D01ahf was used for the sub-ranges.

The amplitudes and phases of the coefficient against the angles of incidence are shown in Figures (6.17) and (6.18) for various heights of the source and are compared with the case of a plane wave. In Figure (6.17), for small angles of incidence, all three curves for spherical waves are very close to the curve for a plane wave; the small oscillations may be due to the stimulation of the transverse wave in the solid. At large angles of incidence, the amplitudes of the spherical waves oscillate rapidly about the value of one. If we examine the curves carefully, we notice that the first main peak for a spherical wave occurs close to the point where the amplitude for a plane wave becomes one, when the height of source increases. Figure (6.18) has similar features. In Figure (6.18) the phase for the plane waves is plotted with a positive sign to make comparison easier. As in the case of the fluid-fluid interface, the oscillation of the reflection coefficient for a spherical wave and the phase of the reflection coefficient for a spherical wave having a different sign from

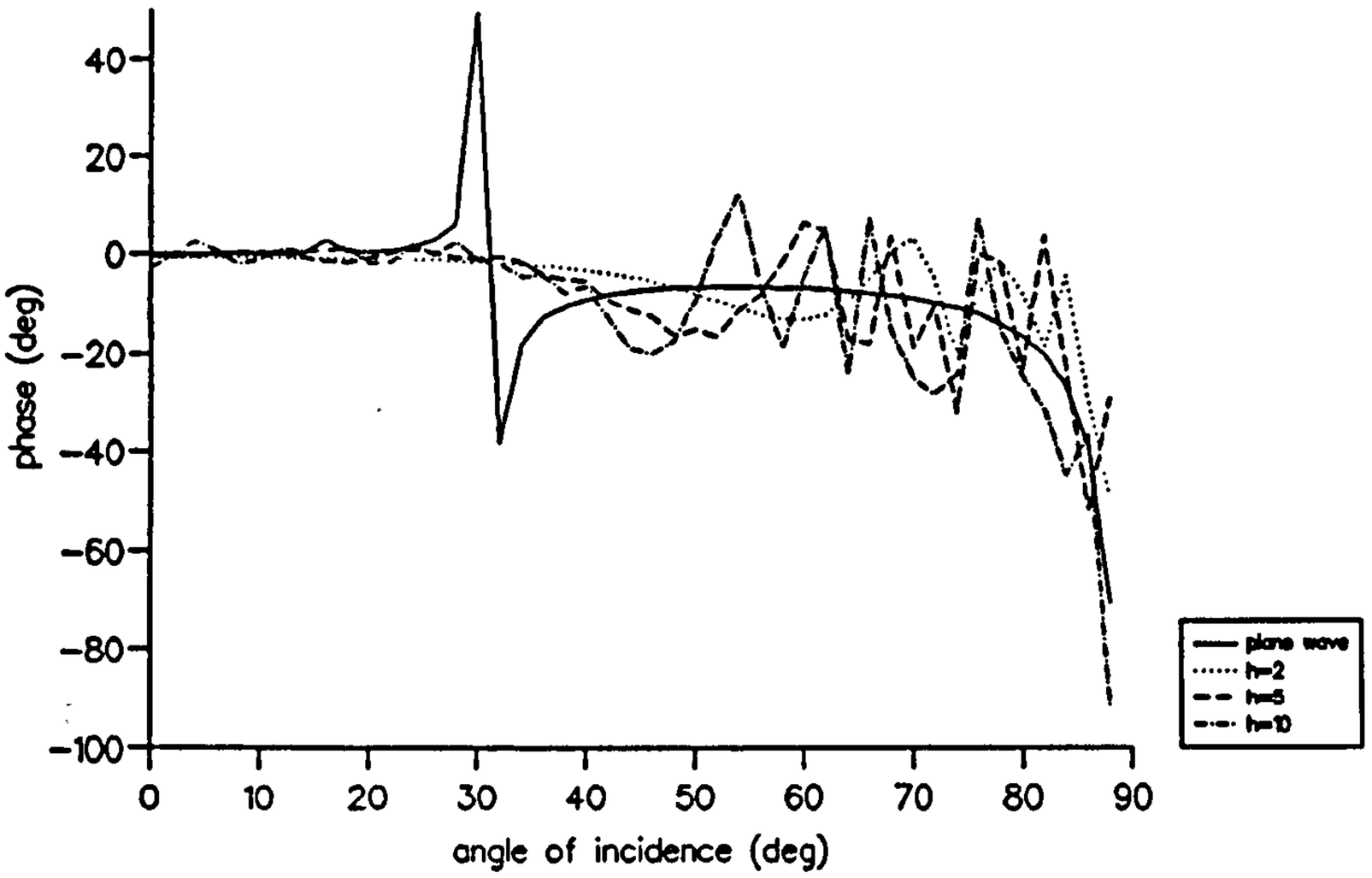

Figure 6.18 Comparison between phases of the reflection coefficients of spherical pressure waves in water incident on a water-steel plane interface for different source heights, and, for a plane wave. Frequency 1000 Hz.

that of a plane wave are probably due to the diffracted wave in the medium containing the source.

From the results described above (particularly Figures (6.6) and (6.17)) we find that when the boundary is acoustically harder than the propagation medium supporting an incident wave, the amplitude of the reflected wave is predicted to be greater than that of the incident wave at some large angles of incidence, but the amplitude for plane waves is always less than one, and again the spherical wave reflection coefficient is oscillatory about that for a plane wave. Also in the case of a hard boundary, the phases of reflected spherical waves and reflected plane waves have an opposite sign. These are the main differences between spherical waves and plane waves and they are probably due to the presence of the diffracted wave in the source medium in the case of spherical wave propagation.

6.4 Spherical waves in layered media

From an experimental point of view, the study of spherical wave propagation is especially important, since it is more easy to simulate a spherical wave source than a plane wave. Previously, we have considered spherical wave propagation in the cases of a two-medium system. The study of waves in a two-medium system has theoretical importance but it has a limited practical application. In this section, we shall study a more realistic case: that is, sound transmission through an infinite solid plate in a fluid with a point source located in the fluid.

The method for solving this problem is similar to that we have used in previous chapters, but the manipulation is little more complicated. A solution of the problem of spherical wave propagation in the fluid-solid-fluid system can be found in a paper by Piquette [46]. As we mentioned earlier he obtained some strange results from the numerical integration of the solution. He calculated the reflection coefficient of a spherical wave at the normal incidence angle on the interface between a fluid and a solid, and the transmission coefficient of a spherical wave on the solid-fluid interface also at the normal incidence angle. His numerical results show that, for some material combinations, the reflection coefficient or the transmission coefficient can be greater than one. He called this phenomenon "overpressure". It can be seen from Chapter 5 that this so called "overpressure" does not happen for a plane wave. Piquette carried out an experiment intended to verify his numerical results; however he could not find the 'overpressure' experimentally. In this chapter we are going to show numerically that the reflection and transmission coefficients for a spherical wave at normal incidence are very similar to those for a normally-incident plane wave.

The boundary conditions at an interface between a fluid and a solid were given in the preceding section. Those conditions must be satisfied at both surfaces of the solid plate. We choose the z-axis to be normal to the plate. The origin is on one surface of the plate and the other surface is at $z = -l$.

A point source is located at $(0,\ h)$. The boundary conditions are

$$w_1 = w_2, \qquad p_1 = t_{zz}, \qquad t_{zx} = 0, \qquad \text{at } z = 0,$$

$$w_2 = w_3, \qquad p_3 = t_{zz}, \qquad t_{zx} = 0, \qquad \text{at } z = -l.$$

The solution obtained by using Lamb's integral can be found in the paper by Piquette [46], and is in a slightly different form,

$$\varphi_1 = \int_0^\infty \frac{J_0(r\xi)e^{-|h-z|q_1\xi}}{q_1}\,d\xi + \int_0^\infty R\frac{J_0(r\xi)e^{-(h+z)q_1\xi}}{q_1}\,d\xi, \tag{6.40}$$

$$\phi_l = \int_0^\infty L_a\frac{J_0(r\xi)e^{-zq_l\xi}}{q_l}\,d\xi + \int_0^\infty L_b\frac{J_0(r\xi)e^{+zq_l\xi}}{q_l}\,d\xi, \tag{6.41}$$

$$\psi_t = \int_0^\infty T_a\frac{J_0(r\xi)e^{-zq_t\xi}}{q_t}\,d\xi + \int_0^\infty T_b\frac{J_0(r\xi)e^{+zq_t\xi}}{q_t}\,d\xi, \tag{6.42}$$

$$\varphi_3 = \int_0^\infty T\frac{J_0(r\xi)e^{-zq_3\xi}}{q_3}\,d\xi, \tag{6.43}$$

where R, L_a, L_b, T_a, T_b, and T are the integrand coefficients. ϕ_l and ψ_t represent the longitudinal and transverse wave potentials in the plate, respectively. The first term in both ϕ_l and ψ_t corresponds to a wave with a phase moving in the positive z-direction and the second term corresponds to one moving in the negative z-direction. The integrand coefficients are determined by the boundary conditions. Firstly from the boundary conditions we obtain six integral equations; the sufficient condition for the existence of solutions of the integral equations gives a system of six algebraic equations with R, L_a, L_b, T_a, T_b, and T as unknowns. After solving this system of equations we obtain the integrand coefficients. Basically solutions (6.40) to (6.43) are the same as those given by Piquette, except that the integrand coefficients differ by exponential factors. The integrand coefficients are very complicated. Piquette did not present them in his paper. Our version of them is given in Appendices (B) and (D). The new form of solution obtained by transformation for the reflected wave is similar to the solution (6.30) in the case of a fluid-solid interface except for a different integrand coefficient for reflection.

As in (6.19) and (6.20), the reflection coefficient in the fluid is defined by the pressure ratio of the reflected wave to the incident wave φ_r/φ_i, where

φ_r represents the second term in (6.40), φ_i the first term in (6.40), and the transmission coefficient in the fluid is defined by the pressure ratio of the transmitted wave and the incident wave, $(\rho_3\varphi_3)/(\rho_1\varphi_i)$.

One can also investigate the alternative form for the complex conjugate solution of the problem using the integral representation (1.5) which has the Hankel function in the integrand, resulting in the following potential forms:

$$\begin{aligned}\varphi_1 &= i\int_0^\infty H_0^{(1)}(|z-h|\sqrt{\kappa_1^2-x^2})cos(rx)\,dx \\ &+ i\int_0^\infty RH_0^{(1)}((h+z)\sqrt{\kappa_1^2-x^2})cos(rx)\,dx, \qquad (6.44)\end{aligned}$$

$$\begin{aligned}\phi_l &= i\int_0^\infty L_a H_0^{(1)}((h-z)\sqrt{\kappa_l^2-x^2})cos(rx)\,dx \\ &+ i\int_0^\infty L_b H_0^{(1)}((h+d+z)\sqrt{\kappa_l^2-x^2})cos(rx)\,dx, \qquad (6.45)\end{aligned}$$

$$\begin{aligned}\psi_t &= i\int_0^\infty T_a H_0^{(1)}((h+d-z)\sqrt{\kappa_t^2-x^2})cos(rx)\,dx \\ &+ i\int_0^\infty T_b H_0^{(1)}((h+d+z)\sqrt{\kappa_t^2-x^2})cos(rx)\,dx, \qquad (6.46)\end{aligned}$$

$$\varphi_3 = i\int_0^\infty TH_0^{(1)}((h-z)\sqrt{\kappa_1^2-x^2})cos(rx)\,dx. \qquad (6.47)$$

Again the integrand coefficients may be determined by the boundary conditions. The coefficient elements for the boundary equations are given in Appendix (C).

By use of NAG integration routines, the data for plotting pressure contours near the origin has been calculated from both equations (6.40) and (6.44). The numerical integrations from equations (6.40) and (6.44) give very similar results, the difference being normally less than 1 dB for media having different acoustical properties. However, if the media are acoustically similar, the difference in the predicted values of the pressure increases. An example of the calculations based on (6.40) and based on (6.44) is given in Table (6.5). Comparing Tables (6.5) and (6.4) shows that the calculations for air-steel-air and air-steel are very similar, and in fact they both are similar to the results for the rigid reflection.

Air-Steel-Air, source height $h = 1$ m, plate thickness l=0.008m						
coordinates	(0,0)	(0,.05)	(0,.1)	(.05,0)	(.05,.05)	(.05,.1)
(6.40)	57.519	57.509	57.477	52.865	52.869	52.879
(6.44)	57.520	57.509	57.477	52.867	52.870	52.880
Water-Steel-Water, source height $h = 2$m, plate thickness l=0.01m						
coordinates	(0,0)	(0,.05)	(0,.1)	(.05,0)	(.05,.05)	(.05,.1)
(6.40)	45.048	45.143	45.417	44.659	44.758	45.045
(6.44)	51.265	51.262	51.253	51.079	51.076	51.068

Table 6.5 Comparison between calculations of total pressures using transformed equation (6.40) and (6.44) at various coordinates. The direct wave was calculated from the functional expression for both cases, frequency 1000 Hz.

The integration of (6.40) uses less CPU time than that of (6.44), but sometimes the integration of (6.40) had convergence difficulties. As was the case with a fluid-solid interface, the difficulties are caused by a singularity in the integrand coefficient and the poor behaviour of the integrand around the singularity. For the reflection, the singularity is located between $(0,\ \kappa_1)$. and it is between $(\kappa_1,\ \infty)$ for the transmission. In order to overcome the difficulties the first thing is to pinpoint the location of the singularity. We have used routine C05agf to locate the zero in the denominator of the integrand coefficients for the reflection and the transmission respectively. For the reflection , the interval was split at the singularity k_s' into two sub-intervals $(0,\ k_s')$ and $(k_s',\ k_s' + 10^{-3})$; and two sub-intervals $(\kappa_1,\ k_s")$ and $(k_s",\ k_s" + 10^{-3})$ for the transmission.

The integrand changes sign in these two sub-intervals; for example, if in the interval $(\kappa_1,\ k_s")$ the integrand is negative, it must be positive in $(k_s",\ k_s" + 10^{-3})$. However, the calculations with the routine D01ajf over the two sub-intervals were still very difficult to converge near the singularities, so we used the routine D01ahf instead.

D01ahf is more flexible, but less reliable in the sense that it uses few criteria for abnormal termination as described in Chapter 3. The calculated results were carefully checked by changing the relative tolerance t_r. The calculations for the reflected wave were very stable.

For the transmission, when choosing a large relative tolerance (e.g., $t_r =$

10^{-4}) it was found that the modulus of the transmission coefficient could be greater than 1 (in fact even greater than 2 or 3) for some materials at high frequencies (e.g., aluminum at $5000Hz$). If the specified accuracy is increased by using a smaller tolerance, the modulus reduces. However increasing the specified accuracy further (*e.g.*, $t_r = 10^{-12}$) led to deviation from unity again. In other words, the calculation was very unstable. When monitoring the process of the calculation it was found that in the interval (κ_1, k_s") the integrand was occasionally negative when it should be positive. This may be because the value of k_s" can only be obtained within the computer precision, and the adaptive routine required abscissae beyond the computer precision. For this reason, we have to avoid using a smaller interval around the singularity when a difficulty occurs. Since the integrand is a monotonic function, the method of "ignoring the singularity" can be convergent to the proper answer [75]. The calculation was actually performed on the intervals (κ_1, k_s" $- 10^{-15}$) and (k_s" $+ 10^{-15}$, k_s" $+ 10^{-3}$). The tolerance for D01ahf was chosen to be as small as possible for different materials, and the largest tolerance was 10^{-9}.

As in the cases in previous sections, the pressure contours were calculated for plotting on the $r-z$ coordinate plane with the interval between calculation points being 50mm in both the r and z-directions. The pressure contours obtained by using solution (6.40) are almost identical to those obtained by using the solution for spherical wave reflection at a rigid boundary and the solution for spherical wave reflection at an interface between a fluid and a solid. Figure (6.19) is for 500 Hz. The calculation for 1000 Hz gives the contour curves which are the same as those in Figure (6.1).

The reflection coefficients at the centre point of the plate on the source side and the transmission coefficients at the centre point of the opposite side were calculated for various material combinations and they are shown in Table (6.6). The value of the transmission coefficient for the water-steel-water at 5000 Hz was obtained over the whole integration interval, and if we ignore the small interval around the singularity the result is 0.8389. By comparing Table (6.6) with Table (4.2) for plane waves, it can be seen that the reflection and transmission coefficients for spherical waves are quite similar to those

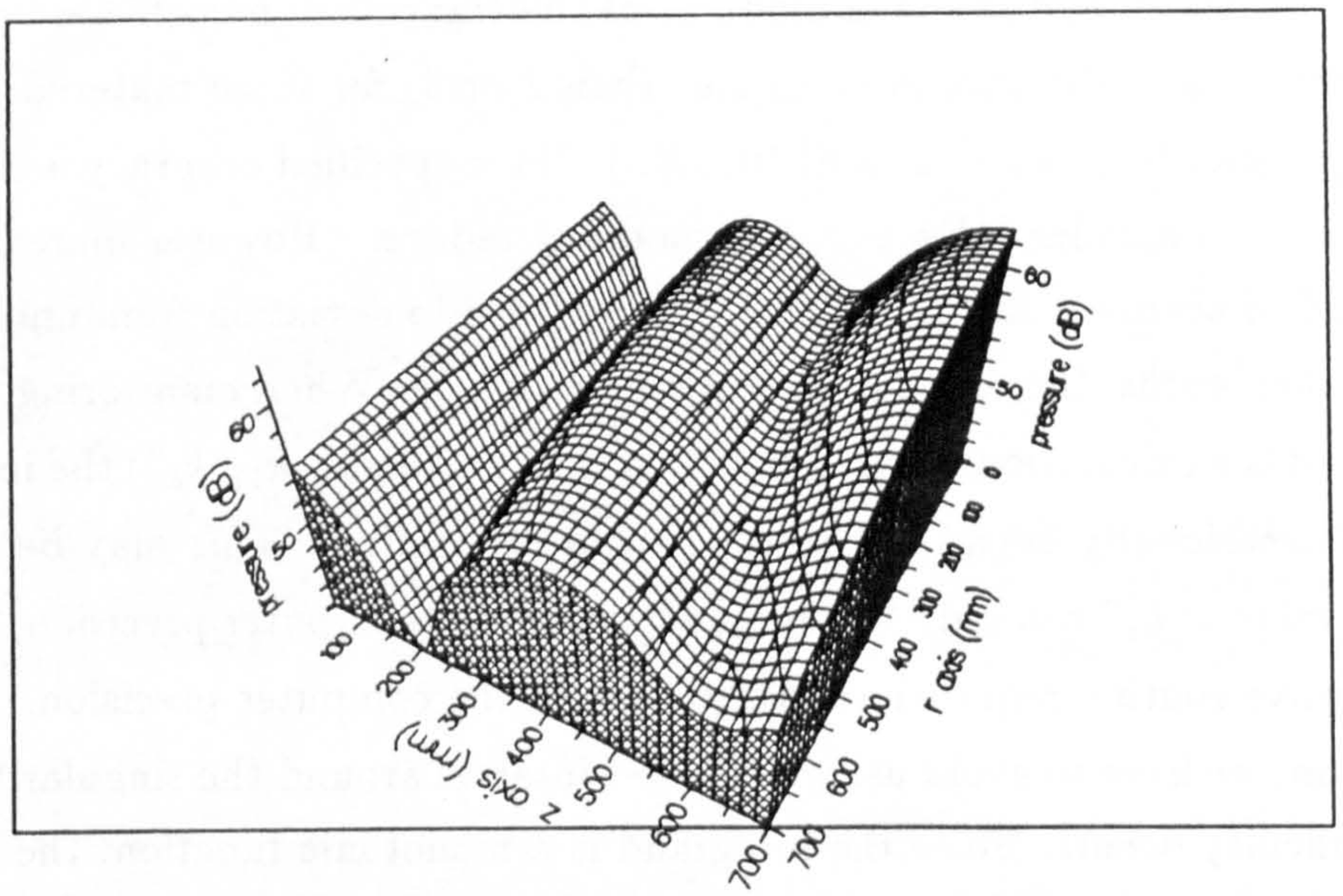

Figure 6.19 Pressure contours for spherical wave reflection at the source side boundary of an air-steel-air combination. frequency: 500 Hz, source height: 1m, thickness of plate: 0.008m.

for plane waves. In general the moduli of the reflection and transmission coefficients for spherical waves are less than those for plane waves except that the moduli of the transmission coefficients at 5000 Hz are greater. It is thought that, from the physical point of view, the results for the reflection and for the transmission at 1000 Hz are reasonable because of spherical spreading, and the results for transmission at 5000Hz may be less reliable: i.e., the values could be too large. To check the results at 5000 Hz, a higher precision program than that being used is needed. Nevertheless, we do not find the so called "overpressures". The pressures of reflection and transmission are always less than the incident pressure. It is likely that the "overpressures" predicted by Piquette were the results of computing error caused by the numerical integration around the singularity in the integrand coefficient.

As before, the boundary conditions guarantee energy conservation at the two interfaces. Piquette has calculated the time average power crossing the two interfaces within a circular area of radius r and has obtained the surprising result that the power crossing the fluid-solid interface is much less

	aluminium	brass	steel	lead
reflection (modulus)				
1000 Hz	0.0455	0.1513	0.1672	0.2222
5000 Hz	0.2325	0.5816	0.6156	0.7491
transmission (modulus)				
1000 Hz	0.9771	0.9570	0.9673	0.9480
5000 Hz	0.9860	0.8997	0.8386	0.6448

Table 6.6 Calculations of the reflection and transmission coefficients for spherical wave propagation at a metal plate in water, the point source height $h = 2$m, the thickness of the plate $l = 0.01$m.

than that crossing an area in the second solid-fluid interface with the same radius. This extra energy is too large to be explained by the "backward wave" phenomenon. We have done a similar calculation and found that the energy transmitted into the solid is very similar to that transmitted out over the same area. A result for water-steel-water at 1000 Hz is shown in Table (6.7). It is likely that the extra energy obtained by Piquette was caused by

radius (m):	2	4	6	8	10
energy into solid	0.2662	0.3705	0.4108	0.4316	0.4443
energy out of solid	0.2668	0.3706	0.4109	0.4317	0.4444

Table 6.7 Calculations of the time average power crossing a circle area. Point source height h=2m, the thickness of the plate 0.01m.

the numerical error for the transmission term. We found that the calculation for the transmission was very difficult for large values of r so we were not able to give a reliable result for a large area.

The behaviours of the reflection and transmission coefficients were examined numerically for the water-steel-water combination and for the water-aluminum-water combination at 5000 Hz and the results are shown in Figures (6.20) to (6.27). The corresponding curves for plane waves were also plotted for comparison. It can be seen that the curves for spherical waves are quite similar to those for plane waves. In particular, the phase changes of the reflection coefficients (Figures (6.21) and (6.25)) give an interesting result. When the results for plane waves were obtained it was considered doubtful whether the curves for spherical waves would also have that sudden phase

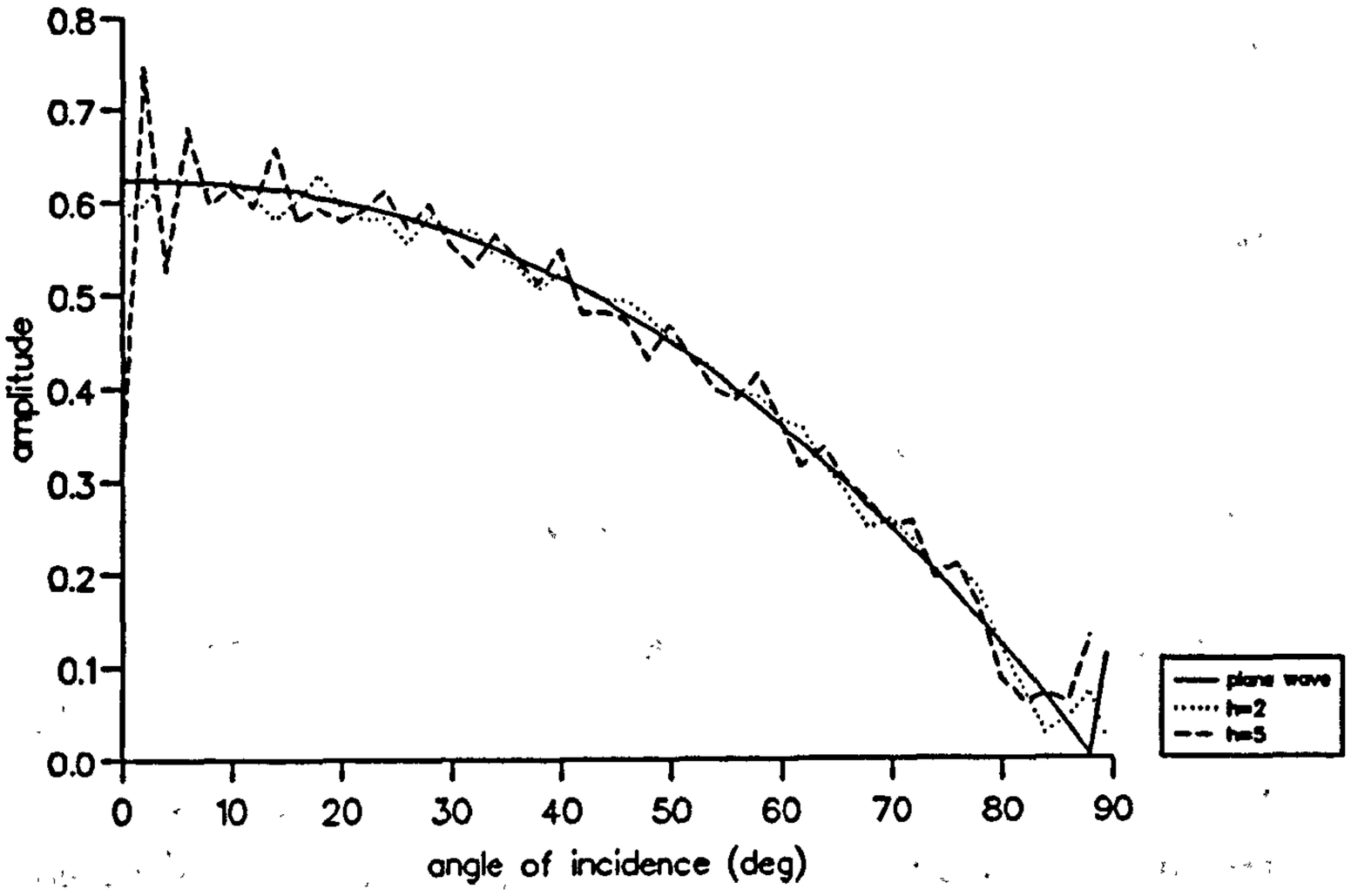

Figure 6.20 Comparison between the predicted amplitudes of reflection coefficients for spherical waves and plane waves in the presence of a water-steel-water combination. Frequency 5000 Hz, thickness of plate 0.01m.

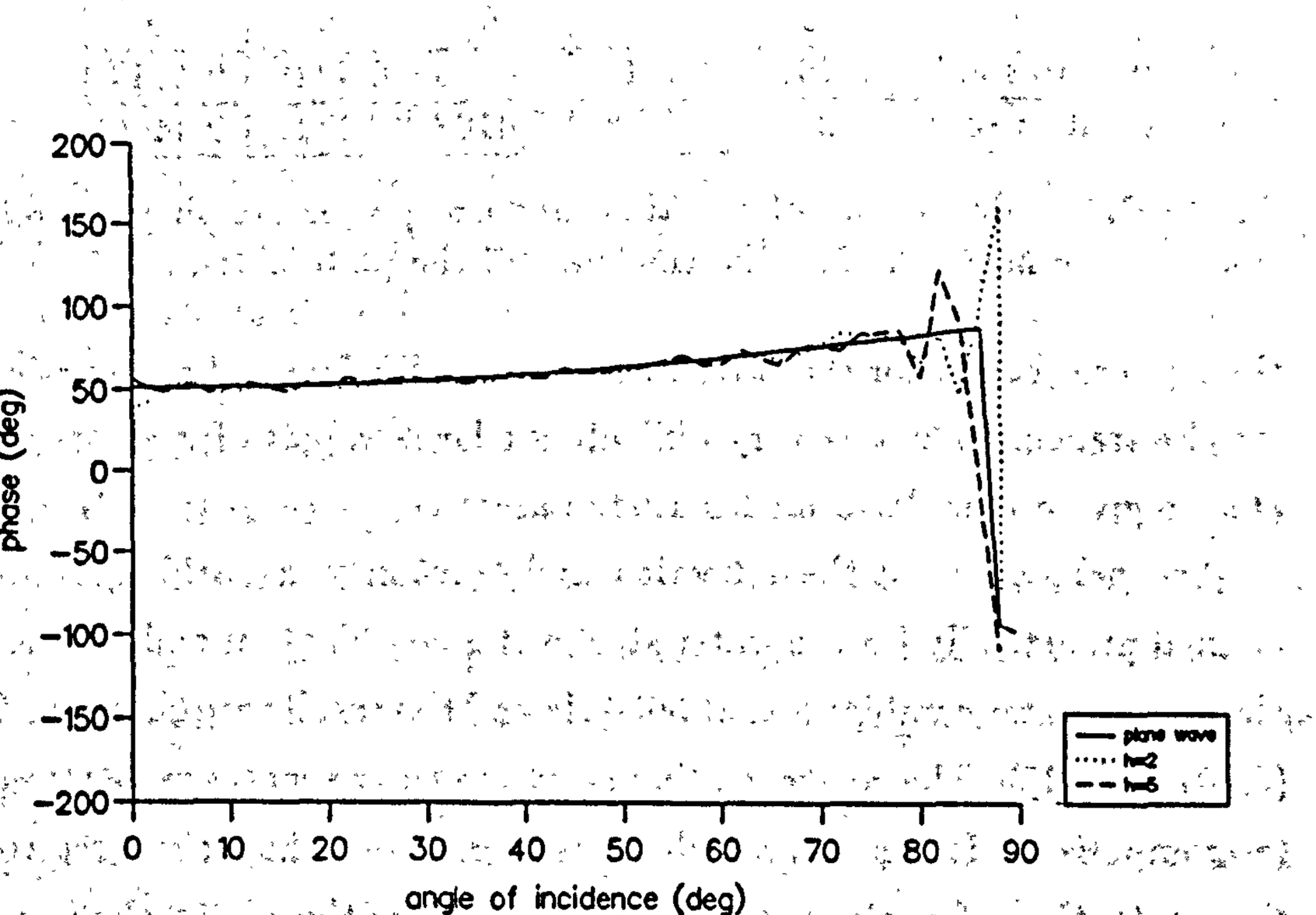

Figure 6.21 Comparison between the predicted phases of reflection coefficients for spherical waves and plane waves in the presence of a water-steel-water combination. Frequency 5000 Hz, thickness of plate 0.01m.

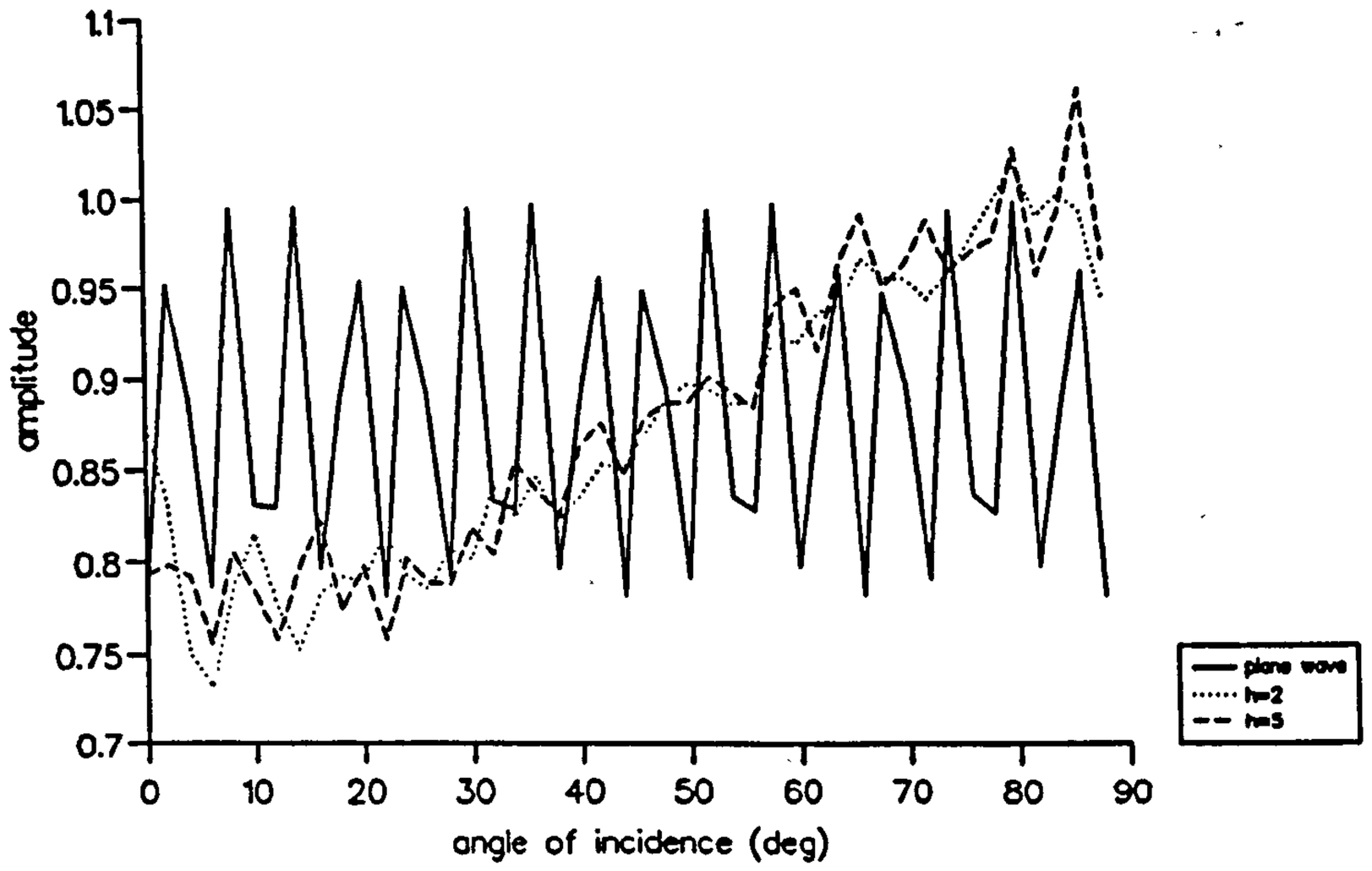

Figure 6.22 Comparison between the predicted amplitudes of transmission coefficients for spherical waves and plane waves in the presence of a water-steel-water combination. Frequency 5000 Hz, thickness of plate 0.01m.

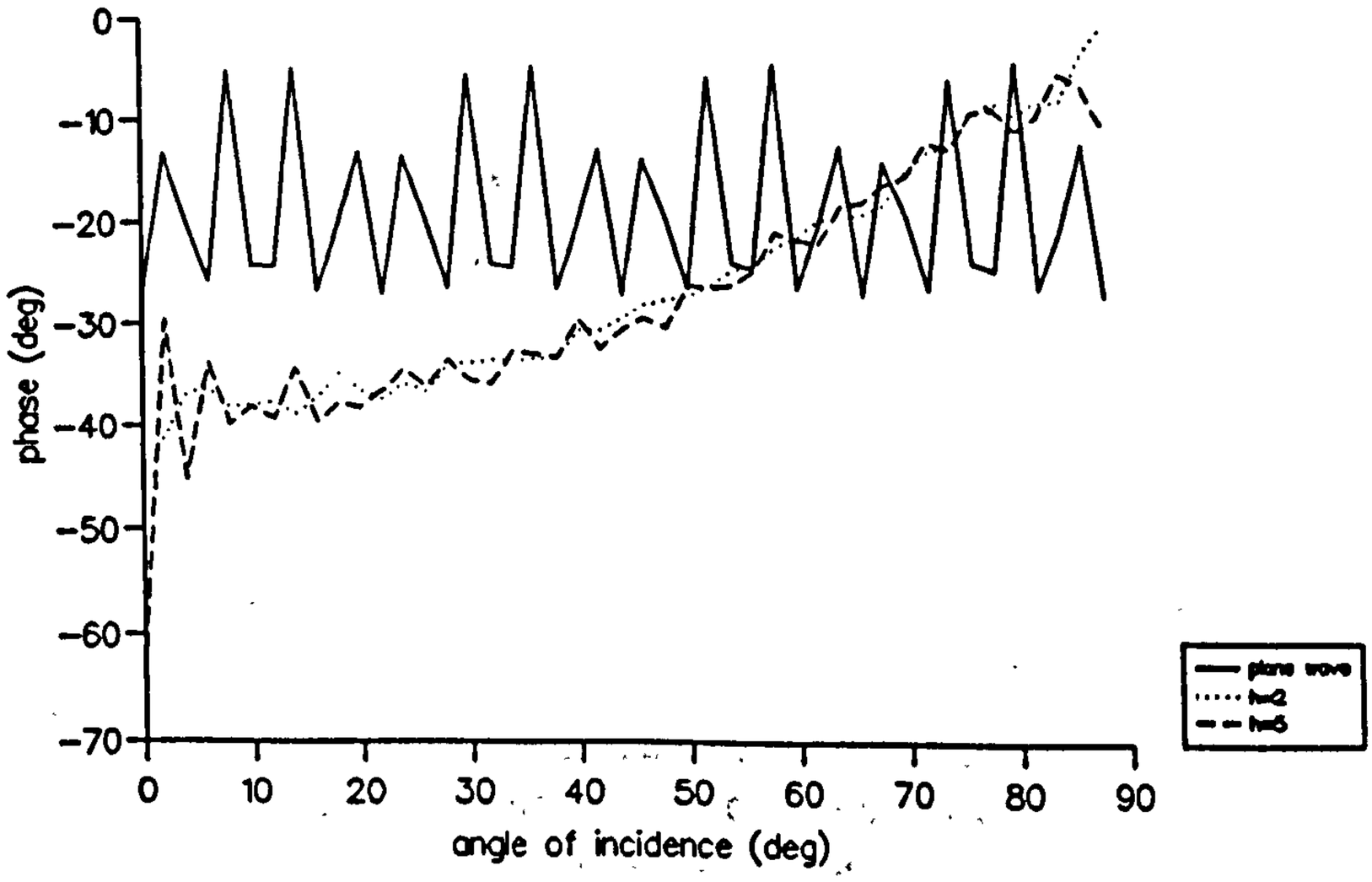

Figure 6.23 Comparison between the predicted phases of transmission coefficients for spherical waves and plane waves in the presence of a water-steel-water combination. Frequency 5000 Hz, thickness of plate 0.01m.

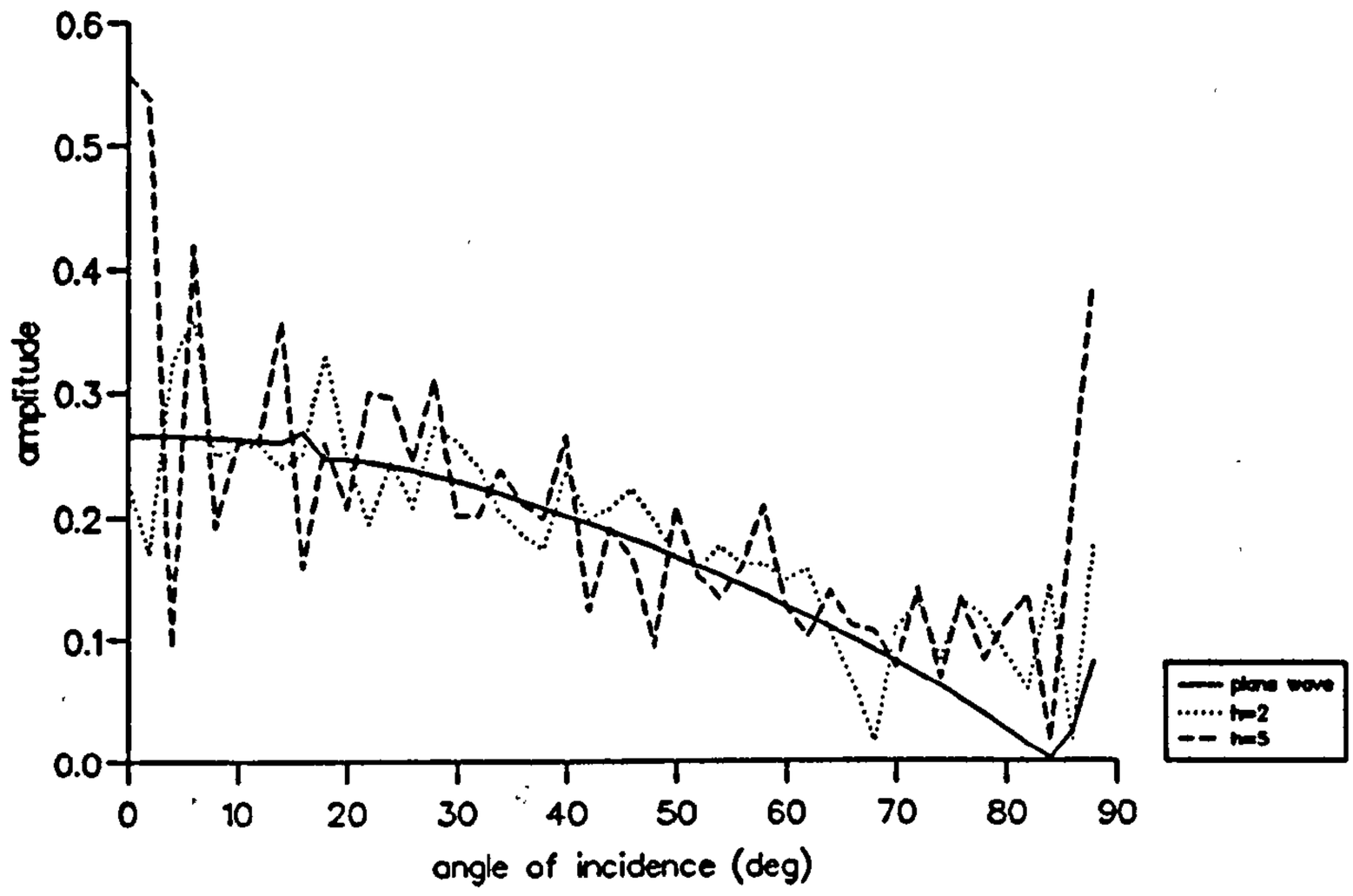

Figure 6.24 Comparison between the predicted amplitudes of reflection coefficients for spherical waves and plane waves in the presence of a water-aluminum-water combination. Frequency 5000 Hz, thickness of plate 0.01m.

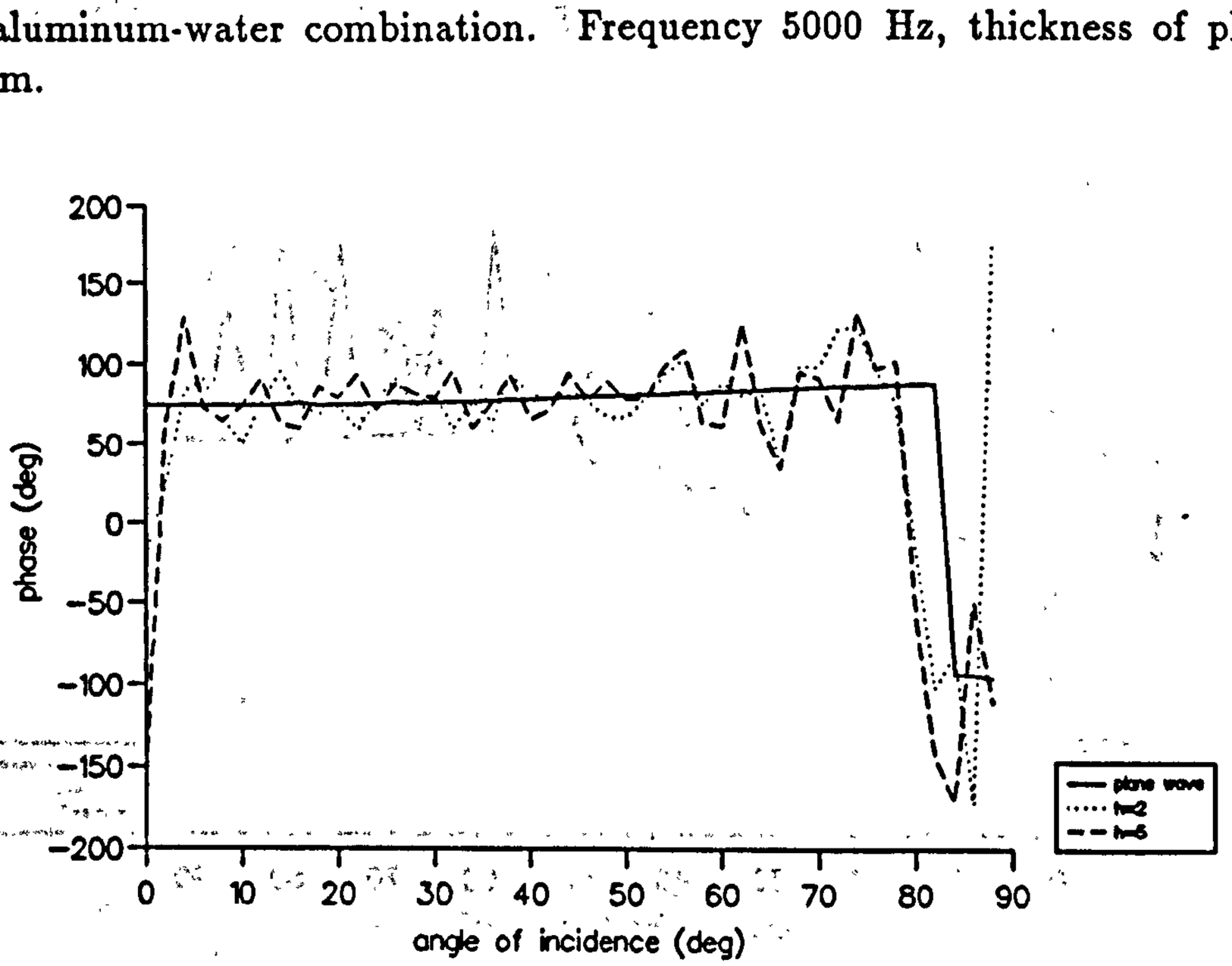

Figure 6.25 Comparison between the predicted phases of reflection coefficients for spherical waves and plane waves in the presence of a water-aluminum-water combination. Frequency 5000 Hz, thickness of plate 0.01m.

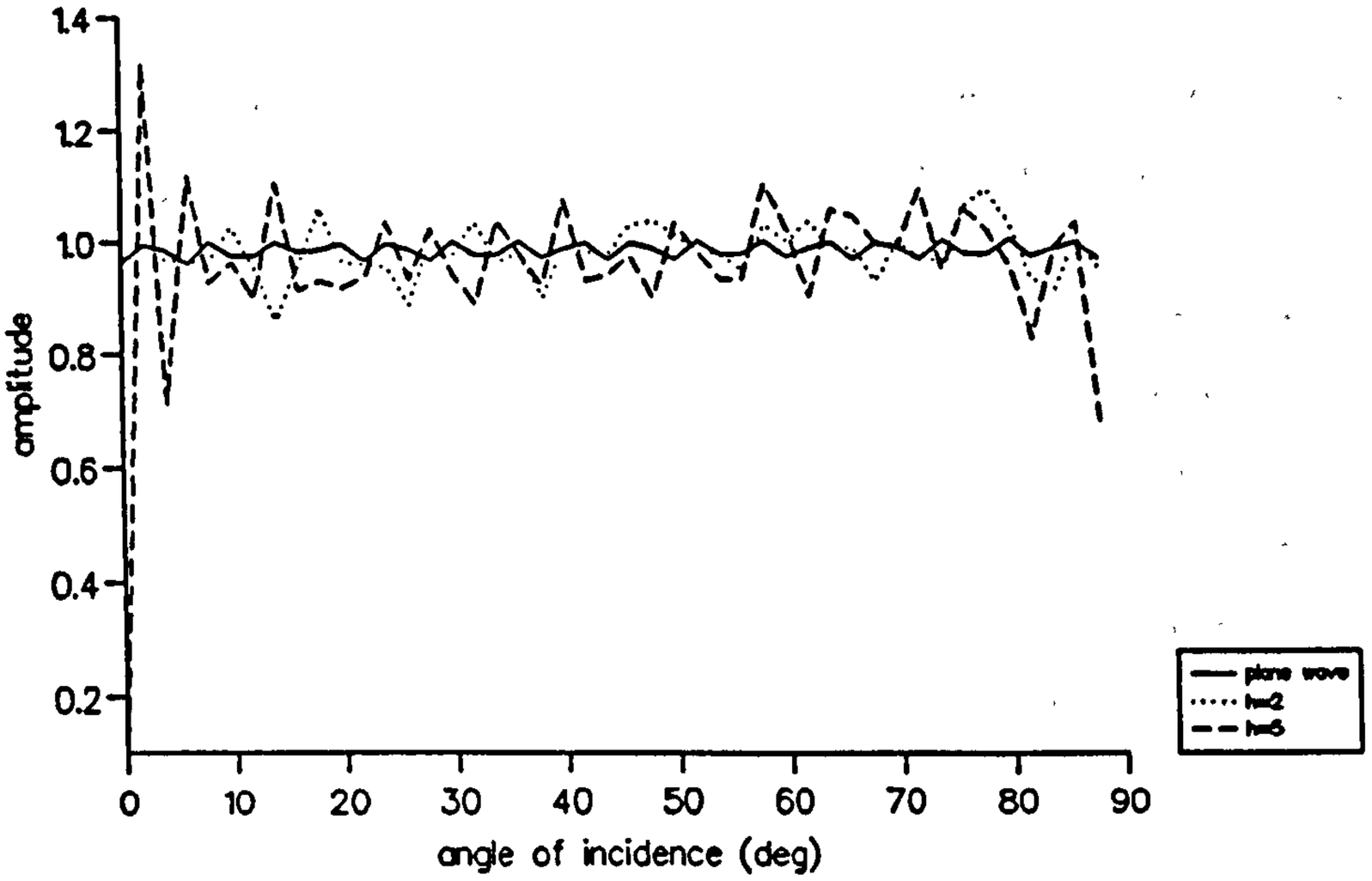

Figure 6.26 Comparison between the predicted amplitudes of transmission coefficients for spherical waves and plane waves in the presence of a water-aluminum-water combination. Frequency 5000 Hz, thickness of plate 0.01m.

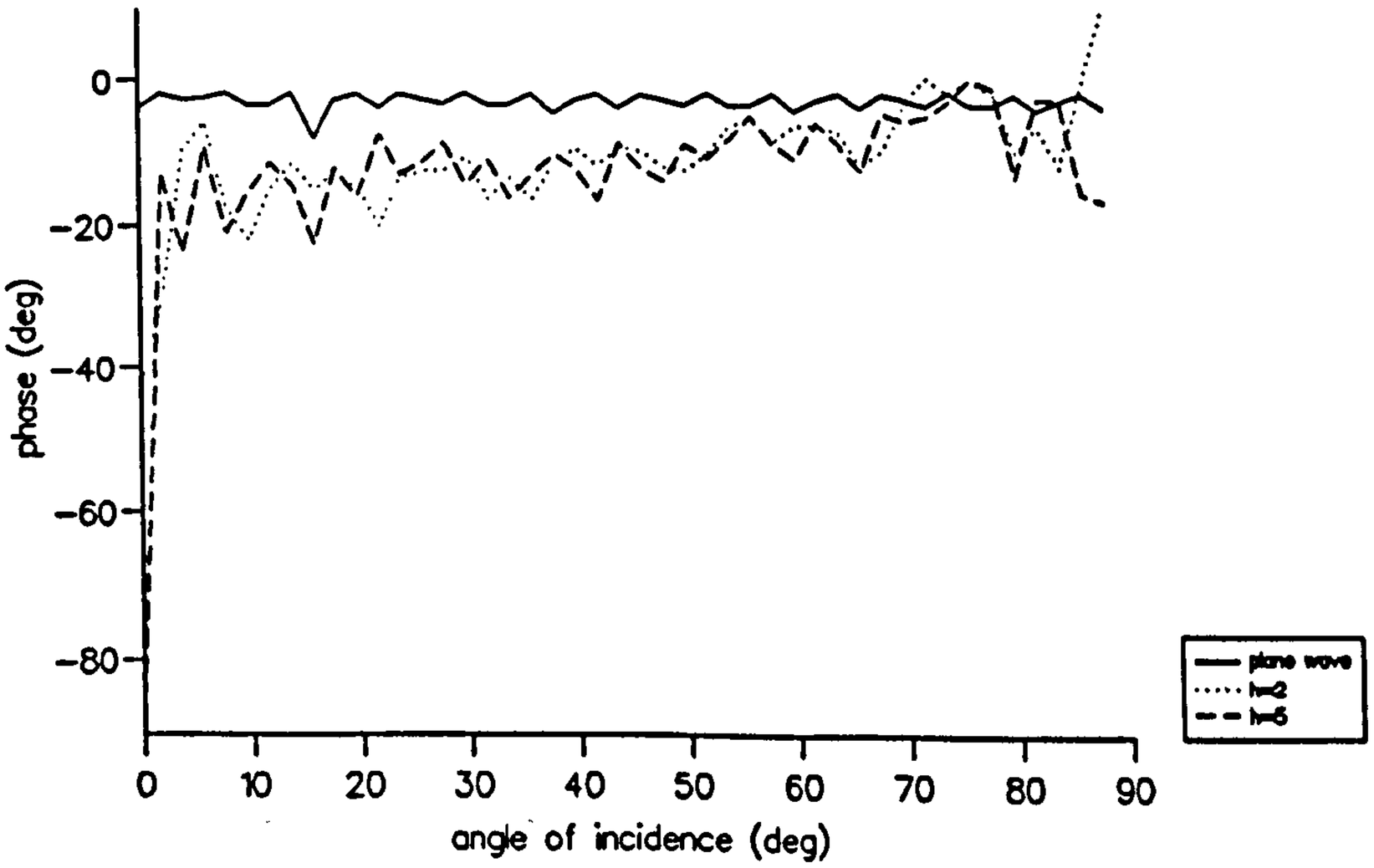

Figure 6.27 Comparison between the predicted phases of transmission coefficients for spherical waves and plane waves in the presence of a water-aluminum-water combination. Frequency 5000 Hz, thickness of plate 0.01m.

jump from positive to negative at near-grazing incidence. However, the results of the calculations for spherical waves also show this feature. It also can be seen that in general, the amplitudes of the coefficients are smaller than unity except at some large angles of incidence.

There are differences between the curves for the transmission coefficients. The amplitudes and phases of the transmission coefficients for spherical waves slightly increase with increasing angle of incidence, however, they are as oscillatory as those for plane waves. If we examine the curves carefully, we find that the oscillatory features of the curves for $h = 5$m are closer to those for the corresponding curves for plane waves than those for $h = 2$m, in general. An interesting fact is that for the three medium system, the phase of the reflection coefficient for a spherical wave has the same sign as that of a plane wave.

A complete explanation of the features of the reflection and transmission coefficients for spherical wave propagation in the case of a solid plate in a fluid is difficult and it may require detailed knowledge of the wave field in the solid plate.

Chapter 7

Experiment

7.1 Choice and design of experiment

In general, the purpose of scientific research is to predict or to explain a natural phenomenon. Evaluation of a theory depends on the comparison between a theoretical result obtained from the theory and a natural phenomenon. In the case of explaining a known natural phenomenon the comparison is straightforward, but for *predicting* a natural phenomenon, in order to make a comparison, the best way is to simulate the realistic situation and measure the quantity with which the theory is concerned: i.e., to perform an experiment, and then make a comparison between the measured data and the theoretical prediction.

From the viewpoint of physical science, the best verification of a theory is through experiments. Sometimes when a direct experimental test is difficult, the theoretical result may be tested indirectly. However, it is obvious that the most convincing verification will be obtained by directly comparing theoretical results and experimental data. A complete scientific investigation should always include both theoretical predictions and experimental verification.

In earlier chapters, based on a theory of linear wave propagation and an integral representation for a spherical wave, we have obtained some theoretical results for spherical wave propagation. It has been found that spherical wave reflection at a plane boundary has some interesting features.

For example, the prediction of "backward waves", i.e., for a spherical

wave reflection at a hard boundary, the time average energy flux component could be in the direction opposite to that in which the wave is supposed to travel, in some small regions above a point source, and in some transmission regions; the critical angle of total reflection for a spherical wave is larger than that of a plane wave; and at normal incidence the reflection and transmission coefficients for a spherical wave are smaller than those of a plane wave.

Among those theoretical results, the most interesting result is the prediction of localized "backward waves". The measurement of energy flux is possible by measuring pressure and pressure gradient or pressure and particle velocity, using sound intensity measurement techniques, but equipment for doing this was not readily available. However, we have obtained pressure contours for several cases of spherical wave reflection and transmission at a plane interface. We can make an indirect test by checking the pressure field obtained by using the spherical wave reflection theory which also predicts the "backward waves". The simplest experimental test is the measurement of pressure in a two-dimensional space.

In Chapter 6, the pressure contours were calculated for spherical wave incidence at a plane interface between air and water. The theoretical result shows a minimum pressure area in the transmitted wave field in Figure (6.3). A simple experimental test of this prediction would be to measure sound pressure on either side of an air-water interface in an anechoic environment. Unfortunately, such an arrangement again was not feasible with the equipment available, so we have considered instead a different experiment that could be performed in a conventional anechoic chamber.

In Chapter 6, we have obtained a theoretical result for an infinite extended plate in a spherical wave field. The theoretical results predict that at 500Hz in the reflection area there are two troughs and at 1000Hz three troughs. These are shown in Figures (6.1) and (6.19). The figures also show the spherical features near the upper left corners and that the peaks are bending over towards the source. Calculations show that these results are the same as those for the reflection at a rigid boundary.

The solution for spherical wave reflection at a rigid boundary is well

known, but as an absolutely rigid boundary cannot be realized so an experiment was carried out to measure the pressure field for spherical wave reflection by a suitable plate.

We expect that the results from the theoretical studies of reflection at an infinite interface should show some resemblance to data obtained near finite interfaces, so we have carried out experiments using a plate of finite area and compared the experimental data with calculations for infinitely extended plates or rigid planes. A simple experimental model corresponding to the theoretical problem studied in Chapter 6 is to place a finite size plate in a spherical wave field. At least we would expect that the theoretical result for the reflection of the spherical wave from an infinite rigid plane should be very similar to the data obtained from this finite plate near the central area of the plate.

The details of the measurement methods and the equipment are described in this section. The detailed experimental procedure is given so that anyone can easily check the experimental method and the reproducibility of the results. A list of equipment is given in Appendix (F)

We have adopted a method similar to that used by Lawhead and Rudnick [10]. A spherical wave is generated from an open end of a brass tube which is coupled to a driver unit. The amplitude of the sound pressure is measured. The receiver is a condenser microphone (details are given later).

In the experiment a digital FFT analyzer and a computer controlled system have been used. The output signal from a FFT analyzer is amplified by a power supply and then sent to the driver unit. The received signal is first preamplified and then is sent to the FFT analyzer.

A computer controlled system was made to enable us to speed up the measurement and to facilitate the production of pressure contours in a vertical plane.

In general measurements in three dimensions provide more detailed information about a wave field. Here, however we need to measure the pressure field only in two dimensions, since the ideal wave field should be symmetrical about the centre axis which passes through the point source and is normal

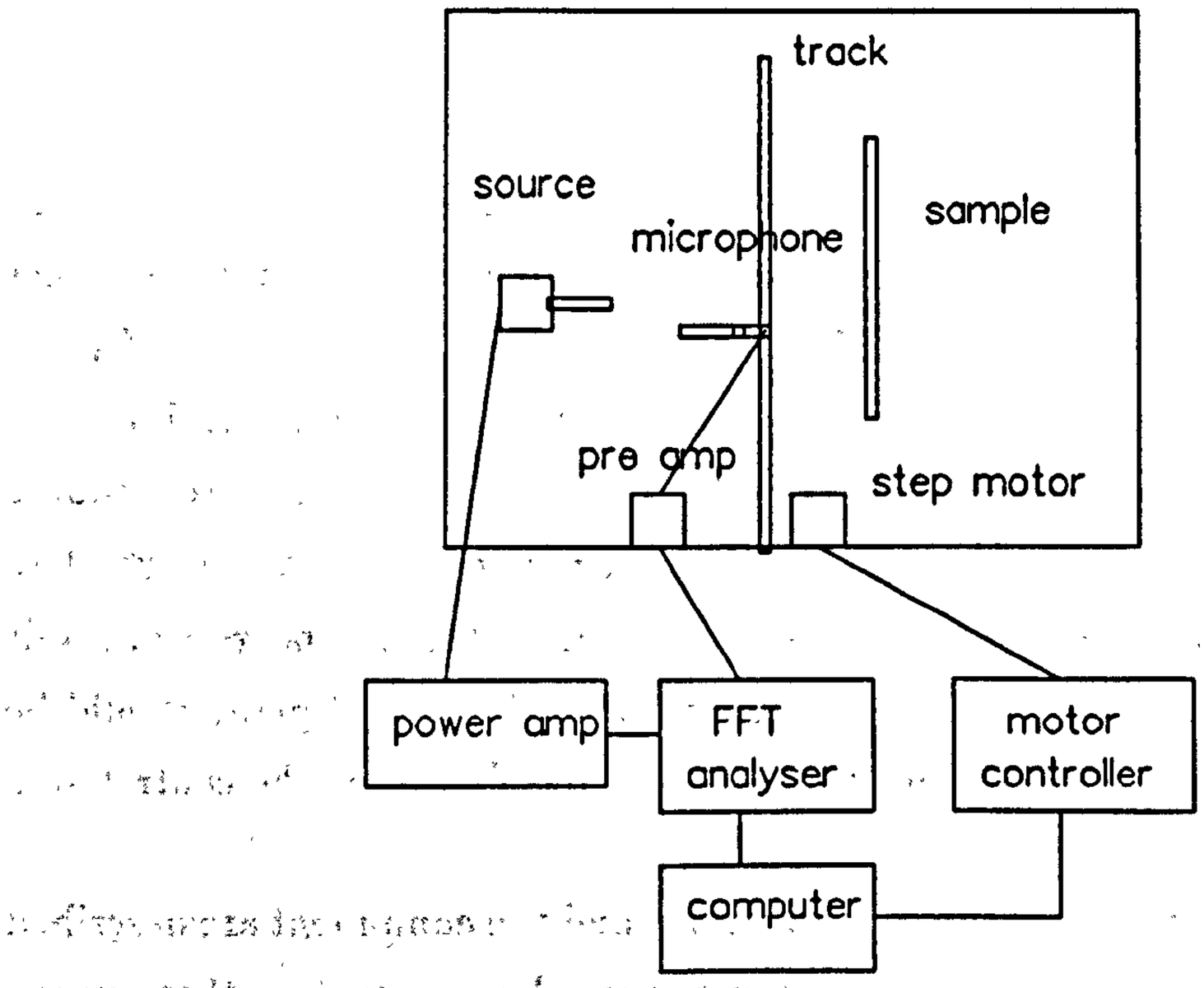

Figure 7.1 Schematic diagram of the equipment connection.

to the reflecting plate. In reality, the wave we generated was not completely spherical because of external disturbances. We have made measurements in less disturbed regions.

A personal computer was used to control the whole measurement system. The computer controls the position of the single microphone in the direction parallel to the sample, and controls a FFT analyzer which is used to process and store data. The location of the microphone is adjusted by a device consisting of a track with a pulley system, a stepping motor and a stepping motor controller. A schematic diagram of the equipment is shown in Figure (7.1). Once the microphone is moved into position the FFT analyzer starts to process and store data. After it is finished the microphone is moved to the next point. This procedure is repeated until the last designated point has been measured.

Along the normal to the sample, the microphone tracking device is moved manually.

The computer controlled system and the FFT analyzer enabled a large

number of closely spaced measurements to be made in a convenient manner.

The experiment was conducted in the OU/Silsoe anechoic chamber at the Silsoe Research Institute, about 20 miles from the Open University. The working space in the chamber is about 2m × 2m × 2m. An expanded metal grille is used as a working floor at about 10cm above the top of the floor wedges.

Circular discs about 1.2 m in diameter and 8 mm thick made from steel or aluminium have been used. The discs were suspended vertically in the centre of the chamber. A cylindrical coordinate system similar to that of the theoretical model was used. The origin was at the centre of the disc on the reflecting surface, with the z-axis perpendicular to the disc and passing through the source point in the region $z > 0$. We have measured at selected (r, z) points, with the axis for r (regarded here as a Cartesian coordinate because of the circular symmetry in any z-plane) pointing vertically upwards, in both the regions $z > 0$ and $r > 0$. The points lie within an area of 0.7m × 0.7m in the r-z Cartesian coordinate system. The measurement points closest to the disc were at a distance of 0.05m from it and the distance between two consecutive measurement points was 0.05m in both the r- and z-directions.

The microphone used in the experiments was a Brüel & Kjaer (B & K) 1/2" (24 mm) type 4165. This type of microphone is suitable for free field measurement. The open circuit frequency response is from 2.6Hz to 20 kHz.

The microphone was preamplified by a B & K type 2639 preamplifier with an adapter JE0002. The linear lower limit of the preamplifier with use of microphone type 4165 is 17 dB in the frequency range 20Hz-200 kHz. The upper limit with the type 4165 microphone is 146 dB for distortion less than 3 %.

The preamplifier is operated by a B & K type 2807 two channel power supply. Since the cable connected between the anechoic chamber and the control room is not suitable for sending a signal from the preamplifier to the power supply over a long distance, it was found necessary to keep the power supply in the anechoic chamber.

The received signal was processed finally in an Ono Sokki CF 910 two

channel mini FFT analysis system. The CF 910 provides a spectrum analyzer covering the frequency range of 0Hz - 40kHz, and data can be stored in a 3.5-inch micro-floppy disk by using the built-in disk drive. The amplitude frequency response is flat to within 0.3 dB (max). The Ono Sokki FFT analyzer has an important feature. It can average a number of readings automatically. The choice of the number of averages depends on two factors, time and error. Choosing a large number of averages will give small error, but require a longer experiment. Given the practical constraint on the experimental work and its relative importance to this research, an error test has been carried out to check the measuring system.

The Ono Sokki FFT analyzer also provided the source drive signal. Two types of signals have been used. Initially a white random noise signal was used since this allowed convenient examination of the frequency dependence of the pressure field. Subsequently , however a single frequency sine wave signal was used to obtain more accurate results at particular frequencies.

The output signal was amplified first by a B & K type 2706 power amplifier, which has a frequency response range of 10Hz - 20 kHz and then sent to a 45 watt Tannoy drive unit. A brass tube was coupled to the drive unit so that a spherical wave was generated at the end of the tube. The tube is about 30cm long and has a circular open end with about 2cm internal diameter. A test of the sphericity of the wave produced is described in the next section.

The initial version of the microphone tracking device had a trolley.which rolled along a track 1.8m long. The track consists of two rods, of 1cm and 0.5cm diameters respectively. The small rod serves as a guide to prevent the trolley rotating. The trolley carries the microphone. The track was fixed vertically to a T shaped platform. The stepping motor was also fixed to the platform. The microphone seat was driven by the stepping motor through pulley systems located at the two ends of the track. Initially there were two problems with this device. One problem was that it was difficult to keep the guide rod straight and the other problem was that there was too large a clearance between the trolley and the rod. Because of these problems,

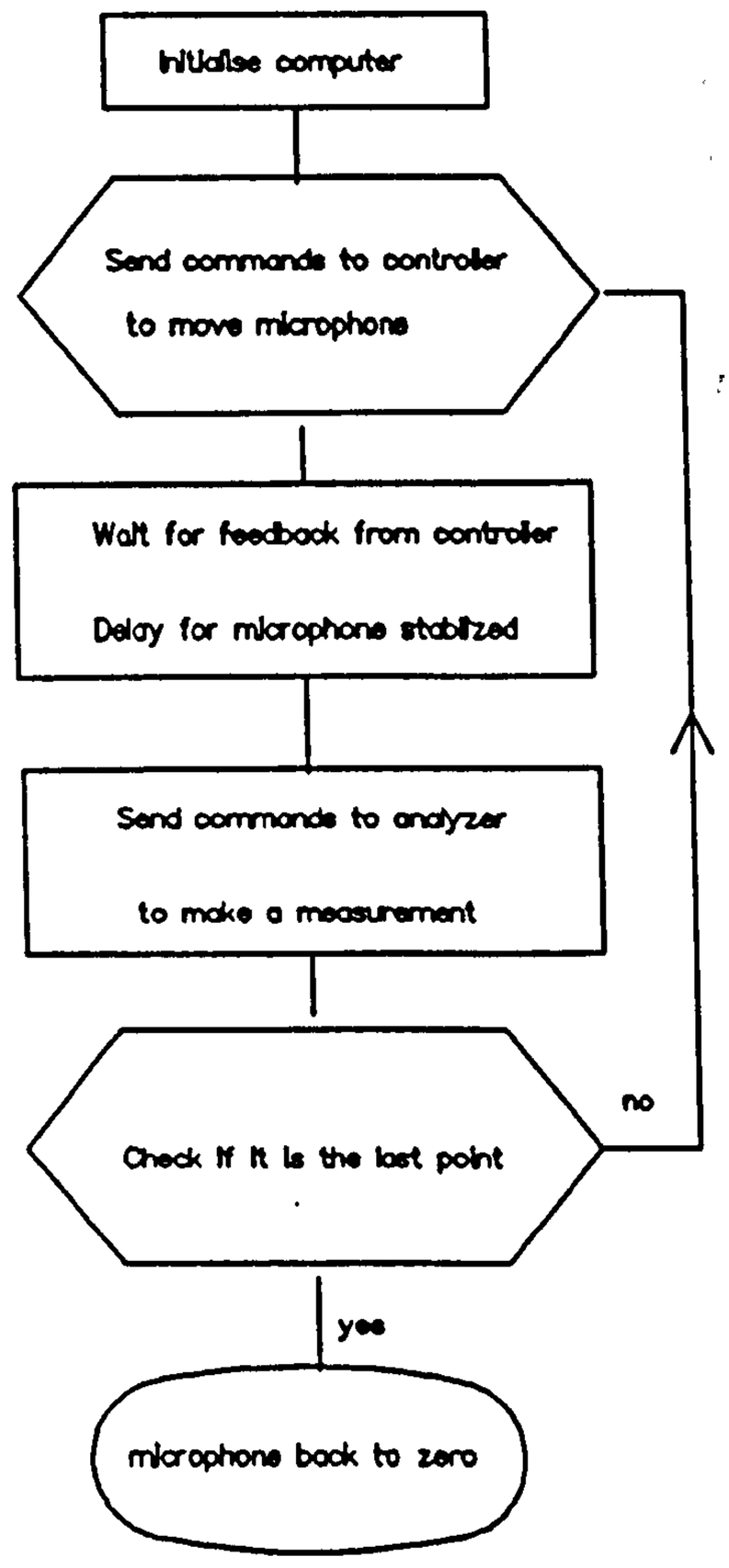

Figure 7.2 Flowchart of computer control program.

this device could not guarantee the position of microphone. Subsequently it was modified. In the improved tracking device, the microphone was fitted to a seat which was able to slide along a guide. This track has a $\prod$ shaped cross section, with outside dimensions, 1.5cm×1.5cm. This microphone track device was portable, and was supported on two bars. The purpose of the two bars was to make the level adjustment easy.

The stepping motor was controlled by a NIP 6.1122.01 controller.

The centre of the measurement system was a Zenith Z-150 personal computer desktop system. The computer has 128K RAM memory and has one built-in RS-232 serial input/output port. The communication between the

computer and the stepping motor controller was through the RS-232 interface. An IEEE 488 interface was installed for parallel communication with a FFT analyzer. The control program was written in Basic. The flow chart is given in Figure (7.2).

The data stored in the Ono Sokki analyzer was transferred to the Zenith computer first and than sent to a VAX mainframe from the Zenith computer. The program for data transfer had been written by a previous researcher.

The procedure for carrying out the measurements was as follows.

Step 1: set up the system in the control room. Switch on all equipment for warm up while the next two steps are carried out.

Step 2: set up the equipment in the chamber.

Step 3: position the microphone track device. Fix the two platform bars to the floor at a suitable distance from the centre line and adjust the bars so that the track is vertical. Adjust the zero point vertically 5cm below the centre z-axis and horizontally 5cm apart from the plate.

Step 4: calibrate.

Step 5: take a measurement with the tracking device at one position. Start the program. Take 15 measurement points at interval of 5cm each over a 70cm distance. Note the reference pressure value and the position of the track etc.

Step 6: make the next measurement. Repeat Step 3 but adjust the zero point horizontally 5cm away from the last position, (make a further calibration occasionally), and repeat Step 5. Repeat this procedure 14 times and finish.

Step 7: final calibration.

The measuring system introduces a random error when using a white noise signal; two measurements with the same set-up could provide different readings. An experiment has been carried out to test the equipment system. The equipment was set up in the anechoic chamber as described above but without the plate, and with a microphone fixed at 1m from the source. 30 measurements were taken and 30 readings obtained which are denoted by x_i. The sample average $\hat{x}$ is given by

$$\hat{x} = (\sum x_i)/N,$$

where N is the total number of readings. The Bessel formula was used for the calculation of the standard error,

$$\hat{\delta} = \sqrt{\sum_{i=1}^{n}(x_i - \hat{x})^2/(N-1)}.$$

The standard error changes with variation of the number of averages. A previous researcher has suggested that 128 averages is a suitable choice [69]. We took the next highest number 256 for the upper limit of the error test. The result is shown in Table (7.1).

Number of averages	32	64	128	256
f=500Hz				
mean value	55.07	55.01	54.94	54.88
standard error	0.75	0.52	0.31	0.31
f=1000Hz				
mean value	54.37	54.28	54.30	54.20
standard error	0.71	0.51	0.36	0.37

Table 7.1 Standard error

From Table (7.1), it can be seen that in general the errors decrease with an increase in the number of averages. The errors obtained for the 128 and 256 averages are rather similar. At a frequency of 1000Hz the error for 256 averages is slightly greater than that for 128 averages. This is because that the specification of the accuracy of the Ono Sokki analyzer is 0.3 dB (for sound pressure against frequency); hence the the second place of decimals in the measurements has no significant meaning.

For the experiment using the single frequency sine wave signal, the equipment error is negligible. When the microphone is stationary, good reproducibility was possible even when using only 16 averages. In fact using 8 averages seemed to be adequate, but we chose the next highest number of averages, 16, since it did not have a large influence on the length of time of the experiment.

7.2 Validation of point source and chamber

The use of a tube attached to a loudspeaker driver to produce a spherical wave has been widespread [10]. However a point source test has been carried out for the source used here. This test also serves as a check on the anechoic chamber and our experimental technique. The disc was removed for this test, of course. The procedure is the same as that described for the experiment with the disc in place, but with a smaller density of measurement points.

Initially, a random white noise signal was used for experiments. One measurement can give the frequency response of the pressure field from 0Hz to 40 kHz. When the wavelength is similar to the dimensions of the instruments inside the chamber, the effects of the instruments on the pressure field will not be negligible, so we chose a smaller frequency range from 0Hz to 10 kHz for the point source test. In order to save time we used 64 averages, since the accuracy was not crucially important for this measurement. From the results of the measurements we found that the spherical wave is badly distorted above 1000Hz at a distance of 1m away from the source.

The results are shown in Figures (7.3) to (7.5) as two-dimensional contours for the frequencies 500Hz, 1000Hz and 2000Hz. The small dots on the figures indicate the measurement locations. The contour curves were produced by using the UNIMAP software with the default method of interpolation.

Figures (7.3) to (7.5) show that in the area close to the source the wave pattern had a good spherical shape, but as the distance from the source increases, the spherical wave pattern disappears.

The main cause of the distortion was the grille which provided a working solid floor for accurate positioning of the microphone. Removal of the grille each time would have required considerable extra working time and additional assistance. Consequently, the presence of the grille during the measurements had to be tolerated, and minimized insofar as possible. We may explain this distortion in the following way. At any observation point we mainly received two signals if we ignore the reflections from the ceiling, floor and walls. One was directly from the source and the other was the reflection

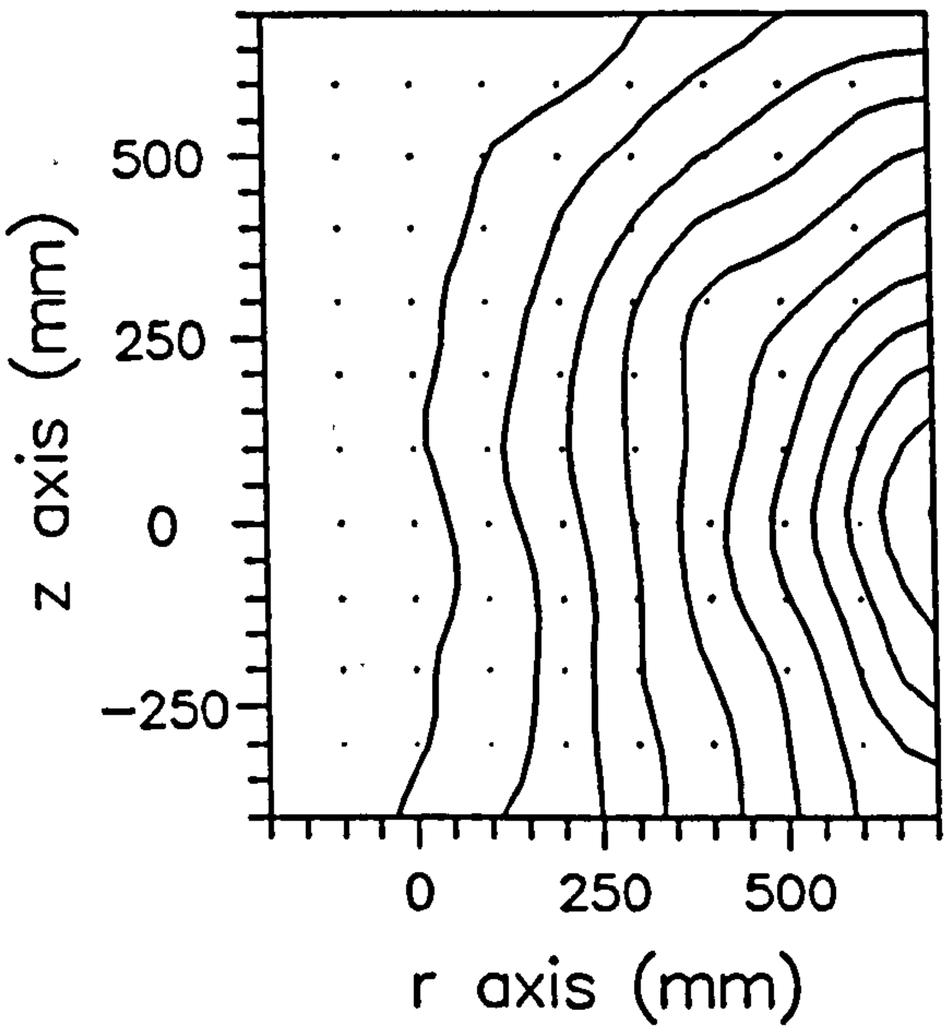

Figure 7.3 Measured pressure contours around the point source. The source is located at (1000, 0). Random white noise; output signal, at 500Hz.

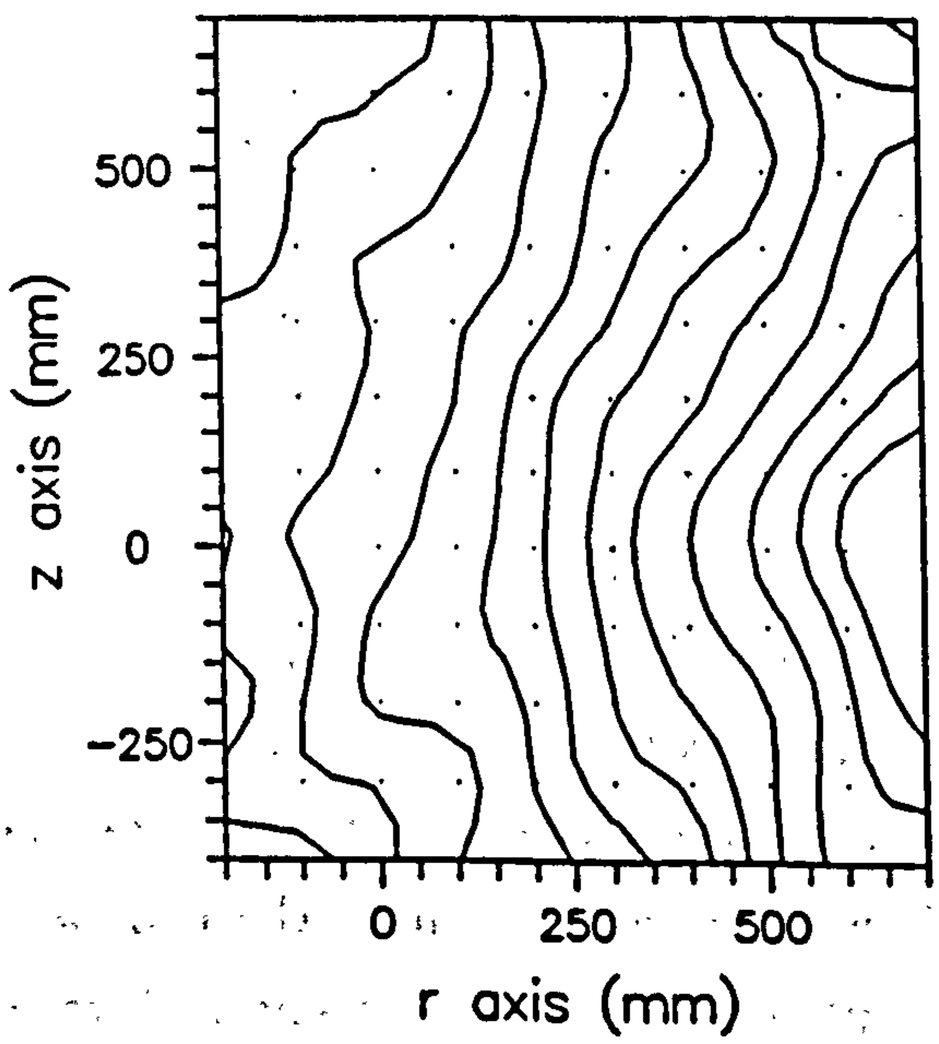

Figure 7.4 Measured pressure contours around the point source. The source is located at (1000, 0). Random white noise; output signal, at 1000Hz.

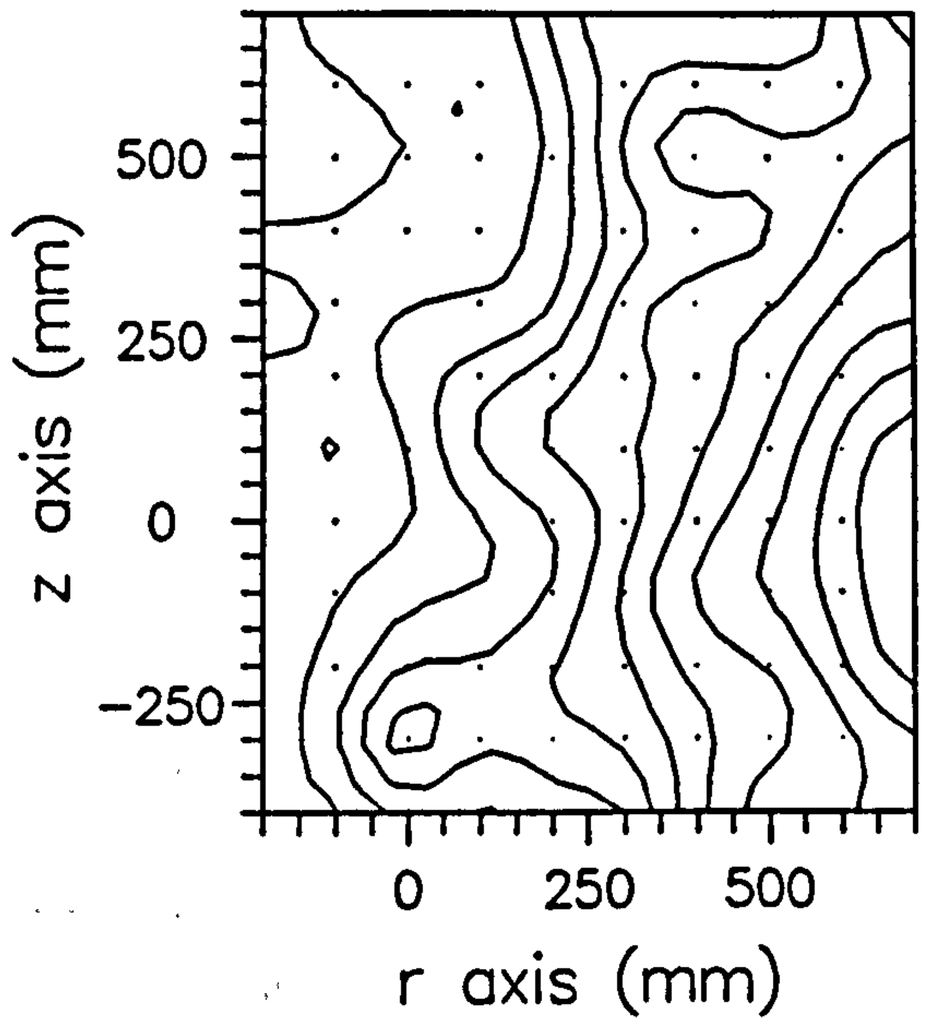

Figure 7.5 Measured pressure contours around the point source. The source is located at (1000, 0). Random white noise; output signal, at 2000Hz.

from the grille. At an observation point near the source, the distance from the point to the source along the path of the direct wave is much less than that along the path of the wave reflected by the grille, so the amplitude of the reflected wave from the grille is much smaller than that of the direct wave even if we could assume a large reflection coefficient for the grille. The wave field is dominated by the direct wave near the source. However, as the distance between the point of observation and the source increases, the difference between the two path lengths becomes smaller so the influence of the wave reflected from the grille is not negligible. The consequence is distortion of the direct spherical wave by the wave reflected from the grille.

It is obvious that the reflections from the side walls tend to be cancelled out, insofar as the walls themselves have the same shapes, since the measurement is taken on the central vertical plane. One may argue on the other hand that the reflection from the ceiling, the floor and the wall facing the source may have contributed to the distortion. First of all the surfaces of the anechoic room which is constructed from absorbent wedges in a conventional way, have a very small reflection coefficient, so they should not produce

significant reflections near the centre of the room. Another argument for neglecting the reflection from the surfaces of the chamber is supplied by the result shown in Figure (7.3).

For spherical waves we should have symmetry about a central axis coinciding with the z-axis; however from Figure (7.3) we see that the central line of symmetry seems to shift upwards with increasing distance from the source. This suggests the influence of the wave reflected by the grille rather than the effects of the reflections from the ceiling, the floor and the wall facing the source. Reflections from the ceiling and the floor should have been cancelled out on the z-axis, since it is near the central line of the chamber. When an observation point is moved away from the source, it is getting closer to the wall which is facing the source. In this case, the effect of the wave reflected by the wall facing the source could become larger. However it cannot make any contribution to 'the central symmetrical line shifting' since this reflected wave is symmetrical about the z-axis.

The results of the subsequent experiment showed this 'central symmetrical line shifting' more clearly for both 500Hz and 1000Hz.

From Figures (7.3) to (7.5) we can also see that the curves are not very smooth. As well as the system error, such erratic results may have been caused by errors in the assumed microphone location.

There were mainly two problems while doing the initial tests with a random white noise signal. One of the problems was that the microphone track device was not very accurate, and the microphone did not move vertically. In compensating for this, the guide rod had to be set at a slight angle to the vertical, but nevertheless the accuracy could not be guaranteed. Another problem arose from the technique of setting up the initial position of the microphone track device. We used the grille floor as the level gauge. In fact when a person stands on the grille it bends so the initial position could not possibly be very accurate.

The wave field at 500Hz conforms better to spherical wave propagation than that at 1000Hz. This is because of the well-known result that if a wave has a larger wavelength relative to the size of an object the wave shape

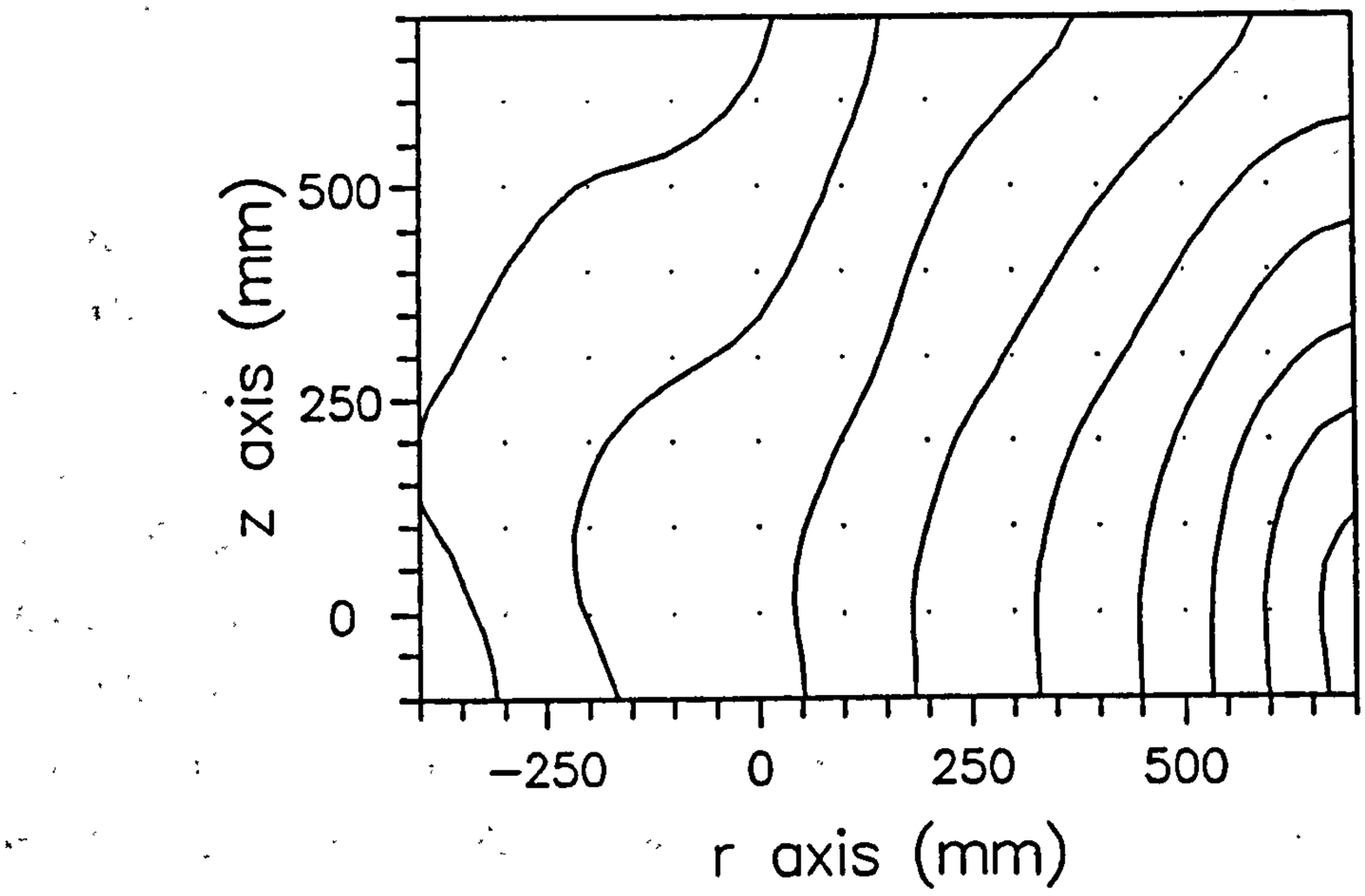

Figure 7.6 Measured pressure contours around the point source. The source is located at (1000, 0). Sine wave signal, at 500Hz.

will have less distortion when passing through the object, and so the grille provides less reflection at 500Hz.

The point source test was repeated using single frequency sine waves at 500Hz and at 1000Hz. This signal was very stable. This time we used the modified microphone track device described in a earlier section, and we also improved the technique of setting up the initial position of the device. The level gauge was set by a wire crossing the anechoic room parallel to the z-axis, and the ends of the wire were tied to posts at opposite sides of the room. A linear scale was marked on the wire for the z-coordinate. The vertical gauge line was set by a wire freely suspended from the top of the track with a weight at the end of the wire. When the level of the device was adjusted the vertical line had to pass the end of the microphone and through a mark on the level gauge line. This ensured that the track was vertical and fixed the distance between the microphone and the reflector disc. The experimenter stood near a support point for the floor to reduce unnecessary floor curvature during the setting up.

The results show that the contour surfaces were much smoother than

those obtained when using the random white noise signal. This suggests that the new results were more accurate since we would expect smooth continuous changes in a realistic pressure field.

From Figures (7.6) and (7.7) again we can see clearly that the line of central symmetry shifts upwards with increasing distance from the source. Figure (7.7) shows that about 1 m from the source the reflected wave becomes more important; as with the random white noise, the reflected wave has less effect at 500Hz than 1000Hz.

From the point source test, we conclude that 1) we can have a reasonably good spherical wave below the frequency of 1000Hz and within 1 m of the source, and 2) the measurement technique is reliable.

7.3 Comparison between measurements and theory

In this section, we examine the the results from two sets of experiments. In the first experiments a steel reflector and random white noise were used. In the second series an aluminium reflector, single frequency sine wave signals at 500Hz and 1000Hz respectively, and a modified microphone track device were used.

7.3.1 Steel disc

Using the random white noise we carried out reflection measurements in front of the steel disc. 128 averages of the field were taken in each measurement position. The experimental procedure and the equipment were as described in section 7.1. The first version of the microphone track device was used.

The results are presented as three-dimensional surface contours at 500Hz and 1000Hz in Figures (7.8) and (7.9) respectively. The reflecting surface of the disc is at z=0, normal to the z-axis, and the source is located at (0, 1000). The (r, z) measurement points are now in the regions $0 \leq r \leq 0.7$m and $0 \leq z \leq 0.7$m Comparing Figures (6.1) and (6.19) from the theoretical

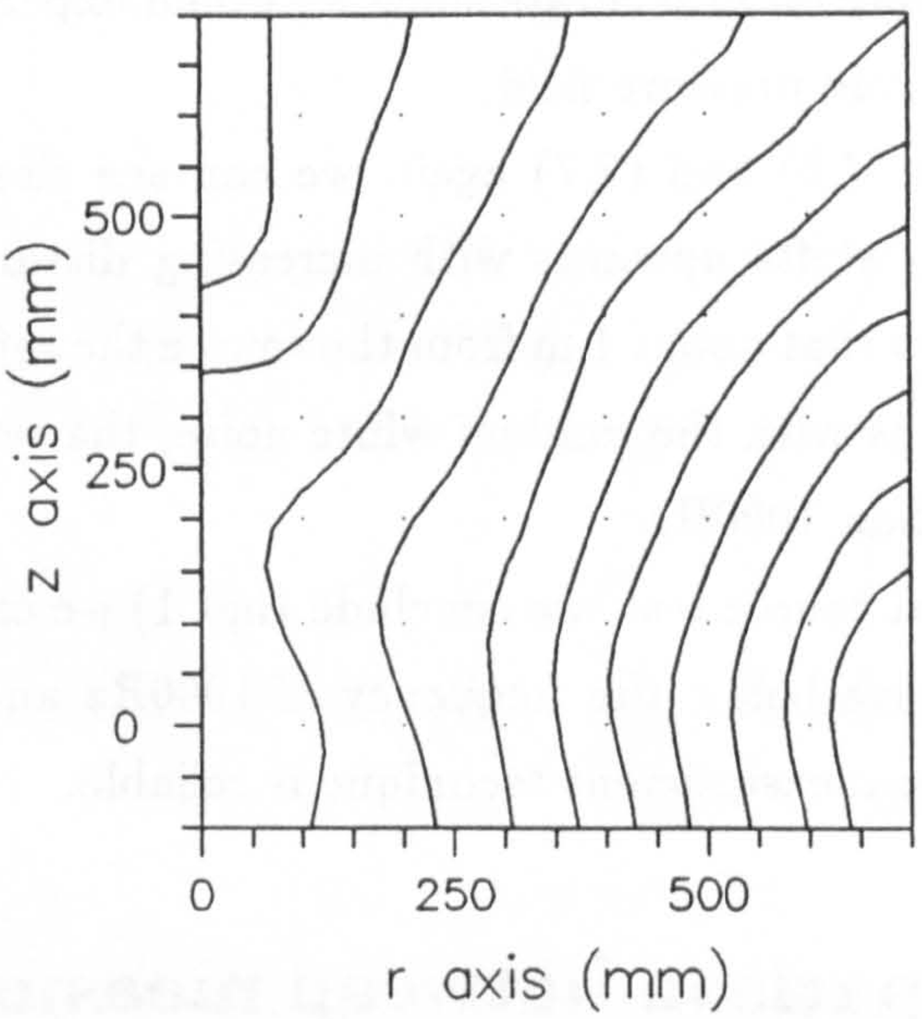

Figure 7.7 Measured pressure contours around the point source. The source is located at (1000, 0). Sine wave signal, at 1000Hz.

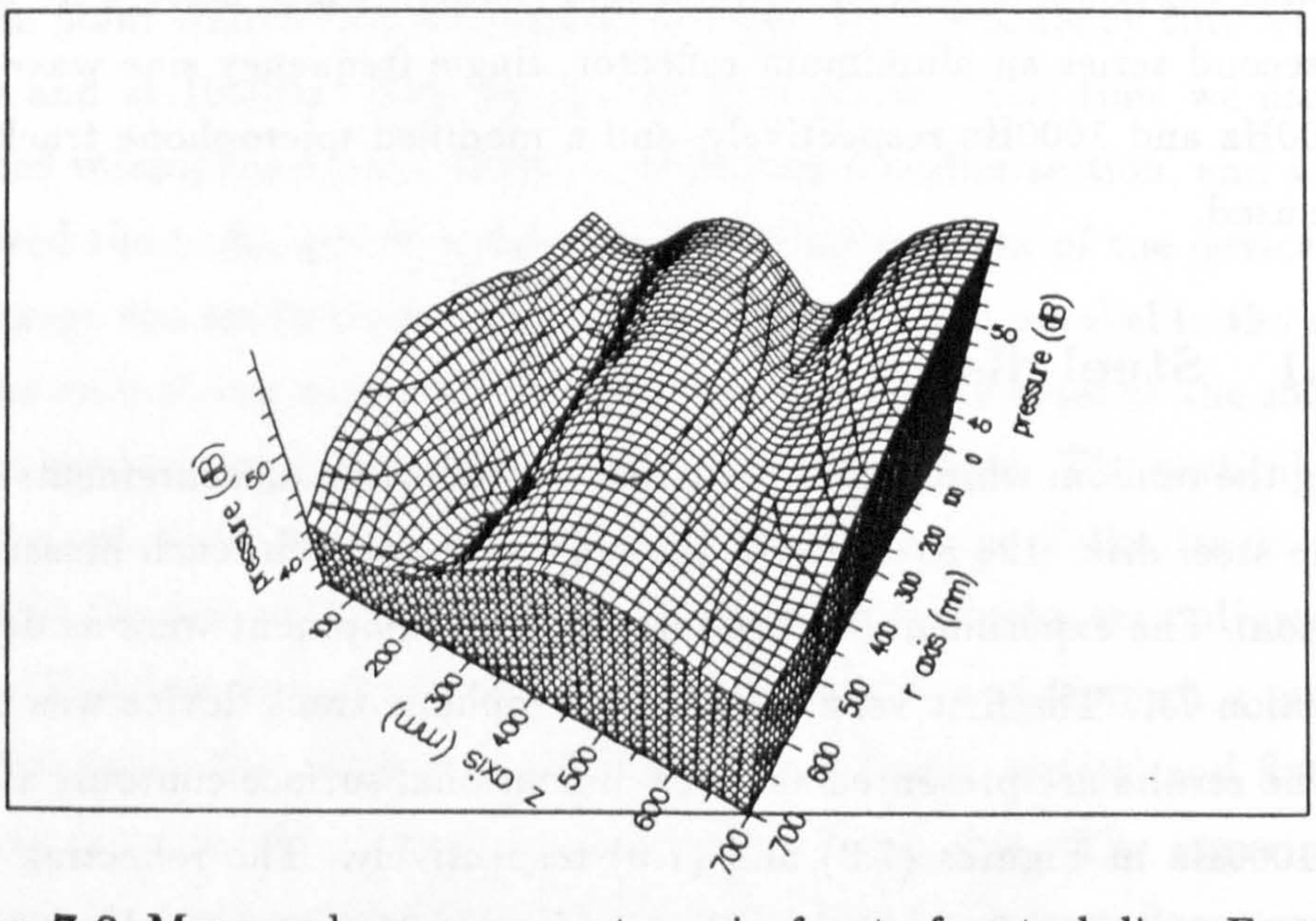

Figure 7.8 Measured pressure contours in front of a steel disc. Frequency 500Hz; source location (0, 1000); the reflecting surface is normal to the z-axis and at z=0; thickness of the plate 0.008m

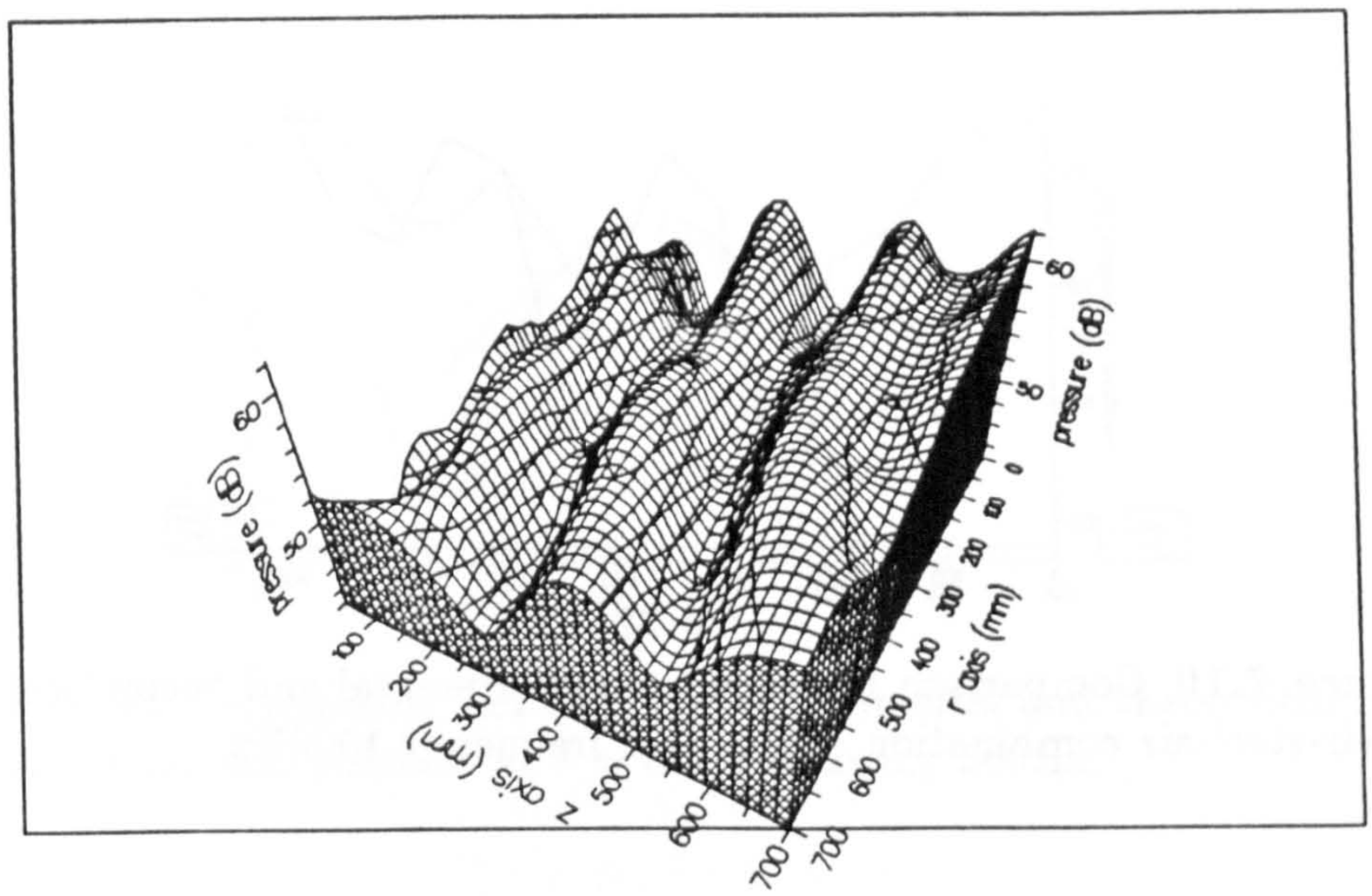

Figure 7.9 Measured pressure contours in front of a steel disc. Frequency 1000Hz; source location (0, 1000); the reflecting surface is normal to the z-axis and at z=0; thickness of the plate 0.008m

results with Figures (7.8) and (7.9) we find that the wave patterns are in good agreement. At 500Hz, there are two troughs in both theoretical and experimental results, and three troughs at 1000Hz. Small local peaks in Figure (7.9) may be the results of the reflected wave from the grille and of the error in the microphone position. From Figures (7.8) and (7.9) we can see the effect of the disc edge near the point (700, 0).

More detailed comparisons are given in Figures (7.10) to (7.15). We select three typical sections: on the central axis $r = 0$ m, at $r = 0.3$ m, and near the edge of the disc $r = 0.7$ m.

The curves in Figures (7.10) to (7.15) are plotted without interpolation so the comparisons are made between the values of the pressure from the calculation and from the experiment for the points at z= 50mm to 700mm with interval of 50mm. The peak amplitudes tend to decrease with increasing distance between the source and the observation point in all of Figures (7.10) to (7.15). This result is a feature of spherical wave propagation.

In Figures (7.12) and (7.15) the experimental results do not show the value at $z = 0.7$ m because the Zenith computer crashed while doing the

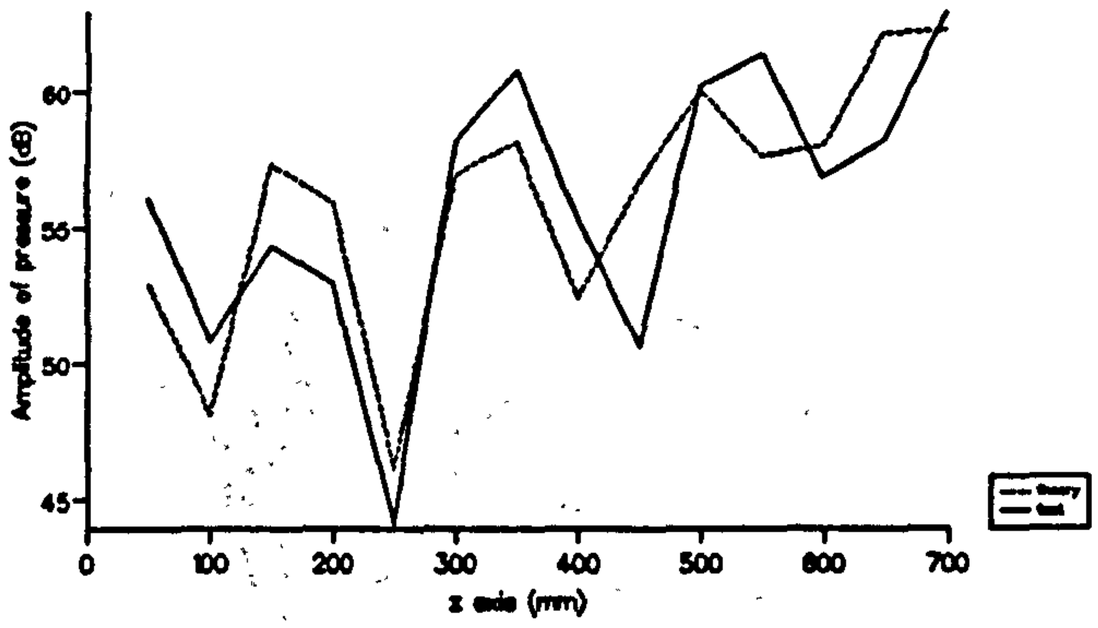

Figure 7.10 Comparison between the experimental and theoretical results for air-steel-air combination at $r = 0$m; frequency 1000Hz.

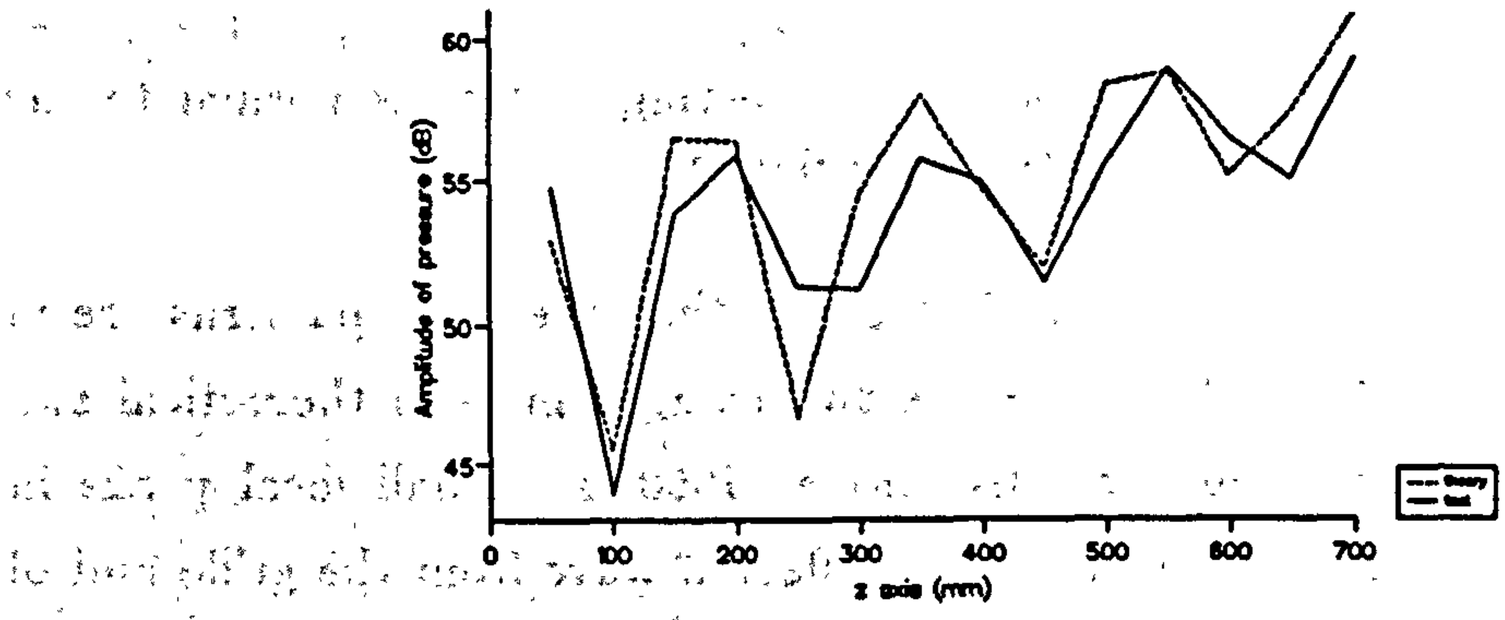

Figure 7.11 Comparison between the experimental and theoretical results for air-steel-air combination at $r = 0.3$m; frequency 1000Hz.

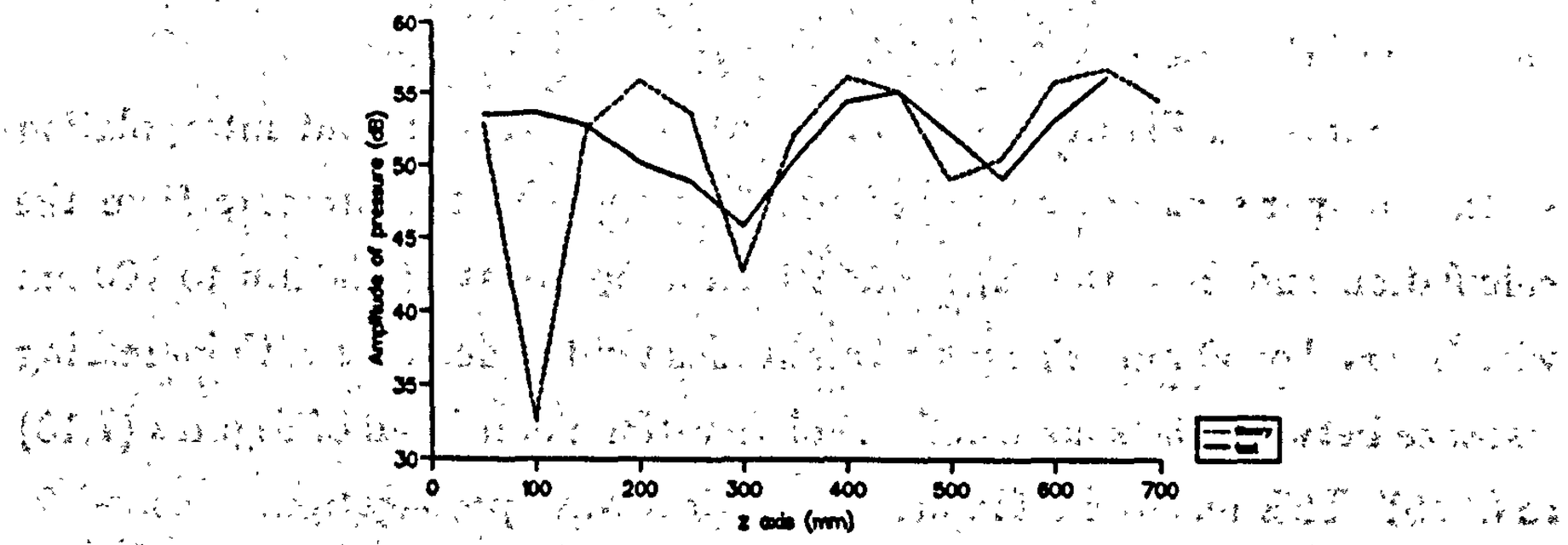

Figure 7.12 Comparison between the experimental and theoretical results for air-steel-air combination at $r = 0.7$m; frequency 1000Hz.

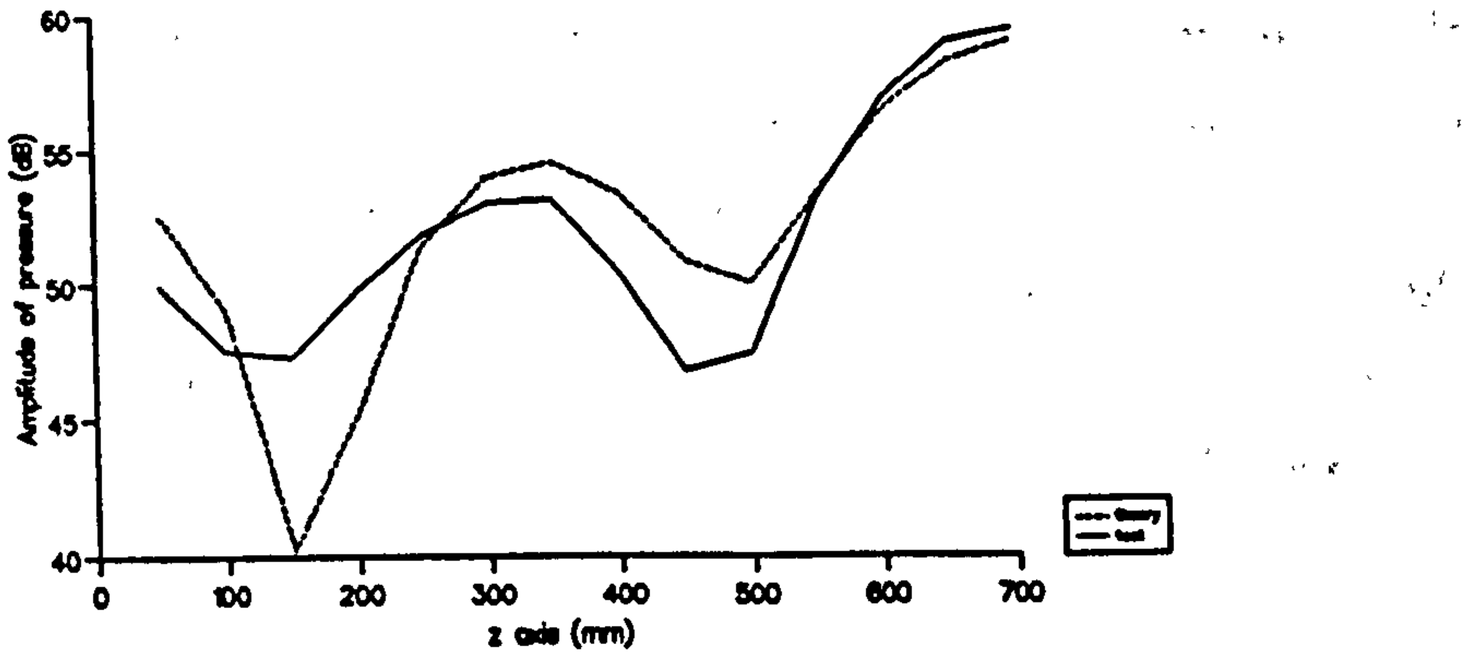

Figure 7.13 Comparison between the experimental and theoretical results for air-steel-air combination at $r = 0$m; frequency 500Hz.

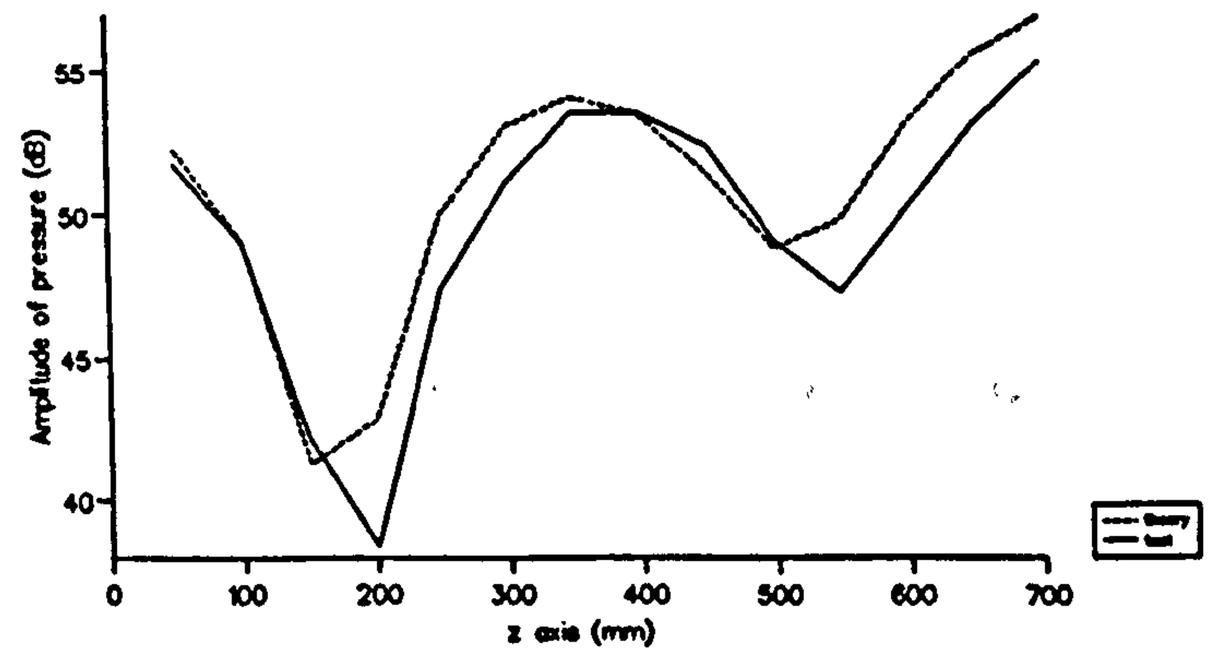

Figure 7.14 Comparison between the experimental and theoretical results for air-steel-air combination at $r = 0.3$m; frequency 500Hz.

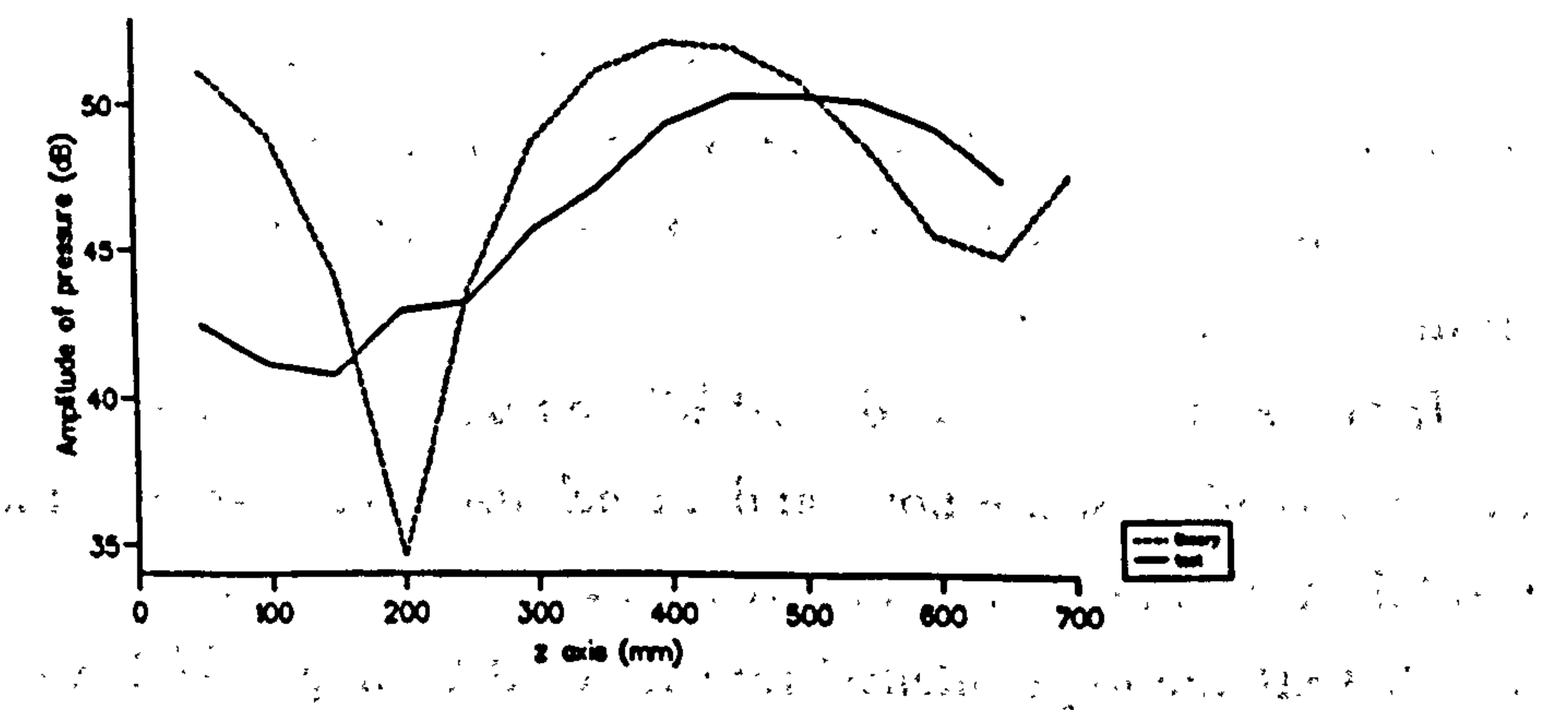

Figure 7.15 Comparison between the experimental and theoretical results for air-steel-air combination at $r = 0.7$m; frequency 500Hz.

last measurement at the last three points and there was no time to repeat the measurement. Since we decided to modify the experiment later, the last three points were not measured again.

At 1000Hz, (Figures (7.10) and (7.11)) there is general agreement between the theory and the test, but in Figure (7.12) for a small value of z there is a large discrepancy. The curve for the measurement in Figure (7.12) was obtained at $r = 0.7$ m, and this position is beyond the edge of the disc so we could not have had a strong reflection to create a deep trough as shown by the theoretical model. However the complete disappearance of the first trough for the test curve could also have been the result of a measurement error, as we shall see later from studying the results of the next experiments. The differences in the positions of the peaks and troughs may be due to the influence of the reflection from the grille.

At 500Hz, the curves in Figure (7.14) for $r = 0.3$m are in a good agreement; at the centre of the disc ($r = 0$m in Figure (7.13)), although the curves agree in shape, there is a large difference in the value at the first trough. From the point source test, we have found that the wave at 500Hz has a better spherical pattern than that at 1000Hz, but the curves in Figure (7.13) show a worse discrepancy than those in Figure (7.10) for the reflection test at the centre of the disc. A possible reason for this is the scattering effect. A wave at 500Hz has a wavelength about 0.6m which is twice as large as the wavelength for a wave of of 1000Hz, and we should remember that the radius of the disc is 0.6 m. When a wavelength is close to the size of an obstacle the scattering effect becomes more important. Near the edge of the disc again we can see the edge effect. The value of the pressure for the experiment at $z = 200$mm could be the result of a measurement error as we shall see later from the next experiments.

In this section we have described the results of the measurement obtained by using random white noise and a steel disc. We have seen that the experimental results are broadly in agreement with the theoretical results. However we felt that the experimental results could be improved if we could modify the technique and the device for positioning the microphone, and use a sta-

ble signal. In the next section, we shall present results from the improved experiment.

7.3.2 Aluminium disc

The theoretical calculation in Chapter 6 showed that a metal plate could be considered as a very good rigid boundary for a point source in air. The material of the metal does not make much difference. For the second set of experiments, an aluminium disc was used. We did not expect to find any large difference between measured data obtained with a steel and that with an aluminium disc according to the theoretical result, but it was felt to be interesting to see if we could find any meaningful difference beyond that attributable to improved experimentation. It should be noted that as a result of the improved procedures the ratio of the signal to the background noise was increased. The background noise was about 5dB. In the test with a steel disc, the signal was generally greater than 40dB and in the test with an aluminium disc the signal was generally greater than 70dB.

The results shown in Figures (7.16) and (7.17) for a aluminium disc are very similar to those for a steel disc of the same radius and thickness. However the curves are smoother. This improvement is particularly noticeable for the 1000Hz curves. There is no significant difference in the patterns. The detailed comparison at several cross sections are given in Figures (7.18) to (7.23). From the detailed comparisons, again we find the decay feature expected for spherical spreading. The edge effects for both the frequency of 500Hz and the frequency of 1000Hz are shown in Figures (7.23) and (7.20) respectively, but the first trough occurs at $z = 100$mm in Figure (7.18), in contrast to Figure (7.10). In the centre of the disc at 500Hz (in Figure (7.16)) the large difference occurs again at the first trough, which we believe to be a scattering effect.

The main discrepancy between the theoretical results and the experimental results is caused by the difference between the infinite plate mathematical model and the finite plate of the experimental model. The differences in the positions of maxima and minima may be caused by the reflections from the

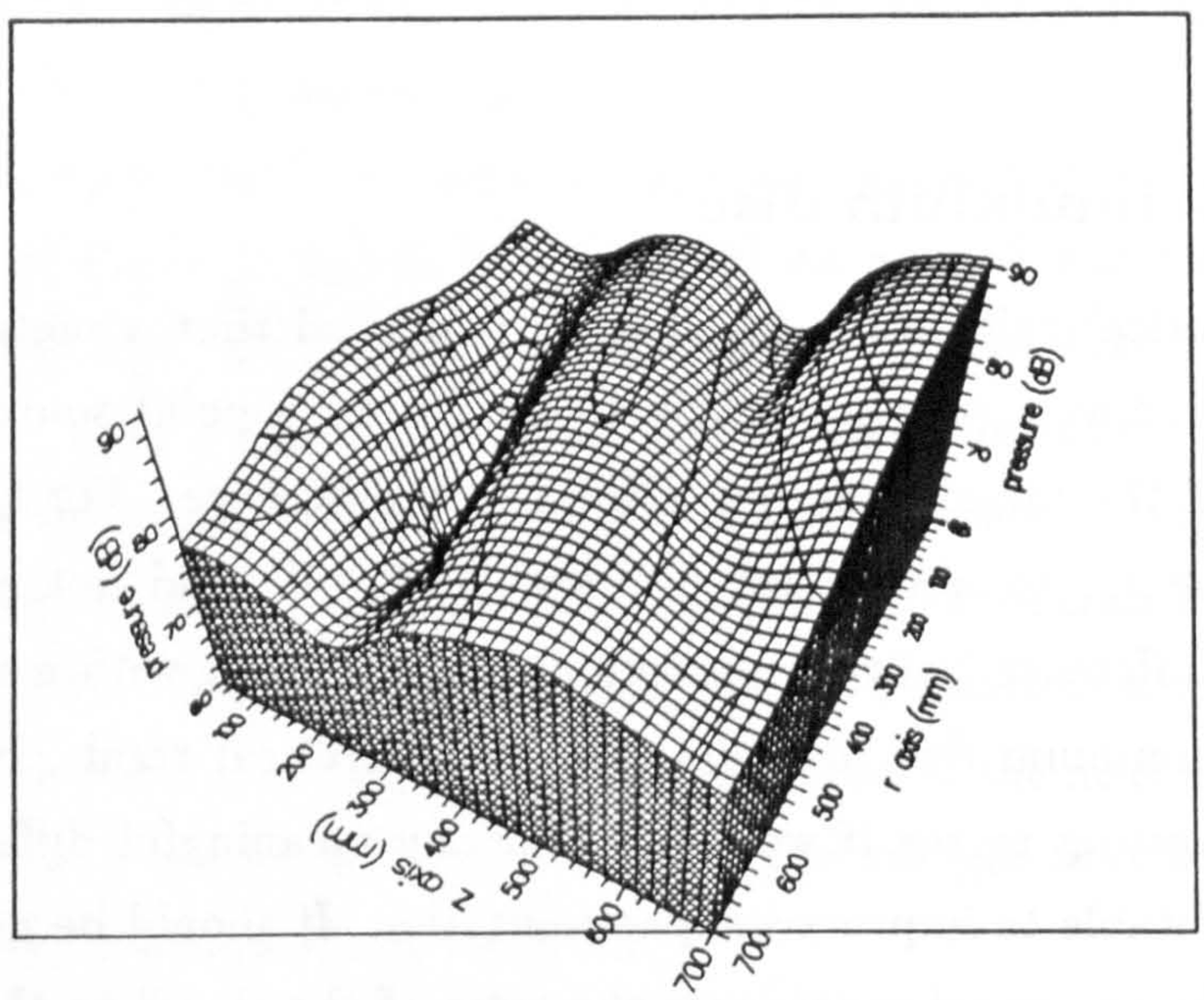

Figure 7.16 Measured pressure contours in front of an aluminium disc. Frequency 500Hz; source location (0, 1000); the reflecting surface is normal to the z-axis and at z=0; thickness of the plate 0.008m.

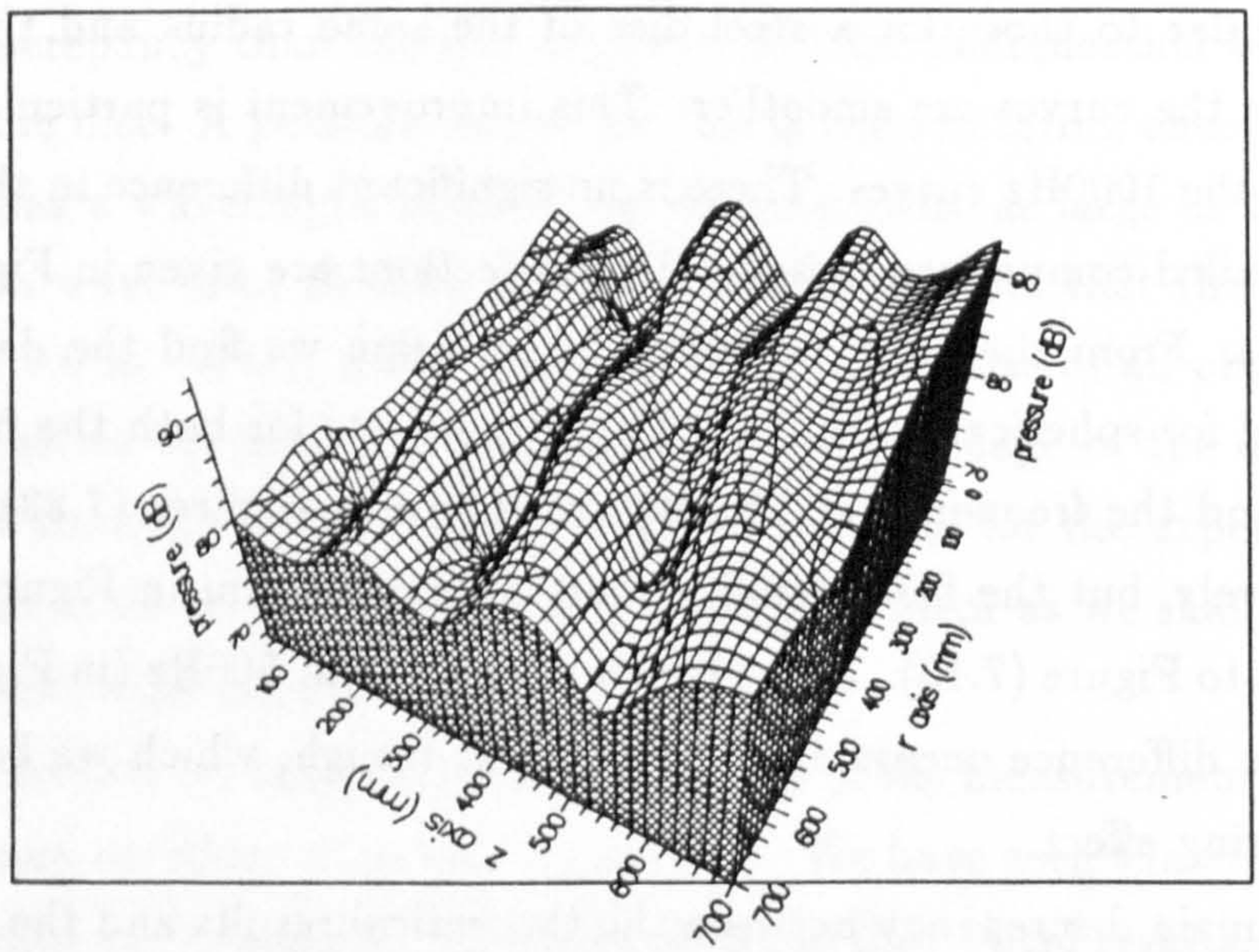

Figure 7.17 Measured pressure contours in front of an aluminium disc. Frequency 1000Hz; source location (0, 1000); the reflecting surface is normal to the z-axis and at z=0; thickness of the plate 0.008m.

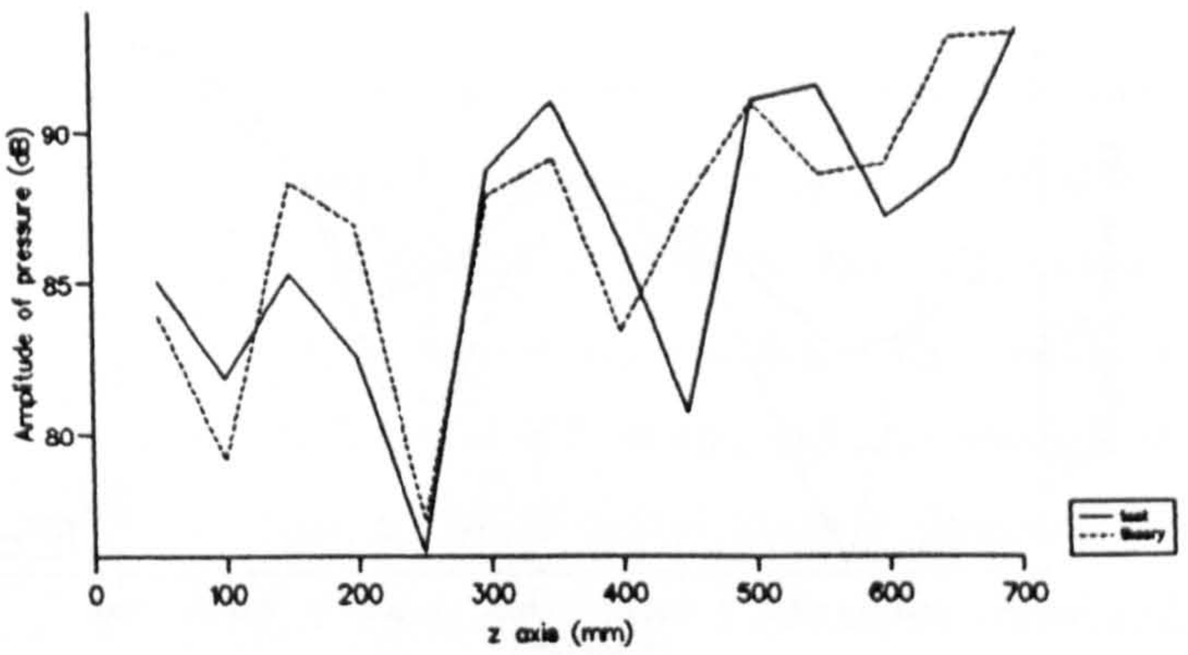

Figure 7.18 Comparison between the experimental and theoretical results for air-aluminium-air combination at $r = 0$m; frequency 1000Hz.

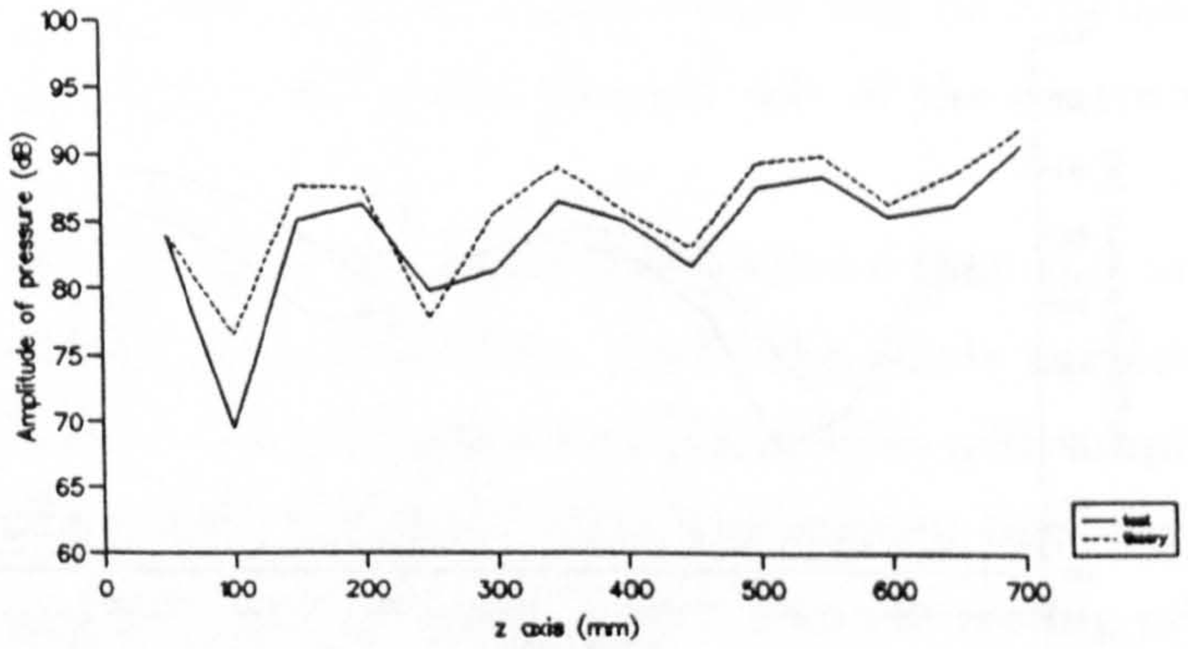

Figure 7.19 Comparison between the experimental and theoretical results for air-aluminium-air combination at $r = 0.3$m; frequency 1000Hz.

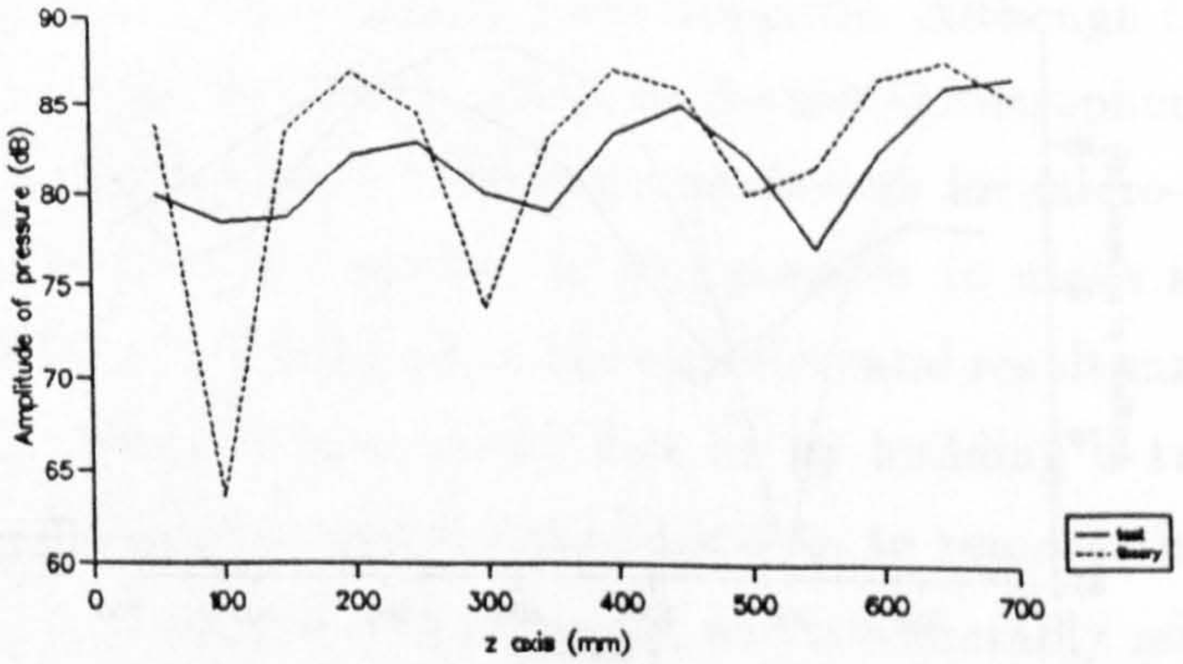

Figure 7.20 Comparison between the experimental and theoretical results for air-aluminium-air combination at $r = 0.7$m; frequency 1000Hz.

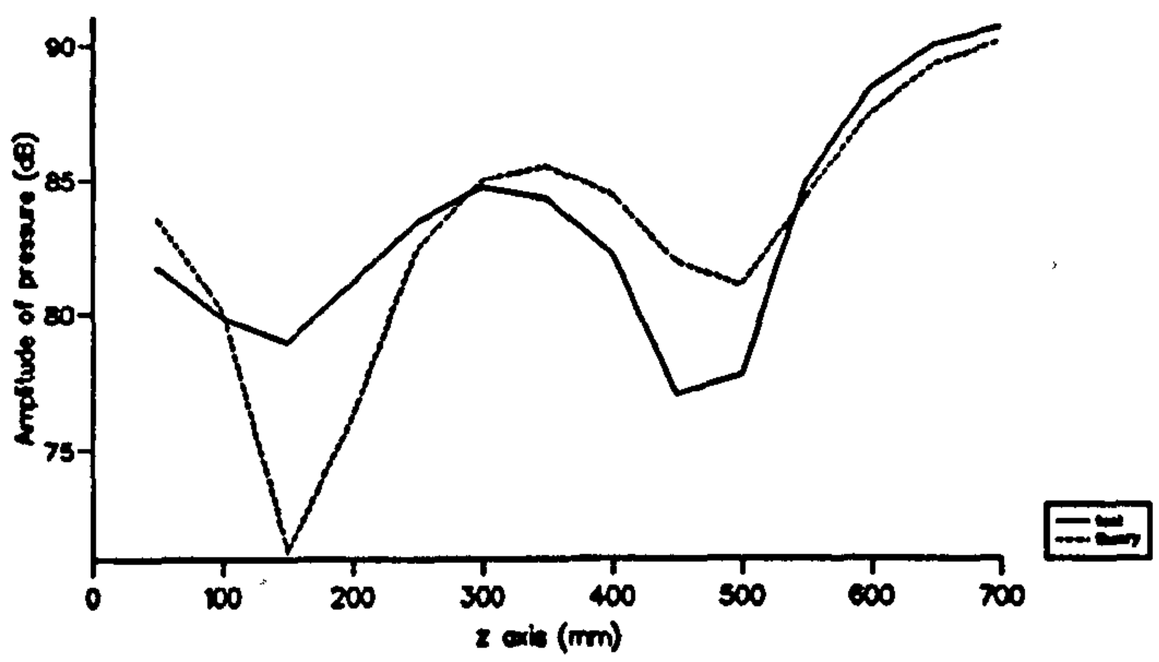

Figure 7.21 Comparison between the experimental and theoretical results for air-aluminium-air combination at $r = 0$ m; frequency 500Hz.

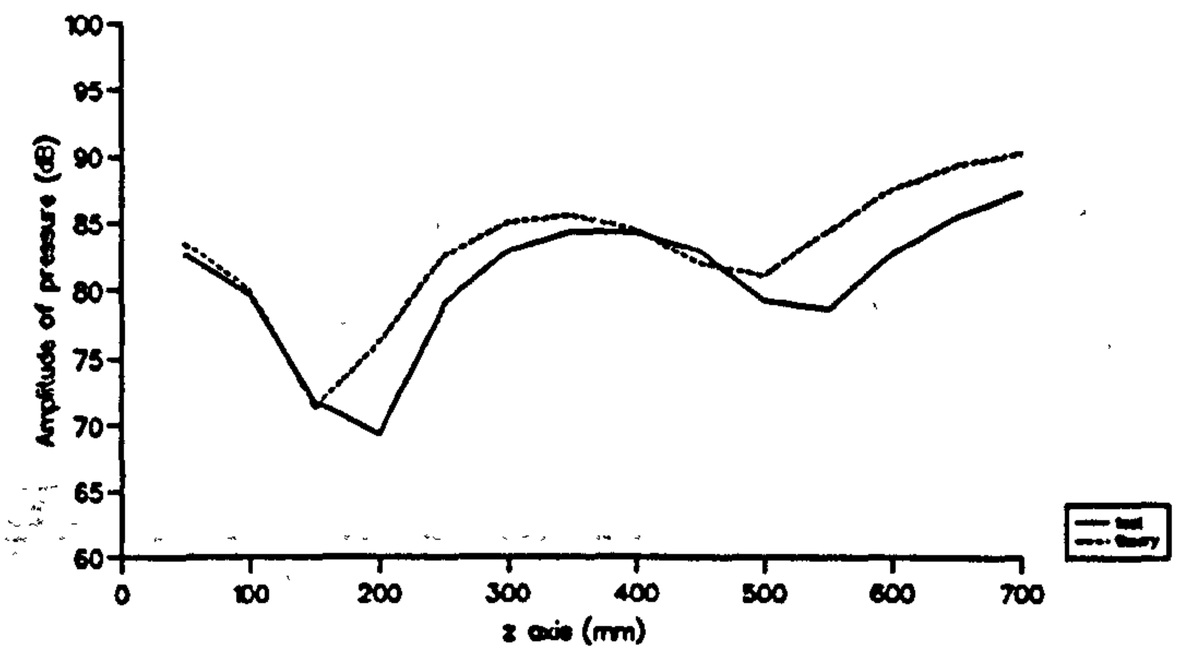

Figure 7.22 Comparison between the experimental and theoretical results for air-aluminium-air combination at $r = 0.3$m; frequency 500Hz.

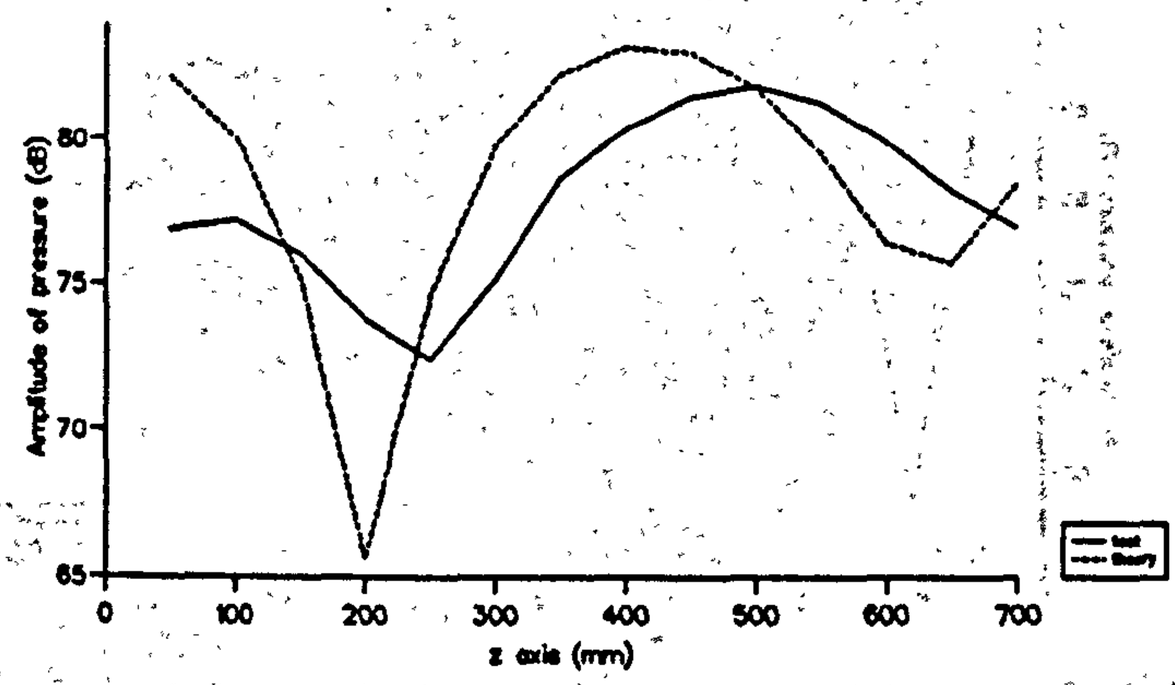

Figure 7.23 Comparison between the experimental and theoretical results for air-aluminium-air combination at $r = 0.7$m; frequency 500Hz.

grille.

The pressure field on the transmission side has also been measured for the frequency at 500Hz. The measured area is from -0.008 m to -0.408 m in the z-direction and from 0 m to 0.7 m in the r-direction. The result is shown in Figure (7.24). It is very different from the result of the numerical calculation for the transmission field of the infinite model, in Figure (7.25), because at 500Hz the scattering effect takes on a dominant role. A possible explanation for the minimum in Figure (7.24) can be obtained by considering plane waves. Let us consider the area behind the disc and assume that two plane waves are propagating towards the centre from the edges of the disc at each side of a diameter. When the waves have a frequency of 500Hz, and the diameter of the disc is about 1.2m; a peak will be obtained at about the centre and two minima will occur on each side of the centre as we obtained in Figure (7.24).

The theoretical result in Figure (7.25) shows that the contour lines are almost parallel to the surface of the disc. The whole surface of the disc in this area acts like a source to generate a plane wave with amplitude decay. In the experimental result of Figure (7.24), the contour lines are almost normal to the plate surface near the z-axis. There is an interesting minimum line. It will be interesting to see if these results are consistent with existing diffraction theory, but this matter has not been pursued in this theses.

For the experiments with the single frequency sine wave signal, the errors are mainly caused by the reflection from the grille. Although the microphone track device has been modified, setting up the initial microphone position still consumed a lot of time since there were no devices for micro-adjustment. If the experimenter was not careful, it was possible to make an error in the microphone position. It is felt that the experimental result may be improved by moving the source closer to the disc or by building a two-dimensional microphone track device, which would allow us to remove the grille, ensure the accurate positioning of a microphone, and considerably reduce the length of the time for experiments. A possible design will be discussed in the last chapter.

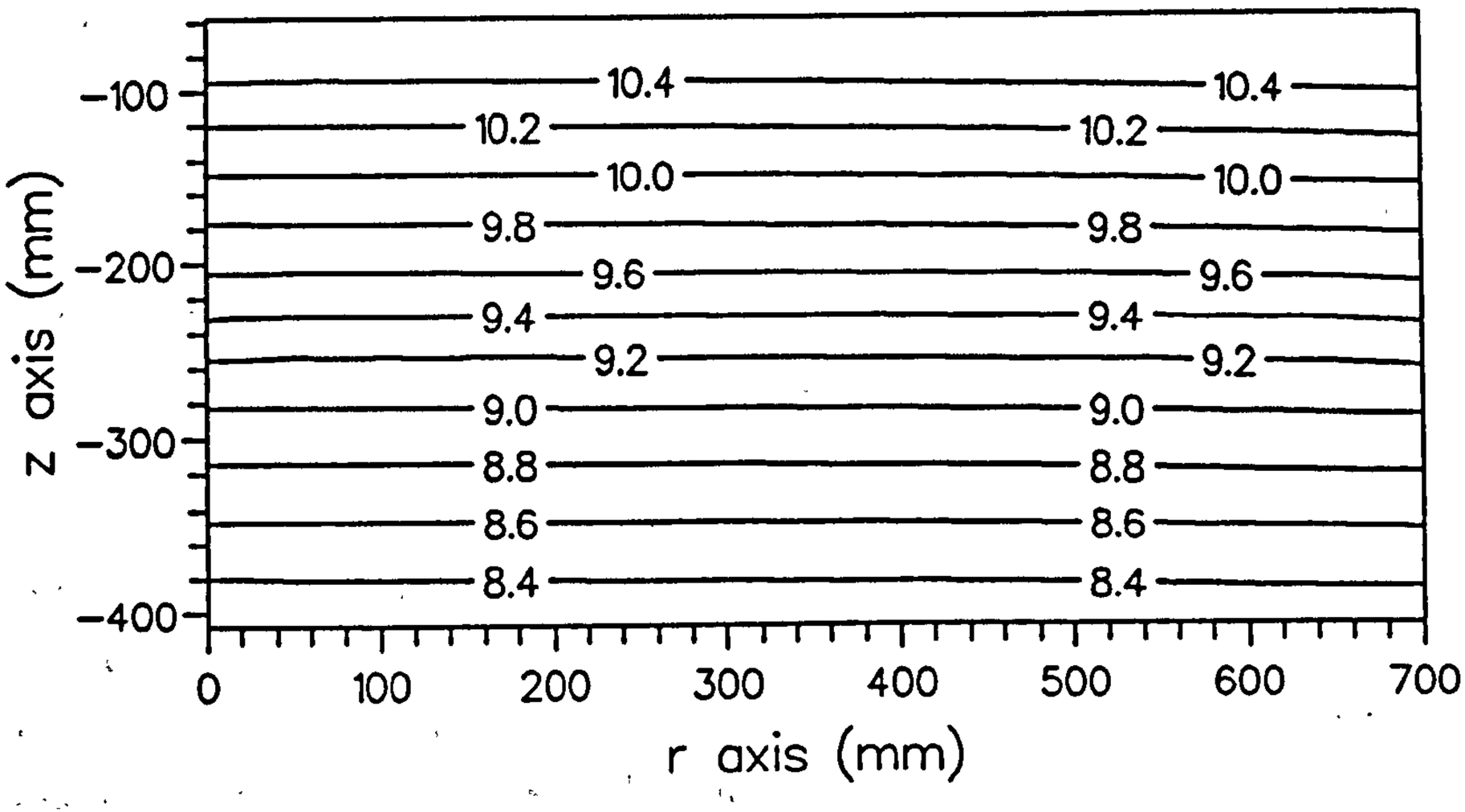

Figure 7.24 Transmission pressure contours from the theory for air-aluminium-air combination. Frequency 500Hz; source height 1m; thickness of the plate 0.008m.

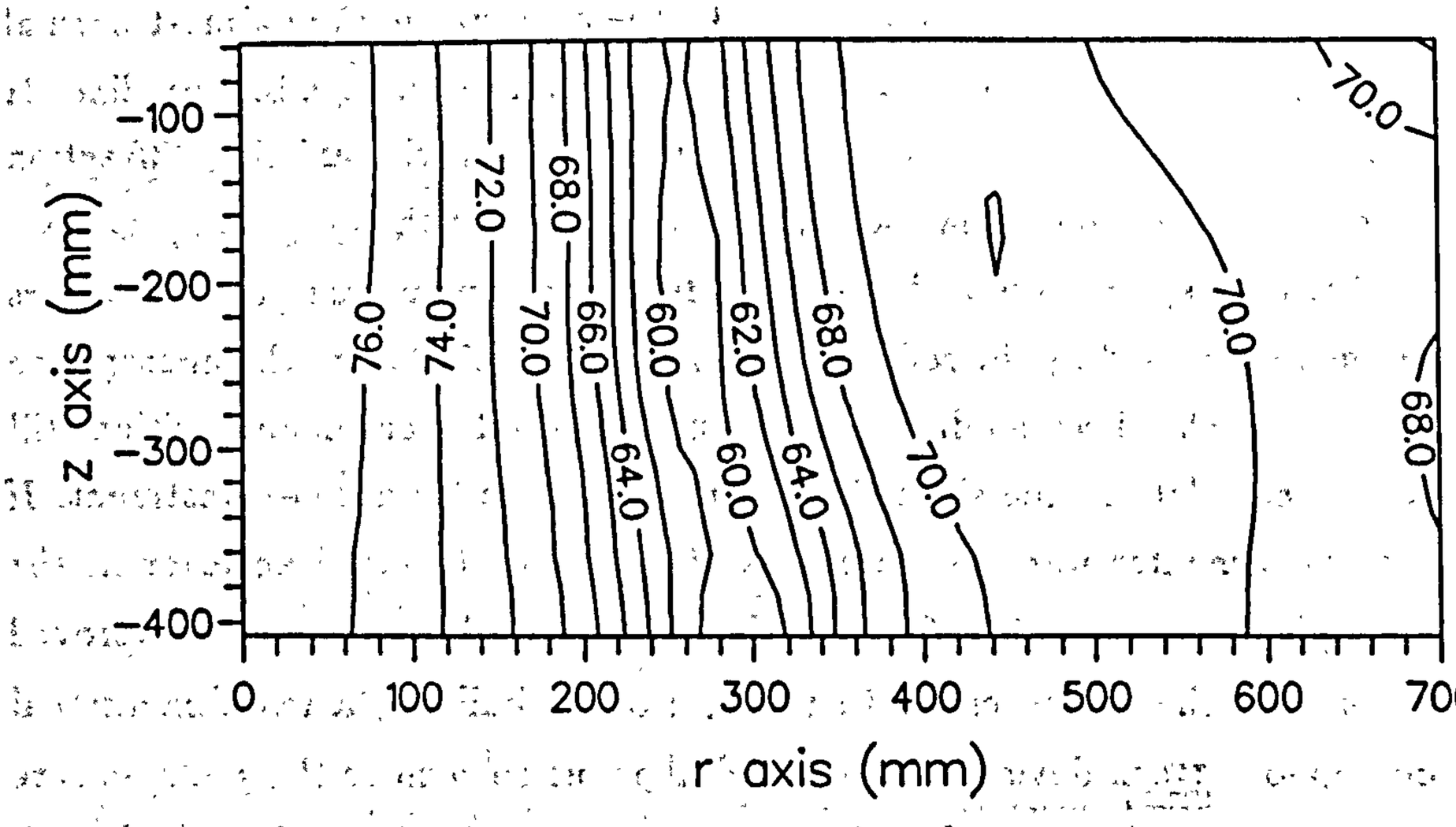

Figure 7.25 Transmission pressure contours from the experiment for air-aluminium-air combination. Frequency 500Hz; source height 1m; thickness of the plate 0.008m.

From the above we can see that the theoretical and experimental results are in fairly good agreement. The two results support one another. Therefore we can reasonably believe that the theoretical results for pressure fields which we have obtained in the earlier chapters could describe spherical wave reflection at a plane interface in reality very well if the reflection area is large compared with the wavelength, and compared with the source height. If the source height is large and the reflection area is small, the incident wave at the reflection surface would behave more like a plane wave rather than a spherical wave regardless of the wavelength. However, when the reflection area is finite, for small wavelengths the correspondence between the wave field in the medium containing the source and the wave field predicted above a reflection area of infinite extent is closer than that for large wavelengths. In the case that the source height and the reflection area are similar, the ratio of the wavelength to the smallest dimension of the reflection area is an important criterion when we consider using the theoretical result of infinite surface model to predict a realistic wave field with a finite reflection area.

The experimental method which we have used in this study can produce good results and is reliable. The technique is particularly suitable for acoustical scattering experiments.

The experimental results only confirm the validity of the predicted pressure distribution. The prediction of the "backward wave" phenomenon would have to be tested by different means involving, perhaps, the measurement of sound intensity.

Chapter 8

Conclusion

8.1 Review of the results

The subject of this thesis is the study of the reflection and transmission of spherical waves at plane boundaries. The research has been based on a theory of linear elastic wave propagation, combined with Lamb/Sommerfeld's integral representation for spherical waves. A new integral representation for spherical waves has been obtained by transforming Lamb's integral representation. New forms of integral expressions for the incident, reflected, and transmitted waves have been obtained through transformations of some existing solutions for the reflection of spherical waves at plane boundaries. The new solutions together with existing solutions have been checked numerically in some cases to see if they satisfy the law of energy conservation and the results are satisfactory. The theoretical result for spherical wave reflection at a rigid boundary has been tested by experiment. Theoretical and experimental results show a good agreement within the constraints of the model differences and external interference on the measurements. We believe that the resulting theory of linear spherical waves should give a good description of the phenomenon of spherical wave reflection and transmission at infinite plane boundaries. In practice, the theoretical result can provide a good approximation when the dimension of a boundary surface is large compared with the distance between a point source and the boundary, and with the wavelength.

One contribution made in the study is to the understanding of the widely-used Lamb's formula

$$\frac{exp(-ik\sqrt{r^2+z^2})}{\sqrt{r^2+z^2}} = \int_0^\infty \frac{J(r\xi)exp(-|z|\sqrt{\xi^2-k^2})\xi}{\sqrt{\xi^2-k^2}}\, d\xi. \qquad (8.1)$$

In this thesis, this integral representation for spherical waves has been studied analytically and numerically. The analytical study has shown (in Chapter 5) that the integral in formula (8.1) is convergent and a new proof of formula (8.1) has been offered when the variables r, z, k and ξ are real quantities. The proof also indicates that the argument of the exponential function on the left side of equation (8.1) must have a minus sign for positive real k and ξ.

A new form of formula (8.1), obtained from the convergence analysis, is

$$\frac{exp(-ik\sqrt{r^2+z^2})}{\sqrt{r^2+z^2}} = \int_{ik}^\infty J(r\sqrt{k^2+x^2})exp(-|z|x)\, dx \qquad (8.2)$$

where the integration path is from ik to $i0$ on the imaginary axis and from 0 to ∞ on the real axis. Since the integral in formula (8.2) has no singularity, it allows more accurate numerical integration than does the integral in (8.1).

One of the features of this research is that we have used up-to-date research tools. REDUCE software for symbolic manipulation has been used in the analytical study, and the numerical investigation has been carried out with the help of the software from the NAG library. For the experimental study, we have used a computer controlled measurement system with a digital FFT analyzer.

The numerical results in Chapter 6 have shown that when a spherical wave impinges on a plane interface between two semi-infinite fluids from an acoustically soft medium to a harder one (an example was given for the case of a kerosene-water interface), with increasing angle of incidence, the energy reflected from the interface decreases until a critical angle is reached, at which time no average energy penetrates into the harder medium. Beyond the critical angle, at some angles there is some net time average transmitted energy but at other angles there is no net time average transmitted energy. This may be associated with the interference between the incident and diffracted

waves. The critical angle for a spherical wave is dependent not only on the material constants of the two media, but also on the frequency and the distance between the source and the interface. The critical angle for a spherical wave is greater than that for a corresponding plane wave. However as the distance between the source and the interface increases, the critical angle for a spherical wave tends to that for a plane wave. This is what we expect since a plane wave can be considered as a far field approximation of a spherical wave.

At a plane interface between two media, the variations, with angle of incidence, of the reflection and transmission coefficients for spherical waves are very similar to those of plane waves, but they are both frequency and source height dependent. As the source height increases, the curves for the reflection and transmission coefficients as functions of incidence angle for spherical waves tend to those of plane waves.

Predictions we have obtained for spherical wave incidence on a fluid-solid-fluid system suggest that the moduli of the reflection coefficient at the interface between the fluid and the solid, and of the transmission coefficient at the interface between the solid and the fluid at normal incidence are consistent with those of a corresponding plane wave. The values of the moduli for a spherical wave are generally smaller than those for a plane wave because of the energy spreading except for the transmission coefficients at 5000 Hz. Nevertheless, all values are less than unity. We believe that the numerical predictions of "overpressures" at normal incidence obtained by Piquette [46] in the corresponding case are most likely due to numerical errors. Nevertheless, some of the numerical results we have obtained indicate that "overpressures" are possible for angles of incidence near grazing. One possible explanation is the constructive interference between the reflected and the diffracted waves at the interface (see Section 6.2).

An interesting numerical result from studies of energy flux is the possibility of "backward waves" associated with spherical wave reflection and transmission at an acoustically hard boundary. It was found that in some regions above a point source, both the direct and reflected waves should travel

upwards away from the boundary; however the normal component of the local time average energy flux of the superposition of the two waves may be in the direction downwards to the boundary. A similar situation happens for the transmitted waves; the normal components of the local time average energy flux may be in the direction upwards towards the boundary although the transmitted wave should travel away from the boundary. This so called "backward wave" phenomenon will be discussed in the next section.

Some hypothesized solutions for spherical wave reflection and transmission based on the integral representation

$$\frac{exp(ik\sqrt{r^2+z^2})}{\sqrt{r^2+z^2}} = i\int_0^\infty H_0^{(1)}(z\sqrt{k^2-x^2})cos(rx)\,dx \qquad (8.3)$$

were also obtained and studied numerically, (Expression (8.3) of course gives the complex conjugate of expression (8.1) or (8.2)). We were not able to prove whether these solutions satisfy the equations of motion but have suggested and shown that the representation (8.3) and the corresponding hypothesized solutions might have potential applications because of their numerical stability.

8.2 Discussions and suggestions for further work

8.2.1 On Lamb's integral for spherical waves

We have shown the validity of formula (8.1) for real variables in Chapter 5. The proof uses the method of power series expansion and the theory of differential equations. As was pointed out in Chapter 5, if we could have proved equation (5.19), we could have avoided having to use the theory of differential equations. Unfortunately we could not. It is felt that it might be possible to prove equation (5.19) by dividing it into two parts, and proving results for each part *viz.*

$$\int_0^k J_0(r\sqrt{k^2+x^2})sin(zx)\,dx = \int_0^k J_0(z\sqrt{k^2+x^2})sin(rx)\,dx \qquad (8.4)$$

and

$$\int_0^\infty J_0(r\sqrt{k^2+x^2})exp(-zx)\,dx = \int_0^\infty J_0(z\sqrt{k^2+x^2})exp(-rx)\,dx. \quad (8.5)$$

In fact we know that the equation

$$\int_0^\infty exp(-at)J_0(bt)\,dx = \int_0^\infty exp(-bt)J_0(at)\,dx \quad (8.6)$$

is valid.

The formula for real variables can be applied only to the situation where energy absorption can be neglected. This is the case that we have been studying. For waves propagating in a medium of energy absorption, the wavenumbers becomes complex. Our analysis in Chapter 5 is invalid for complex wavenumbers. There is a difficulty in using the method of power series expansion for a complex wavenumber because it is not easy to find suitable expansions which will give a simple series expression of the integrand for the integration. A possible method to deal with a complex wavenumber is borrowed from the ideas of Sonine and Gegenbauer. One of the mathematical problems which we need to solve is the convergence of an improper double integration. A discussion of improper double integration is given in Appendix (A).

Extension of the new integral formulations to complex wavenumbers will have many practical applications. For example, acoustic-seismic coupling have been of interest to geophysicists and others for over fifty years. An analysis of acoustic-seismic coupling based on plane continuous harmonic waves and a simple structural model of a poroelastic surface layer above an elastic sub-strata has been published ([86] to [88]) and has been shown to give tolerable agreement with measured data. A theoretical problem of general interest is that of acoustic-to-seismic coupling from a point source. Many existing studies are based on the Lamb/Sommerfeld integral, [89], [90]. It is felt that if we could derive a new integral in the form of (8.2) with a complex wavenumber and use this new integral to study spherical wave reflection and transmission at porous boundaries, we should be able to improve our understanding of acoustic-seismic coupling. Applications of

this theoretical work could include the interpretation and predication of air-coupling in seismic surveys, and interpretation of bottom interacting sonar data near grazing angles to obtain the properties of seabed sediments [91].

8.2.2 On the experiment

It is felt that one of the important factors that would ensure a better pressure contour measurement is more accurate positioning of the microphone. To achieve this using the existing equipment, we have to carefully set up the initial microphone position at each z coordinate, which increases the experimental time. Even so, the accuracy is not absolutely guaranteed because of human error.

The best way to obtain an accurate microphone position is to design a completely automatic measurement system. In order to ensure the accuracy of the microphone position, a possible design is to use an optoelectronic device, and control the two-dimensional movement of the microphone by a gear box through a pulley system. This is not difficult to achieve since we have been using a computer controlled system. With use of an optoelectronic device, we only need to carefully set up a microphone position gauge once for the whole measurement. The only requirement for the microphone moving system is that the microphone moves in a straight line and parallel to the microphone position gauge. Two small step motors could be used. One would control the gear box and the other would control the position of the microphone. The step motor that we have been using is too large for the job. Use of a single step motor would be possible but it would require a good design of the gear box system.

Apart from increasing the accuracy of microphone position, another advantage of using an optoelectronic device is that we can have a flexible compact microphone moving system; therefore we can reduce the interference caused by the presence of the structure of the microphone moving system.

The use of finite plates in experiments means that we have a system for studying diffraction effects. Theories of diffraction around plates could be tested by such a system.

8.2.3 On backward waves

Among the results we have obtained is the interesting prediction of circumstances in which the time average energy of a wave propagates in the direction opposite to that in which the wave is supposed to be travelling. Very probably these instances of "backward waves" are related to the well known locally closed loop time average sound intensity trajectories [92]. Simple examples associated with interference effects are shown in Figures.4.8(a) and 4.12(a) and (c) of [92]. Complicated cases may be obtained from a Helmholtz resonator (Fig.4.20 in [92]) and a point-force excited, water-loaded plate (Fig.4.21 in [92]). It should be noted that closed intensity loops do not occur in the interference between two orthogonally plane travelling waves (see e.g. Fig.4.8(b) in [92]).

The explanation of spherical wave reflection and transmission mentioned earlier [66], [49], suggests that the closed intensity loop may occur for transmitted waves as a result of the wave re-entering into the source medium [66].

A feature of the backward wave is that the time average energy flux and the corresponding wavenumber (or its components) is (are) of opposite sign(s). Another known example where where the energy flux and the wavenumber along the waveguide axis may have opposite signs at certain modes may be found in the elastic waveguide [94], [95]. In this case, coupled longitudinal and transverse waves travel along an elastic solid plate of infinite extent. An experiment [96] has confirmed the existence of such modes by measuring wave speed against frequency, but the experiment could not verify the opposite sign of the energy flux and the wavenumber.

The backward waves we have predicted are simpler than other cases. We have found the phenomenon either in a transmitted wave or in the interference of two travelling waves. If we can determine the conditions under which the backward spherical waves occur or the closed intensity loops occur, and test those conditions by experiments (e.g., intensity measurement), it will help us to understand more about the backward wave and may provide guidance for the understanding of the other instances of backward waves.

Bibliography

[1] H.Lamb, *On the propagation of tremors over the surface of an elastic solid*, Phil. Trans. Roy. Soc. A203, 1904.

[2] W.Thomson and P.G.Tait, *Treatise on Natural Philosophy,* Part II, Cambridge Press, 1890.

[3] A.Sommerfeld, Ann.d.Physik., 28, 665, 1909.

[4] A.Sommerfeld, *Partial differential equations in physics*, Academic press, 1949.

[5] J.A.Stratton, *Electromagnetic theory*, McGraw-Hill, 1941.

[6] B.Van der Pol, *Theory of the reflection of the light from a point source by a finitely conducting flat mirror, with an application to radiotelegraphy*, Phyica, v.2, p.843-853, 1935.

[7] K.A.Norton, *The propagation of radio waves over the surface of the earth and in the upper atmosphere*, Proc. Inst. Radio Eng., v.25, n.9, p.1203-1236, 1937.

[8] I.Rudnick, *The propagation of an acoustic wave along a boundary*, J.Acoust.Soc.Am., v.19, p.348-356, 1947.

[9] D.I.Paul, *Acoustical radiation from a point source in the presence of two media*, J.Acoust.Soc.Am., v.29, n.10, 1957.

[10] R.B.Lawhead and I.Rudnick *Measurements on an acoustic wave propagated along a boundary*, J. Acoust. Soc. Am., v23. n.541-545, 1957.

[11] W.A.Ewing, W.S.Jardetzky and F.Press, *Elastic waves in layered media*, McGraw-Hall, 1957.

[12] U.Ingard, *On the reflection of a spherical sound wave from an infinite plane*, J. Acoust. Soc. Am. v.23, n.3, p.329-335, 1951.

[13] H.Weyl, Ann.Physik, v.60, p.481-500, 1919.

[14] R.B.Lawhead and I.Rudnick, *Acoustic wave propagation along a constant normal impedance boundary*, J.Acoust.Soc.Am., v.23, n.5, p.546-549, 1951.

[15] L.M.Brekhovskikh, *Waves in layered media*, Academic press, 1980.

[16] A.Schoch, *The reflection, refraction , and diffraction of sound*, Ergeb. Exakt. Naturw., 23, p127-234, 1950.

[17] L.M.Brekhovskikh and Lysanov, *Fundamentals of ocean acoustics*, Springer-Verlag, Berlin, 1982.

[18] P.E.Doak, *The reflexion of a spherical acoustic pulse by an absorbent infinite plane and related problems*, Proceedings of the Royal Society, A, Vol.215, p.233, 1952.

[19] M.E.Delany and E.N.Bazley, *Monopole radiation in the presence of an absorbing plane*, J.Sound Vib. v.13, n.3, p.269-279, 1970.

[20] N.Bleistein, *Uniform asymptotic expansion of integrals with a stationary point near an algebraic singularity*, Comm.Pure Appl.Math. 19, 353-370, 1966

[21] A.R.Wenzel, *Propagation of waves along an impedance boundary*, J.Acoust.Soc.Am., v.55, n.5, p.956-963, 1974.

[22] W.K.Van Moorhem, *Reflection of a spherical wave from a plane surface*, J. Sound Vib., v.42, n.2, p.201-208, 1975.

[23] C.F.Chien and W.W.Soroka, *Sound propagation along an impedance plane*, J.Sound Vib., v.43, n.1, p.9-20, 1975.

[24] D.C.Stickler, *Reflection and lateral waves for the Sommerfeld model*, J.Acoust.Soc.Am., 60, 1061-1070, 1976.

[25] T.F.W.Embleton, J.E.Piercy and N.Olson, *Outdoor sound propagation over ground of finite impedance*, J.Acoust.Soc.Am., v.59, n.2, p.267-277, 1976.

[26] Sven-Ingvar Thomasson, *Reflection of waves from a point source by an impedance boundary*, J.Acoust.Soc.Am., v.59, n.4, p.780-785, 1976

[27] R.J.Donato, *Propagation of a spherical waves near a plane boundary with a complex impedance*, J.Acoust.Soc.Am., v.60, n.1, p.34-39, 1976.

[28] M.Briquet and P.Filippi, *Diffraction of a spherical wave by an absorbing plane*, J.Acoust.Soc.Am., v.61, n.3, p.640-646, 1977.

[29] P.J.T.Filippi and D.Habault, *Reflexion of a spherical wave by the plane interface between a perfect fluid and a porous medium*, J.Sound Vib., v.56, n.1, p.97-103, 1978.

[30] K.Attenborough, S.I.Hayek and J.M.Lawther, *Propagation of sound above a porous half-space*, J.Acoust.Soc.Am., v.68, n.5, p.1493-1501, 1980.

[31] D.Habault and P.Filippi, *Ground effect analysis:surface wave and layer potential representations*, J. Sound Vib., v.79, p.529-550, 1981.

[32] K.Attenborough, *Predicted ground effect for highway noise*, J.Sound Vib. v.81, n.3, p.413-424, 1982.

[33] T.Kawai, T.Hidaka and T.Nakajima, *Sound propagation above an impedance boundary*, J.Sound Vib. v.83, n.1, p.125-138, 1982.

[34] A.D.Rawlins, *The field of a spherical wave reflected from a plane absorbent surface expressed in terms of an infinite series of Legendre polynomials*, J. Sound Vib., v.89, n.3, p.359-363, 1983.

[35] M.A.Nobile and S.I.Hayek, *Acoustic propagation over an impedance plane,* J.Acoust.Soc.Am., v.78, n.4, p.1325-1336, 1985.

[36] T.L.Richards, K.Attenborough, N.W.Heap and A.P.Watson, *Penetration of sound from a point source into a rigid porous medium,* J.Acoust.Soc.Am., v.78, n.3, p.956-963, 1985.

[37] N.G.Plumpton and C.T.Tindle, *Saddle point analysis of the reflected acoustic field,* J.Acoust.Soc.Am., 85, 1115-1123, 1989.

[38] K.Attenborough and T.L.Richards, *Solid particle motion induced by a point source above a poroelastic half-space,* J.Acoust.Soc.Am., 86, 1085-1091, 1989.

[39] F..Mechel, *Analysis of spherical wave propagation over absorbing ground,* proc.I.O.A., Vol 11, part 5, 231-256, 1989.

[40] S.Chandler-Wilde, Ph.D. Thesis, The University of Bradford, Bradford, U.K., 1987.

[41] F.R.DiNapoli and R.L.Deavenport, *Theoretical and numerical Green's function field solution in a plane multilayered medium,* J.Acoust. Soc.Am., v.67, n.1, pp.92-105, 1980.

[42] H.W.Marsh and S.R.Elam, Internal Document, Raytheon Co., Marine Research Laboratory, New London, CT 1967.

[43] T.L.Richards and K.Attenborough, *Accurate FFT-based Hankel transforms for predictions of outdoor sound propagation,* J.Sound Vib., v.109, n.1, p.157-167, 1986.

[44] H.Schmidt and J.Glattetre, *A fast field model for three-dimensional wave propagation in stratified environments based in the global matrix method,* J.Acoust.Soc.Am., v.78, n.6, p.2105-2114, 1985.

[45] H.Schmidt and F.B.Jensen, *A full wave solution for propagation in multilayered viscoelastic media with application to Gaussian beam reflection at fluid-solid interfaces,* J.Acoust.Soc.Am., v.77, n.3, p.813-825, 1985.

[46] J.C.Piquette, *Spherical wave scattering by a finite thickness solid plate of infinite lateral extent, with some implications for panel measurements,* J.Acoust.Soc.Am., 83(4), p.1284-1294, 1988.

[47] W.Squire, *Integration for engineers and scientists,* American Elsevier, 1970.

[48] R.Courant and D.Hilbert, *Methods of mathematical physics,* Vol II, Interscience, 1966.

[49] F.G.Friendlander, *Sound pulses,* Cambridge, 1958.

[50] D.Jones, *Acoustic and electromagnetic waves,* Clarendon, 1989.

[51] P.M.Morse and K.U.Ingard, *Theoretical acoustics,* McGraw-Hill, 1968.

[52] L.E.Kinsler, A.R.Frey, A.B.Coppens and J.V.Sanders, *Fundamentals of acoustics,* John Wiley and Sons, 1982.

[53] D.K.Kahaner, *Numerical quadrature by the ϵ-algorithm,* Math. Comp., 26, 689-693, 1972.

[54] H.Weber, *Ueber einige bestimmte Integrale,* Crelle, vol.69, 1868.

[55] O.E.Stanaitis, *A introduction to sequences, series, and improper integrals,* Prentice-Hall, 1969.

[56] R.Courant and F.John *Introduction to calculus and analysis,* V.1 Interscience Publishers, 1965.

[57] G.N.Watson *Theory of Bessel functions,* Cambridge, 1969.

[58] N.J.Sonine, *Recherches sur les fonctions cylindriques et le developpement des fonctions contnues en series,* Math. Ann. XVI. 1-80, 1880.

[59] L.Gegenbauer, *Uber die Bessel'schen functionen,* Wiener Sitzungsberichte, LXXXVIII, (2), 975-1003, 1884.

[60] J.D.Achenbach, *Wave propagation in elastic solids,* North-Holland, 1980.

[61] R.C.Weast, D.R.Lide, M.J.Astle and W.H.Beyer *CRC handbook of chemistry and physics,* CRC Press,Inc., 1990.

[62] I.S.Gradshteyn and I.M.Ryzhik, *Table of integrals, series, and products,* Academic Press, 1980.

[63] M.Abramowitz and I.A.Stegun, *Handbook of mathematical functions,* U.S.Department of Commerce, National Bureau of Standards, 1964.

[64] H,Bateman, *Tables of integral transforms,* McGraw-Hill, 1954.

[65] H.Weber, *Ueber einige bestimmte integrale,* Journal fur Math., LXIX, 222-237, 1869.

[66] P.E.Doak, The arguments are suggested by Prof. P.E.Doak; Private communication.

[67] L.D.Lawson *The physics of charged-particle beams,* Clarendon Press, 1978.

[68] Y.C.Fung, *A first course in continuum mechanics,* Prentice-Hall, 1969.

[69] H.M.Hess, *Acoustical determination of physical properties of porous grounds,* Ph.D. Thesis, The Open University, 1988.

[70] L.Marton, *Methods of experimental physics,* Vol. 1., Academic Press, 1959.

[71] J.Cunningham, *Complex variable methods in science and technology,* D.Van Nostrand, 1965.

[72] R.W.Stephens and A.E.Bate, *Acoustics and vibrational physics,* Edward Arnold, 1966.

[73] A.D.Pierce, *Acoustics: an introduction to its physical principles and applications,* McGraw-Hill, 1981.

[74] H.J.Pain, *The physics of vibrations and waves,* John Wiley and Sons, 1978.

[75] P.J.Davis and P.Rabinowitz, *Methods of numerical integration*, Academic Press, 1975.

[76] A.Ralston and P.Rabinowitz, *A first course in numerical analysis*, McGraw-Hill, 1978.

[77] E.De Doncker, *An adaptive extrapolation algorithm for automatic integration*, Signum Newsletter, 13, 2, 12-18, 1978.

[78] M.A.Malcolm and R.B.Simpson, *Local versus global strategies for adaptive quadrature*, A.C.M. Trans. Math. Software, 1 129-146, 1976.

[79] R.Piessens, E. De Doncker-Kapenga, C.Uberguber and D,Kahaner, *Quadpack, a subroutine package automatic integration*, Springer-Verlag, 1983.

[80] P.Wynn, *On a device for computing the* $e_m(S_n)$ *transformation*, Math. Tables Aids Comp., 10, 91-96, 1956.

[81] T.N.L.Patterson, *The optimum addition of points to quadrature formulae* Math. Comp., 22, 847-856, 1968.

[82] A.S.Kronrod, *Nodes and weights of quadrature formulae*, Consultants Bureau, 1965.

[83] D.K.Kahaner, *Numerical quadrature by the* ϵ*-algorithm*, Math. Comp., 26, 689-693, 1972.

[84] E.H.Wichmann, *Quantum physics*, Berkely Physics Course - Vol.4, McGraw-Hill, 1971.

[85] J.Edwards, *A treatise on the integral calculus*, Vols.I, II, Chelsea, 1922.

[86] J.M.Sabatier, H.E.Bass, L.N.Bolen, K.Attenborough and V.V.S.S.Sastry, *The interaction of airborne sound with porous groud: The theoretical formulation*, J.Acoust.Soc.Am., 79, 1345-1352, 1986.

[87] K.Attenborough, J.M.Sabatier, H.E.Bass and L.N.Bolen, *The acoustic transfer function at the surface of a layered poroelastic soil,* J.Acoust.Soc.Am., 79, 1353-1358, 1986.

[88] J.M.Sabatier, H.E.Bass, L.N.Bolen and K.Attenborough, *Acoustically-induced suismic waves,* J.Acoust.Soc.Am., 80(2), 646-649, 1986.

[89] K.Attenborough and T.L.Richards, *Solid particle motion induced by a point source above a poroelastic ground,* J.Acoust.Soc.Am., 86(3), 1085-1091, 1989.

[90] S.Toom, *Acoustic propagation near porous and elastic boundaries,* Ph.D. Thesis, The Open University, Milton Keynes, England, 1990.

[91] A.E.Yagle and B.C.Levy, A fast algorithm solution of the inverse problem for a layered acoustic medium probed by spherical harmonic waves, J.Acoust.Soc.Am., 78(2), 729-737, 1985.

[92] F.J.Fahy, *Sound intensity,* Elsevier Applied Science, 1989.

[93] G.K.Batchelor, *An introduction to fluid dynamics,* Cambridge, 1967.

[94] I.Tolstoy and E.Usdin, *Dispersive properties of stratified elastic and liquid media: a ray theory,* Geophysics, 18, p844., 1953.

[95] Y.Chen, *Elastic waves in a plate and in layered media,* M.Phil. Thesis, Nottingham University, 1988.

[96] A.H.Meitzler, *Backward-wave transmission of stress pulses in elastic cylinders and plates,* J.Acoust.Soc.Am., 38, p835. 1965.

[97] S.Sasaki, *Back reflection of ultrasonic waves obliquely incident to a solid surface in water,* Jpn.J.Appl.Phys. 2, p198, 1963

[98] J.J.Stamnes, *Role of backward waves in backscattering of ultrasonic beams at a liquid-solid interface,* J.Acoust.Soc.Am. 76(2), p627, 1984.

Appendix A

A formula similar to Lamb's formula

This is a failed attempt to prove formula (1.1) by using a method of integration analysis. Instead of considering formula (1.1), we start from an integral in the following form

$$\int_0^\infty \frac{J_0(r\xi)exp(-|z|\sqrt{\xi^2+k^2})\xi}{\sqrt{\xi^2+k^2}}\,d\xi \tag{A.1}$$

We consider the case where the integral is defined on the real axis, and variables z, r, and k are real.

One of important formulae used in the investigation of Sonine's discontinuous integrals is given by

$$\int_0^\infty J_0(at)\,exp(-p^2t^2)t\,dt = \frac{1}{2p^2}exp(-\frac{a^2}{4p^2}) \tag{A.2}$$

Equation (A.2) was first obtained by Weber [65] in 1868 from a double integral formula but it can be proved directly by expanding $J_0(at)$ in powers of t and integrating term by term, since the integral is convergent. In order to prove formula (1.1), additional to formula (A.2) we need two more formulae, which are given by

$$exp(-2\sqrt{ap}) = \sqrt{\frac{p}{\pi}}\int_0^\infty exp(-\frac{a}{4t}-pt)t^{-1/2}\,dt \tag{A.3}$$

where $Re(a) \geq 0$ and $Re(p) > 0$.

$$\int_0^\infty exp(-\frac{a}{4t}-pt)t^{-3/2}\,dt = 2\sqrt{\frac{\pi}{a}}exp(-2\sqrt{ap}) \tag{A.4}$$

where $Re(a) > 0$ and $Re(p) \geq 0$. They can be obtained by using the method of differentiating with respect to a parameter.

Considering $\sqrt{\xi^2 + k^2} = p$ and $|z| = a$, and applying formula (A.3) to the exponential term in (A.1) we have

$$\int_0^\infty \frac{J_0(r\xi)exp(-|z|\sqrt{\xi^2 + k^2})\xi}{\sqrt{\xi^2 + k^2}}\, d\xi$$

$$= \int_0^\infty \int_0^\infty J_0(r\xi)\frac{1}{\sqrt{\pi}}exp(-\frac{z^2}{4t} - (\xi^2 + k^2)t)t^{-1/2}\, d\xi\, dt \qquad (A.5)$$

where we have exchanged the order of integrals with respect to ξ and t, since they are independent variables.

Next, considering $r = a$, and $t = p^2$, and performing the integration with respect to ξ by formula (A.2) the right hand side of (A.5) becomes

$$\int_0^\infty \frac{1}{2\sqrt{\pi}t}exp(-\frac{r^2}{4t})exp(-\frac{z^2}{4t} - k^2t)t^{-1/2}\, d\xi\, dt \qquad (A.6)$$

Using formula (A.4) to (A.6) gives

$$\int_0^\infty \frac{J_0(r\xi)exp(-|z|\sqrt{\xi^2 + k^2})\xi}{\sqrt{\xi^2 + k^2}}\, d\xi = \frac{exp(-k\sqrt{r^2 + z^2})}{\sqrt{r^2 + z^2}} \qquad (A.7)$$

Thus on substituting $k = i\kappa$ into (A.7) we could obtain Lamb's formula, but the condition on formula (A.4) requires $Re(p) \geq 0$, and this forbids the required substitution.

Although formula (A.4) requires $Re(p) \geq 0$, it is possible that if using (A.4) under another infinite integration, the double infinite integral would be convergent for $Re(p) < 0$, i.e., the substitution $k = i\kappa$ into (A.7) would be valid. In other words, the integration of another divergent integration may be convergent. This idea may be understood by the following example

$$\int_0^1 \frac{1}{\sqrt{1 - x^2}}\, dx = \frac{\pi}{2} \qquad (A.8)$$

The integrand in equation (A.8) becomes infinite at $x = 1$, but the integration is convergent. It is possible that when considering a divergent integral as an integrand of another integral, the double integral may be convergent. Nevertheless it needs a rigorous mathematical analysis to prove the validity of applying (A.4) with $Re(p) < 0$ to (A.7).

Appendix B

The reflection and transmission coefficients

When a reflected plane wave is expressed by the second term in equation (4.43), the reflection coefficient is calculated by the following FORTRAN program

```
pas      ...ratio of densities (fluid/solid)
d      ...thickness of plate
kl      ...wavenumber of the longitudinal wave
kt      ...wavenumber of the transverse wave
ka      ...wavenumber of the wave in fluid
xk      ...the r component of wavenumber
k=dcmplx(xk,0.d0)
im=(0.d0,1.d0)
qa=cdsqrt(ka**2-k**2)
qt=cdsqrt(kt**2-k**2)
ql=cdsqrt(kl**2-k**2)
eda=cdexp(im*qa)
edt=cdexp(im*qt)
edl=cdexp(im*ql)
      ANS2=EDT**2*(-32.*K**8*QA**2+32.*K**6*QT*QL*QA**2+
     . 48.*K**6*KT**2*QA**2+16.*K**6*KL**2*QA**2-32.*K**4*
     . QT*KT**2*QL*QA**2-24.*K**4*KT**4*QA**2-16.*K**4*KT
```

```
     . **2*KL**2*QA**2+8.*K**2*QT*KT**4*QL*QA**2-K**2*KT**
     . 8*PAS**2+8.*K**2*KT**6*QA**2+KT**8*KL**2*PAS**2-KT
     . **8*QA**2)+32.*K**8*QA**2+32.*K**6*QT*QL*QA**2-48.*
     . K**6*KT**2*QA**2-16.*K**6*KL**2*QA**2-32.*K**4*QT*
     . KT**2*QL*QA**2+24.*K**4*KT**4*QA**2+16.*K**4*KT**2*
     . KL**2*QA**2+8.*K**2*QT*KT**4*QL*QA**2+K**2*KT**8*
     . PAS**2-8.*K**2*KT**6*QA**2-KT**8*KL**2*PAS**2+KT**8
     . *QA**2
      ANS1=EDL**2*EDT**2*(32.*K**8*QA**2+32.*K**6*QT*QL*QA
     . **2-48.*K**6*KT**2*QA**2-16.*K**6*KL**2*QA**2-32.*K
     . **4*QT*KT**2*QL*QA**2+24.*K**4*KT**4*QA**2+16.*K**4
     . *KT**2*KL**2*QA**2+8.*K**2*QT*KT**4*QL*QA**2+K**2*
     . KT**8*PAS**2-8.*K**2*KT**6*QA**2-KT**8*KL**2*PAS**2
     . +KT**8*QA**2)+EDL**2*(-32.*K**8*QA**2+32.*K**6*QT*
     . QL*QA**2+48.*K**6*KT**2*QA**2+16.*K**6*KL**2*QA**2-
     . 32.*K**4*QT*KT**2*QL*QA**2-24.*K**4*KT**4*QA**2-16.*
     . K**4*KT**2*KL**2*QA**2+8.*K**2*QT*KT**4*QL*QA**2-K
     . **2*KT**8*PAS**2+8.*K**2*KT**6*QA**2+KT**8*KL**2*
     . PAS**2-KT**8*QA**2)+32.*EDL*EDT*K**2*QT*QL*QA**2*(-
     . 4.*K**4+4.*K**2*KT**2-KT**4)+ANS2
      ANS6=-8.*K**2*KT**6*QA**2+KT**8*KL**2*PAS**2-2.*KT**
     . 8*PAS*QL*QA+KT**8*QA**2
      ANS5=EDT**2*(-32.*K**8*QA**2+32.*K**6*QT*QL*QA**2+
     . 48.*K**6*KT**2*QA**2+16.*K**6*KL**2*QA**2+8.*K**4*QT
     . *KT**4*PAS*QA-32.*K**4*QT*KT**2*QL*QA**2+8.*K**4*KT
     . **4*PAS*QL*QA-24.*K**4*KT**4*QA**2-16.*K**4*KT**2*
     . KL**2*QA**2-8.*K**2*QT*KT**4*KL**2*PAS*QA+8.*K**2*
     . QT*KT**4*QL*QA**2+K**2*KT**8*PAS**2-8.*K**2*KT**6*
     . PAS*QL*QA+8.*K**2*KT**6*QA**2-KT**8*KL**2*PAS**2+2.
     . *KT**8*PAS*QL*QA-KT**8*QA**2)+32.*K**8*QA**2+32.*K
     . **6*QT*QL*QA**2-48.*K**6*KT**2*QA**2-16.*K**6*KL**2
     . *QA**2+8.*K**4*QT*KT**4*PAS*QA-32.*K**4*QT*KT**2*QL
```

```
     . *QA**2-8.*K**4*KT**4*PAS*QL*QA+24.*K**4*KT**4*QA**2
     . +16.*K**4*KT**2*KL**2*QA**2-8.*K**2*QT*KT**4*KL**2*
     . PAS*QA+8.*K**2*QT*KT**4*QL*QA**2-K**2*KT**8*PAS**2+
     . 8.*K**2*KT**6*PAS*QL*QA+ANS6
      ANS4=EDL**2*(-32.*K**8*QA**2+32.*K**6*QT*QL*QA**2+
     . 48.*K**6*KT**2*QA**2+16.*K**6*KL**2*QA**2-8.*K**4*QT
     . *KT**4*PAS*QA-32.*K**4*QT*KT**2*QL*QA**2-8.*K**4*KT
     . **4*PAS*QL*QA-24.*K**4*KT**4*QA**2-16.*K**4*KT**2*
     . KL**2*QA**2+8.*K**2*QT*KT**4*KL**2*PAS*QA+8.*K**2*
     . QT*KT**4*QL*QA**2+K**2*KT**8*PAS**2+8.*K**2*KT**6*
     . PAS*QL*QA+8.*K**2*KT**6*QA**2-KT**8*KL**2*PAS**2-2.
     . *KT**8*PAS*QL*QA-KT**8*QA**2)+32.*EDL*EDT*K**2*QT*
     . QL*QA**2*(-4.*K**4+4.*K**2*KT**2-KT**4)+ANS5
      ANS3=EDL**2*EDT**2*(32.*K**8*QA**2+32.*K**6*QT*QL*QA
     . **2-48.*K**6*KT**2*QA**2-16.*K**6*KL**2*QA**2-8.*K
     . **4*QT*KT**4*PAS*QA-32.*K**4*QT*KT**2*QL*QA**2+8.*K
     . **4*KT**4*PAS*QL*QA+24.*K**4*KT**4*QA**2+16.*K**4*
     . KT**2*KL**2*QA**2+8.*K**2*QT*KT**4*KL**2*PAS*QA+8.*
     . K**2*QT*KT**4*QL*QA**2-K**2*KT**8*PAS**2-8.*K**2*KT
     . **6*PAS*QL*QA-8.*K**2*KT**6*QA**2+KT**8*KL**2*PAS**
     . 2+2.*KT**8*PAS*QL*QA+KT**8*QA**2)+ANS4
R=ANS1/ANS3
```

For the transmitted wave (4.46), the transmission coefficient is calculated by

```
pas     ...ratio of densities (fluid/solid)
d      ...thickness of plate
kl      ...wavenumber of the longitudinal wave
kt      ...wavenumber of the transverse wave
ka      ...wavenumber of the wave in fluid
xk      ...the r component of wavenumber
k=dcmplx(xk,0.d0)
im=(0.d0,1.d0)
qa=cdsqrt(ka**2-k**2)
```

```
      qt=cdsqrt(kt**2-k**2)
      ql=cdsqrt(kl**2-k**2)
      eda=cdexp(im*qa)
      edt=cdexp(im*qt)
      edl=cdexp(im*ql)
           ANS2=16.*EDL**2*EDT*EDA*K**2*QT*KT**4*PAS*QA*(K**2-
     . KL**2)+4.*EDL*EDT**2*EDA*KT**4*PAS*QL*QA*(-4.*K**4+
     . 4.*K**2*KT**2-KT**4)+4.*EDL*EDA*KT**4*PAS*QL*QA*(4.*
     . K**4-4.*K**2*KT**2+KT**4)+16.*EDT*EDA*K**2*QT*KT**4
     . *PAS*QA*(-K**2+KL**2)
      ANS6=-8.*K**2*KT**6*QA**2+KT**8*KL**2*PAS**2-2.*KT**
     . 8*PAS*QL*QA+KT**8*QA**2
      ANS5=EDT**2*(-32.*K**8*QA**2+32.*K**6*QT*QL*QA**2+
     . 48.*K**6*KT**2*QA**2+16.*K**6*KL**2*QA**2+8.*K**4*QT
     . *KT**4*PAS*QA-32.*K**4*QT*KT**2*QL*QA**2+8.*K**4*KT
     . **4*PAS*QL*QA-24.*K**4*KT**4*QA**2-16.*K**4*KT**2*
     . KL**2*QA**2-8.*K**2*QT*KT**4*KL**2*PAS*QA+8.*K**2*
     . QT*KT**4*QL*QA**2+K**2*KT**8*PAS**2-8.*K**2*KT**6*
     . PAS*QL*QA+8.*K**2*KT**6*QA**2-KT**8*KL**2*PAS**2+2.
     . *KT**8*PAS*QL*QA-KT**8*QA**2)+32.*K**8*QA**2+32.*K
     . **6*QT*QL*QA**2-48.*K**6*KT**2*QA**2-16.*K**6*KL**2
     . *QA**2+8.*K**4*QT*KT**4*PAS*QA-32.*K**4*QT*KT**2*QL
     . *QA**2-8.*K**4*KT**4*PAS*QL*QA+24.*K**4*KT**4*QA**2
     . +16.*K**4*KT**2*KL**2*QA**2-8.*K**2*QT*KT**4*KL**2*
     . PAS*QA+8.*K**2*QT*KT**4*QL*QA**2-K**2*KT**8*PAS**2+
     . 8.*K**2*KT**6*PAS*QL*QA+ANS6
      ANS4=EDL**2*(-32.*K**8*QA**2+32.*K**6*QT*QL*QA**2+
     . 48.*K**6*KT**2*QA**2+16.*K**6*KL**2*QA**2-8.*K**4*QT
     . *KT**4*PAS*QA-32.*K**4*QT*KT**2*QL*QA**2-8.*K**4*KT
     . **4*PAS*QL*QA-24.*K**4*KT**4*QA**2-16.*K**4*KT**2*
     . KL**2*QA**2+8.*K**2*QT*KT**4*KL**2*PAS*QA+8.*K**2*
     . QT*KT**4*QL*QA**2+K**2*KT**8*PAS**2+8.*K**2*KT**6*
```

```
     . PAS*QL*QA+8.*K**2*KT**6*QA**2-KT**8*KL**2*PAS**2-2.
     . *KT**8*PAS*QL*QA-KT**8*QA**2)+32.*EDL*EDT*K**2*QT*
     . QL*QA**2*(-4.*K**4+4.*K**2*KT**2-KT**4)+ANS5
      ANS3=EDL**2*EDT**2*(32.*K**8*QA**2+32.*K**6*QT*QL*QA
     . **2-48.*K**6*KT**2*QA**2-16.*K**6*KL**2*QA**2-8.*K
     . **4*QT*KT**4*PAS*QA-32.*K**4*QT*KT**2*QL*QA**2+8.*K
     . **4*KT**4*PAS*QL*QA+24.*K**4*KT**4*QA**2+16.*K**4*
     . KT**2*KL**2*QA**2+8.*K**2*QT*KT**4*KL**2*PAS*QA+8.*
     . K**2*QT*KT**4*QL*QA**2-K**2*KT**8*PAS**2-8.*K**2*KT
     . **6*PAS*QL*QA-8.*K**2*KT**6*QA**2+KT**8*KL**2*PAS**
     . 2+2.*KT**8*PAS*QL*QA+KT**8*QA**2)+ANS4
      ANS1=ANS2/ANS3
T=-ANS1
```

For a spherical wave propagation, the integration coefficient T defined in equation (6.43) for the transmission can be obtained by the following program:

```
pasc=pas    ...ratio of densities (fluid/solid)
h     ...source height
dc=d     ...thickness of plate
klc=kl     ...wavenumber of the longitudinal wave
ktc=kt     ...wavenumber of the transverse wave
kac=k1     ...wavenumber of the wave in fluid
xk     ...the r component of wavenumber
k=dcmplx(xk,0.d0)
im=(0.d0,1.d0)
qt=cdsqrt(k**2-ktc**2)
ql=cdsqrt(k**2-klc**2)
qa=cdsqrt(k**2-kac**2)
eda=cdexp(-d*qa)
edt=cdexp(-d*qt)
```

```
edl=cdexp(-d*ql)
eha=cdexp(-h*qa)

      ANS2=4.*K*PASC*KTC**4*(4.*K**4*QL*EDL*EDT**2-4.*K**4
     . *QL*EDL-4.*K**4*QT*EDL**2*EDT+4.*K**4*QT*EDT-4.*K**
     . 2*QL*EDL*EDT**2*KTC**2+4.*K**2*QL*EDL*KTC**2+4.*K**
     . 2*QT*EDL**2*EDT*KLC**2-4.*K**2*QT*EDT*KLC**2+QL*EDL
     . *EDT**2*KTC**4-QL*EDL*KTC**4)*DHA
      ANS7=-EDL**2*EDT**2*PASC**2*KTC**8*KLC**2+EDL**2*
     . PASC**2*KTC**8*KLC**2+EDT**2*PASC**2*KTC**8*KLC**2-
     . PASC**2*KTC**8*KLC**2
      ANS6=8.*K**2*QA**2*EDL**2*KTC**6+8.*K**2*QA**2*EDT**
     . 2*KTC**6-8.*K**2*QA**2*KTC**6+8.*K**2*QA*QL*EDL**2*
     . EDT**2*PASC*KTC**6-8.*K**2*QA*QL*EDL**2*PASC*KTC**6
     . +8.*K**2*QA*QL*EDT**2*PASC*KTC**6-8.*K**2*QA*QL*
     . PASC*KTC**6-8.*K**2*QA*QT*EDL**2*EDT**2*PASC*KTC**4
     . *KLC**2-8.*K**2*QA*QT*EDL**2*PASC*KTC**4*KLC**2+8.*
     . K**2*QA*QT*EDT**2*PASC*KTC**4*KLC**2+8.*K**2*QA*QT*
     . PASC*KTC**4*KLC**2+K**2*EDL**2*EDT**2*PASC**2*KTC**
     . 8-K**2*EDL**2*PASC**2*KTC**8-K**2*EDT**2*PASC**2*
     . KTC**8+K**2*PASC**2*KTC**8+QA**2*EDL**2*EDT**2*KTC
     . **8-QA**2*EDL**2*KTC**8-QA**2*EDT**2*KTC**8+QA**2*
     . KTC**8-2.*QA*QL*EDL**2*EDT**2*PASC*KTC**8+2.*QA*QL*
     . EDL**2*PASC*KTC**8-2.*QA*QL*EDT**2*PASC*KTC**8+2.*
     . QA*QL*PASC*KTC**8+ANS7
      ANS5=16.*K**4*QA**2*EDL**2*EDT**2*KTC**2*KLC**2-24.*
     . K**4*QA**2*EDL**2*KTC**4-16.*K**4*QA**2*EDL**2*KTC
     . **2*KLC**2-24.*K**4*QA**2*EDT**2*KTC**4-16.*K**4*QA
     . **2*EDT**2*KTC**2*KLC**2+24.*K**4*QA**2*KTC**4+16.*
     . K**4*QA**2*KTC**2*KLC**2-8.*K**4*QA*QL*EDL**2*EDT**
     . 2*PASC*KTC**4+8.*K**4*QA*QL*EDL**2*PASC*KTC**4-8.*K
     . **4*QA*QL*EDT**2*PASC*KTC**4+8.*K**4*QA*QL*PASC*KTC
```

```
. **4+8.*K**4*QA*QT*EDL**2*EDT**2*PASC*KTC**4+8.*K**4
. *QA*QT*EDL**2*PASC*KTC**4-8.*K**4*QA*QT*EDT**2*PASC
. *KTC**4-8.*K**4*QA*QT*PASC*KTC**4-8.*K**2*QA**2*QL*
. QT*EDL**2*EDT**2*KTC**4-8.*K**2*QA**2*QL*QT*EDL**2*
. KTC**4+32.*K**2*QA**2*QL*QT*EDL*EDT*KTC**4-8.*K**2*
. QA**2*QL*QT*EDT**2*KTC**4-8.*K**2*QA**2*QL*QT*KTC**
. 4-8.*K**2*QA**2*EDL**2*EDT**2*KTC**6+ANS6
 ANS4=32.*K**8*QA**2*EDL**2*EDT**2-32.*K**8*QA**2*EDL
. **2-32.*K**8*QA**2*EDT**2+32.*K**8*QA**2-32.*K**6*
. QA**2*QL*QT*EDL**2*EDT**2-32.*K**6*QA**2*QL*QT*EDL
. **2+128.*K**6*QA**2*QL*QT*EDL*EDT-32.*K**6*QA**2*QL
. *QT*EDT**2-32.*K**6*QA**2*QL*QT-48.*K**6*QA**2*EDL
. **2*EDT**2*KTC**2-16.*K**6*QA**2*EDL**2*EDT**2*KLC
. **2+48.*K**6*QA**2*EDL**2*KTC**2+16.*K**6*QA**2*EDL
. **2*KLC**2+48.*K**6*QA**2*EDT**2*KTC**2+16.*K**6*QA
. **2*EDT**2*KLC**2-48.*K**6*QA**2*KTC**2-16.*K**6*QA
. **2*KLC**2+32.*K**4*QA**2*QL*QT*EDL**2*EDT**2*KTC**
. 2+32.*K**4*QA**2*QL*QT*EDL**2*KTC**2-128.*K**4*QA**
. 2*QL*QT*EDL*EDT*KTC**2+32.*K**4*QA**2*QL*QT*EDT**2*
. KTC**2+32.*K**4*QA**2*QL*QT*KTC**2+24.*K**4*QA**2*
. EDL**2*EDT**2*KTC**4+ANS5
 ANS3=EDA*ANS4
 ANS1=ANS2/ANS3
 T=-ANS1
```

The above formulae were produced by REDUCE.

The integration coefficient for the reflection is given in appendix (D).

Appendix C

The element coefficients of system equations

We have tried a form of solution to the problem with using the integral which has the Hankel function in the integrand in the following forms

$$\begin{aligned}\varphi_1 &= i\int_0^\infty H_0^{(1)}(|z-h|\sqrt{k_1^2-k^2})cos(rk)\,dk \\ &+ i\int_0^\infty RH_0^{(1)}((h+z)\sqrt{k_1^2-k^2})cos(rk)\,dk \qquad \text{(C.1)}\end{aligned}$$

$$\begin{aligned}\phi_l &= i\int_0^\infty L_a H_0^{(1)}((h-z)\sqrt{k_l^2-k^2})cos(rk)\,dk \\ &+ i\int_0^\infty L_b H_0^{(1)}((h+d+z)\sqrt{k_l^2-k^2})cos(rk)\,dk \qquad \text{(C.2)}\end{aligned}$$

$$\begin{aligned}\psi_t &= i\int_0^\infty T_a H_0^{(1)}((h-z)\sqrt{k_t^2-k^2})cos(rk)\,dk \\ &+ i\int_0^\infty T_b H_0^{(1)}((h+d+z)\sqrt{k_t^2-k^2})cos(rk)\,dk \qquad \text{(C.3)}\end{aligned}$$

$$\varphi_3 = i\int_0^\infty T H_0^{(1)}((h-z)\sqrt{k_1^2-k^2})cos(rk)\,dk \qquad \text{(C.4)}$$

The integration coefficients may be determened by the boundary conditions. Applying the boundary conditions we can obtain a system equations:

$$\begin{aligned}a(1,1)R + a(1,2)\ L_a\ + a(1,3)L_b + a(1,4)T_a + a(1,5)T_b + b(1,1) = 0 \\ a(2,2)\ L_a\ + a(2,3)L_b + a(2,4)T_a + a(2,5)T_b = 0 \\ a(3,1)R + a(3,2)\ L_a\ + a(3,3)L_b + a(3,4)T_a + a(3,5)T_b + b(3,1) = 0\end{aligned}$$

$$
\begin{aligned}
a(4,2)\ \ L_a\ \ &+a(4,3)L_b + a(4,4)T_a + a(4,5)T_b + a(5,6)T = 0 \\
a(5,2)\ \ L_a\ \ &+a(5,3)L_b + a(5,4)T_a + a(5,5)T_b = 0 \\
a(6,2)\ \ L_a\ \ &+a(6,3)L_b + a(6,4)T_a + a(6,5)T_b + a(6,6)T = 0
\end{aligned}
\tag{C.5}
$$

The coefficient elments of the above system equations are given in the Fortran format by

```
      a(1,1)=HA(1.)*H**2*K*KT**2*PAS*(D**2+2.*D*H+H**2)
      a(1,2)=H*K*(2.*HL(2.)*D**2*QL+4.*HL(2.)*D*H*QL+2.*
     . HL(2.)*H**2*QL+2.*HL(1.)*D**2*H*K**2-HL(1.)*D**2*H*
     . KT**2+4.*HL(1.)*D*H**2*K**2-2.*HL(1.)*D*H**2*KT**2+
     . 2.*HL(1.)*H**3*K**2-HL(1.)*H**3*KT**2)
      a(1,3)=H**2*K*(2.*HLP(2.)*D*QL+2.*HLP(2.)*H*QL+2.*
     . HLP(1.)*D**2*K**2-HLP(1.)*D**2*KT**2+4.*HLP(1.)*D*H
     . *K**2-2.*HLP(1.)*D*H*KT**2+2.*HLP(1.)*H**2*K**2-HLP
     . (1.)*H**2*KT**2)
      a(1,4)=2.*(HT(2.)*D**2*H**2*K**2*QT+2.*HT(2.)*D**2*
     . QT+2.*HT(2.)*D*H**3*K**2*QT+4.*HT(2.)*D*H*QT+HT(2.)
     . *H**4*K**2*QT+2.*HT(2.)*H**2*QT+HT(1.)*D**2*H*K**2-
     . HT(1.)*D**2*H*KT**2+2.*HT(1.)*D*H**2*K**2-2.*HT(1.)
     . *D*H**2*KT**2+HT(1.)*H**3*K**2-HT(1.)*H**3*KT**2)
      a(1,5)=-2.*H**2*(HTP(2.)*D**2*K**2*QT+2.*HTP(2.)*D*
     . H*K**2*QT+HTP(2.)*H**2*K**2*QT+2.*HTP(2.)*QT+HTP(1.
     . )*D*K**2-HTP(1.)*D*KT**2+HTP(1.)*H*K**2-HTP(1.)*H*
     . KT**2)
      a(2,2)=2.*HL(2.)*H*K*QL*(D+H)
      a(2,3)=-2.*HLP(2.)*H*K*QL*(D+H)
      a(2,4)=2.*HT(2.)*D*QT+2.*HT(2.)*H*QT+2.*HT(1.)*D*H*
     . K**2-HT(1.)*D*H*KT**2+2.*HT(1.)*H**2*K**2-HT(1.)*H
     . **2*KT**2
      a(2,5)=H*(2.*HTP(2.)*QT+2.*HTP(1.)*D*K**2-HTP(1.)*D
     . *KT**2+2.*HTP(1.)*H*K**2-HTP(1.)*H*KT**2)
```

```
      a(3,1)=-HA(2.)*H*K*QA*(D+H)
      a(3,2)=-HL(2.)*H*K*QL*(D+H)
      a(3,3)=HLP(2.)*H*K*QL*(D+H)
      a(3,4)=-(HT(2.)*D*QT+HT(2.)*H*QT+HT(1.)*D*H*K**2+HT
     . (1.)*H**2*K**2)
      a(3,5)=-H*(HTP(2.)*QT+HTP(1.)*D*K**2+HTP(1.)*H*K**2
     . )
      a(4,2)=H**2*K*(2.*HLP(2.)*D*QL+2.*HLP(2.)*H*QL+2.*
     . HLP(1.)*D**2*K**2-HLP(1.)*D**2*KT**2+4.*HLP(1.)*D*H
     . *K**2-2.*HLP(1.)*D*H*KT**2+2.*HLP(1.)*H**2*K**2-HLP
     . (1.)*H**2*KT**2)
      a(4,3)=H*K*(2.*HL(2.)*D**2*QL+4.*HL(2.)*D*H*QL+2.*
     . HL(2.)*H**2*QL+2.*HL(1.)*D**2*H*K**2-HL(1.)*D**2*H*
     . KT**2+4.*HL(1.)*D*H**2*K**2-2.*HL(1.)*D*H**2*KT**2+
     . 2.*HL(1.)*H**3*K**2-HL(1.)*H**3*KT**2)
      a(4,4)=2.*H**2*(HTP(2.)*D**2*K**2*QT+2.*HTP(2.)*D*H
     . *K**2*QT+HTP(2.)*H**2*K**2*QT+2.*HTP(2.)*QT+HTP(1.)
     . *D*K**2-HTP(1.)*D*KT**2+HTP(1.)*H*K**2-HTP(1.)*H*KT
     . **2)
      a(4,5)=-2.*(HT(2.)*D**2*H**2*K**2*QT+2.*HT(2.)*D**2
     . *QT+2.*HT(2.)*D*H**3*K**2*QT+4.*HT(2.)*D*H*QT+HT(2.
     . )*H**4*K**2*QT+2.*HT(2.)*H**2*QT+HT(1.)*D**2*H*K**2
     . -HT(1.)*D**2*H*KT**2+2.*HT(1.)*D*H**2*K**2-2.*HT(1.
     . )*D*H**2*KT**2+HT(1.)*H**3*K**2-HT(1.)*H**3*KT**2)
      a(4,6)=HAP(1.)*H**2*K*KT**2*PAS*(D**2+2.*D*H+H**2)
      a(5,2)=2.*HLP(2.)*H*K*QL*(D+H)
      a(5,3)=-2.*HL(2.)*H*K*QL*(D+H)
      a(5,4)=H*(2.*HTP(2.)*QT+2.*HTP(1.)*D*K**2-HTP(1.)*D
     . *KT**2+2.*HTP(1.)*H*K**2-HTP(1.)*H*KT**2)
      a(5,5)=2.*HT(2.)*D*QT+2.*HT(2.)*H*QT+2.*HT(1.)*D*H*
     . K**2-HT(1.)*D*H*KT**2+2.*HT(1.)*H**2*K**2-HT(1.)*H
     . **2*KT**2
```

```
      a(6,2)=HLP(2.)*H*K*QL*(D+H)
      a(6,3)=-HL(2.)*H*K*QL*(D+H)
      a(6,4)=H*(HTP(2.)*QT+HTP(1.)*D*K**2+HTP(1.)*H*K**2)
      a(6,5)=HT(2.)*D*QT+HT(2.)*H*QT+HT(1.)*D*H*K**2+HT(
     . 1.)*H**2*K**2
      a(6,6)=-HAP(2.)*H*K*QA*(D+H)
      b(1,1)=-HA(1.)*H**2*K*KT**2*PAS*(D**2+2.*D*H+H**2)
      b(3,1)=-HA(2.)*H*K*QA*(D+H)
```

where H is the source height, D is the thickness of the plate, PAS is the density ratio, ρ_1/ρ_s , $KA = k_a$, $KT = k_a$, $KL = k_l$,

HA(1.) ... $H_0^{(1)}(QA * H)$,
HA(2.) ... $H_0^{(2)}(QA * H)$,
HT(1.) ... $H_0^{(1)}(QT * H)$,
HT(2.) ... $H_0^{(2)}(QT * H)$,
HL(1.) ... $H_0^{(1)}(QL * H)$,
HL(2.) ... $H_0^{(2)}(QL * H)$,
HAP(1.) ... $H_0^{(1)}(QA * (D + H))$,
HAP(2.) ... $H_0^{(2)}(QA * (D + H))$
HTP(1.) ... $H_0^{(1)}(QT * (D + H))$,
HTP(2.) ... $H_0^{(2)}(QT * (D + H))$,
HLP(1.) ... $H_0^{(1)}(QT * (D + H))$,
HLP(2.) ... $H_0^{(2)}(QL * (D + H))$,
with $QA = \sqrt{k_a^2 - k^2}$, $QT = \sqrt{k_t^2 - k^2}$, $QL = \sqrt{k_l^2 - k^2}$.

The reflection and transmission coefficients are determined by the coefficient elments of the system equations.

Appendix D

An example FORTRAN program

This program calculates the energy crossing a circle area on a surface for reflected wave in the case of fluid-solid-fluid combination. It is the most typical program. The data for pressure contours or the energy flux can be calculated by using the subroutine in it. The program can be used for different problem by changing the expression for the reflected wave.

```
program asafxre
C
integer*4 if, i, np,l,m,loop(2),n,ni,ip,mr
real*8 z, r, ka , kt, kl, h, d, f, pas
real*8 a,b,tofx, fac, tofxal, para(10)
real*8 sing, a1, b1, x0 ,xx,d01ahf, x, d01atf
external fpv,sing, d01baf, d01atf, d01baz,d01bay
common z, r, ka, kt, kl,pas, h, d,xx
c   input data
open(unit=7,file='nem95.dat',status='new')
open(unit=8,file='para95.dat',status='old')
do 500 l=1,10
500 read(8,*) para(l)
write(6,*) para
read(8,*) loop(1)
close(unit=8,status='keep')
c   initialize
```

```
z=0.d0
pas=para(1)/para(2)
f=para(3)
ka=2.d0*3.1415926d0*f/para(4)
kt=2.d0*3.1415926d0*f/para(5)
kl=2.d0*3.1415926d0*f/para(6)
write(6,*) ka,kt,kl
h=para(7)
d=0.01d0
if=0
b=para(9)
fac=para(10)
n=loop(1)
write(7,*) 'asa ref'
c   determining the singularity
a1=ka
b1=ka+0.5d0
x0=ka+1.d-4
xx=sing(a1,b1,x0)
c  integration of the energy flux over finite interval
do 100 i=1,n
a=b
b=a+fac
tofx=d01baf(d01baz,a,b,20,fpv,if)
tofxal=tofxal+tofx
write(6,*) b, tofx,tofxal/ka
write(7,*) b, tofx,tofxal/ka
100 continue
c   integration of the energy flux over semi-infinite interval
c a=b
c b=1.d0
c tofx=-d01baf(d01bay,a,b,20,fpv,if)
```

```
c tofxal=tofxal+tofx
c write(6,*) b, tofx,tofxal/ka
c write(7,*) b, tofx,tofxal/ka
stop
end

c   calculation of the energy flux
function fpv(xr)
integer*4 nlm,lw, if, liw ,i, np,l,m,loop(2),n, ni, ip,mr
parameter (lw=50000,liw=lw/4)
integer*4 iw(liw)
real*8 f, wo(lw), z, r, ka , kt, kl, h, pas, d, xr
real*8 d01amf, d01ahf, d01ajf, fc, xx
real*8 vrr, vir, frj, fij, frm,fim, abac,reac, err, acc
real*8 v3r,v3i,v2r,v2i,v1r,i1i,i1r,i2r,i3r,i4r,i4i
real*8 int, intrp, intip, intrv, intiv, intr, inti,a1,a0
complex*16 dir, im, ref, fp, fv, ans
external d01ajf, d01ahf, d01amf, d01atf
external vrr, vir,frm,fim,frj,fij
common z, r, ka, kt,kl, pas, h, d,xx
if=0
im=dcmplx(0.d0,1.d0)
nlm=-1
abac=1.d-14
reac=1.d-3
acc=1.d-6
a0=0.d0
a1=ka+2.d0
r=xr
if=0
c   particle velocity for the reflected wave
v1r=d01ahf(a0,xx,acc,np,err,vrr,nlm,if)
```

```
if(if .ne. 0) write(6,*) 1
v2r=d01ahf(xx,a1,acc,np,err,vrr,nlm,if)
if(if .ne. 0) write(6,*) 2
call d01amf(vrr,a1,1,abac,reac,v3r,err,wo,lw,iw,liw,if)
if(if .ne. 0) write(6,*) 3
```

```
call d01amf(vir,a0,1,abac,reac,v3i,err,wo,lw,iw,liw,if)
if(if .ne. 0) write(6,*) 4

intrv=v3r+v2r+v1r
intiv=v3i+v2i
fv=dcmplx(intrv,-intiv)

c   particle velocity for the direct wave
      ANS=(dSQRT(H**2-2.*H*Z+R**2+Z**2)*Im*KA*(H-Z)+H-Z)/(cdExp
     .(dSQRT(H**2-2.*H*Z+R**2+Z**2)*Im*KA)*dSQRT(H**2-2.*H
     . *Z+R**2+Z**2)*(H**2-2.*H*Z+R**2+Z**2))
c   pressure for the reflected wave
if=-1
call d01atf(frj,a0,ka,abac,reac,i1r,err,wo,lw,iw,liw,if)
if(if. gt. 0.0) write(6,*) 1,err
if=-1
call d01atf(fij,a0,ka,abac,reac,i1i,err,wo,lw,iw,liw,if)
if(if. gt. 0.0) write(6,*) 2,err

if=-1
call d01amf(frm,a1,1,abac,reac,i4r,err,wo,lw,iw,liw,if)
if(if. gt. 0.0) write(6,*) 3,err
if=-1
call d01amf(fim,a0,1,abac,reac,i4i,err,wo,lw,iw,liw,if)
if(if. gt. 0.0) write(6,*) 4,err
if=-1
```

```
i2r=d01ahf(a0,xx,acc,np,err,frm,nlm,if)
if(if. gt. 0.0) write(6,*) 5,err
if=-1
i3r=d01ahf(xx,a1,acc,np,err,frm,nlm,if)
if(if. gt. 0.0) write(6,*) 6,err

intr=-i1r+i2r+i3r+i4r
inti=-i1i+i2i+i3i+i4i
fp=dcmplx(intr,inti)
c   pressure for the direct wave
dir=cdexp(-im*ka*dsqrt((h-z)**2+r**2))/dsqrt((h-z)**2+r**2)
c   the energy flux of the reflected wave
fpv=dimag(fp*fv*r)
c   the energy flux of the sum of the direct and reflected wave
c fpv=dimag(fp*fv*r)+dimag(dir*dconjg(ans)*r)
return
END

c   calculation of real part of the particle velocity
function vrr(x)
real*8 x, vrr
complex*16 vxr
external vxr
vrr=dreal(vxr(x))
return
end
c   calculation of imaginary part of the particle velocity
function vir(x)
real*8 x, vir
complex*16 vxr
external vxr
vir=dimag(vxr(x))
```

```
return
end

c   calculation of the particle velocity
FUNCTION vxr(xk)
integer if
real*8 besl, xk, s17aef, ka, kt, z, r, pas, h, d, zh,x2,kl,xx
complex*16 k , im,q1,co, vxr
external s17aef,co
common z, r, ka, kt,kl, pas, h,d, xx
if=0
zh=(h+z)
im=(0.d0,1.d0)
k=dcmplx(xk,0.d0)
q1=cdsqrt(k**2-ka**2)
x2=r*dreal(k)
besl= s17aef(x2,if)
vxr=co(k)*(besl*cdexp(-q1*zh))*k
RETURN
end

c   calculation of real part of pressure contribution
c   on imaginary axis
function frj(x,frjv,n)
integer*4 j,n
real*8 x(n), frjv(n)
complex*16 fx
external fx
do 100 j=1,n
100 frjv(j)=dreal(fx(2,x(j)))
return
end
```

```
c    calculation of imaginary part of pressure contribution
c    on imaginary axis
function fij(x,fijv,n)
real*8 x(n), fijv(n)
complex*16 fx
external fx
do 100 j=1,n
100 fijv(j)=dimag(fx(2,x(j)))
return
end
c    calculation of real part of pressure contribution
c    on real axis
function frm(x)
real*8 x, frm
complex*16 fx
external fx
frm=dreal(fx(1,x))
return
end
c    calculation of imaginary part of pressure contribution
c    on real axis
function fim(x)
real*8 x, fim
complex*16 fx
external fx
fim=dimag(fx(1,x))
return
end
c    calculation of pressure for reflected wave
FUNCTION fx(i,xk)
integer if, i
real*8 besl,xk,s17aef,ka,kt,z,r,pas,h,d, zh, kl, x2, xx
```

```
complex*16 k , x1,  im,q1, q2, co, fx, xxk
external s17aef, co
common z, r, ka, kt, kl, pas, h,d,xx
if=0
zh=(h+z)
im=(0.d0,1.d0)
if(i.eq.1) goto 100
xxk=dcmplx(0.d0,xk)
k=cdsqrt(ka**2+xxk**2)
q1=cdsqrt(k**2-ka**2)
x2=r*dreal(k)
besl= s17aef(x2,if)
fx=-co(k)*(besl*cdexp(-q1*zh))/im
goto 200
100 continue
xxk=dcmplx(xk,0.d0)
k=cdsqrt(ka**2+xxk**2)
q1=cdsqrt(k**2-ka**2)
x2=r*dreal(k)
besl= s17aef(x2,if)
fx=co(k)*(besl*cdexp(-q1*zh))
200 continue
RETURN
end
c   the integration coefficient for reflection
function co(k)
real*8 h, w, ct, pas, ca,kt,kl,ka,x,d,z,r,pa,ps,pasc
real*8 klc,ktc,kac, dc,xk, xx
complex*16 eda,edt,edl, qt, ql,qa
complex*16 xa, xt, xl, k, co,nm, dn,im
complex*16 ans1,ans2,ans3,ans4,ans5,ans6,ans7,ans8
common z, r, ka, kt, kl, pas, h, d,xx
```

```
pasc=pas
dc=d
klc=kl
ktc=kt
kac=ka
im=(0.d0,1.d0)
qt=cdsqrt(k**2-ktc**2)
ql=cdsqrt(k**2-klc**2)
qa=cdsqrt(k**2-kac**2)
eda=cdexp(-d*qa)
edt=cdexp(-d*qt)
edl=cdexp(-d*ql)

      ANS1=K**(-1.)*KTC**4*(-8.*QA**2*EDL**2*EDT**2*QL*QT-
     . 8.*QA**2*EDL**2*EDT**2*KTC**2-8.*QA**2*EDL**2*QL*QT+
     . 8.*QA**2*EDL**2*KTC**2+32.*QA**2*EDL*EDT*QL*QT-8.*QA
     . **2*EDT**2*QL*QT+8.*QA**2*EDT**2*KTC**2-8.*QA**2*QL
     . *QT-8.*QA**2*KTC**2-EDL**2*EDT**2*KTC**4*PASC**2+
     . EDL**2*KTC**4*PASC**2+EDT**2*KTC**4*PASC**2-KTC**4*
     . PASC**2)+K**(-3.)*KTC**8*(QA**2*EDL**2*EDT**2-QA**2
     . *EDL**2-QA**2*EDT**2+QA**2+EDL**2*EDT**2*KLC**2*
     . PASC**2-EDL**2*KLC**2*PASC**2-EDT**2*KLC**2*PASC**2
     . +KLC**2*PASC**2)
      nm=32.*K**5*QA**2*(EDL**2*EDT**2-EDL**2-EDT**2+1.)+
     . 16.*K**3*QA**2*(-2.*EDL**2*EDT**2*QL*QT-3.*EDL**2*
     . EDT**2*KTC**2-EDL**2*EDT**2*KLC**2-2.*EDL**2*QL*QT+
     . 3.*EDL**2*KTC**2+EDL**2*KLC**2+8.*EDL*EDT*QL*QT-2.*
     . EDT**2*QL*QT+3.*EDT**2*KTC**2+EDT**2*KLC**2-2.*QL*
     . QT-3.*KTC**2-KLC**2)+8.*K*QA**2*KTC**2*(4.*EDL**2*
     . EDT**2*QL*QT+3.*EDL**2*EDT**2*KTC**2+2.*EDL**2*EDT
     . **2*KLC**2+4.*EDL**2*QL*QT-3.*EDL**2*KTC**2-2.*EDL
     . **2*KLC**2-16.*EDL*EDT*QL*QT+4.*EDT**2*QL*QT-3.*EDT
```

```
     . **2*KTC**2-2.*EDT**2*KLC**2+4.*QL*QT+3.*KTC**2+2.*
     . KLC**2)+ANS1
      ANS3=K**(-3.)*KTC**8*(QA**2*EDL**2*EDT**2-QA**2*EDL
     . **2-QA**2*EDT**2+QA**2-2.*QA*EDL**2*EDT**2*QL*PASC+
     . 2.*QA*EDL**2*QL*PASC-2.*QA*EDT**2*QL*PASC+2.*QA*QL*
     . PASC-EDL**2*EDT**2*KLC**2*PASC**2+EDL**2*KLC**2*
     . PASC**2+EDT**2*KLC**2*PASC**2-KLC**2*PASC**2)
      ANS2=K**(-1.)*KTC**4*(-8.*QA**2*EDL**2*EDT**2*QL*QT-
     . 8.*QA**2*EDL**2*EDT**2*KTC**2-8.*QA**2*EDL**2*QL*QT+
     . 8.*QA**2*EDL**2*KTC**2+32.*QA**2*EDL*EDT*QL*QT-8.*QA
     . **2*EDT**2*QL*QT+8.*QA**2*EDT**2*KTC**2-8.*QA**2*QL
     . *QT-8.*QA**2*KTC**2+8.*QA*EDL**2*EDT**2*QL*KTC**2*
     . PASC-8.*QA*EDL**2*EDT**2*QT*KLC**2*PASC-8.*QA*EDL**
     . 2*QL*KTC**2*PASC-8.*QA*EDL**2*QT*KLC**2*PASC+8.*QA*
     . EDT**2*QL*KTC**2*PASC+8.*QA*EDT**2*QT*KLC**2*PASC-
     . 8.*QA*QL*KTC**2*PASC+8.*QA*QT*KLC**2*PASC+EDL**2*EDT
     . **2*KTC**4*PASC**2-EDL**2*KTC**4*PASC**2-EDT**2*KTC
     . **4*PASC**2+KTC**4*PASC**2)+ANS3
      ANS1=8.*K*QA*KTC**2*(4.*QA*EDL**2*EDT**2*QL*QT+3.*QA
     . *EDL**2*EDT**2*KTC**2+2.*QA*EDL**2*EDT**2*KLC**2+4.
     . *QA*EDL**2*QL*QT-3.*QA*EDL**2*KTC**2-2.*QA*EDL**2*
     . KLC**2-16.*QA*EDL*EDT*QL*QT+4.*QA*EDT**2*QL*QT-3.*
     . QA*EDT**2*KTC**2-2.*QA*EDT**2*KLC**2+4.*QA*QL*QT+3.
     . *QA*KTC**2+2.*QA*KLC**2-EDL**2*EDT**2*QL*KTC**2*
     . PASC+EDL**2*EDT**2*QT*KTC**2*PASC+EDL**2*QL*KTC**2*
     . PASC+EDL**2*QT*KTC**2*PASC-EDT**2*QL*KTC**2*PASC-
     . EDT**2*QT*KTC**2*PASC+QL*KTC**2*PASC-QT*KTC**2*PASC
     . )+ANS2
      dn=32.*K**5*QA**2*(EDL**2*EDT**2-EDL**2-EDT**2+1.)+
     . 16.*K**3*QA**2*(-2.*EDL**2*EDT**2*QL*QT-3.*EDL**2*
     . EDT**2*KTC**2-EDL**2*EDT**2*KLC**2-2.*EDL**2*QL*QT+
     . 3.*EDL**2*KTC**2+EDL**2*KLC**2+8.*EDL*EDT*QL*QT-2.*
```

```
     . EDT**2*QL*QT+3.*EDT**2*KTC**2+EDT**2*KLC**2-2.*QL*
     . QT-3.*KTC**2-KLC**2)+ANS1
      co=nm/dn
return
end
c   the dinominator of the integration coefficient
function dn(xk)
real*8 h,w,ct,pas,ca,kt, kl, ka,x, d, z, r,pa,ps,pasc
real*8 klc,ktc,kac, dc,xk, dn, xx
complex*16 eda,edt,edl, qt, ql,qa
complex*16 xa, xt, xl, k, im, dnc
complex*16  ans1,ans2,ans3,ans4,ans5,ans6,ans7,ans8
common z, r, ka, kt, kl, pas, h, d,xx
pasc=pas
dc=d
k=dcmplx(xk,0.d0)
klc=kl
ktc=kt
kac=ka
im=(0.d0,1.d0)
qt=cdsqrt(k**2-ktc**2)
ql=cdsqrt(k**2-klc**2)
qa=cdsqrt(k**2-kac**2)
eda=cdexp(-d*qa)
edt=cdexp(-d*qt)
edl=cdexp(-d*ql)
ANS3=K**(-3.)*KTC**8*(QA**2*EDL**2*EDT**2-QA**2*EDL
. **2-QA**2*EDT**2+QA**2-2.*QA*EDL**2*EDT**2*QL*PASC+
. 2.*QA*EDL**2*QL*PASC-2.*QA*EDT**2*QL*PASC+2.*QA*QL*
. PASC-EDL**2*EDT**2*KLC**2*PASC**2+EDL**2*KLC**2*
. PASC**2+EDT**2*KLC**2*PASC**2-KLC**2*PASC**2)
```

```
      ANS2=K**(-1.)*KTC**4*(-8.*QA**2*EDL**2*EDT**2*QL*QT-
     . 8.*QA**2*EDL**2*EDT**2*KTC**2-8.*QA**2*EDL**2*QL*QT+
     . 8.*QA**2*EDL**2*KTC**2+32.*QA**2*EDL*EDT*QL*QT-8.*QA
     . **2*EDT**2*QL*QT+8.*QA**2*EDT**2*KTC**2-8.*QA**2*QL
     . *QT-8.*QA**2*KTC**2+8.*QA*EDL**2*EDT**2*QL*KTC**2*
     . PASC-8.*QA*EDL**2*EDT**2*QT*KLC**2*PASC-8.*QA*EDL**
     . 2*QL*KTC**2*PASC-8.*QA*EDL**2*QT*KLC**2*PASC+8.*QA*
     . EDT**2*QL*KTC**2*PASC+8.*QA*EDT**2*QT*KLC**2*PASC-
     . 8.*QA*QL*KTC**2*PASC+8.*QA*QT*KLC**2*PASC+EDL**2*EDT
     . **2*KTC**4*PASC**2-EDL**2*KTC**4*PASC**2-EDT**2*KTC
     . **4*PASC**2+KTC**4*PASC**2)+ANS3
      ANS1=8.*K*QA*KTC**2*(4.*QA*EDL**2*EDT**2*QL*QT+3.*QA
     . *EDL**2*EDT**2*KTC**2+2.*QA*EDL**2*EDT**2*KLC**2+4.
     . *QA*EDL**2*QL*QT-3.*QA*EDL**2*KTC**2-2.*QA*EDL**2*
     . KLC**2-16.*QA*EDL*EDT*QL*QT+4.*QA*EDT**2*QL*QT-3.*
     . QA*EDT**2*KTC**2-2.*QA*EDT**2*KLC**2+4.*QA*QL*QT+3.
     . *QA*KTC**2+2.*QA*KLC**2-EDL**2*EDT**2*QL*KTC**2*
     . PASC+EDL**2*EDT**2*QT*KTC**2*PASC+EDL**2*QL*KTC**2*
     . PASC+EDL**2*QT*KTC**2*PASC-EDT**2*QL*KTC**2*PASC-
     . EDT**2*QT*KTC**2*PASC+QL*KTC**2*PASC-QT*KTC**2*PASC
     . )+ANS2
      dnc=32.*K**5*QA**2*(EDL**2*EDT**2-EDL**2-EDT**2+1.)+
     . 16.*K**3*QA**2*(-2.*EDL**2*EDT**2*QL*QT-3.*EDL**2*
     . EDT**2*KTC**2-EDL**2*EDT**2*KLC**2-2.*EDL**2*QL*QT+
     . 3.*EDL**2*KTC**2+EDL**2*KLC**2+8.*EDL*EDT*QL*QT-2.*
     . EDT**2*QL*QT+3.*EDT**2*KTC**2+EDT**2*KLC**2-2.*QL*
     . QT-3.*KTC**2-KLC**2)+ANS1
      dn=dreal(dnc)
      return
      end
c     calculation of the point for singularity
      function sing(a,b,x0)
```

```
integer if
real*8 a,b,xx,dn, eps, zero, c05agf,sing,x0
external c05agf,dn
if=-1
xx=x0
h=1.d-6
zero=0.d0
eps=1.d-16
call c05agf(xx,h,eps,zero,dn,a,b,if)
sing=xx
write(6,*) xx
return
end
```

Appendix E

Decompostion of the reflected wave term

According to the description of spherical wave reflection above a boundary with a refractive index less than unity [66], a reflection wave term, e.g.,

$$\int_{i\kappa_1}^{\infty} \frac{\rho_2 x - \rho_1\sqrt{x^2+\kappa_1^2-\kappa_2^2}}{\rho_2 x + \rho_1\sqrt{x^2+\kappa_1^2-\kappa_2^2}} J_0(r\sqrt{x^2+\kappa_1^2}) exp(-hx)\,dx \text{ at } z=0, \quad \text{(E.1)}$$

for the reflection at a kerosene-water interface, can be considered as a combination of a reflected wave and a diffracted wave. It would be interesting to know some features of these two waves so we have tried to decompose the two waves. We assume that the reflected wave and the diffracted wave, at the interface $z = 0$, have the forms

$$\frac{exp(i\kappa_1\sqrt{r^2+h^2})}{\sqrt{r^2+h^2}} \quad \text{(E.2)}$$

and

$$\int_{i\kappa_1}^{\infty} \frac{\rho_2 x - \rho_1\sqrt{x^2+\kappa_1^2-\kappa_2^2}}{\rho_2 x + \rho_1\sqrt{x^2+\kappa_1^2-\kappa_2^2}} J_0(r\sqrt{x^2+\kappa_1^2}) exp(-hx)\,dx,$$

$$-\frac{exp(i\kappa_1\sqrt{r^2+h^2})}{\sqrt{r^2+h^2}} \quad \text{(E.3)}$$

respectively. It is not difficult to see that the sum of (E.2) and (E.3) gives the reflection term (E.1). The calculations of the 'reflected wave' (E.2) and the 'diffracted wave' (E.3), and the reflection term (E.1) are shown in Figures (E.1) to (E.4).

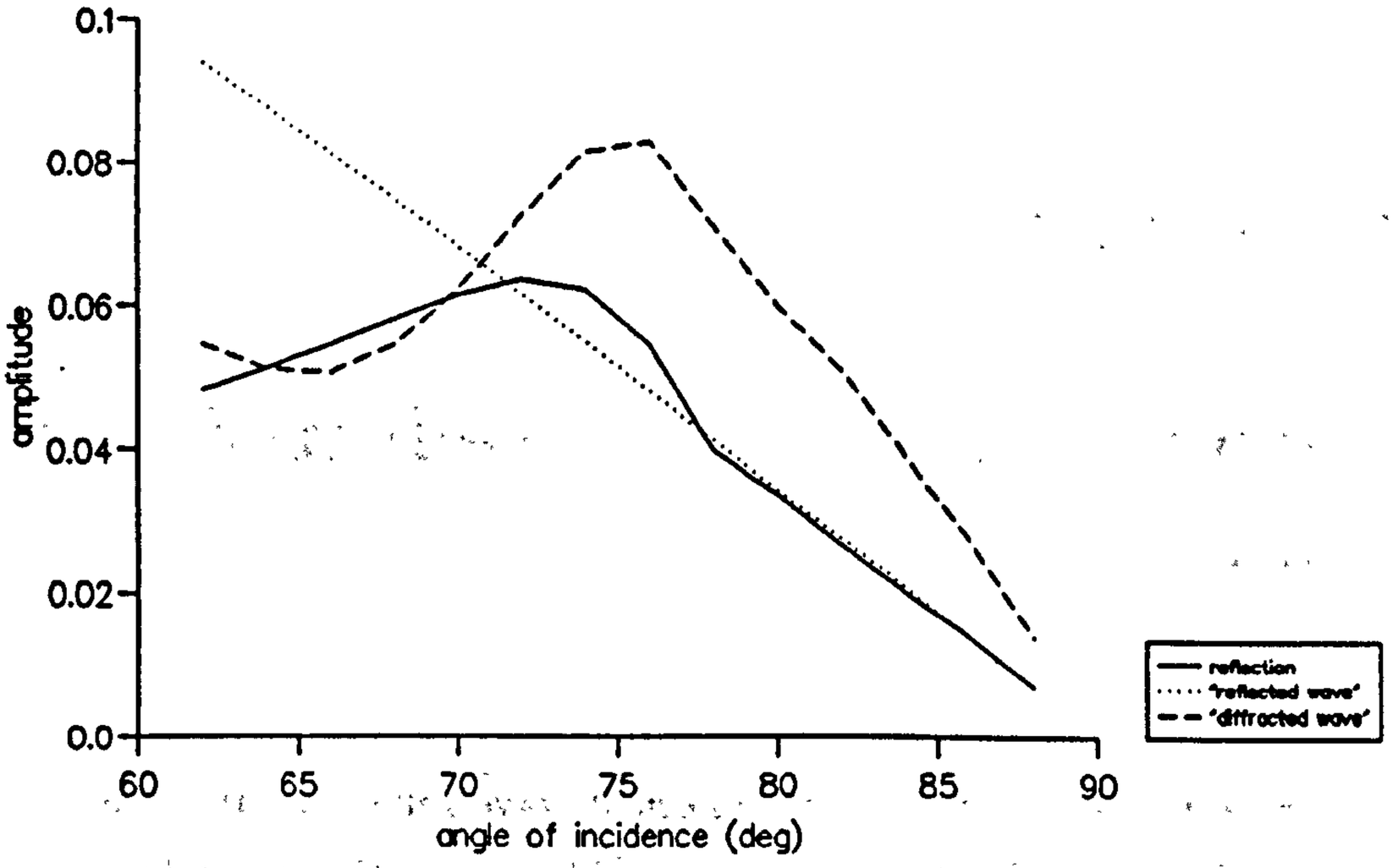

Figure E.1 Amplitudes of various waves for the decomposition of the reflection at a kerosene-water interface. The source is in the kerosene, at $h = 5$m, frequency 1000Hz.

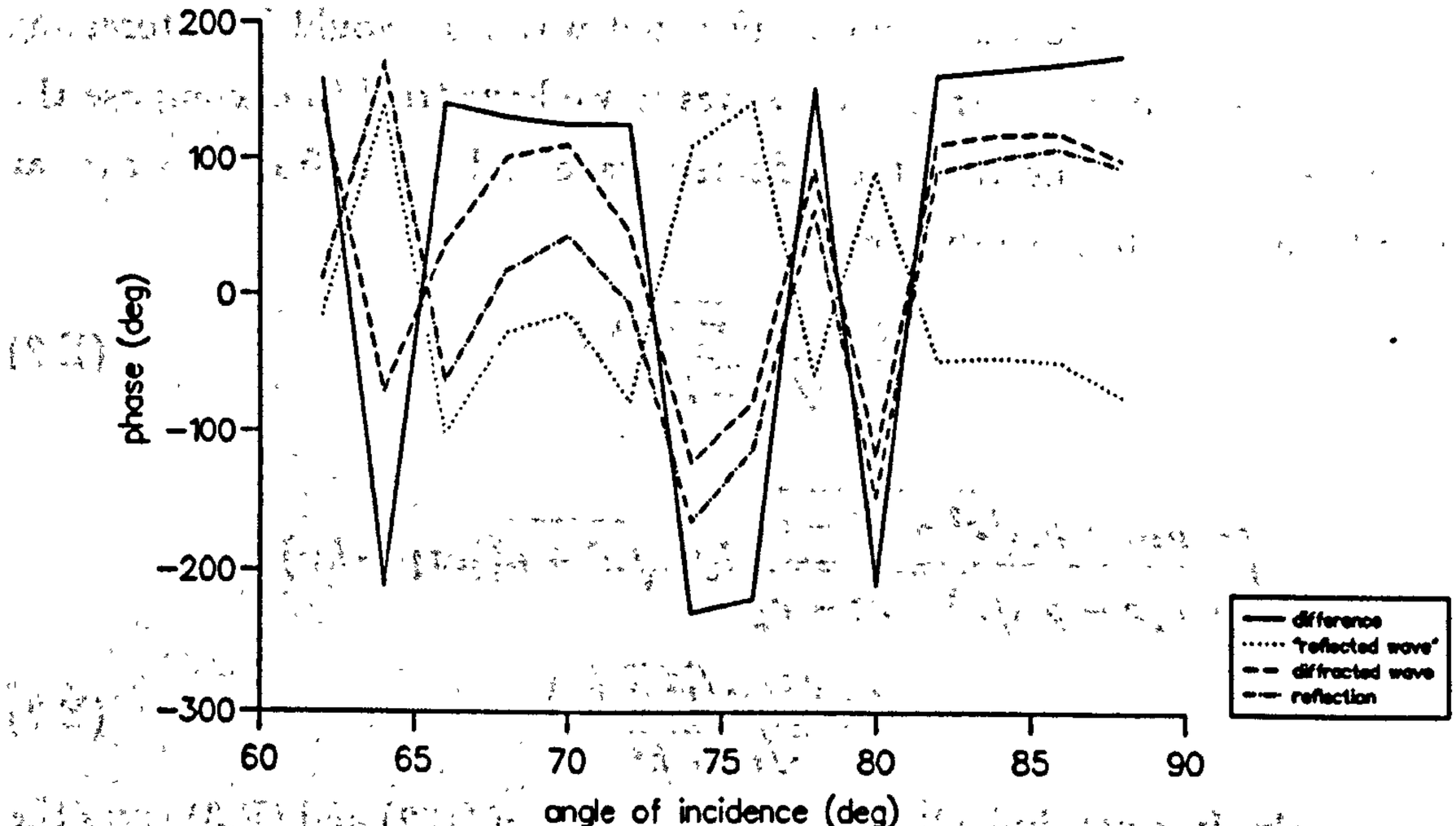

Figure E.2 Phases of various waves for the decomposition of the reflection at a kerosene-water interface. The source is in the kerosene, at $h = 5$m, frequency 1000Hz.

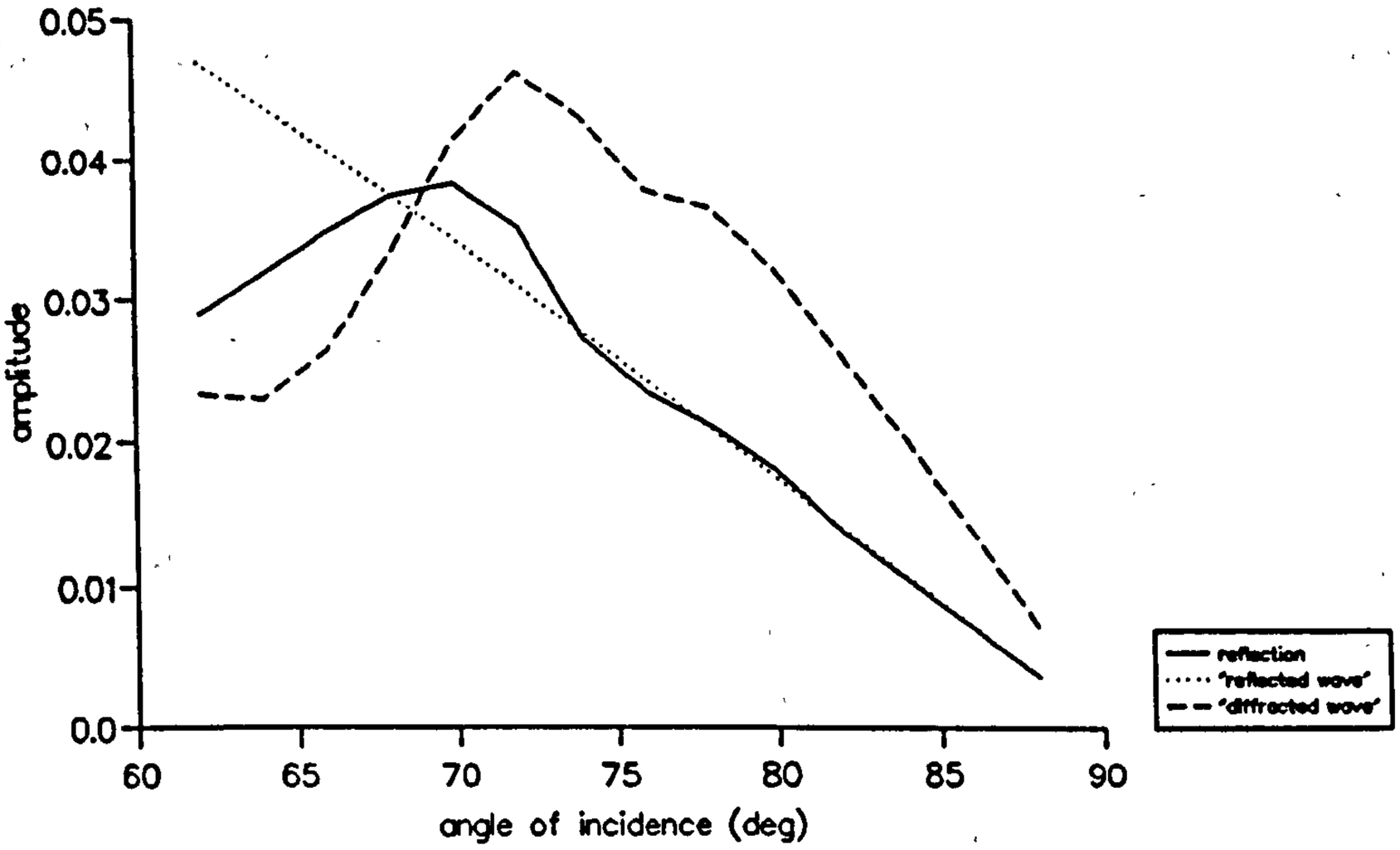

Figure E.3 Amplitudes of various waves for the decomposition of the reflection at a kerosene-water interface. The source is in the kerosene, at $h = 10$m, frequency 1000Hz.

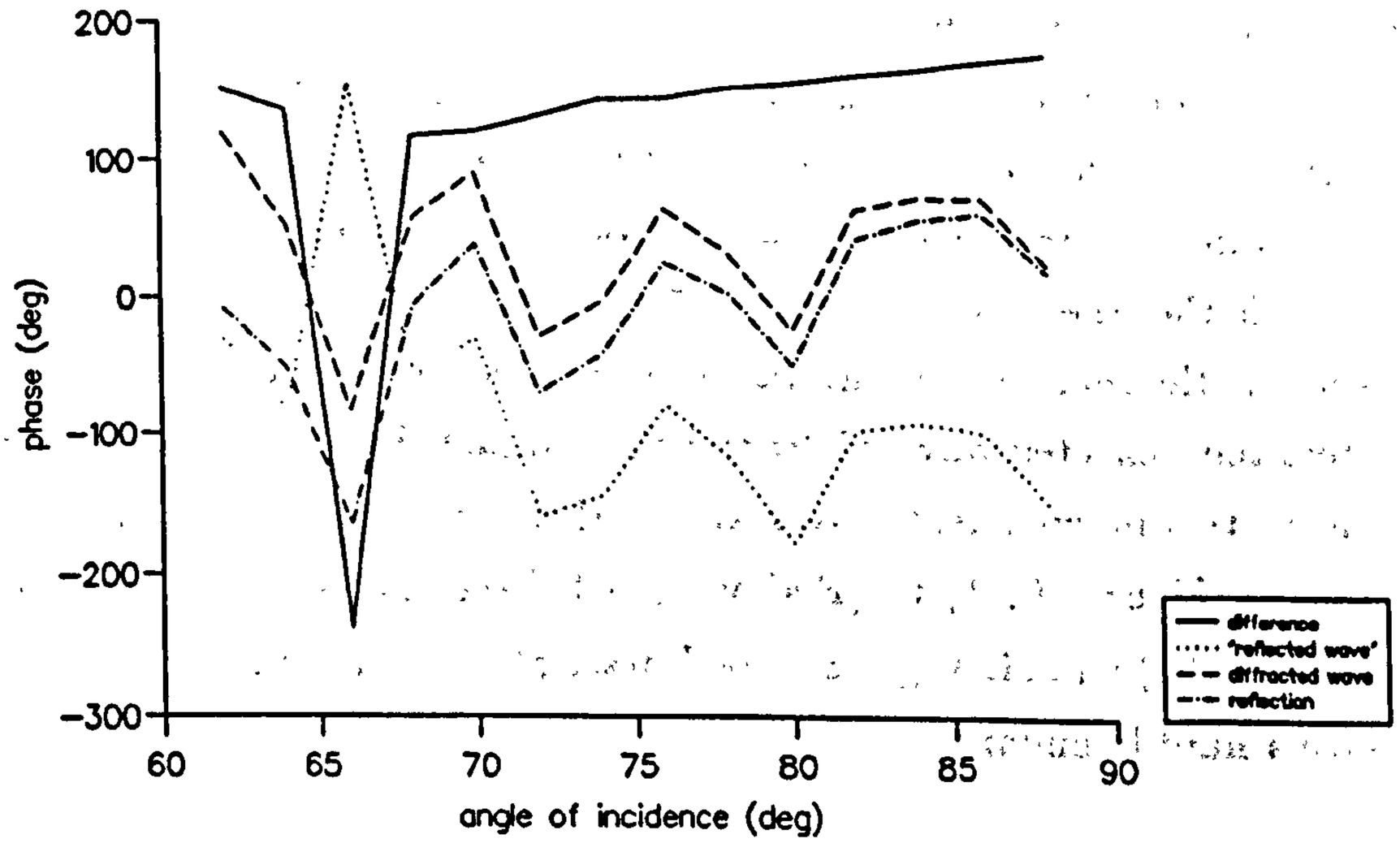

Figure E.4 Phases of various waves for the decomposition of the reflection at a kerosene-water interface. The source is in the kerosene, at $h = 10$m, frequency 1000Hz.

Figure (6.6) in Section 6.2 shows that beyond the critical angle the amplitude of the reflection coefficient for spherical waves oscillates about that for a plane wave. The amplitude of the incident wave is a linear monotonic decreasing function when r (or angle of incidence) increases. If we plot the amplitude of the reflection term (E.1) against the angle of incidence, we can see that it does not behave in this way (see the curves labelled by "reflection" in Figures (E.1) and (E.3)). Therefore, the ratio of the amplitudes of the incident wave and the reflection term appears to oscillate. An explanation is that the interference between a reflected wave and a diffracted wave may determine the feature of the reflection term (E.1) and caused the oscillation.

In Figures (E.2) and (E.4) the curves labelled "difference" give the phase difference between the 'reflected wave' (E.2) and the 'diffracted wave' (E.3). The curves of phase difference for source heights at $h = 5$m and $h = 10$m are quite different, there is only one trough in (E.4) but there are three in (E.2). From the curves for the phase difference it can be seen that the peaks of amplitude of the reflection term in Figures (E.1) and (E.3), obtained from (E.1), cannot be caused by a constructive interference between the 'reflected wave' (E.2) and the 'diffracted wave' (E.3), therefore the oscillation of the reflection coefficients in Figure (6.6) cannot be the result of the interference between the 'reflected wave' (E.2) and the 'diffracted wave' (E.3).

It is difficult to judge from the information provided in Figures (E.1) to (E.4) whether the decomposition of (E.1) by (E.2) and (E.3) is appropriate to represent the reflected and diffracted waves. An experiment may be needed to test the 'reflected wave' (E.2) and the 'diffracted wave' (E.3). If we could identify two independent waves and if these two waves have the features shown in Figures (E.1) to (E.4) we can believe that the decomposition of (E.1) by (E.2) and (E.3) gives a good description of spherical wave reflection above a hard boundary.

Appendix F

A list of equipment

1. Microphone: Bruel & Kjaer 1/2" (24 mm), type 4165.
2. Microphone preamplifier: Bruel & Kjaer type 2639, with an adapter JE0002.
3. Power supply: Bruel & Kjaer type 2807.
4. FFT anlyser: Ono Sokki CF 910 two channel mini FFT analysis system.
5. Power amplifier: Bruel & Kjaer type 2706.
6. Source: 45 watt Tannoy drive unit.
7. Step motor: Berger Lahr, RDM59/50.
8. Motor controllor: Berger Lahr, NIP 6.1122.01.
9. Personal computer: Zenith z-150 desktop system.

List of Figures

List of Tables